Universitat Autònoma de Barcelona

Radical dendrimers as Magnetic Resonance Imaging Contrast Agents

Songbai Zhang

Universitat Autònoma de Barcelona

Radical dendrimers as Magnetic Resonance Imaging Contrast Agents

Songbai Zhang

Tesi Doctoral

Programa de doctorat de Química

Directors

José Vidal Gancedo i Vega Lloveras Monserrat

Departament de Química

2021

Memoria presentada para aspirar al grado de doctor por:

Songbai Zhang

Visto Bueno:

José Vidal Gancedo Vega Lloveras Monserrat

En Bellaterra, a 29 de Octubre de 2021

Dr. José Vidal Gancedo and **Dr. Vega Lloveras Monserrat**, of the Spanish National Research Council at the Materials Science Institute of Barcelona (ICMAB-CSIC)

CERTIFY

That **Songbai Zhang**, graduate in Chemistry, has performed, under their management, the research work entitled **"Radical dendrimers as Magnetic Resonance Imaging Contrast Agents"**. This work has been performed under the mark of the Chemistry Ph. D. program of the Chemistry Department of the Autonomous University of Barcelona.

An in witness whereof this is signed by

Directors UAB Tutor

José Vidal Gancedo Vega Lloveras Monserrat Rosa Mª Sebastián Pérez

Ph.D. Student

Songbai Zhang

En Bellaterra, a 29 de Octubre de 2021

“What is reasonable is real; that which is real is reasonable.”

Georg Wilhelm Friedrich Hegel

Dedicated to my family

Acknowledgments

I would like to express my gratitude to China Scholarship Council (CSC) for financing me during the last four years. I acknowledge sincerely my supervisors José Vidal Gancedo and Vega Lloveras. They offered me specialized guidelines and extraordinary assistance in completing this Thesis with their immense knowledge and plentiful experience and constant patience. I would like to extend my thanks to Dr. Luiz Pinto, Dr. Flonja Liko and Dr. Pilar Elías for their valuable help and numerous useful advices for the specific experiments when I entered the laboratory. I would like to acknowledge Nikita, Ehsan, and Yufei. With their help, I was able to complete my Thesis smoothly. I am deeply gratefully to members of the Nanomol family, Amable, Arnau, Alejandro, Nerea, Ángel, José, David, Aida, Lidia Ballell, so forth, thanks for their help whenever I needed it. And I also would like to thank all the members for having a nice atmosphere in working here.

I would like to thank Miriam Royo and Daniel Pulido for providing us OEG-based dendrimers and Joaquín C. García for the oligo(styryl)benzenes fluorescent dendrimers, which made part of this Thesis possible.

I also would like to appreciate the staff from Servei de Ressonància Magnètica Nuclear (RMN); they helped me to finish many measurements of NMR spectra. Thanks especially to Silvia Lope for her expertise and help with MRI experiments. I would like to thank Wu Shuang, Pilar Calero and Ana Paula Candiota from Departament de Bioquímica i Biologia Molecular of UAB for their help on the animal experiments. I would like to thank Salva from Laboratori Luminescència i Espectroscòpia Biomolècules (LLEB) for his always kind assistance of fluorimetry measurement. Thanks to Óscar from Servei d'Anàlisi Química for his professional analysis of ESI-MS spectra. I would like to thank Sohini for her help to master the method of measuring quantum yield. I would like to thank Miriam her assistance in the *in vitro* cytotoxicity. Thanks to Judith for her help with TEM images.

I spent a cheerful four years period, attributed to many friends. I would like to thank the members of radio patio ICMAB. It was a meaningful and joyful time to spend with all of you. I also thank my officemate, Sergi Martin for his help any time in my office. I must thank all the Chinese friends whom I met here, Qian Wenjie, Zhang Qiaoming, Chen Yu, Ma Zheng, Wang Hailing, Tan Fangchang, Zhang Yajie, Gan Lei, Zhang Xiaodong,

Li Jinghai, Duan Wenchao, Li Zhen and others not specifically mentioned here. Thanks for their support and assistance during the last four years.

Last but not least, I would like to thank my family, my parents, my brother and my wife. Without your support, I could not reach to this moment, nor to finish this Thesis, thanks to you!

Abbreviations

Å: ångström unit.

ACN: Acetonitrile.

AcOH: Acetic Acid.

B_0: External Magnetic Field.

bis-MPA: 2,2-bis(hydroxymethyl)propionic acid.

BOC: tert-butyloxycarbonyl protecting group.

br: broad.

d: doublet.

DCE: Dynamic Contrast Enhanced

DCM: Dichlorometane.

DIEA: N,N-Diisopropylethylamine.

DLS: Dynamic light scattering.

DMF: Dimethylformamide.

DMSO: Dimethyl sulfoxide.

DNP: Dynamic Nuclear Polarization.

DTPA: diethylenetriaminepentaacetic acid.

EDTA: 2,2',2",2'"-(Ethane-1,2-diyldinitrilo)tetraacetic acid.

EPR: Electron Paramagnetic Resonance.

eq.: Equivalent.

EU: Endotoxin Units.

AcOEt: Ethyl acetate.

G: Gauss, magnetic field unit.

GPC: Gel Permeation chromatography.

HATU: 1-[Bis(dimethylamino)methylene]-1H-1,2,3-triazolo[4,5-b]pyridinium 3- oxid hexafluorophosphate.

HPLC: High Performance Liquid Chromatography.

I: Nuclear spin quantum number.

IC50: half maximal inhibitory concentration.

IC: Internal conversion.

IR-ATR: Infrared spectroscopy-Attenuated Total Reflectance.

ISC: intersystem crossing.

GBCAs: gadolinium-based contrast agents.

GL261: Glioma 261.

Gn: Dendrimer of x generation.

Gn': Dendrimer of x generation ended in aldehyde.

LB: Line broadening.

m: multiplet.

MALDI-TOF: Matrix-Assisted Laser Desorption/ Ionization-Time Of Fly.

MeOH: Methanol.

MRC-5: Medical Research Council cell strain-5.

MRI: Magnetic Resonance Imaging.

MS: Mass Spectrometry.

MTT: 3-(4,5-Dimethylthiazol-2-yl)-2,5-diphenyltetrazolium bromide.

MTS: (3-(4,5-dimethylthiazol-2-yl)-5-(3-carboxymethoxyphenyl)-2-(4-sulfophenyl)-2H-tetrazolium).

MWCO: Molecular weight cut-off.

m/z: Mass to charge ratio.

NMR: Nuclear Magnetic Resonance.

ORCAs: Organic Radical Contrast Agents.

OEG: Oligoethylene glycol.

OSB: oligo(styryl)benzene

PTM: Perchlorotriphenylmethyl radical.

PROXYL: 2,2,5,5-tetramethylpyrrolidin-1-oxyl radical.

r_1: Longitudinal relaxivity.

r_2: Transverse relaxivity.

s: singlet.

SEC: Size-exclusion chromatography.

t: triplet.

T_1: Longitudinal relaxation time or Spin-Lattice relaxation time.

T_2: Transverse relaxation time or Spin-Spin relaxation time.

TE: Time echo.

TEA: Trimethylamine.

TEM: Transmission electron microscope.

TEMPO: (2,2,6,6-Tetramethylpiperidin-1-yl)oxyl radical.

TFA: Trifluoroacetic acid.

THF: Tetrahydrofuran.

TLC: Thin layer chromatography.

UV-Vis: Ultraviolet-visible spectrophotometry.

Wt: Wild type.

XTT: 2,3-bis-(2-methoxy-4-nitro-5-sulfophenyl)-2H-tetrazolium-5-carboxanilide.

δ: Chemical shift (ppm).

γ: Gyromagnetic constant.

ω_0: Larmor frequency.

^{31}P: ^{31}P NMR spectrum with $\{^1H\}$ disengaged.

^{13}C: ^{13}C NMR spectrum with $\{^1H\}$ disengaged.

Summary

The main objective of this Thesis is to develop metal-free contrast agents (CA) for magnetic resonance imaging (MRI) to overcome the established toxicity of the most widely used CA in clinical diagnosis based on Gd(III) complexes. Dendrimers are monodisperse polymers with a well-defined molecular structure, which can be a perfect support for anchoring organic radicals, what is called 'radical dendrimer'. In this way, the relaxivity can be improved and a shielding effect can be provided to the radicals offering them protection against reduction.

One of the greatest challenges in the synthesis of CA for biomedical applications is to make them water-soluble. Besides, CA should present high relaxivity and low toxicity. In this Thesis we use different strategies to prepare water-soluble radical dendrimers, by playing with different types of dendrimers, linkers and supramolecular structures.

Amino acids can be ideal linkers for preparing water-soluble radical dendrimers because they provide an amino group for radical coupling, and an acid group that can provide negative charges conferring high solubility and low toxicity. Tyrosine and lysine have been chosen as linkers between polyphosphorhydrazone (PPH) dendrimer branches and PROXYL radicals. In the group it had been started the synthesis of four generations of PPH radical dendrimers with tyrosine as linker (Gn-Tyr(PROXYL)-COOLi, n=0-3). They are fully soluble in water, present high relaxivity (from 1.39 $mM^{-1}s^{-1}$ in G0 to 12.96 $mM^{-1}s^{-1}$ in G3), and no cytotoxicity. Lysine has been properly anchored to four generations of PPH dendrimers (Gn-Lys(BOC)-COOMe, n=0-3). However, under acid conditions the generations higher than G0 showed lysine release through P-N bond cleavage, preventing the obtaining of radical dendrimers with this linker. We have been able to determine that G1-Lys(BOC)-COOLi presents lysine release at pH 7.7. Therefore, these new lysine-functionalized PPH dendrimers can be used to prepare pH-controlled degradable dendrimers or pH-controlled release, opening a new field of research.

Another strategy has been the use of dendrimers that are water-soluble themselves, in particular oligoethylene glycol (OEG) based dendrimers. Two generations of OEG-based dendrimers fully functionalized with 5 and 20 PROXYL radicals have been synthesized and characterized. They are soluble in water, non-cytotoxic and have a good relaxivity: G1-OEG-PROXYL radical dendrimer has a similar r_1 relaxivity value (3.4 $mM^{-1}s^{-1}$) than Gd-DTPA (3.2 $mM^{-1}s^{-1}$) widely used in clinics.

A third possibility is the use of amphiphilic compounds to prepare self-assembled supramolecular structures such as nanoparticles. We have used dendritic-linear-dendritic polymers based on (bis-MPA) dendrons at the end of a poly(ethylene glycol) chain. Three different generations have been synthesized by click chemistry (G1-, G2- and G3-MPA-PEG20k-TEMPO) and we have obtained homogeneous suspension of G2 nanoparticles (G2NPs) in water. While G2NPs form spherical nanoparticles, G2 directly dissolved in water forms nanofibers. They are non-cytotoxic and G2NPs present slightly higher relaxivity than G2, probably because of the higher rigidity of the former.

We have also explored the possibility of obtaining not only magnetic but also fluorescent dendrimers to have bimodal CA for potential MRI and fluorescence imaging applications. We have synthesized six radical dendrimers based on fluorescent oligo(styryl)benzenes. In organic solvents these compounds present simultaneously fluorescence and relaxivity. In order to obtain these compounds in aqueous solution, CTAB micelles have been prepared to encapsulate them. Such systems, with the radical dendrimers inside, maintain both magnetic and fluorescent properties.

Finally, the contrast ability *in vivo* of G3-Tyr(PROXYL)-COONa (G3) radical dendrimer has been described in healthy and GL261 glioblastoma-bearing mice. Biodistribution studies show enhancement mostly in kidney cortex and pelvis, as well as a selective accumulation of the radical dendrimer in the brain tumor. G3 provides similar contrast enhancement than commercial Gd-based CA and a longer circulation time.

Index

Chapter 1 Introduction and Objectives

1.1 Imaging modalities

The term “molecular imaging” has been used to describe techniques that directly or indirectly monitor and record the spatiotemporal distribution of molecular species or cellular processes for biochemical, biologic, diagnostic or therapeutic applications.[1] Several imaging techniques have been developed to these purposes, including optical fluorescence imaging (OFI), positron emission tomography (PET), single photon emission computed tomography (SPECT), X-ray based computed tomography (CT) and magnetic resonance imaging (MRI).[2] Among them, MRI is the most versatile and widely used clinical diagnostic tool nowadays, showing some advantages over the others (Table 1-1).

MRI provides images of soft tissue anatomy in excellent detail, with high spatial resolution (~1 mm), non-destructive and non-invasive characteristics due to the absence of ionizing radiation, unlimited penetration depth and long effective imaging window. This method is largely used for non-invasive diagnostic routine in detection and staging of cancer, pathologies of the brain such as stroke or neurodegenerative disease, musculoskeletal disease or in cardiac imaging, among others. On the other hand, other clinical imaging techniques such as optical fluorescence imaging (OFI) shows high sensitivity but low resolution in *in vivo* tissues and low penetration depth. X-ray based computed tomography (CT) presents high resolution (0.5-1 mm) but presents safety concerns due to the ionizing radiation like positron emission tomography (PET) and single photon emission computed tomography (SPECT).

Table 1-1. Features of available and emerging imaging modalities (adapted from reference [2] with modifications).

Modalities	Spatial Resolution	Depth of Penetration	Imaging time	Sensitivity (mol/L)	Multiplexing Capability	Safety	Cost	Clinical Availability	Imaging/Contrast Agent	Information Provided
OFI	Highest in vitro cell imaging Low in vivo tissue imaging (2-3 mm)	< 1 cm	s–min	High (10^{-9}-10^{-12})	Yes	Relatively safe	Low	Optical guided surgery	Organic fluorophores Quantum dots Polymer dots Upconversion materials, etc.	Functional information: biomarker, physiological information, receptor, and etc.
CT	High (0.5–1 mm)	Unlimited	min	Low for soft tissues (ND)	No	Ionizing radiation	Relatively high	Yes	Iodinated molecules Gold nanoparticles Bi2S3, TaOx, etc.	Mainly 3D anatomy
MRI	High (~1 mm)	Unlimited	(min)	Very Low, Better than CT for soft tissues (10^{-3}-10^{-5})	No	No ionizing radiation	High	Yes	$Gd^{3+}$and Mn^{2+} complexes, Superparamagnetic iron oxide nanoparticles, ^{19}F enriched materials, etc.	3D anatomy Physiological information
PET	low 5–7 mm	Unlimited	s–min	Very High (10^{-11}-10^{-12})	No	Ionizing radiation	High	Yes	Radioisotopes: ^{18}F, ^{64}Cu, ^{68}Ga, ^{89}Zr, etc.	3D distributions of PET nuclides
SPECT	low 8–10 mm	Unlimited	min	High (10^{-10}-10^{-11})	Yes	Ionizing radiation	Relatively high	Yes	Radioisotopes: ^{99m}Tc, ^{111}In, ^{177}Lu, etc.	3D distributions of SPECT nuclides

1.2 Nuclear Magnetic Resonance (NMR) and Magnetic Resonance Imaging (MRI)

Magnetic resonance imaging which is based on nuclear magnetic resonance (NMR), was developed for clinical use in the 1980s to study structural aspects of tissues. More recently, this technique has provided functional insights due to several MRI innovations. Indeed, *in vivo* magnetic resonance spectroscopy using contrast agents has made it possible to obtain information on basic cellular mechanisms at the molecular level.

Nuclear spin is the basis of all magnetic resonance research. Many atomic nuclei have spin, characterized by the nuclear spin quantum number (I). Spin behaves as expected from a classical description of a rotating object but fits the quantum mechanical descriptions of angular momentum. Thus, nuclear spin is associated with an angular momentum (μ) which, in absence of an external magnetic field shows a random direction. When an external magnetic field (B_0) is applied, the nuclear magnetic moments are oriented preferentially along the magnetic field. As a result, the degenerated energy states from the nucleus are split in different levels which are filled following a Boltzman distribution. Additionally, this interaction forces the spin to precess around the magnetic field B_0 (rotational movement around B_0) that depends on the magnetic field and the gyromagnetic constant (γ) which is characteristic of each isotope of the nuclei. The frequency of the precession is called Larmor frequency (ω_0)

$$\omega_0 = \gamma B_0 \tag{1-1}$$

For any I, there are 2I+1 energy levels. In particular, for a nucleus with spin I = ½ there are only two energy levels, the low energy level occupied by the spins aligned with B_0 and the high energy level occupied by spins aligned against B_0, with an energy difference of:

$$\Delta E = \gamma \hbar B_0 = \hbar \omega_0 \tag{1-2}$$

Where $\hbar$ is Planck's constant (h) divided by 2π.

At room temperature, there is only a slight excess of spins aligned along the magnetic field (i.e. in the lower energy level) compared to those aligned against the field if the nuclei have a positive gyromagnetic ratio. Although the excess of spins in the lower energy level is quite small (often approximately 1 ppm) it yields a net magnetic moment, which is the signal detected in an NMR experiment. Bloch[3] showed that for any ensemble of spins with I = ½, the net magnetization was given by:

$$M_0 = \frac{\rho_0 \gamma^2 \hbar B_0}{4kT} \pi r^2 \quad (1\text{-}3)$$

where ρ_0 is the spin density, K is the Boltzmann constant and T is the temperature.

The spin magnetization vector (M_0) is parallel to the external magnetic field B_0, thus, in the Z-axis direction (M_z). In the initial equilibrium state, M_z equals M_0. Once another magnetic field B_1 with energy that equals to the energy gap ΔE is applied (created by a radiofrequency pulse), the magnetization vector M_0 can rotate to XY transverse plane and produce M_{XY_0}. The recovery of the initial equilibrium state takes place through relaxation processes changing the magnetization and these data are those which are measured in a magnetic resonance imaging experiment. By taking the vector sum over all spins, the behavior of the spins in a magnetic field can be described by the Bloch equations.[3]

$$\frac{dM_X}{dt} = \gamma(M_y B_0 + M_z B_1 \sin(\omega t)) - \frac{M_X}{T_2} \quad (1\text{-}4)$$

$$\frac{dM_y}{dt} = \gamma(-M_X B_0 + M_z B_1 \sin(\omega t)) - \frac{M_y}{T_2} \quad (1\text{-}5)$$

$$\frac{dM_Z}{dt} = \gamma(M_X B_1 \sin(\omega t) + M_y B_1 \cos(\omega t)) - \frac{M_Z - M_o}{T_1} \quad (1\text{-}6)$$

In a more simplified way: when the applied energy is removed, the spin magnetization can recover its initial state M_0 along the Z direction. During this process, the magnetization M_z increases. The increasing process can be described by this equation:

$$M_z = M_0(1 - e^{-\frac{t}{T_1}}) \quad (1\text{-}7)$$

The time constant T_1 is the longitudinal relaxation time also called the spin-lattice relaxation time because the longitudinal process results from the release of energy to the environment. In other words, it is the result of non-radiative interactions between the spin system and the lattice. Strictly, relaxation time T_1 is defined as the time when the magnetization vector M_Z increases to 63% (1-1/e) of the maximum M_0.

While the longitudinal magnetization vector M_Z increases to the M_0, the transverse magnetization vector M_{XY_0} decreases to zero. Due to the heterogeneous magnetic field experienced, the spins of the magnetization vector lose their coherence. This process can be expressed by the equation:

$$M_{XY} = M_{XY_0} e^{\frac{-t}{T_2}} \quad (1\text{-}8)$$

Here, the time constant T_2 is the transverse relaxation time or spin-spin relaxation time because the relaxation comes from the spin-spin interactions. The value of the T_2 is defined as the time that it takes the magnetization to decrease to 37% (1/e) of the initial M_{XY_0}.

The graphical representations of longitudinal and transverse magnetization with different relaxation times (short and long T_1 or T_2) are presented in Figure 1-1. It is clearly observed that the longitudinal relaxation with short T_1 is faster in recovering the initial value than with long T_1, as well as in the transverse relaxation process, the relaxation with short T_2 is also faster than with long T_2.

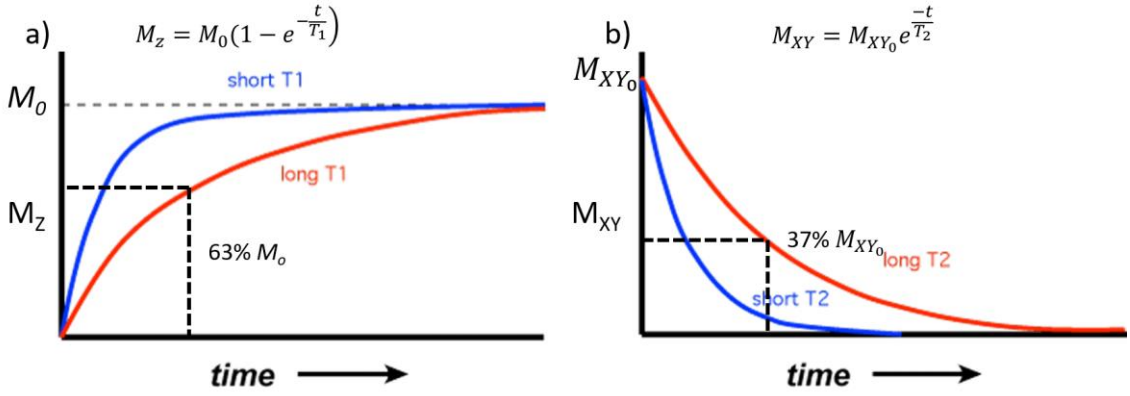

Figure 1-1. The graphical representations of longitudinal and transverse magnetization change with time with different T1 and T2 relaxation times.

In NMR, we pay much attention to the chemical shift of protons. However, in MRI, we are interested in finding the location of the protons in water or fat. In order to differentiate the position of the protons, a gradient field is designed. With the aid of the gradient field, the recognition of protons in different locations can be achieved by slice selection, frequency encoding, and phase encoding processes. In this way, we can give a specific position in a 2-D plane with different frequencies or phases. When the exam finishes, the signal can be transferred to a voxel by Fourier transform. Finally, the image at different location can be obtained.[4]

1.3 MRI with contrast agents

One limitation of MRI techniques is their low sensitivity, inherent to the nuclear magnetic resonance, because of the low energy difference between the ground and excited states which are filled following a Boltzman distribution, with only slight excess in the lower state in the thermal equilibrium. In order to overcome the lack of sensitivity, the use of contrast agents (CAs) for ^{1}H visualization are needed to enhance the contrast of the images in most MRI clinical diagnostic techniques.

Signal intensity in most of the MRI experiments stems largely from the local value of the longitudinal relaxation rate ($1/T_1$) and the transverse relaxation rate ($1/T_2$) of water protons contained in tissues. Contrast agents are used to shorten the longitudinal T_1 or the transverse T_2 relaxation times. Signal tends to increase (brighter signals) with shortening T_1 (increasing $1/T_1$ rate) and decrease (darker signals) with shortening T_2 (increasing $1/T_2$ rate).

The extent to which the contrast agent can modify the relaxation rate ($1/T_1$ or $1/T_2$) of tissue water ^{1}H per milimolar concentration is defined as relaxivity (r_1 or r_2)[5]. Higher relaxivity values translate to a better image contrast (positive or negative contrast, respectively) and, hence, better MRI efficiency of the system. Pulse sequences that emphasize changes in $1/T_1$ are referred as T_1-weighted, and changes in $1/T_2$ as T_2-weighted scans.

Relaxivity can be obtained from the slope of $1/T_i$ *versus* the concentration of the contrast agent [*CA*].

$$\frac{1}{T_i} = \frac{1}{T_0} + r_i[CA]; \qquad i = 1,2 \tag{1-9}$$

Where $1/T_i$ is the relaxation rate ($1/T_1$ or $1/T_2$) in s^{-1} units, $1/T_0$ is the relaxation rate without contrast agent, r_i (r_1 or r_2) is the relaxivity and [*CA*] the concentration of the contrast agent in mM units. When the contrast agent approaches the water ^{1}H of the tissues, the relaxation time (T_i) change (decreases) depending on the concentration of the CA, at higher concentration higher change. Relaxivity value is usually expressed in $mM^{-1}s^{-1}$ units.

Here, we will describe the working mechanism of a MRI contrast agent to help to understand the parameters that influence the relaxivity. In this Introduction, we pay more attention to the factors influencing the r_1 relaxivity since the contrast agents developed in this Thesis are categorized as T_1 contrast agents and because they are the most important and used ones in many MRI applications. We will describe the theories related to metal-based CA, and then we will explain the similarities to our systems. When a paramagnetic complex, such as gadolinium (III) ion complex, is used as contrast agent, there are two contributions to the relaxivity. The first one is through *inner sphere relaxation* where a water molecule is directly bound to the paramagnetic center (metal) by occupying one of the coordination sites and exchange with water from the bulk (Figure 1-2). The second one is the *outer-sphere relaxation* where water molecules diffuse to the vicinity of the paramagnetic compound (second coordination sphere and beyond, i.e., bulk solvent) and

are relaxed (Figure 1-2).[5] The relaxivity from both the inner sphere (r_1^{IS}) and outer sphere (r_1^{OS}) can be expressed as:

$$r_1 = r_1^{IS} + r_1^{OS} \tag{1-10}$$

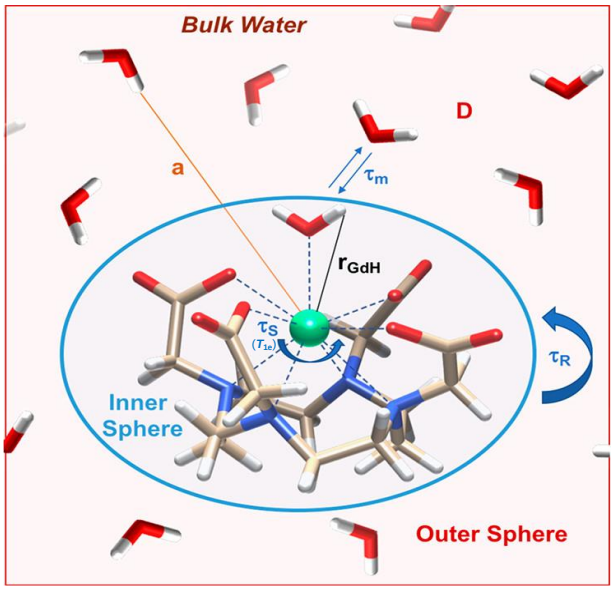

Figure 1-2. Schematic description of the parameters that influence the relaxivity of a MRI contrast agent.[5] We can observe the inner and outer sphere, and the main parameters: τ_R (rotational correlation time or tumbling of the molecule), τ_m (mean residence time of the water in the ligand) and τ_s (also referred as T_{1e}) electronic relaxation time.

The inner sphere stems from the intimate or direct interaction between water and metal ion. Since the molecule of water forms a coordinating bond with the metal, the distance between them is very short, and the metal can relax the water directly. Then, the relaxed water can exchange with another water from the bulk. The relaxivity from the inner sphere can be expressed by the equation:

$$r_1^{IS} = \frac{q[P_m]}{T_{1m}+\tau_m} \tag{1-11}$$

Where q is the number of bound water, P_m is the mole fraction of metal ion, τ_m is the mean residence/exchange time of the water in the ligand (Figure 1-2), T_{1m} is the relaxation time of the bound water (bound relaxation time). In general, T_{1m} is always larger than τ_m, for a simple metal complex. Therefore, the inner relaxivity depends, mainly, on the T_{1m}. According to Solomon-Bloembergen-Morgan (SBM) equations,[6,7] T_{1m} can be expressed as:

$$\frac{1}{T_{1m}} = \frac{1}{T_1^{DD}} + \frac{1}{T_1^{SC}} \tag{1-12}$$

Where T_1^{DD} is the relaxation time from the dipole-dipole (DD) mechanism (through

space) and T_1^{SC} is the relaxation time from the scalar coupling (though bonds).[6] In Gd(III) (ion) complex, due to the water is separated from the Gd ion by two bonds (H-O; O--Gd), the T_1^{SC} is quite small and can be negligible.[7,8] The T_1^{DD} can be expressed as the equation:

$$\frac{1}{T_1^{DD}} = \frac{2}{15}\frac{{\gamma_H}^2 {g_e}^2 \mu_B^2 S(S+1)}{r_{MH}^6}\left[\frac{7\tau_{c2}}{1+\omega_S^2\tau_{c2}^2} + \frac{3\tau_{c1}}{1+\omega_H^2\tau_{c1}^2}\right] \quad (1\text{-}13)$$

Where r_{MH} is the metal ion to water hydrogen distance, γ_H is the proton gyromagnetic constant, g_e is the g factor of the electron, μ_B is the Bohr magneton, μ_0 is the vacuum permeability, and ω_S and ω_H are the Larmor frequencies of the electron and proton, respectively. τ_{ci} (τ_{c1} and τ_{c2}) is the correlation time of the magnetic fluctuation (overall correlation time), which is given in equation:

$$\frac{1}{\tau_{c1}} = \frac{1}{T_{1e}} + \frac{1}{\tau_m} + \frac{1}{\tau_R} \quad (1\text{-}14)$$

Where, $1/\boldsymbol{T_{1e}}$ is the **electronic relaxation time** (sometimes referred to as $\boldsymbol{\tau_S}$, see Figure 1-2) which is usually not taken into account, since its contribution to relaxivity is negligible at the magnetic field strengths that are typically used in the clinic (≥1.5 T).[5] As explained above, $\boldsymbol{\tau_m}$ is the **mean residence/exchange time of the water in the ligand**, while the term $\boldsymbol{\tau_R}$ is the **rotational correlation time** (or tumbling of the molecule, see Figure 1-2).

When the magnetic field is above 0.1 T, the "$7\tau_{c2}$" term of equation ((1-13) can be negligible.[5] Thus, and in turn equation (1-12) is reduced to:

$$\frac{1}{T_{1m}} = \frac{C}{r_{MH}^6}\frac{3\tau_{c1}}{1+\omega_H^2\tau_{c1}^2} \quad (1\text{-}15)$$

Where C is a constant.

The relaxivity from the inner sphere can be expressed by:

$$r_1^{IS} \approx \mathrm{q}P_m\frac{C}{r_{MH}^6}\frac{3\tau_{c1}}{1+\omega_H^2\tau_{c1}^2} \quad (1\text{-}16)$$

Here, we can see that the most important parameters influencing the relaxivity from the inner sphere are, the number of water molecules (q), metal-water hydrogen distance (r_{MH}) and then, through τ_{c1} term, the mean residence time of water (τ_m), and the rotational correlation time or tumbling of the molecule (τ_R). The metal-water hydrogen distance normally is around 3.05 Å for Gd-ligand, determined by proton electron-nuclear double resonance (^{1}H ENDOR).[9,10] As shown in equation (1-16), increasing the number of water molecules (q) should increase the inner-sphere relaxivity, but this may decrease the thermodynamic stability.[11] As commented, the mean residence/exchange time of water (τ_m) is normally smaller than T_{1m} for a small Gd(III) complex, so the influence obtained by tuning this parameter is limited. However, in general, a short residence/exchange time

of water molecules (fast exchange of water molecules) favors relaxivity, and, on the contrary, low exchange rates often limit the relaxivity. We can play more easily with the tumbling of the molecule (rotational correlation time, τ_R) to tune the relaxivity. In general, slow tumbling of the molecule (large size) favors an increase in relaxivity.

As above mentioned, there is also an outer-sphere relaxation that contributes to relaxivity. The very vicinity sphere is sometimes called second-sphere relaxation and can be described by equations (1-11) and (1-13), where the related parameters are denoted with a prime, *q*', *r*', etc.[7] It is difficult to use these equations since the number of water molecules and the distance are unknown. The outer-sphere relaxation itself is complex.

Although the inner and outer-sphere theories have been developed for paramagnetic systems based on metal ions such as Gd(III), they can be used for other paramagnetic systems such as organic radicals. The difference lies in the fact that the parameters that influence relaxivity must be adapted to the specific characteristics of the radicals. In fact, some theories has been proposed in the literature to explain the experimental relaxivity in aqueous solutions of molecular oxygen,[12] or in solutions of nitroxide free radicals in water[13,14] or other solvents.[15]

1.4 Different types of MRI contrast agents

According to the mechanism of action, contrast agents can be classified into four categories, 1) paramagnetic, 2) superparamagnetic, 3) chemical exchange saturation transfer (CEST) and 4) direct detection agents.[5]

Paramagnetic contrast agents are the most widely used and comprise a paramagnetic metal ion that contain unpaired electrons, such as Gd(III)-, Mn(II)- and Fe(III)-complexes. They increase the magnetic resonance signal around them. Among them, Gd(III) complexes are, by far, the most successful and used paramagnetic contrast agents in clinics. *Superparamagnetic* contrast agents are colloidal materials formed by iron oxide particles in suspension, approximately from 5 to 200 nm in diameter. In the presence of an external magnetic field, the total spin of the particle is much larger than the sum of the individual magnetic metal ion spins of the particle (leading to a superspin) which can induce a high relaxivity. Generically, these agents are also referred to as superparamagnetic iron oxide nanoparticles (SPION) and they are classified in three groups depending on the nanoparticles size (ultrasmall, small and micron-sized particles).

They decrease the magnetic resonance signal around them. *CEST contrast agents* are molecules that possess exchangeable protons (usually OH or NH) that resonate at a different chemical shift than the bulk water signal. The exchangeable protons of the CEST agent are saturated by a saturation pulse and their magnetization is transferred to the protons of the bulk water leading to a reduced intensity of the water signal (generating MRI contrast). These three last examples of types of contrast agents are agents not directly detected but their effect on the bulk water signal is clearly observed. *Direct detection agents* do not generate contrast but are directly detected and in general have little background signal. For example, nanoparticles containing perfluorocarbon emulsions, that provide huge amount of ^{19}F atoms, have been used for direct detection in ^{19}F MRI. Here, it is important to comment that another possible way to overcome the low sensitivity of nuclear magnetic resonance is by hyperpolarization processes, in particular by dynamic nuclear polarization (DNP) which results from transferring spin polarization from electrons to nuclei (usually ^{13}C or ^{15}N nuclei). For example, we can hyperpolarize [1-^{13}C] pyruvate for human applications.

According to their effect, contrast agents are divided into two principal classes: T_1 contrast agents and T_2 contrast agents. *T_1 contrast agents* (e.g., paramagnetic contrast agents such as Gd(III) complexes) are also referred to as positive contrast agents because give positive contrast (brightened) images by locally reducing the water ^{1}H longitudinal relaxation time (T_1). In fact, they increase $1/T_1$ and $1/T_2$ values by roughly similar amounts (they have r_2/r_1 ratios of 1-2) but are used to get T_1-weighted images since the percentage change in $1/T_1$ in tissue is much greater than in $1/T_2$. On the other hand, *T_2 contrast agents* (e.g., superparamagnetic iron oxide nanoparticles) are also referred to as negative contrast agents because they lead to negative contrast (darkened) images by locally decreasing the water ^{1}H transverse relaxation time (T_2). Although these contrast agent shortens T_1, the effect on T_2 is very large, i.e. they generally lead to a much larger increase in $1/T_2$ than in $1/T_1$ (they can have r_2/r_1 ratios higher than 10) and are used to get T_2-weighted scans.

As mentioned above, the most commonly used contrast agents in clinics so far are gadolinium-based contrast agents. They present high relaxivities due to the high spin of Gd(III) ion that contains 7 unpaired electrons in its 4f subshell (spin 7/2). Due to the high toxicity of Gd(III) ion, it is used forming complexes with various ligands. The ligand occupies eight of its coordination sites, and the left one can form transient bonding with water molecule. The ligands to chelate gadolinium(III) ion can be linear or macrocyclic, being the macrocyclic ligands more inert than the linear ones. The Gd-based contrast

agents approved for clinical use are listed in Figure 1-3 and consist of a nine-coordinate Gd(III) ion chelated by an octadentate polyaminocarboxylate ligand with a water coligand. The relaxivity values r_1 of Gd complexes are around 3 $mM^{-1}s^{-1}$ at 7 T. For example, in Gd-DTPA it is 3.2 $mM^{-1}s^{-1}$ and in Gd-DOTA it is 2.8 $mM^{-1}s^{-1}$ (rt, 7 T).[16]

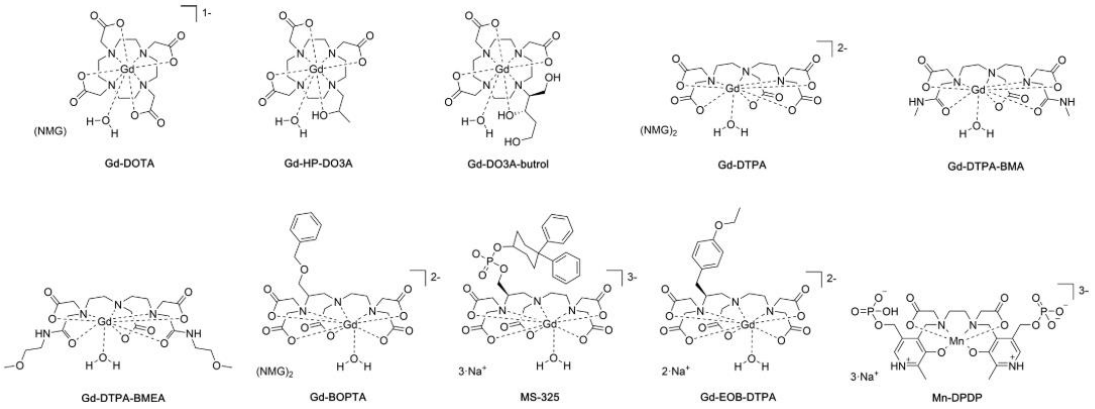

Figure 1-3. Commercially approved T_1 contrast agents.[5]

These Gd-based contrast agents have historically been considered as safe. However, despite the wide use of Gd-based contrast agents in clinical diagnosis due to their high relaxivity, there have been increasing concerns about their safety. First, in 2006, nephrogenic systemic fibrosis (NSF) was identified in patients who have impaired kidneys, which was directly related with exposure to gadolinium ion.[17] In addition, the accumulation of residual toxic Gd(III) ions in the brain and bones of patients with normal renal function has also been reported.[18,19] Based on these facts, some Gd-based contrast agents are being banned and gradually phased out from the market in several countries, like Magnevist® while others directly are no longer commercially available.

Other metal-based contrast agents like manganese-based contrast agents and iron-based contrast agents have also shown toxicity problems related to the metal. For instance, the deposition of Mn(II) in the brain of mice up to 1 month after injection of manganese-based CAs[20] was reported. It is described that the overexposure to Mn(II) can lead to a neurodegenerative disorder.[21] Regarding the iron oxide based contrast agents, they might cause more serious adverse effect than Gd-based CAs. For instance, one of the iron oxide-based contrast agents, ferumoxytol, has been related to the risk of suffer a potentially life-threatening allergy.[22] It has also been reported that the deposition of iron can cause organ dysfunction and lead to the development of chronic diseases such as diabetes, cirrhosis, and heart disease.[23] Overall, all metal-containing CAs, especially those integrating gadolinium, manganese and iron oxide present adverse effects on human health and

safety, principally because of the metals themselves.[24]

The safety concerns of Gd and other metal-based contrast agents are becoming a real safety problem. Since the use of CAs in MRI is of vital importance to gain lifesaving clinical information, it is critical to find alternative imaging probes that possess similar or even better paramagnetic properties than Gd-based contrast agents but lower toxicity.

1.5 MRI contrast agents based on organic radicals

Contrast agents based on organic radicals can be an attractive option as alternative MRI contrast agents since they are organic species free of metals that take advantage of the paramagnetism of the unpaired electron of the organic radicals which can shorten the T_1 relaxation time of water, like Gd-based CA. Especially, with the development of polymer chemistry, more and more attention is paid to these metal-free MRI contrast agents.

1.5.1 Organic radicals

The most commonly used organic radicals for MRI contrast agents are nitroxides (or nitroxyl radicals). Nitroxides contain an unpaired electron located mainly between the oxygen and nitrogen atoms of the N-O$^{\bullet}$ group, the position of which can vary depending on the environment, such as the polarity.[25] The most common nitroxides are five- or six-membered heterocyclic derivatives of pyrrolidine, oxazolidine, imidazolidine, piperidine or isoindoline, among others (Figure 1-4). In these structures, the four adjacent methyl groups protect the radical from reduction or other chemical processes in certain conditions. The most known nitroxides are 2,2,6,6-tetramethylpiperidin-1-oxyl (TEMPO) and 2,2,5,5-tetramethylpyrrolidin-1-oxyl (PROXYL) radicals.

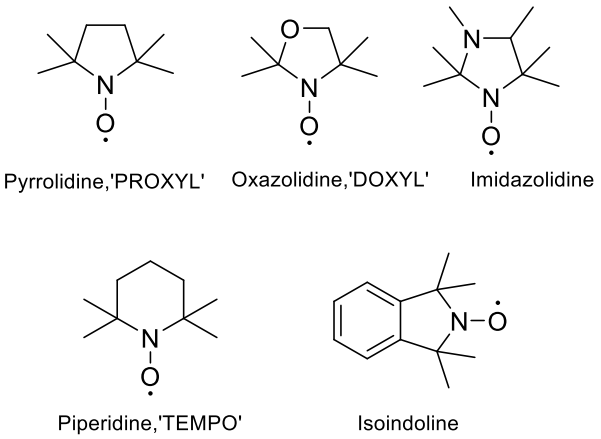

Figure 1-4. Chemical structures of some nitroxides (or nitroxyl radicals).

Based on the special structure, nitroxides have unique chemical reactivity. In general, these compounds are chemical inert, but the reactivity can increase with increasing temperature, which is used in chemical synthesis and polymerization. Nitroxyl free radicals can be reduced or oxidized to form hydroxylamine or oxoammonium cation, respectively (Scheme 1-1). The reduction of nitroxides to the corresponding hydroxylamine can be performed with mild reducing agents such as ascorbic acid, phenylhydrazine, hydrazobenzene, thiols, etc. while oxidizing agents for the oxidation of nitroxides can be chlorine, bromine, nitrogen dioxide, *m*-chloroperbenzoic acid, etc.[26] The formed hydroxylamine or oxoammonium products can produce reversibly nitroxide radicals again under proper conditions.

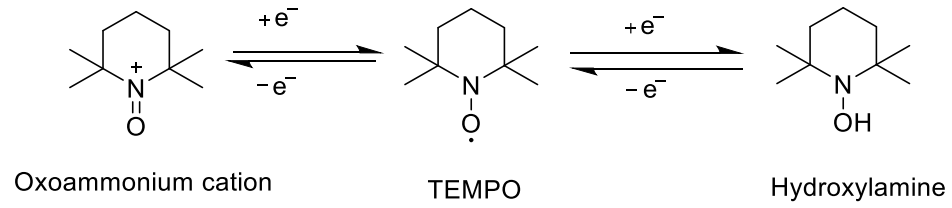

Scheme 1-1. Redox reactions of TEMPO radical.

Traditional spectroscopic methods such as UV-Vis and IR as well as X-ray diffraction can be used to characterize nitroxides but the most important characterization technique for organic radicals is the electron paramagnetic resonance (EPR). The characteristic IR absorption band of the N-O• bond is located at the range from 1340 to 1380 cm^{-1}, depending on the type of nitroxide. They show two characteristic absorption bands in the UV-Vis spectra: a very intense band at around 240 nm and another around 410-460 nm which is very weak. The maximum of the absorption bands in UV-Vis can be shifted by changing the polarity of the environment or by conjugation of the structure.

X-ray diffraction showed that the length of the N-O• bond is in the range of 1.23-1.29 Å, which is an intermediate value between the NO single bond and the NO double bond. On the other hand, if we reduce nitroxyl radicals to their corresponding diamagnetic hydroxylamine species they can be also characterized by ^{1}H NMR. Some commonly used reducing agents include ascorbic acid, sodium dithionite[27] or phenylhydrazine.[28]

As mentioned, an important method to characterize organic radicals is electron paramagnetic resonance. EPR describes the interaction between the unpaired electron/s of the radical and the applied magnetic field, and it gives a characteristic *g*-factor for each kind of radical species. In the case of organic radicals their *g*-factor differs little from the *g*-value of the free electron, 2.0023. The basic concepts of EPR spectroscopy are analogous to those of NMR, but it is the electron spins that are excited instead of the nuclear atomic spins. In the absence of other interactions, there is only one single line in the EPR spectrum. However, when the unpaired electron interacts with other atoms of the molecule with nuclear spin $I \neq 0$, the hyperfine interaction (*a*) causes a split of the signal depending on the nuclear spin and the number of atoms with which it interacts, providing important structural information. For example, in nitroxides, the presence of a nitrogen atom (^{14}N; I = 1) in the zone of maximum spin density of the unpaired electron in the N-O• group is responsible for the characteristic spectrum of these types of radicals, showing a three-line EPR spectrum with the same relative intensity (1:1:1). See more detailed information about EPR in the corresponding EPR Appendix C.

Nitroxides have been extensively investigated in many fields, including nitroxide-mediated polymerization,[29] fluorophore-nitroxide probes,[30] dynamic nuclear polarization (DNP) agents[31] or as organic radical batteries,[32] among others. In biomedical applications, nitroxides have been used as anticancer[33] and antioxidants[34] drugs. Also, it is worth mentioning that nitroxides are prominent spin probes for obtaining structural information of membrane proteins since their microenvironment sensitivity to pH, local dynamics, temperature or viscosity can be reflected by EPR.[25]

1.5.2 Organic radical contrast agents

Nitroxide radicals, and in particular those derived from TEMPO and PROXYL radicals, have been investigated as MRI contrast agents since the 1980s[35] because of their paramagnetic properties, showing similar mechanism of relaxation than Gd-based contrast agents. Nitroxides have important advantages such as low toxicity or easy

elimination from the body. However, they have only one unpaired electron (spin ½), while gadolinium, manganese and iron ions have 7, 5, and 5 unpaired electrons in their 4f, 3d and 3d orbitals, respectively, which makes organic radicals have much lower relaxivities compared with metal-based contrast agents. In addition, the susceptibility of nitroxides to be reduced to diamagnetic hydroxylamine in the body (by ascorbate (vitamin C), glutathione, etc.) is another obstacle for their advancement as MRI contrast agents. Due to these two main drawbacks, i.e. their inherent low paramagnetic relaxivity and rapid bioreduction, the widespread application of nitroxides as MRI CAs has been rather limited at the beginning.

It has been proved that the reduction of radicals is related to their structure. In general, the reduction of piperidine-based systems (TEMPO radicals) is slightly faster than pyrrolidine-based ones (PROXYL radicals) as well as faster for positively charged systems than for negatively charged ones.[36] The stability of nitroxides can be enhanced by replacing the adjacent methyl groups of N-O• by more bulky groups like ethyl or cyclohexyl groups (see Figure 1-5).[37–39] Also, their biostability can be improved by including the radical into host molecules, such as β-cyclodextrin[40] or RNA.[41]

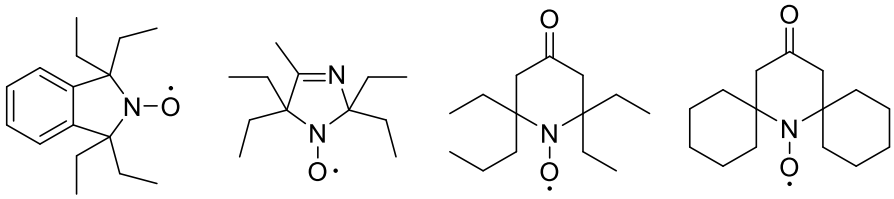

Figure 1-5. Sterically hindered nitroxides with improved resistance to bioreduction.

Since nitroxide radicals present a similar relaxivity mechanism than the paramagnetic metal-based contrast agents, the relaxivity can be improved by anchoring them to big rigid scaffolds. In this way, the rotational correlation time (τ_R) can be slower, increasing the relaxivity. In addition, at the same time, by this way the stability of nitroxides can also be improved (by a protective shield effect offered by the scaffolds). For this reason, numerous efforts have been made to anchor or encapsulate nitroxides into cyclodextrin,[42] chitosan,[43] albumin,[44] carbon nanotubes,[45] virus,[46] polymers,[47–51] etc. The chemical versatility of nitroxides enables the combination of the free radical with macromolecules or other matrix compounds.

The conjunction of nitroxides to polymers not only increases the relaxivity and stability but also provides more opportunities to encapsulate fluorophore, drugs, target

ligands. In this regard, Jeremiah A. Johnson's group prepared nitroxide-loaded macromolecules with also near-infrared fluorophores. They reported nitroxide-functionalized brush-arm star polymer (BASP-ORCA, Figure 1-6) composed by a dense layer of nitroxides at the interface between a rigid poly(acetal) core and a hydrophilic PEG shell. Such structure showed very high per-nitroxide transverse relaxivity, from ~17 to ~44-fold greater than common nitroxides, and good stability[47]. When they increased the nitroxide payload, the corresponding structure showed higher relaxivity than the first one, because more nitroxides were included in the macromolecule,[48] Such enhancement of relaxivity allowed detecting millimetric tumor implant in a murine model.

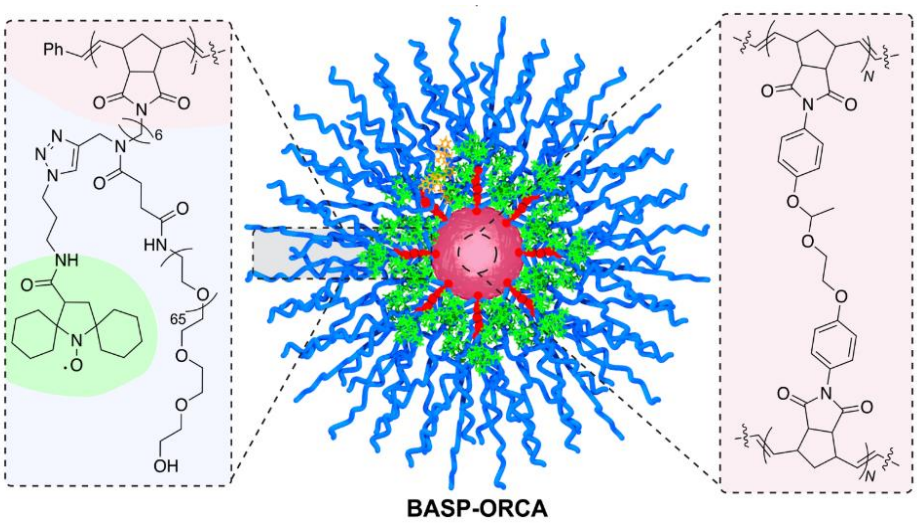

Figure 1-6. Structure of nitroxide loaded brush-arm star polymers (BASP-ORCA).

In this part, we have seen that nitroxide inclusion strategies in bulky scaffolds can be used to prepare high relaxivity contrast agents, especially by anchoring nitroxides to a polymeric scaffold. However, the polydisperse structure of the traditional polymers can be problematic in calculating relaxivity, leading to inaccurate values and unsatisfactory reproducibility. For this reason, we propose to use dendrimers as scaffolds for organic radicals (which differs from polymers by the strict control over their structure, making them nearly perfect monodisperse macromolecules) as metal-free MRI contrast agents in this Thesis.

1.5.3 Radical dendrimers as contrast agents

The strategy of our group to overcome the two main drawbacks of organic radicals

is through the incorporation of many nitroxide units to a dendrimer scaffold, i.e. radical dendrimers. In this way, we can achieve higher molecular relaxivity since the relatively low relaxivity per nitroxide is multiplied by the number of bounded nitroxides and a protective shield effect can be provided to the radicals, by restricting the fast access of reducing agents in such dendrimeric structures.

Dendrimers are monodisperse well defined macromolecules that usually have a globular appearance due to its regular and symmetrical structure. They provide a wide range of unusual properties both physical and chemical due to its symmetry, the presence of internal cavities and the number and variety of functional groups capable of being anchored at the end of their branches. They are constituted by three different domains (Figure 1-7): a *central core* which is either a single atom or an atomic group having at least two identical functional groups, *branches* emerging from the core, constituted of repetitive units having at least one branch junction, whose repetition is organized in a spherical progression called "generations" and *terminal functional groups*, located at the exterior of the dendrimers, which play an important role in their properties.

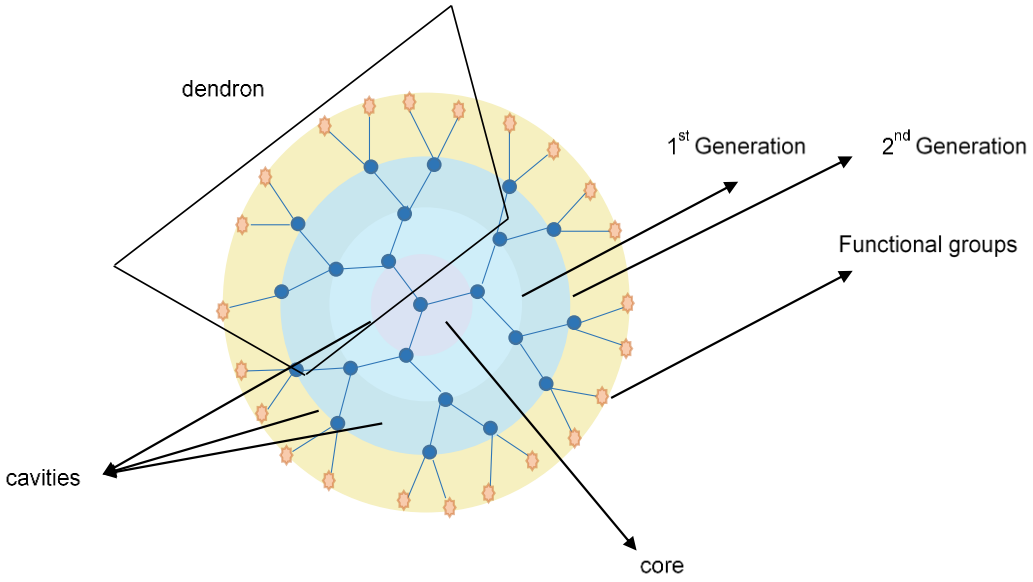

Figure 1-7. Schematic representation of a second generation dendrimer with functional groups on its surface.

There are two main methods for the synthesis of dendrimers.[52] The divergent method (Figure 1-8 a) builds up the dendrimer from a multifunctional core, which extends outward through a series of reactions.[53] By contrast, the convergent method (Figure 1-8 b), in which the dendrimers are built from smaller molecules (dendrons) which, as a final

step, react with a multifunctional core in order to generate the corresponding dendrimer generation of the dendron.[54] Each method has advantages and disadvantages: Dendrimers constructed by the convergent method are easier to purify than those synthesized by the divergent method. However, the size of dendrimers built by the convergent approach is smaller due to the steric effect of the dendron size in the final coupling with the core.

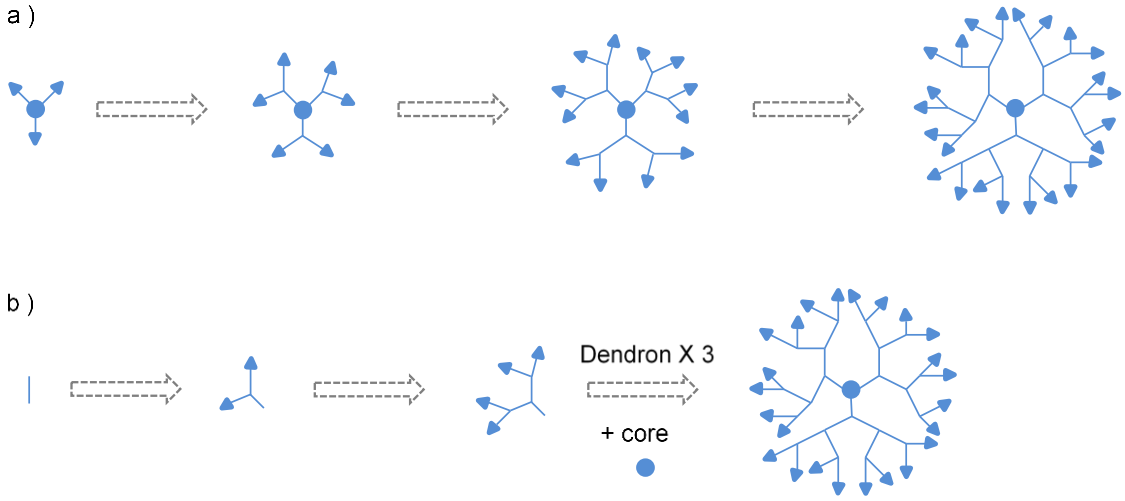

Figure 1-8. Scheme for a) the divergent method for dendrimer growth, b) convergent process for dendrimer synthesis.

The first dendrimer was synthesized by Vögtle[55] and co-workers by the divergent method, in 1978. Then, Tomalia's poly(amidoamine) (PAMAM)[53,56] and Newkome's "arborol" dendrimers[57] received numerous attention and have been thoroughly investigated. Both of these two dendrimeric structures were prepared in a divergent way. PAMAM dendrimer was synthehsized by a Michael addition followed by amidation. Later on, Fréchet et al. synthesized aromatic poly(ether) dendrimers in a convergent way.[58] Researchers have been working on developing many kinds of dendrimers with different atomic cores such as silicon[59] or germanium[60] atom cores. The synthesis of silicon containing dendrimers is mainly carried out by divergent methods. For instance, carbosilane dendrimers are synthesized in very good yields by using alternate alkenylation with Grignard reagents and hydrosilylation.[61] The synthesis of organogermanium dendrimers can be carried out both by divergent and convergent methods.[60] Other examples are cores based on phosphorous built by a nucleophilic substitution of chlorine leading phosphodiester compounds followed by an hydrazone bond,[62] or organic cores such as aromatic rings[63] or amines.[64]

The well-defined structures of dendrimers lay the foundation for wide application in

biomedicine.[65] The interior cavities can be used to encapsulate small drug molecules or genes. The functional groups on the periphery can be modified to improve the water solubility or antiviral ability, for example. The size of the dendrimers can be easily adjusted by changing the different dendrimer generations. When it comes to contrast agents, the precise number of functional groups and the controllable molecular size make dendrimers a suitable candidate scaffold to anchor small molecules to prepare contrast agents.

There have been some reports about MRI contrast agents based on dendrimers.[66] Most of them reported the use of dendrimers as scaffolds to anchor ligands that can be used to stabilize gadolinium ions. One of the most representative example is Gadomer-17.[67] This kind of MRI contrast agents was prepared by anchoring 24 macrocyclic Gd(III)-complexes to a 17 kDa dendrimer, which is under clinical trial. By anchoring the small gadolinium contrast agents to dendrimers, the relaxivity can be apparently enhanced, because of the slow rotation movement of the big molecules.

Radical dendrimers as contrast agents for MRI can provide some advantages: i) first, the stability of radicals can be improved by the protection offered by bulky segments around them, ii) the relaxivity can be increased not only by multiplying by the number of radicals in the macromolecule but also iii) decreasing the rotational correlation time. Moreover, iv) the pharmacokinetic profiles can be improved by controlling the size of the dendrimers (through different generations) which affects their circulation time and biodistribution in the body. The v) versatility of dendrimers chemistry allows us to tune the structural design of these agents to obtain the desired properties like water solubility and their versatile functionalization allows to achieve various functions, such as targeting ability, drug conjunction or multimodal imaging agents.

The first time the term "radical dendrimers" was used was in one of the first publications on dendrimers of the group,[68] in which the synthesis and characterization of a family of polyphosphorhydrazone(PPH)-based dendrimers fully functionalized with organic radicals was described for the first time. Our group synthesized a 5-generation family of PPH-based radical dendrimers with TEMPO as radical end groups (Scheme 1-2) and a comprehensive characterization by EPR, SQUID, ^{1}H NMR, ^{31}P NMR, FT-IR and UV-Vis spectroscopy was carried out.

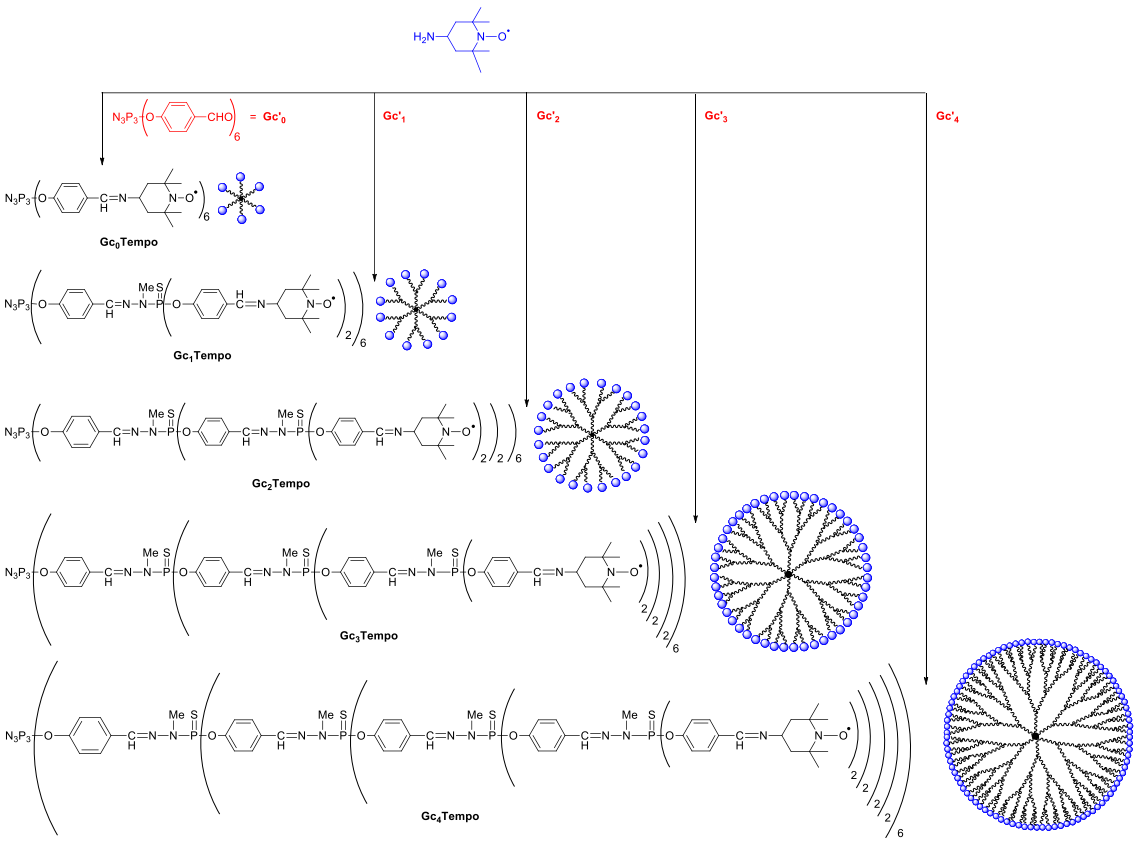

Scheme 1-2. Synthesis of five generations of PPH based radical dendrimers (labeled Gc0-Gc4Tempo), with 6, 12, 24, 48 and 96 TEMPO radical units, respectively, at the periphery. Published by Macromolecules, 2014 [68].

Although some few examples were reported in the past, it is in our group where a systematic work of synthesis and characterization of radical dendrimers has been developed for the first time.[68–75] It is important to highlight that the chemical versatility that dendrimers and radical dendrimers offer allows us to tune the system by playing with the kind of dendrimer, its branches, the radical used, and the linker connecting the radical to the dendrimer. In this way, we can modify the properties of the radical dendrimers at will, opening the perspective of creating a system with optimized properties to fulfill the requests of each application. For example, we can use water solubilizing linkers to obtain water-soluble systems.[73] Other example is the possibility to tune the intramolecular interaction between radicals by using different linkers. For example, we synthesized two generations of PPH-based radical dendrimers with two different linkers, imino and acrylamido ones.[71] With the imino linker the radicals presented a strong intramolecular interaction among radicals while in the radical dendrimers with the acrylamido linkers, they acted mainly as independent radicals, without showing signs of interaction. The control over the interactions between radicals opens the perspective to tune them as

needed in many applications, such as dynamic nuclear polarization (DNP), MRI, organic electronics, or organic batteries.[32] On the other hand, if we change the type of radical–for instance, using perchlorotriphenylmethyl (PTM) radicals–we can take advantage of their redox properties, for example in the design of different devices such as molecular switches. In this regard, three generations of polyphosphorhydrazone dendrimers, fully functionalized with 6, 12, and 24 PTM radicals in the periphery, were capable of undergoing electrochemical reversible switching by multi-electron reduction and oxidation. An electrical input was used to trigger the physical properties of these radical dendrimers in a reversible way, modifying their optical, magnetic, and electronic properties.[72]

Only few reports based on dendrimers fully functionalized with organic radicals have been reported previously.[76–83] Some of them were based only on a cyclotriphosphazene ring as scaffold for the radicals and others were based, mainly, on PAMAM and PPI dendrimers, to study principally their magnetic, structural or electrochemical properties. Only few of them studied their relaxivity properties.[78–80] Recently, radical dendrimers have also been used for their anti-oxidant or anti-tumor properties in TEMPO-terminated polyurethane dendrimers.[84,85]

In the first works described in the past regarding relaxivity studies,[78,80] PAMAM and poly(propylene imine) (PPI) dendrimers were functionalized with PROXYL radical units, or nitronyl nitroxides radicals resulting in high paramagnetic systems. The dendrimers were fully functionalized with up to 32 PROXYL radicals per macromolecule and the relaxivities per molecule obtained significantly increased, up to r_1 ca. 5 $mM^{-1}s^{-1}$ at 1.5 T, compared to those of the monomeric nitroxide with a single spin (0.18 $mM^{-1}s^{-1}$). However, in the highest generation, the relaxivity per nitroxide unit was lower than the free radical[86]. When PAMAM dendrimers (G0-NH_2 to G4-NH_2) were fully functionalized with nitronyl nitroxide (NIT) radicals, the relaxivity per radical unit obtained in G2-NIT and G3-NIT was about half of the value for the monomeric free radical in solution.[80] The authors pointed out aggregation problems in water phase of such nitroxide-based dendrimers for their limited water solubility. Thus, in these two previous reported works, the relaxivity per radical unit decreased in higher generations, which can be explained by the aggregation problems promoted by the lower water solubility of larger generations, which makes radical units inaccessible by water molecules.

In fact, the hydrophobicity of the surface of nitroxide-covered dendrimers may

contribute to their limited applications in MRI. Water solubility of radical dendrimers is an essential property for their *in vivo* applications but is usually an issue difficult to solve, especially in large generation dendrimers. A common strategy used to overcome the lack of water solubility in organic systems is by including water-solubilizing groups such as poly(ethylene glycol) (PEG) chains, like Rajca[87] and Katayama[88] and co-workers did, respectively, on the surface of the dendrimer. However, in this way, the number of nitroxides anchored on the surface is not the maximum possible one since not all the branches are free to be spin labeled and hence the molecular relaxivity should be lower than with fully nitroxide covered surface. In addition, the number of radical units anchored is not well controlled but only statistically known. Rajca and co-workers introduced PEG chains into spirocyclohexyl nitroxides-based PPI dendrimers resulting in a relaxivity per molecule of r_1 ca. 5 $mM^{-1}s^{-1}$ at 7 T in G4-PPI-PEG system with an average number of nitroxide units per macromolecule of ~13, which means a relaxivity per nitroxide unit of ca. 0.42 $mM^{-1}s^{-1}$.[89] The dendrimers showed much shorter rotational correlation time (τ_R) than the free nitroxide. However, although the dendrimer with the longest τ_R possessed the highest r_1, the relaxivity was only weakly dependent on τ_R. The authors pointed out long residence/exchange time of water molecules hydrogen-bonded to the nitroxide radicals as the most probable factor limiting the water r_1.

The relaxation mechanism in nitroxides is considered to be by dipole-dipole mechanism, between the radical and the molecules of water. In these cases, it is not taken into account the two spheres (inner and outer spheres) of relaxation like with Gd-based contrast agents but only one. However, the same parameters that influence the relaxivity are usually used and taken into account, with some differences. The electronic relaxation time T_{1e}, usually contributes very little to the global correlation time in nitroxides, like in Gd-based CA; the mean residence/exchange time (τ_m) of water molecules hydrogen-bonded to the nitroxide radical, and the rotational correlation time (τ_R) of the entire molecule. This last contribution usually has great impact on relaxivity, like in the Gd-based CA. However, in dendrimers it has to be taken into account not only the global rotational motion but also the local rotational motion, i.e. for example nitroxides can rotate through segmental motion faster than through rotation of the entire dendrimer, limiting in this case the relaxivity.

1.6 References

(1) James, M. L.; Gambhir, S. S. A Molecular Imaging Primer: Modalities, Imaging Agents, and Applications. *Physiol. Rev.* **2012**, *92* (2), 897–965.

(2) Zhao, J.; Chen, J.; Ma, S.; Liu, Q.; Huang, L.; Chen, X.; Lou, K.; Wang, W. Recent Developments in Multimodality Fluorescence Imaging Probes. *Acta Pharm. Sin. B* **2018**, *8* (3), 320–338.

(3) Bloch, F. Nuclear Induction. *Phys. Rev.* **1946**, *70* (7–8), 460.

(4) Martín, María Luisa García, and P. L. L. *Preclinical MRI: Methods and Protocols*; Springer: New York, 2018.

(5) Wahsner, J.; Gale, E. M.; Rodríguez-Rodríguez, A.; Caravan, P. Chemistry of MRI Contrast Agents: Current Challenges and New Frontiers. *Chem. Rev.* **2019**, *119* (2), 957–1057.

(6) Lauffer, R. B. Paramagnetic Metal Complexes as Water Proton Relaxation Agents for NMR Imaging: Theory and Design. *Chem. Rev.* **1987**, *87* (5), 901–927.

(7) Caravan, P.; Ellison, J. J.; McMurry, T. J.; Lauffer, R. B. Gadolinium(III) Chelates as MRI Contrast Agents: Structure, Dynamics, and Applications. *Chem. Rev.* **1999**, *99* (9), 2293–2352.

(8) Hao, D.; Ai, T.; Goerner, F.; Hu, X.; Runge, V. M.; Tweedle, M. MRI Contrast Agents: Basic Chemistry and Safety. *J. Magn. Reson. Imaging* **2012**, *36* (5), 1060–1071.

(9) Caravan, P.; Astashkin, A. V; Raitsimring, A. M. The Gadolinium(III)-Water Hydrogen Distance in MRI Contrast Agents. *Inorg. Chem.* **2003**, *42* (13), 3972–3974.

(10) Raitsimring, A. M.; Astashkin, A. V; Poluektov, O. G.; Caravan, P. Applied Magnetic Resollance High-Field Pulsed EPR and ENDOR of Gd 3+ Complexes in Glassy Solutions. *Appl. Magn. Reson* **2005**, *28*, 281–295.

(11) Polasek, M.; Caravan, P. Is Macrocycle a Synonym for Kinetic Inertness in Gd(III) Complexes? Effect of Coordinating and Noncoordinating Substituents on Inertness and Relaxivity of Gd(III) Chelates with DO3A-like Ligands. **2013**.

(12) Hausser, R.; Noack, F. Kernmagnetische Relaxation Und Korrelation Im System Wasser - Sauerstoff. *Zeitschrift fur Naturforsch. - Sect. A J. Phys. Sci.* **1965**, *20* (12), 1668–1675.

(13) Borah, B.; Bryant, R. G. NMR Relaxation Dispersion in an Aqueous Nitroxide System. *J. Chem. Phys.* **1981**, *75* (7), 3297–3300.

(14) Polnaszek, C. F.; Bryant, R. G. Nitroxide Radical Induced Solvent Proton Relaxation: Measurement of Localized Translational Diffusion. *J. Chem. Phys.* **1984**, *81* (9), 4038–4045.

(15) Nientiedt, H. W.; Bundfuss, K.; Müller-Warmuth, W. Frequency and Temperature Dependence of NMR Relaxation for Protic Solvents with Complexes of Nitroxide Radicals. *J. Magn. Reson.* **1981**, *43* (1), 154–166.

(16) Shen, Y.; Goerner, F. L.; Snyder, C.; Morelli, J. N.; Hao, D.; Hu, D.; Li, X.; Runge, V. M. T1 Relaxivities of Gadolinium-Based Magnetic Resonance Contrast Agents in Human Whole Blood at 1.5, 3, and 7 T. *Invest. Radiol.* **2015**, *50* (5), 330–338.

(17) Marckmann, P.; Skov, L.; Rossen, K.; Dupont, A.; Damholt, M. B.; Heaf, J. G.; Thomsen, H. S. Nephrogenic Systemic Fibrosis: Suspected Causative Role of Gadodiamide Used for Contrast-Enhanced Magnetic Resonance Imaging. *J. Am. Soc. Nephrol.* **2006**, *17* (9), 2359–2362.

(18) Zhang, Y.; Cao, Y.; Shih, G. L.; Hecht, E. M.; Prince, M. R. Extent of Signal Hyperintensity on Unenhanced T1-Weighted Brain MR Images after More than 35 Administrations of Linear Gadolinium-Based Contrast Agents. *Radiology* **2017**, *282* (2), 516–525.

(19) Kanda, T.; Osawa, M.; Oba, H.; Toyoda, K.; Kotoku, J.; Haruyama, T.; Takeshita, K.; Furui, S. High Signal Intensity in Dentate Nucleus on Unenhanced T1-Weighted MR Images: Association with Linear versus Macrocyclic Gadolinium Chelate Administration. *Radiology* **2015**, *275* (3), 803–809.

(20) Gallez, B.; Baudelet, C.; Adline, J.; Geurts, M.; Delzenne, N. Accumulation of Manganese in the Brain of Mice after Intravenous Injection of Manganese-Based Contrast Agents. *Chem. Res. Toxicol.* **1997**, *10* (4), 360–363.

(21) Pan, D.; Schmieder, A. H.; Wickline, S. A.; Lanza, G. M. Manganese-Based MRI Contrast Agents: Past, Present, and Future. *Tetrahedron* **2011**, *67* (44), 8431–8444.

(22) Anderson, M. A.; Harrington, S. G.; Kozak, B. M.; Gee, M. S. Strategies to Reduce the Use of Gadolinium-Based Contrast Agents for Abdominal MRI in Children. *Am. J. Roentgenol.* **2020**, *214* (5), 1054–1064.

(23) Kohgo, Y.; Ikuta, K.; Ohtake, T.; Torimoto, Y.; Kato, J. Body Iron Metabolism and Pathophysiology of Iron Overload. *Int. J. Hematol.* **2008**, *88* (1), 7–15.

(24) Akakuru, O. U.; Iqbal, M. Z.; Saeed, M.; Liu, C.; Paunesku, T.; Woloschak, G.; Hosmane, N. S.; Wu, A. The Transition from Metal-Based to Metal-Free Contrast Agents for T 1 Magnetic Resonance Imaging Enhancement . *Bioconjug. Chem.* **2019**, *30*, 2264–2286.

(25) Bordignon, E. EPR Spectroscopy of Nitroxide Spin Probes. *eMagRes* **2017**, *6* (2), 235–254.

(26) Breuer, E.; Aurich, H. U.; Nielsen, A.; Patai, S.; Rappoport, Z. *Nitrones, Nitronates and Nitroxides (1989)*; Breuer, E., Aurich, H. G., Nielsen, A., Eds.; John Wiley & Sons, Inc.: Chichester, UK, 1989.

(27) Ozinskas, A. J.; Bobst, A. M. Formation of N-Hydroxy-amines of Spin Labeled Nucleosides for 1H-NMR. Analysis. *Helv. Chim. Acta* **1980**, *63* (6),

1407–1411.

(28) Lee, T. D.; Keana, J. F. W. In Situ Reduction of Nitroxide Spin Labels with Phenylhydrazine in Deuteriochloroform Solution. A Convenient Method for Obtaining Structural Information on Nitroxides Using Nuclear Magnetic Resonance Spectroscopy. *J. Org. Chem.* **1975**, *40* (21), 3145–3147.

(29) Hawker, C. J.; Bosman, A. W.; Harth, E. New Polymer Synthesis by Nitroxide Mediated Living Radical Polymerizations. *Chem. Rev.* **2001**, *101* (12), 3661–3688.

(30) Hughes, B. K.; Braunecker, W. A.; Ferguson, A. J.; Kemper, T. W.; Larsen, R. E.; Gennett, T. Quenching of the Perylene Fluorophore by Stable Nitroxide Radical-Containing Macromolecules. *J. Phys. Chem. B* **2014**, *118* (43), 12541–12548.

(31) Pinto, L. F.; Marín-Montesinos, I.; Lloveras, V.; Muñoz-Gómez, J. L.; Pons, M.; Veciana, J.; Vidal-Gancedo, J. NMR Signal Enhancement of >50 000 Times in Fast Dissolution Dynamic Nuclear Polarization. *Chem. Commun.* **2017**, *53* (26), 3757–3760.

(32) Badetti, E.; Lloveras, V.; Amadio, E.; Di Lorenzo, R.; Olivares-Marín, M.; Tesio, A. Y.; Zhang, S.; Pan, F.; Rissanen, K.; Veciana, J.; Tonti, D.; Vidal-Gancedo, J.; Zonta, C.; Licini, G. Organic Polyradicals as Redox Mediators: Effect of Intramolecular Radical Interactions on Their Efficiency. *ACS Appl. Mater. Interfaces* **2020**, *12* (41), 45968.

(33) Hong, S. K.; Starenki, D.; Wu, P. K.; Park, J. I. Suppression of B-RafV600E Melanoma Cell Survival by Targeting Mitochondria Using Triphenyl-Phosphonium-Conjugated Nitroxide or Ubiquinone. *Cancer Biol. Ther.* **2017**, *18* (2), 106–114.

(34) Lewandowski, M.; Gwozdzinski, K. Nitroxides as Antioxidants and Anticancer Drugs. *Int. J. Mol. Sci.* **2017**, *18* (11).

(35) Brasch, R. C.; Nitecki, D. E.; Brant Zawadzki, M. Brain Nuclear Magnetic Resonance Imaging Enhanced by a Paramagnetic Nitroxide Contrast Agent: Preliminary Report. *Am. J. Neuroradiol.* **1983**, *4* (5), 1035–1039.

(36) Couet, W. R.; Brasch, R. C.; Sosnovsky, G.; Tozer, T. N. Factors Affecting Nitroxide Reduction in Ascorbate Solution and Tissue Homogenates. *Magn. Reson. Imaging* **1985**, *3* (1), 83–88.

(37) Marx, L.; Chiarelli, R.; Guiberteau, T.; Rassat, A. A Comparative Study of the Reduction by Ascorbate of 1,1,3,3-Tetraethylisoindolin-2-Yloxyl and of 1,1,3,3-Tetramethylisoindolin-2-Yloxyl. *J. Chem. Soc. Perkin Trans. 1* **2000**, No. 8, 1181–1182.

(38) Kirilyuk, I. A.; Bobko, A. A.; Grigor'ev, I. A.; Khramtsov, V. V. Synthesis of the Tetraethyl Substituted PH-Sensitive Nitroxides of Imidazole Series with Enhanced Stability towards Reduction. *Org. Biomol. Chem.* **2004**, *2* (7), 1025–1030.

(39) Okazaki, S.; Mannan, M. A.; Sawai, K.; Masumizu, T.; Miura, Y.; Takeshita, K. Enzymatic Reduction-Resistant Nitroxyl Spin Probes with

Spirocyclohexyl Rings. *Free Radic. Res.* **2007**, *41* (10), 1069–1077.

(40) Franchi, P.; Fanì, M.; Mezzina, E.; Lucarini, M. Increasing the Persistency of Stable Free-Radicals: Synthesis and Characterization of a Nitroxide Based [1]Rotaxane. *Org. Lett.* **2008**, *10* (10), 1901–1904.

(41) Saha, S.; Jagtap, A. P.; Th Sigurdsson, S. Site-Directed Spin Labeling of 2 0-Amino Groups in RNA with Isoindoline Nitroxides That Are Resistant to Reduction †. *Chem. Commun* **2015**, *51*, 13142.

(42) Caglieris, F.; Melone, L.; Canepa, F.; Lamura, G.; Castiglione, F.; Ferro, M.; Malpezzi, L.; Mele, A.; Punta, C.; Franchi, P.; Lucarini, M.; Rossi, B.; Trotta, F. Effective Magnetic Moment in Cyclodextrin-Polynitroxides: Potential Supramolecular Vectors for Magnetic Resonance Imaging. *RSC Adv.* **2015**, *5* (93), 76133–76140.

(43) Akakuru, O. U.; Iqbal, M. Z.; Liu, C.; Xing, J.; Wei, Z.; Jiang, Z.; Fang, Q.; Yuan, B.; Nosike, E. I.; Xia, J.; Jin, Y.; Zheng, J.; Wu, A. Self-Assembled, Biocompatible and Biodegradable TEMPO-Conjugated Nanoparticles Enable Folate-Targeted Tumor Magnetic Resonance Imaging. *Appl. Mater. Today* **2020**, *18*, 100524.

(44) Chan, H. C.; Sun, K.; Magin, R. L.; Swartz, H. M. Potential of Albumin Labeled with Nitroxides as a Contrast Agent for Magnetic Resonance Imaging and Spectroscopy. *Bioconjug. Chem.* **1990**, *1* (1), 32–36.

(45) Rivera, E. J.; Sethi, R.; Qu, F.; Krishnamurthy, R.; Muthupillai, R.; Alford, M.; Swanson, M. A.; Eaton, S. S.; Eaton, G. R.; Wilson, L. J. Nitroxide Radicals@US-Tubes: New Spin Labels for Biomedical Applications. *Adv. Funct. Mater.* **2012**, *22* (17), 3691–3698.

(46) Dharmarwardana, M.; Martins, A. F.; Chen, Z.; Palacios, P. M.; Nowak, C. M.; Welch, R. P.; Li, S.; Luzuriaga, M. A.; Bleris, L.; Pierce, B. S.; Sherry, A. D.; Gassensmith, J. J. Nitroxyl Modified Tobacco Mosaic Virus as a Metal-Free High-Relaxivity MRI and EPR Active Superoxide Sensor. *Mol. Pharm.* **2018**.

(47) Nguyen, H. V. T.; Chen, Q.; Paletta, J. T.; Harvey, P.; Jiang, Y.; Zhang, H.; Boska, M. D.; Ottaviani, M. F.; Jasanoff, A.; Rajca, A.; Johnson, J. A. Nitroxide-Based Macromolecular Contrast Agents with Unprecedented Transverse Relaxivity and Stability for Magnetic Resonance Imaging of Tumors. *ACS Cent. Sci.* **2017**, *3* (7), 800–811.

(48) Nguyen, H. V. T.; Detappe, A.; Gallagher, N. M.; Zhang, H.; Harvey, P.; Yan, C.; Mathieu, C.; Golder, M. R.; Jiang, Y.; Ottaviani, M. F.; Jasanoff, A.; Rajca, A.; Ghobrial, I.; Ghoroghchian, P. P.; Johnson, J. A. Triply Loaded Nitroxide Brush-Arm Star Polymers Enable Metal-Free Millimetric Tumor Detection by Magnetic Resonance Imaging. *ACS Nano* **2018**, *12* (11), 11343–11354.

(49) Garmendia, S.; Mantione, D.; Alonso-De Castro, S.; Jehanno, C.; Lezama, L.; Hedrick, J. L.; Mecerreyes, D.; Salassa, L.; Sardon, H. Polyurethane Based Organic Macromolecular Contrast Agents (PU-ORCAs) for Magnetic Resonance Imaging. *Polym. Chem.* **2017**, *8* (17), 2693–2701.

(50) Chan, J. M. W.; Wojtecki, R. J.; Sardon, H.; Lee, A. L. Z.; Smith, C. E.; Shkumatov, A.; Gao, S.; Kong, H.; Yang, Y. Y.; Hedrick, J. L. Self-Assembled, Biodegradable Magnetic Resonance Imaging Agents: Organic Radical-Functionalized Diblock Copolymers. *ACS Macro Lett.* **2017**, *6* (2), 176–180.

(51) Guo, S.; Wang, X.; Dai, Y.; Dai, X.; Li, Z.; Luo, Q.; Zheng, X.; Gu, Z.; Zhang, H.; Gong, Q.; Luo, K. Enhancing the Efficacy of Metal-Free MRI Contrast Agents via Conjugating Nitroxides onto PEGylated Cross-Linked Poly(Carboxylate Ester). *Adv. Sci.* **2020**, *7* (14).

(52) Touzani, R. Dendrons, Dendrimers New Materials for Environmental and Science Applications. *J. Mater. Environ. Sci.* **2011**, *2* (3), 201–214.

(53) Tomalia, D. A.; Baker, H.; Dewald, J.; Hall, M.; Kallos, G.; Martin, S.; Roeck, J.; Ryder, J.; Smith, P. A New Class of Polymers: Starburst-Dendritic Macromolecules. *Polym. J.* **1985**, *17* (I), 117–132.

(54) Hawker, C. J.; Frechet, J. M. J. Preparation of Polymers with Controlled Molecular Architecture. A New Convergent Approach to Dendritic Macromolecules. *J. Am. Chem. Soc.* **1990**, *112* (21), 7638–7647.

(55) BUHLEIER E; WEHNER W; VOEGTLE F. " CASCADE"-AND" NONSKID-CHAIN-LIKE" SYNTHESES OF MOLECULAR CAVITY TOPOLOGIES. *Synthesis (Stuttg).* **1978**, *2*, 155–158.

(56) Tomalia, D. A.; Baker, H.; Dewald, J.; Hall, M.; Kallos, G.; Martin, S.; Roeck, J.; Ryder, J.; Smith, P. Dendritic Macromolecules: Synthesis of Starburst Dendrimers. *Macromolecules* **1986**, *19* (9), 2466–2468.

(57) Newkome, G. R.; Yao, Z.; Baker, G. R.; Gupta, V. K. Micelles. Part 1. Cascade Molecules: A New Approach to Micelles. A [27]-Arborol. *J. Org. Chem.* **1985**, *50* (11), 2003–2004.

(58) Hawker, C.; Fréchet, J. M. J. A New Convergent Approach to Monodisperse Dendritic Macromolecules. *J. Chem. Soc. Chem. Commun.* **1990**, *15*, 1010–1013.

(59) Rebrov, E. Space-Network Polyorganosiloxanes. In *Dokl. Akad. Nauk SSSR*; **1989**; Vol. 309, pp 376–380.

(60) Huc, V.; Boussaguet, P.; Mazerolles, P. Organogermanium Dendrimers. *J. Organomet. Chem.* **1996**, *521* (1–2), 253–260.

(61) Muzafarov, A. M.; Gorbatsevich, O. B.; Rebrov, E. A. Ignat'eva, GM, Chenskaya, TB. *Myakushev, VD, Bulkin, AF, Papkov, VS., Polym. Sci. Ser. A* **1993**, *35* (11), 1575.

(62) Launay, N.; Caminade, A. -M; Lahana, R.; Majoral, J. -P. A General Synthetic Strategy for Neutral Phosphorus-Containing Dendrimers. *Angew. Chemie Int. Ed. English* **1994**, *33* (15–16), 1589–1592.

(63) Archut, A.; Issberner, J.; Vögtle, F. Dendrimers, Arborols, and Cascade Molecules: Breakthrough into Generations of New Materials. *Org. Synth.*

Highlights III **2008**, *6*, 391–405.

(64) Tomalia, D. A.; Naylor, A. M.; Goddard, W. A. Starburst Dendrimers: Molecular-Level Control of Size, Shape, Surface Chemistry, Topology, and Flexibility from Atoms to Macroscopic Matter. *Angew. Chemie Int. Ed. English* **1990**, *29* (2), 138–175.

(65) Pedziwiatr-Werbicka, E.; Milowska, K.; Dzmitruk, V.; Ionov, M.; Shcharbin, D.; Bryszewska, M. Dendrimers and Hyperbranched Structures for Biomedical Applications. *Eur. Polym. J.* **2019**, *119* (July), 61–73.

(66) Floyd, W. C.; Klemm, P. J.; Smiles, D. E.; Kohlgruber, A. C.; Pierre, V. C.; Mynar, J. L.; Fréchet, J. M. J.; Raymond, K. N. Conjugation Effects of Various Linkers on Gd(III) MRI Contrast Agents with Dendrimers: Optimizing the Hydroxypyridinonate (HOPO) Ligands with Nontoxic, Degradable Esteramide (EA) Dendrimers for High Relaxivity. *J. Am. Chem. Soc.* **2011**, *133* (8), 2390–2393.

(67) Jaspers, K.; Versluis, B.; Leiner, T.; Dijkstra, P.; Oostendorp, M.; van Golde, J. M.; Post, M. J.; Backes, W. H. MR Angiography of Collateral Arteries in a Hind Limb Ischemia Model: Comparison between Blood Pool Agent Gadomer and Small Contrast Agent Gd-DTPA. *PLoS One* **2011**, *6* (1), 2–7.

(68) Badetti, E.; Lloveras, V.; Muñoz-Gómez, J. L.; Sebastián, R. M.; Caminade, A. M.; Majoral, J. P.; Veciana, J.; Vidal-Gancedo, J. Radical Dendrimers: A Family of Five Generations of Phosphorus Dendrimers Functionalized with TEMPO Radicals. *Macromolecules* **2014**, *47* (22), 7717–7724.

(69) Badetti, E.; Lloveras, V.; Wurst, K.; Sebastián, R. M.; Caminade, A. M.; Majoral, J. P.; Veciana, J.; Vidal-Gancedo, J. Synthesis and Structural Characterization of a Dendrimer Model Compound Based on a Cyclotriphosphazene Core with TEMPO Radicals as Substituents. *Org. Lett.* **2013**, *15* (14), 3490–3493.

(70) Lloveras, V.; Badetti, E.; Wurst, K.; Vidal-gancedo, J. Synthesis , X-Ray Structure , Magnetic Properties , and a Study of Intra / Intermolecular Radical – Radical Interactions of a Triradical TEMPO Compound. *ChemPhysChem* **2015**, *16*, 3302–3307.

(71) Lloveras, V.; Liko, F.; Pinto, L. F.; Muñoz-Gómez, J. L.; Veciana, J.; Vidal-Gancedo, J. Tuning Spin-Spin Interactions in Radical Dendrimers. *ChemPhysChem* **2018**, *19* (15), 1895–1902.

(72) Lloveras, V.; Liko, F.; Muñoz-Gómez, J. L.; Veciana, J.; Vidal-Gancedo, J. Redox-Active PTM Radical Dendrimers as Promising Multifunctional Molecular Switches. *Chem. Mater.* **2019**, *31* (22), 9400–9412.

(73) Pinto, L. F.; Lloveras, V.; Zhang, S.; Liko, F.; Veciana, J.; Muñoz-Gómez, J. L.; Vidal-Gancedo, J. Fully Water-Soluble Polyphosphorhydrazone-Based Radical Dendrimers Functionalized with Tyr-PROXYL Radicals as Metal-Free MRI T1 Contrast Agents. *ACS Appl. Bio Mater.* **2020**, *3* (1), 369–376.

(74) Zhang, S.; Lloveras, V.; Pulido, D.; Liko, F.; Pinto, L. F.; Albericio, F.; Royo, M.; Vidal-Gancedo, J. Radical Dendrimers Based on

Biocompatible Oligoethylene Glycol Dendrimers as Contrast Agents for MRI. *Pharmaceutics* **2020**, *12* (8), 1–15.

(75) Lloveras, V.; Vidal-Gancedo, J. Polyphosphorhydrazone-Based Radical Dendrimers. *Molecules* **2021**, *26* (5), 1230.

(76) Bosman, A. W.; Janssen, R. A. J.; Meijer, E. W. Five Generations of Nitroxyl-Functionalized Dendrimers. *Macromolecules* **1997**, *30* (12), 3606–3611.

(77) Kashiwagi, Y.; Kurashima, F.; Kikuchi, C.; Anzai, J. I.; Osa, T. Voltammetric Behavior of Poly(Amidoamine) Dendrimers Containing Nitroxyl Radical End Groups. *Electrochem. commun.* **1999**, *1* (8), 305–308.

(78) Winalski, C. S.; Shortkroff, S.; Mulkern, R. V.; Schneider, E.; Rosen, G. M. Magnetic Resonance Relaxivity of Dendrimer-Linked Nitroxides. *Magn. Reson. Med.* **2002**, *48* (6), 965–972.

(79) Maliakal, A. J.; Turro, N. J.; Bosman, A. W.; Cornel, J.; Meijer, E. W. Relaxivity Studies on Dinitroxide and Polynitroxyl Functionalized Dendrimers: Effect of Electron Exchange and Structure on Paramagnetic Relaxation Enhancement. *J. Phys. Chem. A* **2003**, *107* (41), 8467–8475.

(80) Francese, G.; Dunand, F. A.; Loosli, C.; Merbach, A. E.; Decurtins, S. Functionalization of PAMAM Dendrimers with Nitronyl Nitroxide Radicals as Models for the Outer-Sphere Relaxation in Dentritic Potential MRI Contrast Agents. *Magn. Reson. Chem.* **2003**, *41* (2), 81–83.

(81) Shimono, S.; Tamura, R.; Ikuma, N.; Takahashi, H.; Sakai, N.; Yamauchi, J. Characterization of the Chiral Paramagnetic Multispin System Built on a Cyclotriphosphazene Scaffold. *Chem. Lett.* **2004**, *33* (7), 932–933.

(82) Shimono, S.; Takahashi, H.; Sakai, N.; Tamura, R.; Ikuma, N.; Yamauchi, J. Use of Cyclotriphosphazene as a Molecular Scaffold for Building Chiral Multispin Systems. *Mol. Cryst. Liq. Cryst.* **2005**, *440* (1), 37–52.

(83) Sebby, K. B.; Walter, E. D.; Usselman, R. J.; Cloninger, M. J.; Singel, D. J. End-Group Distributions of Multiple Generations of Spin-Labeled PAMAM Dendrimers. *J. Phys. Chem. B* **2011**, *115* (16), 4613–4620.

(84) Ali, B. M.; Boothapandi, M.; Sultan Nasar, A. S. Nitric Oxide, DPPH and Hydrogen Peroxide Radical Scavenging Activity of TEMPO Terminated Polyurethane Dendrimers: Data Supporting Antioxidant Activity of Radical Dendrimers. *Data Br.* **2020**, *28*, 104972.

(85) Mohamad Ali, B.; Velavan, B.; Sudhandiran, G.; Sridevi, J.; Sultan Nasar, A. Radical Dendrimers: Synthesis, Anti-Tumor Activity and Enhanced Cytoprotective Performance of TEMPO Free Radical Functionalized Polyurethane Dendrimers. *Eur. Polym. J.* **2020**, *122* (August 2019), 109354.

(86) Winalski, C. S.; Shortkroff, S.; Mulkern, R. V.; Schneider, E.; Rosen, G. M. Magnetic Resonance Relaxivity of Dendrimer-Linked Nitroxides. *Magn. Reson. Med.* **2002**, *48* (6), 965–972.

(87) Rajca, A.; Wang, Y.; Boska, M.; Paletta, J. T.; Olankitwanit, A.;

Swanson, M. A.; Mitchell, D. G.; Eaton, S. S.; Eaton, G. R.; Rajca, S. Organic Radical Contrast Agents for Magnetic Resonance Imaging. *J. Am. Chem. Soc.* **2012**, *134* (38), 15724–15727.

(88) Niidome, T.; Gokuden, R.; Watanabe, K.; Mori, T.; Naganuma, T.; Utsumi, H.; Ichikawa, K.; Katayama, Y. Nitroxyl Radicals-Modified Dendritic Poly(l -Lysine) as a Contrast Agent for Overhauser-Enhanced MRI. *J. Biomater. Sci. Polym. Ed.* **2014**, *25* (13), 1425–1439.

(89) Rajca, A.; Wang, Y.; Boska, M.; Paletta, J. T.; Olankitwanit, A.; Swanson, M. A.; Mitchell, D. G.; Eaton, S. S.; Eaton, G. R.; Rajca, S. Organic Radical Contrast Agents for Magnetic Resonance Imaging. *J. Am. Chem. Soc.* **2012**, *134* (38), 15724–15727.

1.7 Objectives

The safety concerns of traditional metal-based MRI contrast agents used in clinical diagnosis make crucial the development of new MRI contrast agents (CA) free of metals to avoid the side effects of the metal ions.

The **general objective** of this Thesis is to develop metal-free contrast agents based on organic radical dendrimers as alternative to Gd-based CA. One of the greatest challenges in the synthesis of contrast agents based on organic macromolecules for biomedical applications is to make them water-soluble. Thus, our goal is to obtain radical dendrimers soluble in water. In addition to this, they should present high relaxivity and low toxicity.

1. For this reason, the **first objective** of this Thesis is the **preparation of water-soluble radical dendrimers** and we propose different strategies to achieve this goal:

1.1. *Using amino acids as the linker between the dendrimers' branches and radicals.* We propose two different amino acids, i.e. tyrosine and lysine derivatives since both can react with chlorine ended Gn PPH dendrimers through phenolic hydroxyl group or amine group, respectively. Then, they provide an available amino group for radical coupling, for example, with a 3-carboxy-PROXYL radical, and the remaining methyl ester group can be hydrolyzed to form the water-solubilizing salt. Both amino acids present different structures that can influence on the relaxivity or other properties of the final radical dendrimers.

1.2. Another possibility is *to use water-soluble dendrimers by themselves* such as (diethylenetriaminepentaacetic acid) DTPA-core based dendrimers containing oligoethylene glycol (OEG) branches. In this case, the dendrimers could present good solubility both in water and organic solvents, something important when it comes to synthesizing and characterizing them.

1.3. A third possibility is to obtain water-soluble dendrimers by *joining dendrons to water-solubilizing polyethylene glycol (PEG) chains*.

1.4. Finally, related to solubility, it is also possible *to form nanoparticles based on radical dendrimers* that, although not soluble in water, can generate stable suspensions.

2. As a **second objective**, we want to explore the possibility of **obtaining dendrimers not only with magnetic properties but also with fluoresce properties**. This would give us the possibility of having bimodal contrast agents that could be used both for potential MRI and fluorescence imaging applications. To achieve this goal we can take advantage of using fluorescent oligo(styryl)benzene dendrimers.

3. Finally, as a **third objective**: in order to determine the suitability as contrast agents of the systems obtained, it is very important to carry out ***in vitro*** MRI (relaxivity) and cytotoxicity studies as well as ***in vivo*** toxicity and **MRI studies** (biodistribution and tumor enhancement) in healthy and tumor-bearing mice.

Chapter 2 Polyphosphorhydrazone-based radical dendrimers

2.1 Introduction

In 1997, the group of Anne-Marie Caminade and Jean-Pierre Majoral reported for the first time the synthesis of polyphosphorhydrazone (PPH) dendrimers or the so-called phosphorous dendrimers.[1] They started from hexachlorocyclotriphosphazene core and by iterative substitution of chlorine atoms with *p*-hydroxybenzaldehyde and condensation with dichlorophosphonomethylhydrazide (H_2N-N(Me)P(S)Cl_2), they obtained a family of PPH dendrimers from generation G0 to G8 ended in chlorine (Gn) and aldehyde (Gn') end groups. Since the first report about the synthesis of this family of dendrimers, enormous attention has been paid to these PPH dendrimers being used in many applications, such as catalysis, nanocarriers, bioimaging, etc.

2.1.1 Chemical reactivity and properties of PPH dendrimers

Thanks to the chemical versatility of these PPH dendrimers with chlorine (Gn) or aldehyde (Gn') functional groups as terminal groups, there exist numerous ways to obtain these dendrimers with different structures depending on the different demands. The chlorine atoms can be replaced by phenol or amine derivatives (Scheme 2-1). The phenol can be functionalized with different species in order to achieve different functions. For example, ferrocene functionalized phenols for studying electrochemical properties,[2] fluorophores functionalized phenols for interchromophoric interactions,[3] phosphonate functionalized phenols as precursors of anti-HIV derivatives.[4] Regarding the replacement of chlorine atoms end groups by amine groups, it is worth mentioning that the two chlorine atoms probably hold different reactivity depending on the amines.[5] For example, bisallylamine led to a monosubstitution of the P(S)Cl_2 moieties, regardless of the number of equivalents added.[6] Similarly, allylamine can also be used to obtain monosubstituted dendrimer.[6] After one chlorine group is substituted by an amine, the remaining one can still react with other compounds, such as amine or phenol derivatives. Based on this fact, different replacements can occur resulting in multifunctional dendrimers. Besides, linear amine as well as cyclic amines can replace the chlorine atoms such as

tetraazacyclotetradecane or pentadecane and tetraazacyclotetradecanedione.[7]

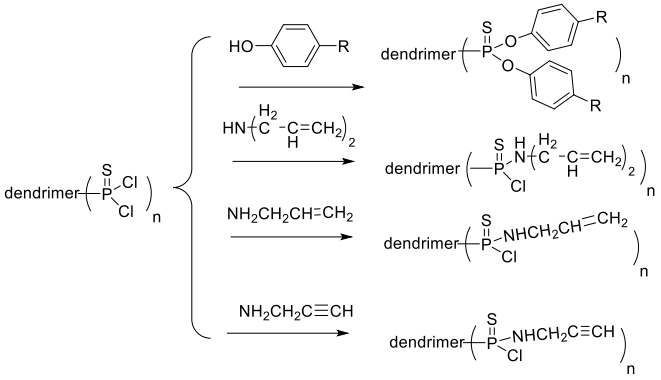

Scheme 2-1. Description of possible reactions on chlorine ended PPH dendrimers with phenol or amine derivatives.

On the other hand, aldehyde end groups can react with amines like hydrazine to form Schiff base (imine) (Scheme 2-2). Also, phosphonates can be added into the unsaturated bonds (C=O) of the aldehydes to obtain olefinic compounds with cis or trans configuration by the known Witting reaction, like, (acetylmethylene)triphenylphosphorane and (cyanomethylene)triphenylphosphorane.[8,9] The aldehyde groups of the PPH dendrimers can also react with ester, phosphonate and carboxylic acid derivatives of phosphonates forming α,β-unsaturated functional groups which also possess different *Z* and *E* isomers, which is known as the Horner-Wadsworth-Emmons reaction[10] (Scheme 2-2). Our group has made use of this Horner-Wadsworth-Emmons reaction to prepare PTM radical functionalized dendrimers.[11] The chemical versatility of the PPH dendrimers makes them very attractive for different applications such as drug delivery or imaging agents.

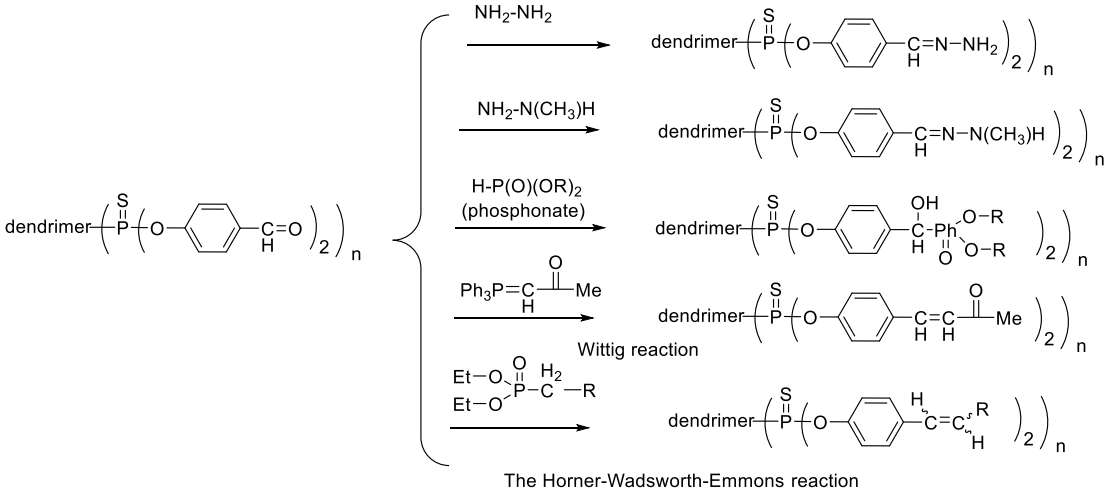

Scheme 2-2. Description of possible reactions on aldehyde ended PPH dendrimers.

PPH dendrimers (Gn and Gn') from G0 to G8 present good solubility in the common organic solvents such as chloroform, tetrahydrofuran, dichloromethane, dioxane, etc.[1] However, PPH dendrimers are not soluble in water. In order to make this kind of dendrimers soluble in water, it is necessary to modify the end group, for example, introducing water-soluble organic compounds,[12] cations,[13] nions.[14]

When PPH dendrimers are used as biomaterials, it is important to consider their stabilities. PPH dendrimers with aldehyde end groups are stable up to 250 ºC. A series of dendrimers with different cores, generations and end groups were researched to investigate the factors influencing their thermal stabilities. It indicated that the end group plays an important role but the core and generation have less influence on the stability of the dendrimer.[15] There are also a few reports about the degradability of the dendrimer core, G0.[16,17]

The toxicity of PPH dendrimers is another important property to take into account when these dendrimers are used as biomaterials. Researchers have confirmed that ionic charges have an apparent influence on the toxicity of the material. It was confirmed that quaternary ammonium terminal groups possess higher cytotoxicity than tertiary ammonium groups.[18] An alternative way to decrease the cytotoxicity of the dendrimers and ensure their water solubility is the introduction of negatively charged entities on the surface of the dendrimer, such as azabisphosphonate and azabiscarboxylate terminal groups.[19]

2.1.2 Biomedical applications of PPH dendrimers

As mentioned above, PPH dendrimers have been widely studied in different fields, especially in biomedical applications. For instance, a series of hexachlorocyclotriphosphazene (G0) based dendrimers containing two chalcone moieties were found to act as anti-tumor species *in vitro* (Scheme 2-3). They were active against prostatic adenocarcinoma PC-3 and carcinoma LNCaP cell lines in classical MTT assays with IC50 about 100 μM.[20]

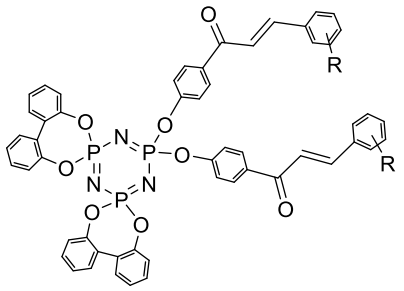

R: -H, 2-CH_3, 3-CH_3, 4-CH_3, 2-F, 3-F, 4-F, 2-Cl

Scheme 2-3. Structure of PPH dendrimers containing chalcone moieties.

A novel multivalent Gn-N-(pyridin-2-ylmethylene) ethanamine (copper (II) chelator moiety)-conjugated PPH dendrimers with chlorine as end groups and its corresponding mononuclear copper(II) complex was prepared (Scheme 2-4). The MTS assay against HL60 cell line indicated a direct relationship between the growth inhibitory effect and the number of dendrimer terminal moieties and/or the amount of copper complexed with the dendrimer. The number of terminal moieties has an apparent influence on the antiproliferative potency of the dendrimers and the complexation of dendrimers with Cu(II) boosts this effect. It is interesting that the dendrimer alone without Cu(II) also showed the growth inhibition effects for G3 on some cancer cells.[21]

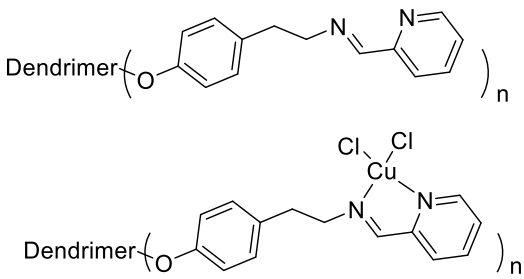

Scheme 2-4. Structure of dendrimers with N-(pyridin-2-ylmethylene) ethanamine ligand.

Six tyrosine-derived $[Mn(EDTA)(H_2O)]^{2-}$ moieties were coupled to a cyclotriphosphazene core to prepare an MRI contrast agent. This dendrimer complex has six-fold higher relaxivity than one Mn(II) containing ligand.[22] Six EDTA chelators were firstly grafted on the surface of the dendrimer and then complexed with Mn(II) (Scheme 2-5). Compared to the clinically used $[Gd(DTPA)(H_2O)]^{2-}$, the dendrimer has a higher r_1 relaxivity, with the result that blood MR signal intensity was two times higher than that of mice injected with $[Gd(DTPA)(H_2O)]^{2-}$ at 4.7 T. Furthermore, blood clearance and elimination were fast through the renal and hepatobiliary routes. The imaging and pharmacokinetic properties indicate that these Mn(II)/dendrimer chelating agents could

be advantageous for patients with chronic kidney disease.

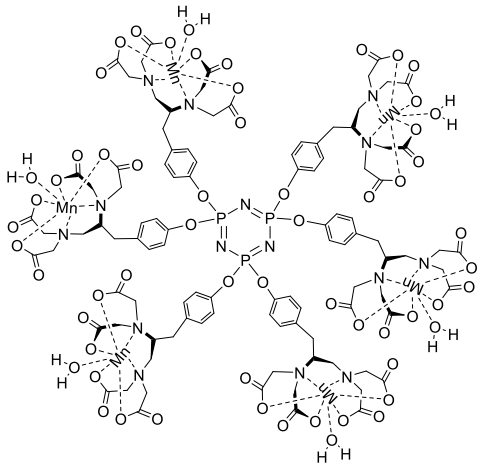

Scheme 2-5. Hexameric dendrimer with Mn(II) chelate.

2.1.3 PPH radical dendrimers

As explained in the Introduction, the conception of radical dendrimers was formally proposed in 2014 with a family of polyphosphorhydrazone dendrimers fully functionalized with TEMPO radicals, from G0 to G4 generations, having from 6 to 96 TEMPO units, respectively (Scheme 2-6).[23] Different techniques were used to characterize the PPH radical dendrimers such as EPR, ^{1}H NMR, ^{31}P NMR, UV-Vis, FT-IR and SQUID. By EPR, a strong spin-exchange interaction of the radicals at the periphery of the PPH dendrimers could be observed, and these interactions depended on the dendrimer generation as well as on the temperature. The spin-exchange interaction was much stronger at high generation and temperature. We obtained monocrystals of the zero generation radical dendrimer based on cyclotriphosphazene ring (G0) and by EPR it was proved that the relative orientation of the dendrimer branches in solution was similar as in the solid state determined by X-Ray diffraction: three branches above the cyclotriphosphazene ring and the other three below it (Scheme 2-6).[24]

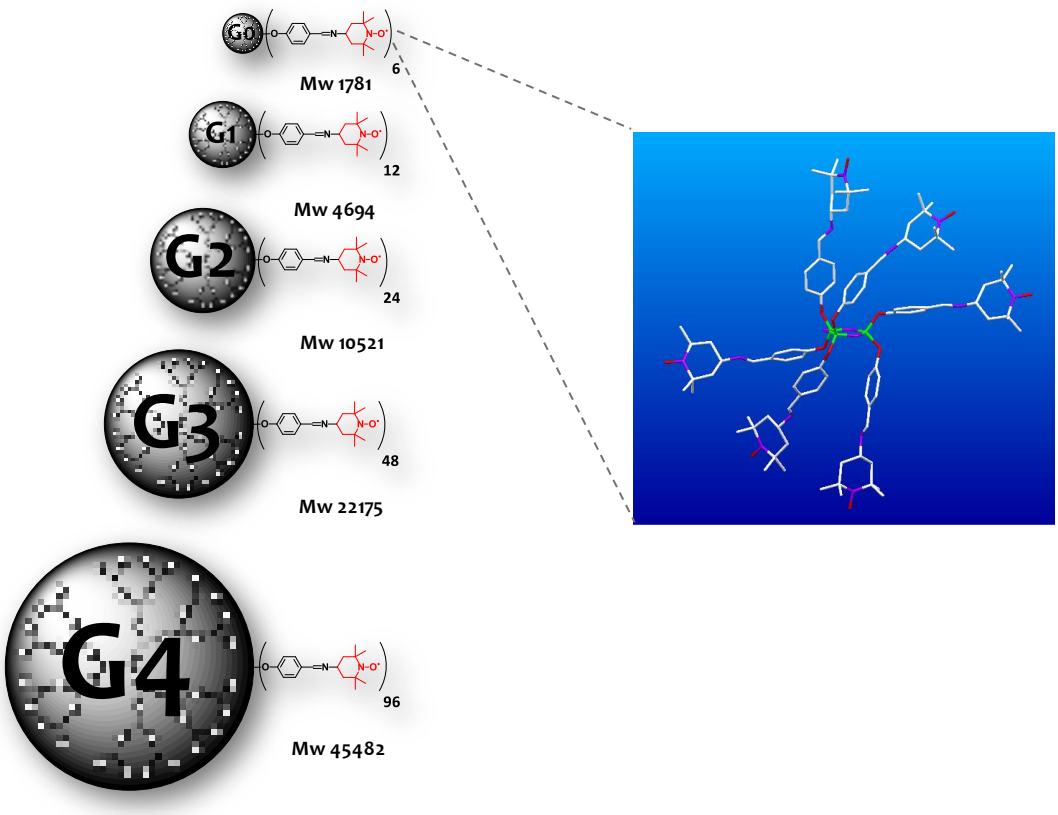

Scheme 2-6. Left) Five generations of PPH-based radical dendrimers from G0 to G4 with 6, 12, 24, 48, and 96 TEMPO radical units, respectively, at the periphery. Right) X-ray crystal structure of G0-TEMPO.

As mentioned in the Introduction, other PPH radical dendrimers have been synthesized and studied in our group, in which we have determined the influence of the linker on the spin-exchange interactions among the radicals or on tuning their solubility, or we have played with different organic radicals to achieve different applications (see the review on *Molecules*).[25]

2.2 Synthesis of PPH dendrimers from G0 to G4

We synthesized PPH dendrimers from generation G0 to G4 ended in chlorine atoms (Gn) or aldehyde groups (Gn') as previously reported[1,11] with some modifications. The synthetic route is shown in Scheme 2-7. We started from commercial hexachlorocyclotriphosphazene (G0). By nucleophilic substitution between the chlorine of G0 and phenol of *p*-hydroxybenzaldehyde under basic conditions with Cs_2CO_3 to scavenge the hydrochloric acid, dendrimer G0' was obtained (**1**). Subsequently, G0' (**1**) dendrimer reacted with dichlorophosphonomethylhydrazide (**9**) to obtain G1 (**2**). After

the synthesis of G0' (**1**) dendrimer and G1 (**2**) dendrimer with aldehyde and chlorine as end groups respectively, we repeated the same synthetic process in order to prepare dendrimers G1' (**3**), G2 (**4**), G2' (**5**), G3 (**6**), G3' (**7**) and G4 (**8**). Since these dendrimers have phosphorus atoms, this allows us to characterize them and follow the reaction by ^{31}P NMR. ^{31}P NMR is a very powerful tool since it provides information about the achievement or not of full substitution of the branches or their degree of functionalization. Moreover, Gn' dendrimers have the characteristic aldehyde groups which allow us to follow easily the reaction by IR and ^{1}H NMR.

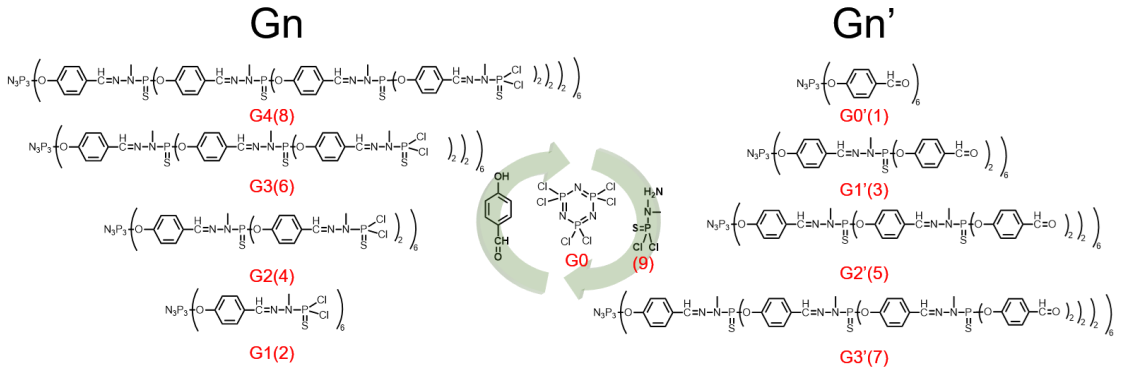

Scheme 2-7. Synthesis of PPH dendrimers from G0 to G4 generations.

First of all, dendrimer G0' (**1**) was synthesized by substitution of chlorine atoms of dendrimer core (G0) with *p*-hydroxybenzaldehyde in basic media (Cs_2CO_3). The reaction was carried out at 0 ºC for 15 min, then at room temperature overnight. After that, the solid part was filtrated, and the solution part was precipitated with *n*-pentane three times to get dendrimer G0'.

Next, in order to synthesize dendrimer G1, it was necessary to prepare a dichlorophosphonomethylhydrazide intermediate (**9**). This intermediate was prepared with thiophosphorylchloride and methylhydrazine (Scheme 2-8). Methylhydrazine was added into the solution of thiophosphorylchloride drop by drop and the reaction was initially performed at -60 ºC in an acetone bath during the addition to avoid subproducts. Herein, two equivalents of methylhydrazine were needed, because one equivalent acted as a reagent and the other one as a base to scavenge the hydrochloric acid. After the addition of methylhydrazine, the reaction was kept in the acetone bath for 30 min, then, the acetone bath was removed, and the reaction continued at room temperature overnight. After removing the salt by filtration, the prepared dichlorophosphonomethylhydrazide was stored in $CHCl_3$ and used directly.

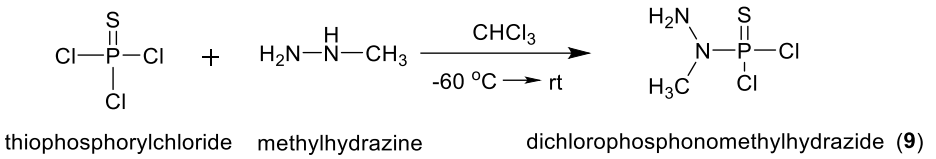

Scheme 2-8 Synthesis of dichlorophosphonomethylhydrazide (**9**).

Dendrimer G1 (**2**) was prepared with the obtained dichlorophosphonomethylhydrazide (**9**) and G0' (**1**). The reaction proceeded initially in an ice bath for 30 min and then stirred at room temperature overnight. After purification by precipitation with *n*-pentane, dendrimer G1 (**2**) was obtained. Dendrimer G1' (**3**) was synthesized in a similar way to dendrimer G0' (**1**) but starting with dendrimer G1 (**2**) instead of dendrimer G0.

However, when we moved to the synthesis of dendrimer G2 (**4**), we found that the reaction time played an important role. At first, we carried out the reaction at 0 ºC for 30 min and then the reaction proceeded at room temperature overnight. However, we did not get the pure product after purification by precipitation according to ^{31}P NMR, as shown in Figure 2-1. Then, we decided to carefully follow the reaction by ^{31}P NMR. As shown in Figure 2-2, the peaks at 64.0 and 63.3 ppm were singlets after one hour of reaction, but then each singlet split into two peaks after overnight reaction at room temperature, which indicated the molecular structure changed during that time. Therefore, we performed this reaction within a short time. Finally, we found that one hour was enough to finish this reaction. In this way, we were able to synthesize dendrimer G2 (**4**) successfully, and it was well characterized by NMR (^{31}P NMR, ^{1}H NMR, ^{13}C NMR) and IR.

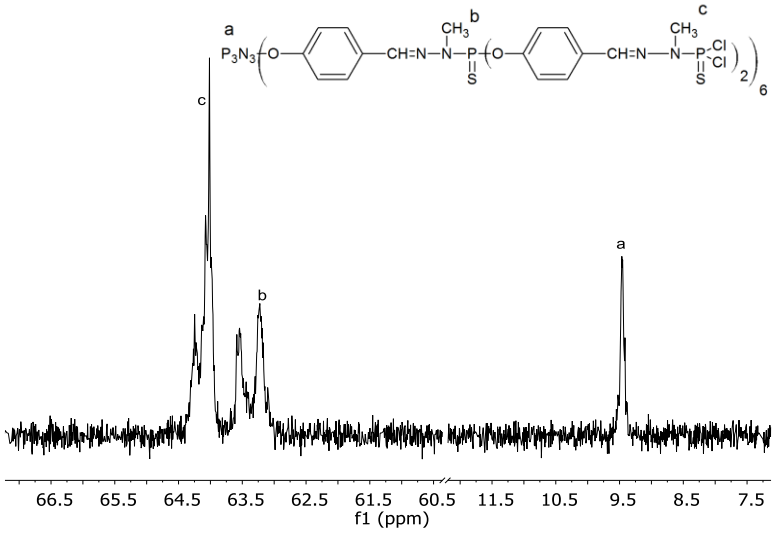

Figure 2-1. ^{31}P NMR of G2 (**4**) after overnight reaction ($CDCl_3$, 250 MHz).

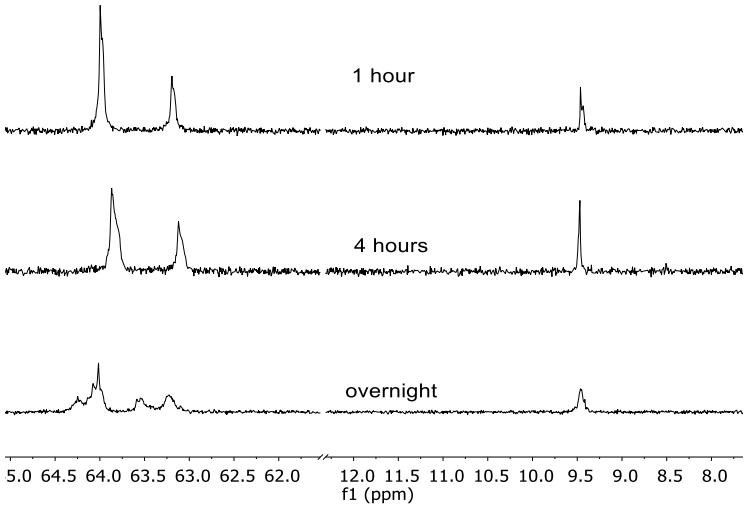

Figure 2-2. Follow-up of G2 (**4**) reaction by ^{31}P NMR ($CDCl_3$, 250 MHz).

Next, G2' (**5**) dendrimer was synthesized in a similar way to G1' (**3**) dendrimer. Specifically, G2 (**4**) dendrimer reacted overnight with 4-hydroxylbenzaldehyde with Cs_2CO_3 as a base. Dendrimer G2' (**5**) was obtained after purification by precipitation with *n*-pentane. After we obtained G2' dendrimer (**5**), G3 (**6**) dendrimer was synthesized in a similar way to G2 dendrimer (**4**). Specifically, the reaction between G2' dendrimer (**5**) and dichlorophosphonomethylhydrazide (**9**) proceeded within two hours and the reaction was followed by ^{31}P NMR to ensure the complete substitution. The product G3 (**6**) dendrimer was obtained after purification by precipitation. G3' (**7**) dendrimer was prepared in a similar way to G2' (**5**), and G4 (**8**) dendrimer was prepared based on G3' (**7**) in a similar way. The experimental conditions of the synthesis of Gn' dendrimers and Gn dendrimers are reflected in the Table 2-1 and Table 2-2, respectively.

Table 2-1. Experimental conditions for the synthesis of Gn' dendrimers.

Compound	Gn (eq)[1]	Cs_2CO_3 (eq)	aldehyde (eq)[2]	temperature (ºC)	time	Yield (%)
G0'	1	16	8	0-r.t.	overnight	84%
G1'	1	32	16	0-r.t.	overnight	81%
G2'	1	64	32	0-r.t.	overnight	73%
G3'	1	128	64	0-r.t.	overnight	92%

[1] n=0, 1, 2, 3
[2] Aldehyde means 4-hydroxylbenzaldehyde

Table 2-2. Experimental conditions for the synthesis of Gn dendrimers.

Compound	Gn' (eq)[1]	hydrazide (eq) [2]	temperature (ºC)	time	Yield (%)
G1	1	14	0-r.t.	overnight	95%
G2	1	20	0	1 hour	94%
G3	1	30	0	2 hours	92%
G4	1	80	0	1 hour	85%

[1] n=0, 1, 2, 3
[2] Hydrazide means dichlorophosphonomethylhydrazide

In conclusion, we have synthesized Gn and Gn' PPH dendrimers from G0 to G4 generations. The synthetic conditions for higher generation are a bit different from lower generation (G1). Higher generations require less reaction time than a low generation. All the synthesized dendrimers were well characterized by NMR (^{1}H, ^{31}P, ^{13}C) and IR. ^{31}P NMR is a useful tool to characterize the PPH dendrimer: G0' dendrimer showed one singlet after condensation with 4-hydroxylbenzaldehyde and the chemical shift changed from 21 ppm corresponding to the core (G0) to 7.2 ppm. For higher aldehyde ended dendrimer generations (G1' to G3'), the chemical shift of phosphorus peaks of the most exterior phosphorus can be found at around 61 ppm. After Gn' dendrimers were transformed to Gn dendrimers, one more phosphorus peak can be found at around 63 ppm because the dichlorophosphonomethylhydrazide that contains one phosphorus reacted with the aldehyde. According to ^{1}H NMR, we can clearly see the peak of aldehyde of Gn' dendrimers at around 9.8 ppm and this characteristic peak disappeared after the reaction with dichlorophosphonomethylhydrazide. The disappearance of the aldehyde groups can also be observed in ^{13}C NMR. The carbons of aldehydes were at around 190 ppm, which disappeared after the aldehyde reacted with dichlorophosphonomethylhydrazide. In the corresponding IR spectra, the aldehyde group of dendrimer Gn' was at 1700 cm^{-1}, but this band disappeared once the aldehyde ended dendrimers Gn' changed to chlorine ended dendrimers Gn. Both the NMR (^{31}P NMR, ^{1}H NMR and ^{13}C NMR) and the IR confirmed the successful synthesis of the dendrimers from G0' to G4.

2.3 PPH radical dendrimers with Tyrosine as linker (Gn-Tyr(PROXYL)-COOLi, n=0-3)

In order to prepare water-soluble PPH dendrimers, one way is to anchor hydrophilic

compounds, for example, D-oxylose[26] or helicon.[27] Another option is the introduction of cations or anions in the structure, for example, ammonium[18] or carboxylate groups.[10] However, dendrimers with anions show less cytotoxicity compared with cations.[28]

Amino acids could be ideal linkers for preparing water-soluble dendrimers because they contain an amine and acid groups, which provide us with the opportunity of using one amine group to couple with 3-carboxy-PROXYL and the acid group can be converted to carboxylate salt to make our radical dendrimers water-soluble (Scheme 2-9). We chose two different amino acids as linkers, tyrosine and lysine. To anchor them to the dendrimer, tyrosine has a phenol group that is able to substitute the chlorines of the Gn dendrimers, while lysine has an extra amine group that can also react with Gn dendrimers by substitution of chlorine atoms.

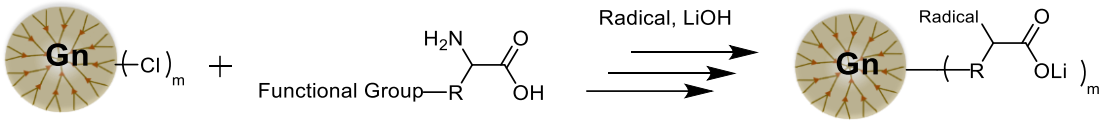

Scheme 2-9. Synthetic scheme to afford amino acid functionalized water-soluble PPH dendrimers.

In our group, we started with tyrosine amino acid to prepare water-soluble dendrimers.[29] The reaction between the tyrosine and Gn dendrimer was performed in a similar way than the synthesis of Gn' dendrimers since they are essentially between the Gn dendrimers and *p*-hydroxyphenyl (phenol) group. After the coupling of the tyrosine amino acid on the surface of the dendrimer, the BOC group was deprotected by TFA. The deprotected amine group was coupled with 3-carboxy-PROXYL radical. Finally, the acid group was converted to the salt. In this way, we prepared water-soluble radical dendrimers from G0 to G3 (Scheme 2-10).

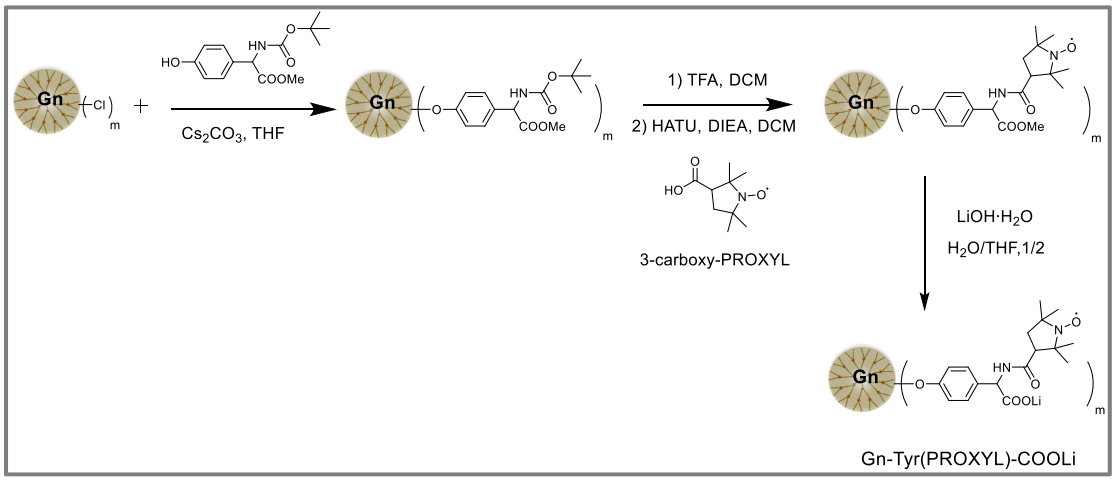

Scheme 2-10. Synthetic route of radical dendrimers Gn-Tyr(PROXYL)-COOMe (n=0, 1, 2, 3; m=6, 12, 24, 48) with **tyrosine** as linker.

The tyrosine radical dendrimers began to be characterized by EPR, MALDI-TOF and SEC and I continued to improve the characterization with these and other techniques such as TEM and DLS as well as performing stability and cytotoxicity studies. Importantly, by EPR we can know the presence of radicals and the number of radical units (Figure 2-3). The number of radical units in the radical dendrimer matched very well with the theoretical value.

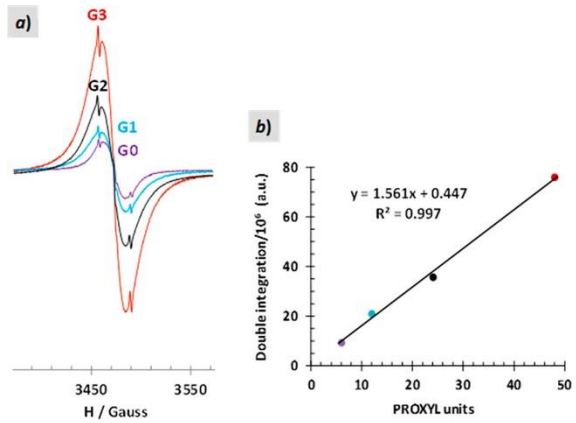

Figure 2-3. (a) X-band EPR spectra (100 mM phosphate buffer pH 7.4, 300 K) of 0.21 mM solutions of Gn-Tyr(PROXYL)-COOLi (n =0-3) dendrimers obtained under identical conditions. (b) Double integral of the EPR spectra of Gn-Tyr(PROXYL)-COOLi dendrimers (0.21 mM, 100 mM PB pH 7.4, 180 K) vs number of PROXYL units.

Furthermore, DLS was used to determine the average hydrodynamic diameter of Gn-Tyr(PROXYL)-COOLi dendrimers (Table 2-3 and Figure 2-4). It indicated that the hydrodynamic diameter ranged from 2.8 nm for G0-, to 4.8 nm for G3-Tyr(PROXYL)-COOLi, being similar to other water-soluble dendrimers in the same range of molecular

weight.[30,31] It is worth remarking that none of the Gn-Tyr(PROXYL)-COOLi dendrimer generations presented significant aggregation at physiological pH (<0.2% by volume). This is also consistent with the Z-potential data obtained (Table 2-3), which reflects the good stability in solution of such species. TEM image of G3-Tyr(PROXYL)-COOLi was obtained using the negative stain technique with uranyl acetate (see Figure 2-5), observing a very homogeneous particle size distribution with an average diameter of d = 4.86 ± 0.05 nm, which is in agreement with the data obtained by DLS.

Table 2-3. Hydrodynamic diameters of Gn-Tyr(PROXYL)-COOLi dendrimers (100 mM phosphate buffer (PB) pH 7.4 at 300 K) shown in the Z-average with standard deviation values (N = 5) and their corresponding Z-potential in water.

Compound	Hydrodynamic diameters (nm)	Z-potential (mV)
G0-Tyr(PROXYL)-COOLi	**2.81 ±0.58**	**-57.6**
G1-Tyr(PROXYL)-COOLi	**3.44 ±0.75**	**-68.1**
G2-Tyr(PROXYL)-COOLi	**4.23 ±1.30**	**-84.1**
G3-Tyr(PROXYL)-COOLi	**4.78 ±1.23**	**-59.2**

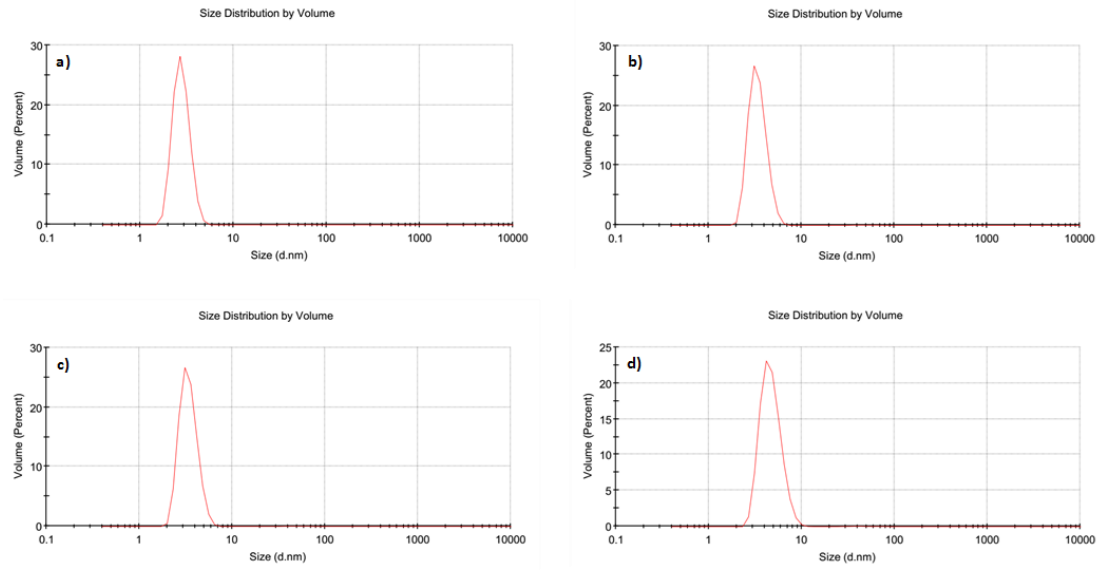

Figure 2-4. Average result created from the record of frequency curves (N = 5) obtained from the volume particle size distribution, for a) G0-, b) G1-, c) G2- and d) G3-Tyr(PROXYL)-COOLi dendrimers, provided by Malvern Zetasizer Software.

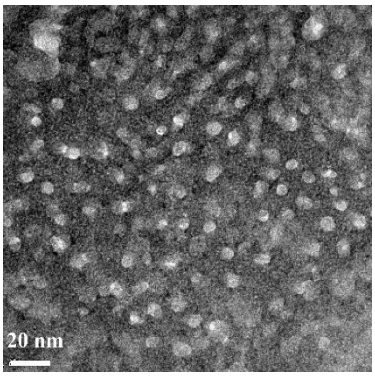

Figure 2-5. TEM image of G3-Tyr(PROXYL)-COOLi dendrimer using the negative stain technique with uranyl acetate, d = 4.86 ± 0.05 nm.

One of the most important properties of radical dendrimers, when they are used as contrast agents, is relaxivity. We performed the MRI phantom experiments of the tyrosine functionalized radical dendrimers to measure the relaxivities. The results indicated that the relaxivities of radical dendrimers per molecule increased from 1.39 $mM^{-1}s^{-1}$ to 12.96 $mM^{-1}s^{-1}$ from G0 to G3 generations. It is worth mentioning that the increase of relaxivity was not only observed per molecule but also per radical unit (0.20 $mM^{-1}s^{-1}$ for PROXYL, 0.23 $mM^{-1}s^{-1}$ for G0 and 0.27 $mM^{-1}s^{-1}$ for G3), which could result from the big molecular size (slow tumbling) of high generation radical dendrimers (Figure 2-6).

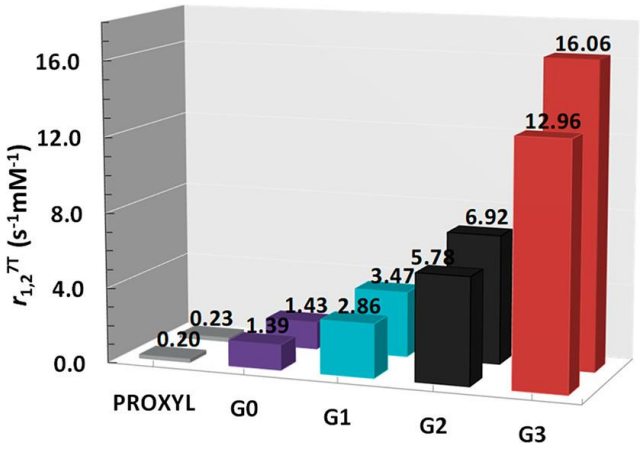

Figure 2-6. Longitudinal (r_1) and transverse (r_2) relaxivity per molecule of Gn-Tyr(PROXYL)-COOLi, n=0-3 dendrimers determined at 7T in 100 mM phosphate buffer pH 7.4, 300 K.

In vitro viability assays were performed with the fetus normal lung tissue cell line (MRC-5) to evaluate the toxicity of Gn-Tyr(PROXYL)-COOLi dendrimers (n=0-3). The cells were incubated with Gn-Tyr(PROXYL)-COOLi dendrimers (n=0-3) of various concentrations ranging from 0.016 to 2mM per radical unit for 24 and 48 h. MTT assay

was used to determine cell viability. As a result, Gn-Tyr(PROXYL)-COOLi dendrimers (n=0-3) did not display any cytotoxicity *in vitro*, in the tested concentration range (Figure 2-7). It is known that nitroxides themselves are not considered cytotoxic[32–34] and negatively charged dendrimers do not interact with biological environment, since they are repelled by the negatively charged cell membrane.[28] The combination of these two attributes is confirmed by our results, giving biocompatible dendrimers better suitable for clinical applications.

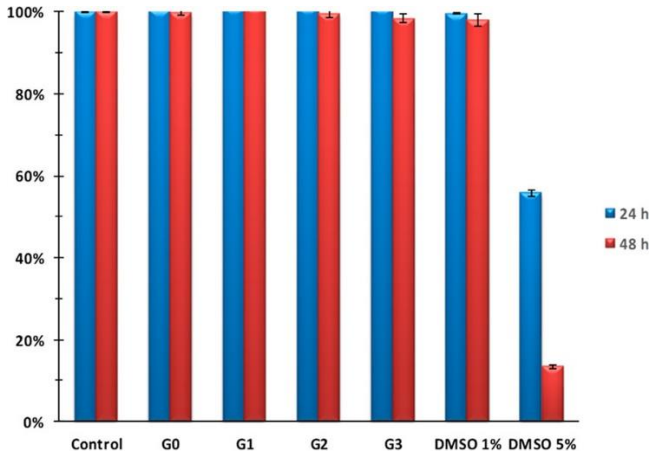

Figure 2-7. In vitro cell viability assays conducted with the fetus normal lung tissue cell line (MRC-5) incubated with Gn-Tyr(PROXYL)-COOLi dendrimers (n =0−3) in a concentration of 2 mM per radical unit for 24 and 48 h.

In conclusion, we have successfully prepared a series of radical dendrimers with tyrosine as a linker between the radical and the dendrimers. These radical dendrimers showed high water solubility thanks to the carboxylate salt in the tyrosine linker. Remarkably, the phantom MRI experiments showed that the relaxivity r_1 of G3 radical dendrimers G3-Tyr(PROXYL)-COOLi (ca. 13 $mM^{-1}s^{-1}$) is four times higher than the most widely used CA in clinics, Gd-DPTA (3.2 $mM^{-1}s^{-1}$) or Gd-DOTA (2.8 $mM^{-1}s^{-1}$). *In vitro* cell viability assays showed no toxicity for these radical dendrimers.

2.4 Attempted synthesis of PPH radical dendrimers with Lysine as linker (PROXYL-Lys(Gn)-COOLi, n=0-3). Route 1.

After we confirmed the successful preparation of radical dendrimers as MRI contrast agents with tyrosine as a linker, we tried to use another amino acid as linker, lysine. The

main difference between lysine and tyrosine is the rigidity. In lysine, there is an alkyl chain, but in tyrosine, there is an aromatic ring. We believe the different structures could induce a difference in the spin-spin interaction of radicals. Accordingly, we can check the influence of the different linkers in the relaxivity values or other influences on our radical dendrimers.

In order to synthesize lysine functionalized radical dendrimers, we used, in the beginning, a different synthetic route from tyrosine functionalized Gn-Tyr(PROXYL)-COOLi radical dendrimers. Instead of starting with the anchoring of the amino acid lysine on the surface of PPH dendrimers, we synthesized the PROXYL-Lys(BOC)-COOMe radical ligand firstly (Scheme 2-11). Next, the BOC group was removed by deprotection with TFA, obtaining PROXYL-Lys-COOMe ligand. Then, this ligand was used to couple to the Gn PPH dendrimers, by substitution of chlorine with the deprotected amine. Finally, the acid group was hydrolyzed with LiOH to form the salt, to provide us water-soluble radical dendrimers (Scheme 2-11).

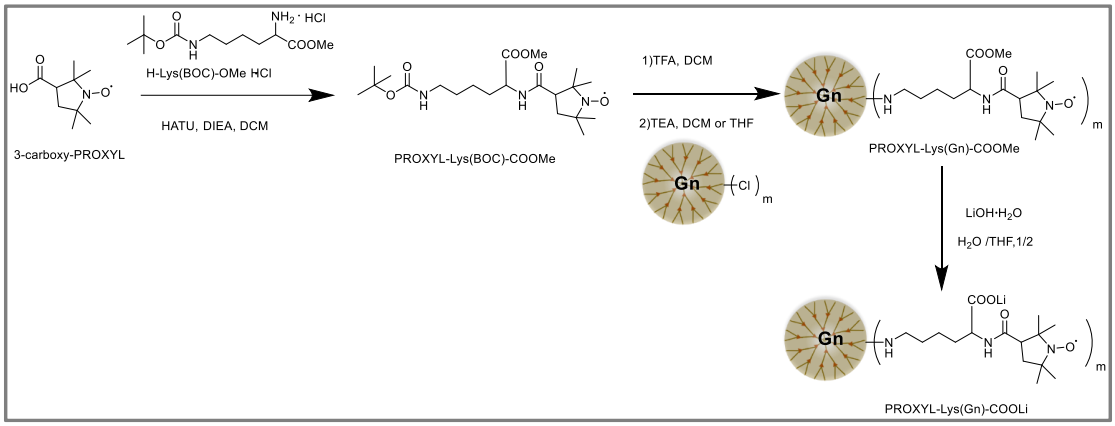

Scheme 2-11. Synthetic route of PROXYL-Lys(Gn)-COOLi (n=0, 1, 2, 3; m=6, 12, 24, 48) radical dendrimers with **lysine** as linker. **ROUTE 1**.

2.4.1 Synthesis of PROXY-Lys-COOMe ligand

First, we synthesized the PROXYL-Lys(BOC)-COOMe (**10**) radical ligand, by amidation between the amine group of H-Lys(BOC)-OMe and the carboxylic acid group of the 3-carboxy-PROXYL with HATU as the coupling agent and DIEA as the base (Scheme 2-12). This reaction was performed at room temperature overnight. After that, the crude was extracted with DCM/H_2O three times. Then, the product PROXYL-Lys(BOC)-COOMe (**10**) was purified by column chromatography on silica gel, and was characterized by IR. In the IR spectrum, we can observe the band of amide at 1665 cm^{-1}

and the band of the NH of carbamate at 3323 cm^{-1}. EPR was also used to characterize the ligand PROXYL-Lys(BOC)-COOMe (**10**). The EPR spectrum showed that the intensity of the third peak was lower than the first two peaks, which is indicative of slower rotational time (tumbling) of the radical due to the radical was coupled to another (larger) molecule, lysine, in our case (Figure 2-8).

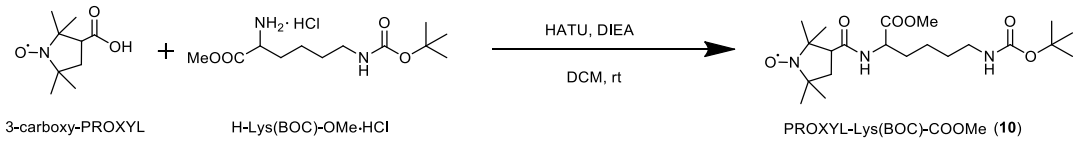

Scheme 2-12. Synthesis of PROXYL-Lys(BOC)-COOMe (**10**) radical ligand.

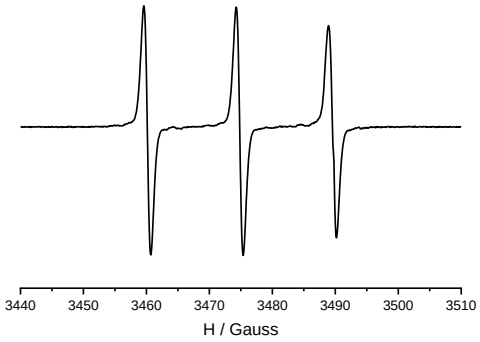

Figure 2-8. EPR spectrum of PROXYL-Lys(BOC)-COOMe (**10**) ligand.

Then, the obtained PROXYL-Lys(BOC)-COOMe (**10**) was deprotected with TFA (Scheme 2-13), which is the most commonly used deprotecting agent for BOC group to obtain PROXYL-Lys-COOMe (**11**) ligand. The reaction was performed in an ice bath for 30 min at first and then proceeded at room temperature overnight. Then, the product was purified by washing with DCM and MeOH three times, respectively. The obtained product was characterized by IR and EPR, showing also a three-line pattern similar to ligand **10** (Figure 2-9).

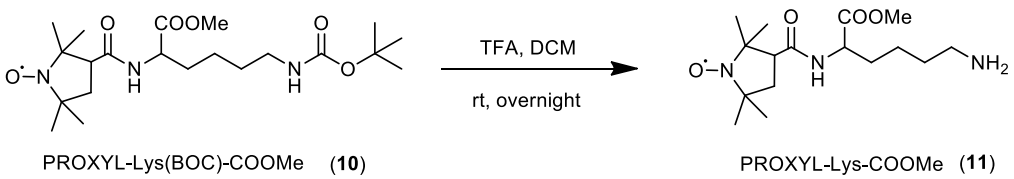

Scheme 2-13. Deprotection of PROXYL-Lys(BOC)-COOMe (**10**) with TFA to afford ligand PROXYL-Lys-COOMe (**11**).

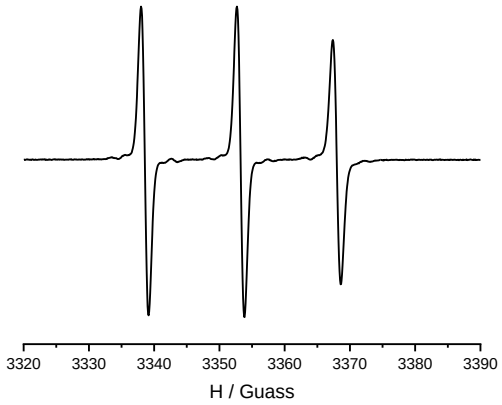

Figure 2-9. EPR spectrum of PROXYL-Lys-COOMe (**11**) ligand.

2.4.2 Attempted synthesis of PROXY-Lys(G0)-COOMe and PROXY-Lys(Gn)-COOLi n=0-3

Once we got the radical ligand PROXYL-Lys-COOMe (**11**), we were able to take advantage of the primary amine group to replace the chorine of the Gn PPH dendrimer to prepare the radical dendrimers PROXYL-Lys(Gn)-COOMe. First, we started with G0 to synthesize radical dendrimer PROXYL-Lys(G0)-COOMe (**12**), in basic conditions (Cs_2CO_3) (Scheme 2-14). After overnight reaction, the reaction solution was filtrated to remove Cs_2CO_3. Subsequently, the product was purified by column chromatography on silica gel. The product was characterized by IR and EPR. In the EPR spectrum, we observed spin-exchange interaction between radicals since we observed two broad bands between the three principal lines, which indicated that the radicals were anchored on the dendrimer G0 and interacting among them intramolecularly (Figure 2-10).

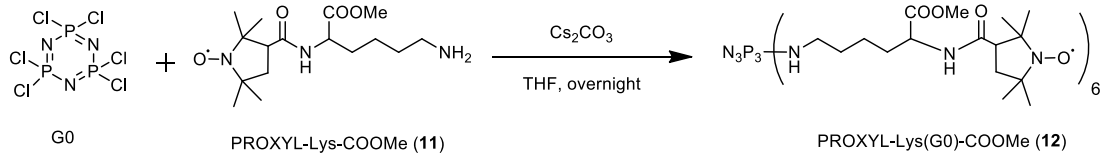

Scheme 2-14. Synthesis of radical dendrimer PROXYL-Lys(G0)-COOMe (**12**).

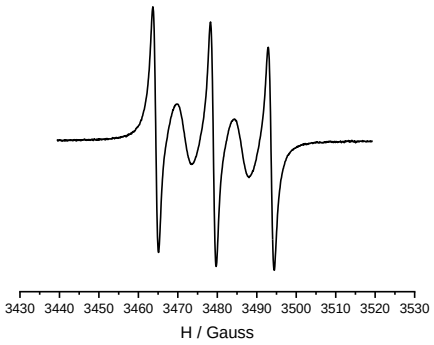

Figure 2-10. EPR of radical dendrimer PROXYL-Lys(G0)-COOMe (**12**).

Then, in order to make the radical dendrimer PROXYL-Lys(G0)-COOMe (**12**) water-soluble, we transformed the methyl ester to carboxylate salt with an excess of LiOH in THF/H_2O (Scheme 2-15). The excess of LiOH was removed by ultrafiltration. After drying by lyophilization, the product PROXYL-Lys(BOC)-COOLi (**13**) was obtained as a white powder. It was characterized by EPR and MRI together with the other generations (see below).

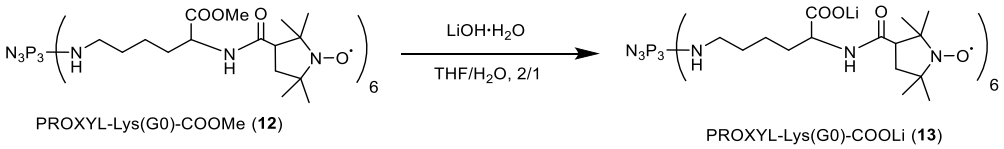

PROXYL-Lys(G0)-COOMe (**12**)

PROXYL-Lys(G0)-COOLi (**13**)

Scheme 2-15. Last step of the synthesis to obtain water-soluble PROXYL-Lys(G0)-COOLi (**13**) dendrimer.

Then, we moved to prepare PROXYL-Lys(Gn)-COOLi radical dendrimers from G1 to G3, in a similar way, but we changed the base from Cs_2CO_3 to trimethylamine (TEA). First, the PROXYL-Lys-COOMe (**11**) radical ligand reacted with the Cl-ended dendrimer with TEA as a base. After the reaction proceeded overnight or two days, the formed salt between the TEA and hydrochloric acid was removed by filtration. The solution was dried and then dissolved in THF/H_2O (2/1, v/v). LiOH•H_2O was added to hydrolyze the ester of the radical dendrimers to get the corresponding lithium salt (Scheme 2-16). The excess of LiOH was removed by ultrafiltration, and the products were dried by the lyophilization.

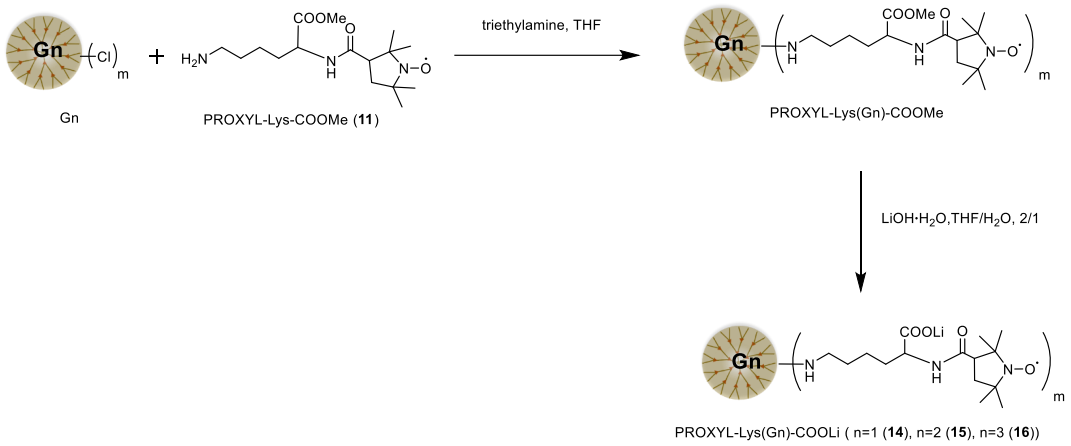

Scheme 2-16. Synthetic scheme to obtain PROXYL-Lys(Gn)-COOMe radical dendrimers and subsequent hydrolysis with LiOH to obtain PROXYL-Lys(Gn)-COOLi (n=1 (**14**), 2 (**15**), 3 (**16**); m= 12, 24, 48).

The obtained compounds as PROXYL-Lys(Gn)-COOLi radical dendrimers from G0 to G3, were characterized by EPR and MRI phantoms. From the shape of the EPR spectra obtained, we could observe that only G0 showed some interaction between radicals, but from G1 to G3 the EPR spectra only showed a three-line pattern, which was surprising and not expected if all branches were substituted, indicating that most probably there was not fully radical substitution. We also used EPR to make a quantitative analysis to determine the number of radical units anchored on the dendrimers. The quantitative EPR study confirmed the previous assumption, showing that the number of radicals anchored on the dendrimers was much lower than the expected theoretical ones. Also, the MRI phantom experiments performed showed that the relaxivity values were much lower than the expected ones (Figure 2-11). The relaxivities were very low indicating that the dendrimers structures contain only few PROXYL radicals. Therefore, we did not get radical dendrimers fully functionalized by PROXYL radicals but only with few radicals in the structure as determined by EPR and MRI studies.

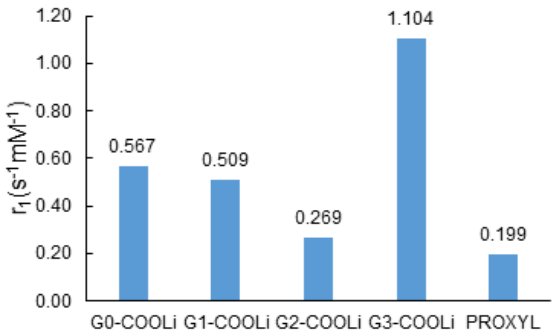

Figure 2-11. Longitudinal (r_1) relaxivities of PROXYL-Lys(Gn)-COOLi (Gn-COOLi) n=0-3 radical dendrimers per molecule determined at 7T in 100 mM phosphate buffer pH 7.4, 300 K.

In order to try to explain these results, we think there are three possible reasons to explain why the radical dendrimers did not present full radical substitution:

1) The first explanation could be that the radical ligand PROXYL-Lys-COOMe (**11**) did not anchor on the surface of Gn dendrimers in all positions. Interestingly, as explained before, in the radical dendrimer PROXYL-Lys(G0)-COOMe (**13**), there existed interaction between radicals resulting from radicals grafted on the dendrimer, according to the EPR spectrum. In dendrimer G0, we have six chlorine atoms connected to the ring. It is well known that the substitution of one chlorine is easier than the substitution of two chlorines on the same phosphorus, which is called "cis effect", resulting in cis geminal products.[35–37] Due to the radicals are located at the same side of the dendrimer core ring it is possible to produce some interaction between them (and see the interaction in the EPR spectrum). Therefore, it is plausible to think that we got G0 radical dendrimer with only three chlorine atoms substituted and that the radicals are on the same side of the dendrimer core (Scheme 2-17). For dendrimers from G1 to G3, the reaction between radical ligand and dendrimers might be hindered by the bulky hindrance of the ligand PROXYL-Lys-COOMe (**11**).

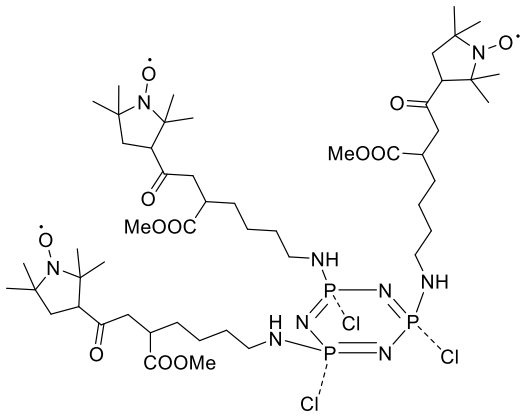

Scheme 2-17. Possible structure obtained for the attempted synthesis of PROXYL-Lys(G0)-COOMe (**12**) (and the COOLi derivative **13**) with tri-radical substitution instead of full radical substitution.

2) TFA can also affect the nitroxide radicals through Golubev disproportion[38-40] (Scheme 2-18). Some acids can oxidize nitroxides into oxoammonium and hydroxylammonium. However, then, under basic conditions, for example, $NaHCO_3$, these products can form nitroxide radicals again, in a reversible way. In our case, when the PROXYL-Lys(BOC)-COOMe radical ligand was deprotected with TFA, the radical character of PROXYL units could possibly be

partially lost. And then, although we used a base in the next step, the radical character could not be totally recovered.

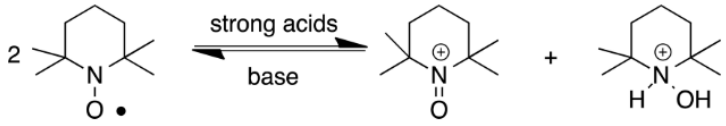

Scheme 2-18. Golubev disproportion of the nitroxide radical with acid.[38]

3) It is also possible that the obtained radical dendrimers were not stable during the hydrolysis or purification processes, for instance, inducing some degradation of the dendrimer structure.

We had to propose another route to prepare these radical dendrimers so that all the end groups could be fully functionalized with radicals. In addition, the radicals have to be prevented from TFA. Therefore, we can firstly anchor amino acid lysine on the surface of Gn PPH dendrimers. After lysine deprotection, radical units can be anchored on these lysine functionalized dendrimers. Also, in this way, we can take advantage of ^{1}H NMR for the first steps which is not possible in the previous route.

2.5 Synthesis of PPH radical dendrimers with Lysine as linker (Gn-Lys(PROXYL)-COOLi, n=0,1). Route 2.

Since the first route was not successful, we changed to another synthetic way similar to the formation of radical dendrimers with tyrosine as linker (Scheme 2-19). First, the lysine amino acid derivative is coupled through the free amine to the Gn PPH dendrimers with chlorine atoms as the end group. Second, the BOC group of the dendrimer Gn-Lys(BOC)-COOMe is removed with TFA, obtaining Gn-Lys-COOMe. Then, the lysine functionalized PPH dendrimers with free amine group are coupled with 3-carboxy-PROXYL. Finally, the radical dendrimers can be hydrolyzed to make radical dendrimers soluble in water. The advantage of this reaction procedure is that the full functionalization of dendrimers with amino acid can be verified by NMR. The main difference of structure between the previous PROXYL-Lys(Gn)-COOLi radical dendrimers (from route 1) and the new Gn-Lys(PROXYL)-COOLi radical dendrimers (from route 2) is the position of the hydrophilic groups (COOLi). In the radical dendrimers of the first route, the hydrophilic groups (COOLi) are closer to the radical end groups, i.e. to the dendrimer

surface while in the radical dendrimers of the second route these are located more in the interior, further from the radical end groups（Scheme 2-20）.

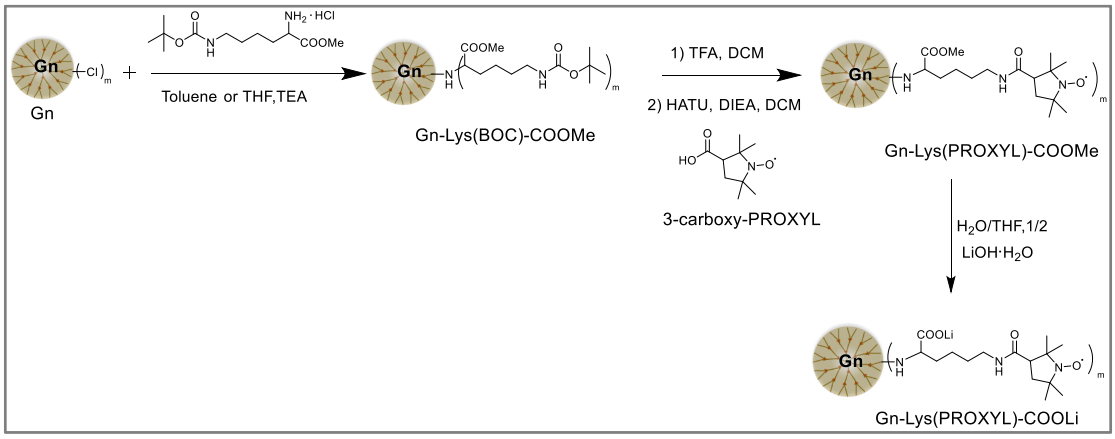

Scheme 2-19. Synthesis of Gn-Lys(PROXYL)-COOMe radical dendrimers (n=0, 1, 2, 3; m=6, 12, 24, 48) with **lysine** as linker. **ROUTE 2**.

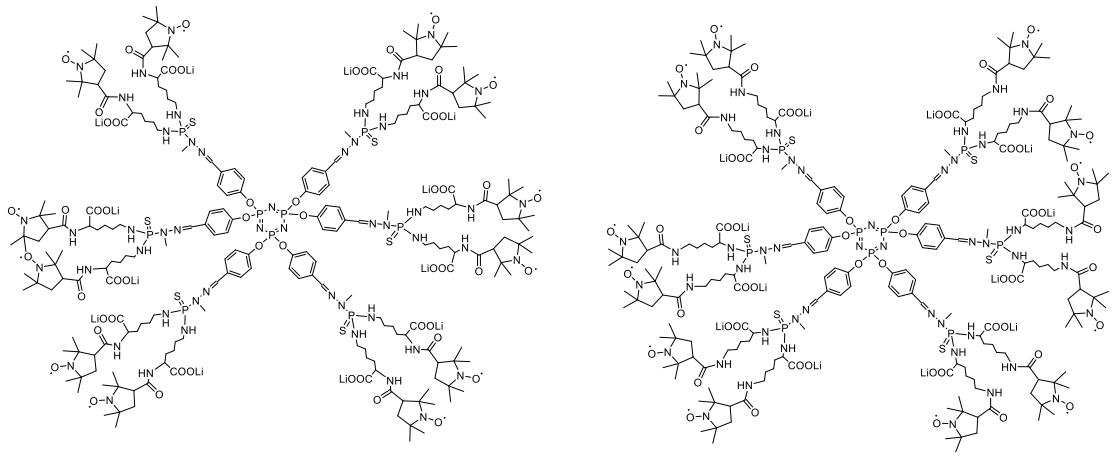

Scheme 2-20. Chemical structure of left) radical dendrimer PROXYL-Lys(G1)-COOLi from the Route 1 and right) G1-Lys(PROXYL)-COOLi from the new Route 2.

2.5.1 Synthesis of dendrimers Gn-Lys(BOC)-COOMe n=0-3

At first, we synthesized the dendrimer **G0-Lys(BOC)-COOMe** (**17**) by coupling the lysine amino acid derivative and the dendrimer G0 in basic conditions (Scheme 2-21).

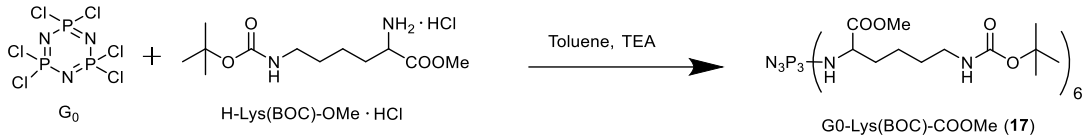

Scheme 2-21. Synthesis of dendrimer G0-Lys(BOC)-COOMe (**17**).

The reaction between the G0 and lysine was originally performed at room temperature for 24 h, but we did not obtain the desired product according to the ^{31}P NMR spectrum (Figure 2-12). As shown in Figure 2-12, there is more than one peak, indicating the incomplete substitution of chlorine atoms. If all the chlorine groups were completely substituted there should appear only one peak. In order to make all the chlorine atoms be substituted, we decided to increase the temperature to 105 ℃, and follow the reaction by ^{31}P NMR. The ^{31}P NMR spectra at different times are shown in Figure 2-13. We can clearly see that the intensities of the peaks at around 11 ppm and 22.5 ppm decreased with time, which means the chlorine atoms have been gradually substituted. After 9 days at 105 ℃ only one peak at 15 ppm appeared, which indicated all the chlorine atoms were substituted. The dendrimer G0-Lys(BOC)-COOMe (**17**) was obtained after precipitation and was characterized by ^{1}H NMR, ^{31}P NMR, ^{13}C NMR and MALDI-TOF confirming it was successfully obtained. In the ^{31}P NMR, the phosphorus peak at 15 ppm was shifted from the phosphorus peak of G0 dendrimer at 21 ppm. In the MALDI-TOF spectrum, the molecular ion peak can be found at 1690 m/z.

As we mentioned before, the chlorine groups of the dendrimer core have different reactivity when one of the two chlorine atoms is substituted by an amine because the first substitution could induce an increase of the electronegativity of phosphorus, thus, making the second chlorine less susceptible to be substituted. As a result, an incomplete substitution product can be obtained, for this reason it is necessary to increase the temperature to make all chlorine groups substituted.[41]

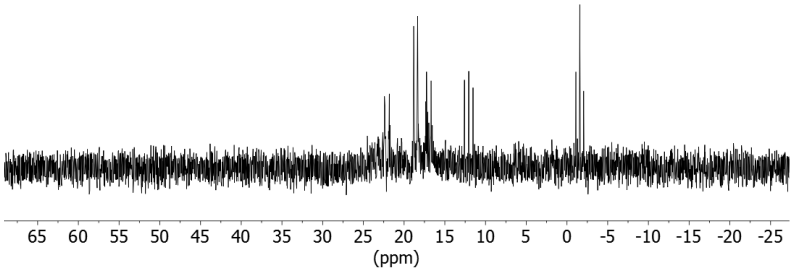

Figure 2-12. ^{31}P NMR spectrum of the reaction to form G0-Lys(BOC)-COOMe (**17**) dendrimer at room temperature, after 24 hours.

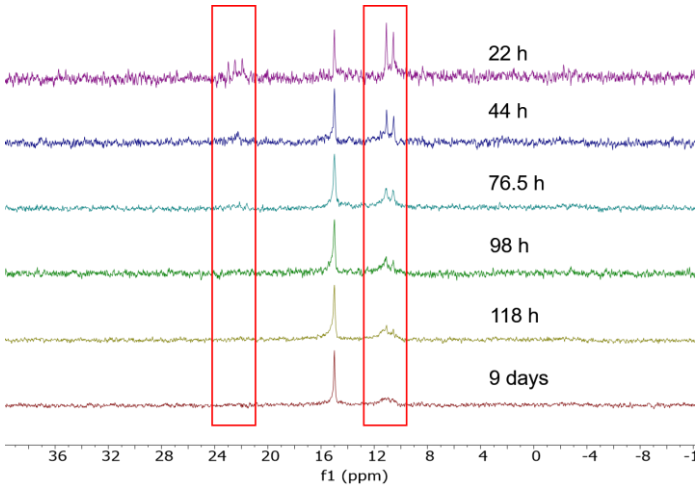

Figure 2-13. Follow-up by ^{31}P NMR of the synthesis of dendrimer G0-Lys(BOC)-COOMe (**17**) (LB=3).

The synthesis of **G1-Lys(BOC)-COOMe** (**18**) dendrimer was carried out in softer conditions (Scheme 2-22). In this case, we found that this reaction was completed at room temperature and overnight. The product was purified by extraction with 0.05 M HCl in dichloromethane. ^{31}P NMR, ^{1}H NMR, ^{13}C NMR and MALDI-TOF confirmed the structure of the G1-Lys(BOC)-COOMe (**18**). It is worth mentioning that ^{31}P NMR was able to confirm the anchoring of lysine derivative through the chemical shift of the most exterior phosphorous of G1 (**2**) dendrimer that changed from 63 ppm to 68 ppm, as well as the complete substitution of chlorine atoms because of the appearance of only two phosphorus peaks in the final spectrum (from the two different phosphorous from the structure). By MALDI-TOF mass spectrometry we obtained the quasi-molecular ion peak at 4537.9 m/z from the adduct $[M+Na]^+$.

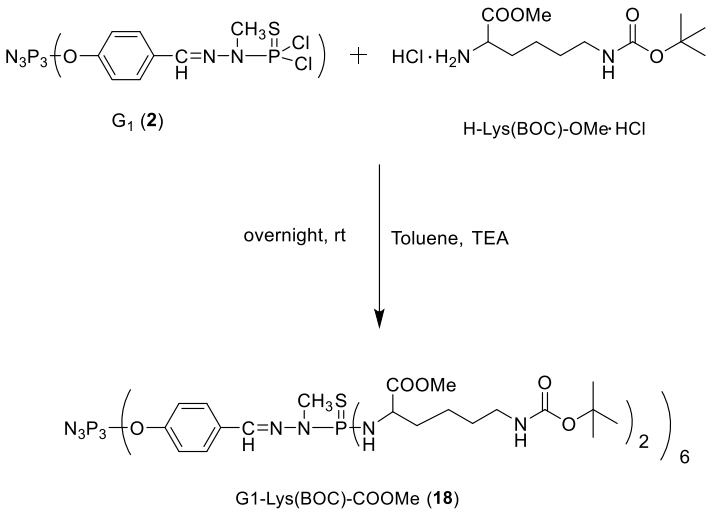

Scheme 2-22. Synthesis of G1-Lys(BOC)-COOMe (**18**) dendrimer.

Thus, we have noticed that the functionalization of G0 and G1 dendrimers required very different reaction conditions. For G0 dendrimer, it was needed a high temperature and long reaction time, but for G1 derivative, the reaction was finished at room temperature and with much less reaction time. This phenomenon could result from the different reactivity of the chlorine end groups between G0 (connected to the phosphorous from the N_3P_3 core ring) and G1 (connected to the phosphorous from the branches) dendrimers.

G2-Lys(BOC)-COOMe (**19**) dendrimer was synthesized in a similar way than G1-Lys(BOC)-COOMe (Scheme 2-23) dendrimer, and characterized by ^{31}P NMR and ^{1}H NMR. Similarly, we can also observe in ^{31}P NMR that the most exterior phosphorus peak shifted from 63 ppm of G2 (**4**) dendrimer to 67 ppm, and that appeared only three peaks from the three different phosphorous atoms, confirming the anchoring of lysine derivative and the complete substitution of all chlorine atoms.

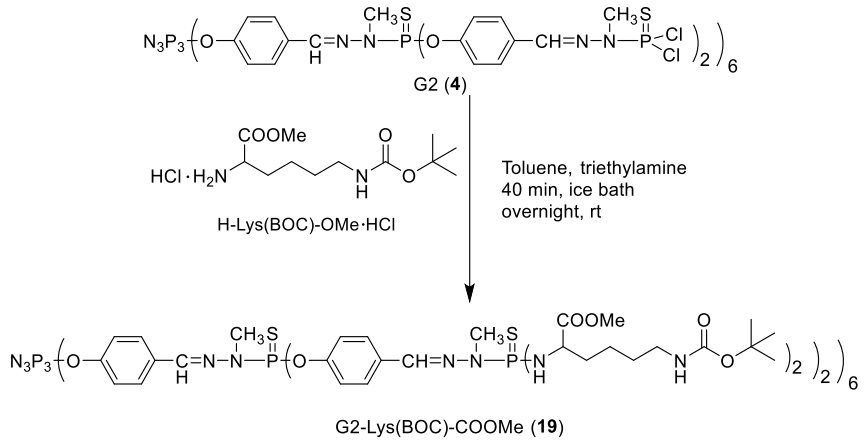

Scheme 2-23 Synthesis of G2-Lys(BOC)-COOMe (**19**) dendrimer.

We synthesized initially **G3-Lys(BOC)-COOMe** (**20**) dendrimer in the same solvent than the others (toluene) but we found that the product precipitated during the synthesis process, which was checked by ^{31}P NMR. For this reason, we changed the solvent to THF, in which the solubility of the product was better than in toluene. In addition, the reaction needed more time than G1-Lys(BOC)-COOMe (**18**) and G2-Lys(BOC)-COOMe (**19**) (Scheme 2-24). After purification by column chromatography on silica gel, G3-Lys(BOC)-COOMe (**20**) was successfully characterized by ^{31}P NMR and ^{1}H NMR. Again, the shift of the most exterior phosphorus peak from 63 to 67 ppm suggested that the lysine was anchored to G3 dendrimer and the appearance of only four phosphorus peaks meant that all chlorine atoms were substituted.

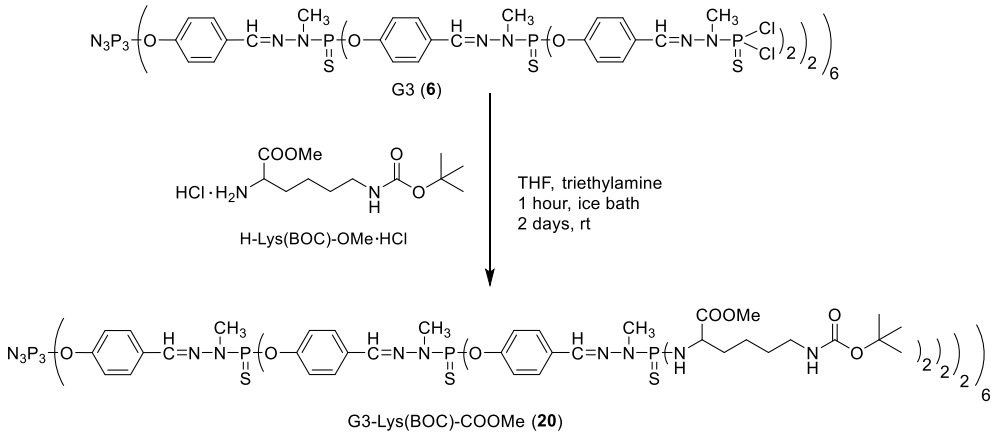

Scheme 2-24. Synthesis of G3-Lys(BOC)-COOMe (**20**) dendrimer.

At this stage, we successfully synthesized Gn-Lys(BOC)-COOMe dendrimers by functionalizing Gn PPH dendrimers with lysine amino acids from G0 to G3. Different reaction conditions were used to synthesize these dendrimers, for example, changing the temperature, the solvents and the time. All the products were well characterized by ^{1}H NMR, ^{31}P NMR, ^{13}C NMR (G0, G1 and G2) and MALDI-TOF (G0 and G1).

2.5.2 Synthesis of radical dendrimers Gn-Lys(PROXYL)-COOMe n=0,1 and Gn-Lys(PROXYL)-COOLi n=0,1

After obtaining Gn-Lys(BOC)-COOMe dendrimers from G0 to G3, we proceeded to prepare Gn-Lys(PROXYL)-COOMe radical dendrimers. First, it was necessary to deprotect the BOC group in order to get the amine group to couple with the 3-carboxy-PROXYL radical.

We started with dendrimer G0-Lys(BOC)-COOMe (**17**), using TFA as a deprotecting agent to remove BOC (Scheme 2-25). The reaction was performed in DCM overnight. Then, the solvent was removed under vacuum followed by washing with DCM and MeOH to remove the residual TFA, obtaining G0-Lys-COOMe (**21**) dendrimer. MALDI-TOF mass spectrometry clearly showed the molecular ion peak at 1090 m/z. Before NMR characterization, DIEA was added to neutralize the possible residual amount of TFA. ^{1}H NMR confirmed that the BOC group was removed due to the disappearance of the BOC peak at 1.4 ppm. ^{31}P NMR also showed only one phosphorus peak, at 16 ppm.

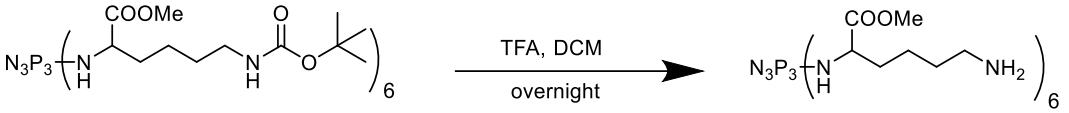

G0-Lys(BOC)-COOMe (**17**) G0-Lys-COOMe (**21**)

Scheme 2-25. Deprotection step of G0-Lys(BOC)-COOMe (**17**) dendrimer with TFA to obtain G0-Lys-COOMe (**21**).

G0-Lys-COOMe (**21**) dendrimer was then coupled to 3-carboxy-PROXYL using HATU as coupling agent (Scheme 2-26). The G0-Lys(PROXYL)-COOMe (**22**) product was obtained after purification by column chromatography on silica gel. The MALDI-TOF spectrum showed the molecular ion peak at 2100 m/z, which indicated that all the six chlorine atoms were substituted. We also could obtain the ^{1}H NMR spectrum after reduction of PROXYL radical units with phenylhydrazine, confirming the structure of G0-Lys(PROXYL)-COOMe. By EPR (Figure 2-14), we observed broad lines between the three main narrow lines resulting from some intramolecular spin-exchange interactions between radicals, indicating that radicals were anchored on the dendrimer surface and interacting between them. Also, quantitative EPR study showed that this radical dendrimer has the same area (double integral) than G0-Tyr(PROXYL)-COOMe and around 6 times more than PROXYL free radical.

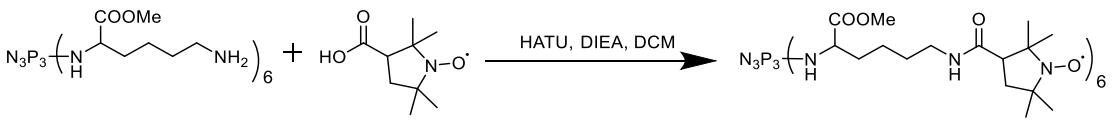

G0-Lys-COOMe (**21**) 3-carboxy-PROXYL G0-Lys(PROXYL)-COOMe (**22**)

Scheme 2-26. Synthesis of G0-Lys(PROXYL)-COOMe (**22**) radical dendrimer.

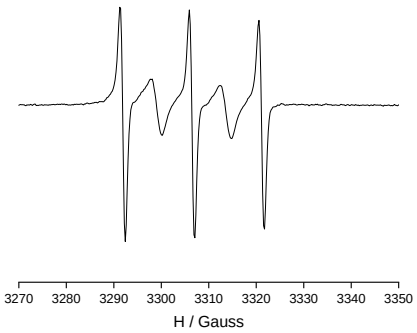

Figure 2-14. EPR spectrum of G0-Lys(PROXYL)-COOMe (**22**) dendrimer (300 K, in CH_2Cl_2)

The last step was the hydrolysis of G0-Lys(PROXYL)-COOMe (**22**) to obtain G0-Lys(PROXYL)-COOLi (**23**). It was dissolved in THF/H_2O (2/1, v/v). LiOH•H_2O was added to hydrolyze the ester of the radical dendrimers to get the corresponding lithium salt (Scheme 2-27). The excess of LiOH was removed by ultrafiltration, and the product was dried by the lyophilization. Although we obtained low amount of product we could characterize it by quantitative EPR study, showing the same area (double integral) than the precursor G0-Tyr(PROXYL)-COOLi and also around 6 times that of PROXYL free radical, confirming the integrity of the compound.

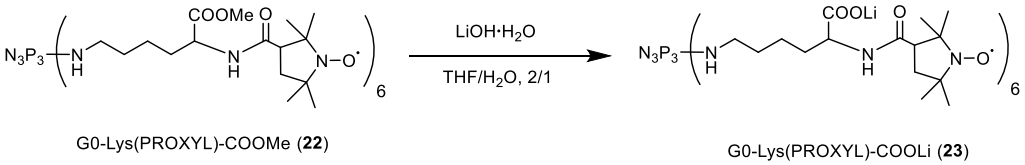

G0-Lys(PROXYL)-COOMe (**22**)

G0-Lys(PROXYL)-COOLi (**23**)

Scheme 2-27. Hydrolysis of G0-Lys(PROXYL)-COOMe (**22**) to obtain G0-Lys(PROXYL)-COOLi (**23**).

Then we moved to G1 dendrimer. We used the same methodology than for G0 to deprotect the BOC group of G1-Lys(BOC)-COOMe (**18**) (Scheme 2-28) and G2-Lys(BOC)-COOMe (**19**) and then couple 3-carboxy-PROXYL in a one-pot synthesis. During the reaction process, we observed the formation of some solid. After the reaction finished, we removed the excess of 3-carboxy-PROXYL by extraction with water/DCM and the solid produced was removed by filtration. We characterized the products obtained from G1-Lys(BOC)-COOMe (**18**) and G2-Lys(BOC)-COOMe (**19**) by EPR. In the EPR spectra, we could see two broad peaks between three main peaks indicating spin-exchange interaction between radicals (Figure 2-15). However, quantitative EPR and MALDI-TOF indicated that the two products were not obtained.

The MALDI-TOF spectrum of the possible G1-Lys(PROXYL)-COOMe product showed a maximum ion peak was at 496 m/z (Figure 2-16), much lower than the

corresponding molecular ion peak.

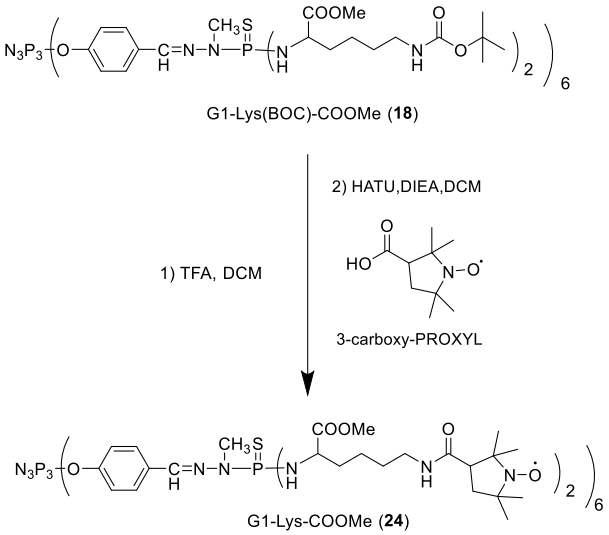

Scheme 2-28. BOC deprotection of G1-Lys(BOC)-COOMe (**18**) dendrimer and coupling with 3-carboxy-PROXYL in one-pot synthesis. The same procedure was followed for G2-Lys(BOC)-COOMe (**19**).

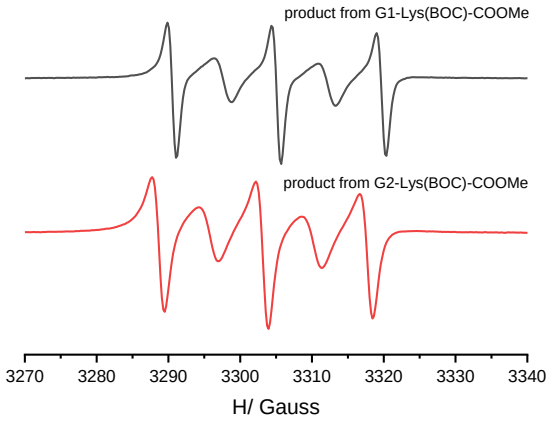

Figure 2-15. EPR spectra of the products obtained from G1-Lys(BOC)-COOMe (**18**) and G2-Lys(BOC)-COOMe (**19**) after deprotection with TFA and coupling with 3-carboxy-PROXYL (DCM, 300 K).

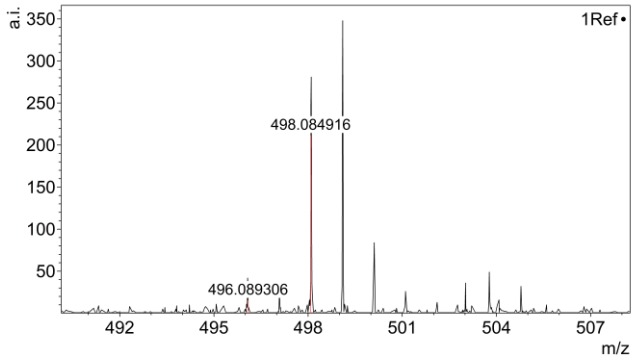

Figure 2-16. MALDI-TOF of the product obtained from G1-Lys(BOC)-COOMe (**18**) after BOC deprotection with TFA and coupling with 3-carboxy-PROXYL (positive matrix).

Quantitative EPR was performed to measure the number of radicals per molecule (Figure 2-17). The double integrals of the quantitative EPR spectra are listed in Table 2-4 and Table 2-5.

In Table 2-4, we have assumed that the products obtained were G1-Lys(PROXYL)-COOMe and G2-Lys(PROXYL)-COOMe. However, when we compared the EPR intensities taking into account the molecular weight of the G0-Lys(PROXYL)-COOMe, G1-Lys(PROXYL)-COOMe and G2-Lys(PROXYL)-COOMe, they were not proportional to the number of radical units. Considering there was precipitation during the deprotection process, we deduced that some kind of degradation release occurred probably due to the cleavage of P-N bond with acid, which resulted in the release of lysine amino acid, being the rest of the dendrimer insoluble. Thus, after removal of the precipitate, we presumably had in solution the lysine released. The lysine amino acid after BOC deprotection with TFA possessed two free amine groups so that two equivalents of 3-carboxy-PROXYL could couple to it, forming a diradical, in both cases for G1 and G2 species, that has a molecular weight 496.65 g/mol (Scheme 2-29) like the mass obtained by MALDI-TOF. This kind of diradical could also produce spin-exchange interaction between the radicals. Therefore, if we take into account that the product we had in solution was this kind of diradical, the concentration of radicals changed as well, as shown in Table 2-5. And now, the intensity of the quantitative EPR study shows good linearity with the concentration of radical (Figure 2-18) indicating that, most probably, we obtained this diradical species in both cases.

Therefore, we can conclude that it was not possible to deprotect G1-Lys(BOC)-COOMe (**18**) and G2-Lys(BOC)-COOMe (**19**) with TFA, since this acid produced some branch release of the dendrimer.

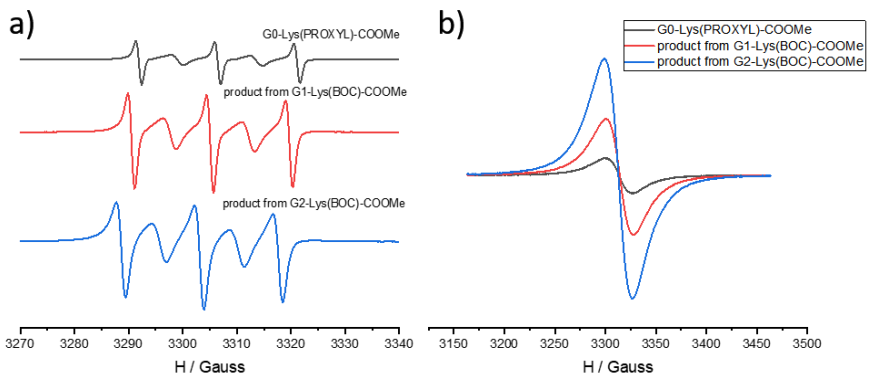

Figure 2-17. EPR spectra obtained from a quantitative EPR study in DCM at a) 300 K and b) 130 K of G0-Lys(PROXYL)-COOMe (**22**) and the products from G1-Lys(BOC)-COOMe (**18**) and G2-Lys(BOC)-COOMe (**19**) after BOC deprotection with TFA and coupling with 3-carboxy-PROXYL.

Table 2-4. Quantitative EPR data taking into account the molecular weight of G1-Lys(PROXYL)-COOMe and G2-Lys(PROXYL)-COOMe radical dendrimers as products. There is no correlation.

Sample[1]	Mw (g/mol)	Mass (mg)	Volume (mL)	Concentration of compound (mM)	Concentration of radical (mM)	EPR double integral (a.u.)
G0-PROXYL	2099.46	1.228	2.785	0.21	1.26	$2.9x10^6$
G1-PROXYL	5031.18	1.37	1.296	0.21	2.52	$9.9x10^6$
G2-PROXYL	12773	4.38	1.632	0.21	5.04	$21.6x10^6$

[1] Gn-PROXYL means Gn-Lys(PRXOYL)-COOMe

Table 2-5 Quantitative EPR data taking into account the molecular weight of diradical as products.

Sample[1]	Mw (g/mol)	Mass (mg)	Volume (mL)	Concentration of compound (mM)	Concentration of radical (mM)	EPR double integral (a.u.)
G0-PROXYL	2099.46	1.228	2.785	0.21	1.26	$2.9x10^6$
diradical	496.65	1.37	1.296	2.13	4.26	$9.9x10^6$
diradical	496.65	4.38	1.632	5.40	10.80	$21.6x10^6$

[1] G0-PROXYL means G0-Lys(PRXOYL)-COOMe

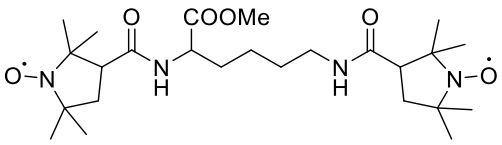

Diradical
Molecular Weight: 496.65 g/mol

Scheme 2-29. Chemical structure of the formed diradical from the lysine release of dendrimers G1-Lys(BOC)-COOMe (**18**) and G2-Lys(BOC)-COOMe (**19**) after TFA addition.

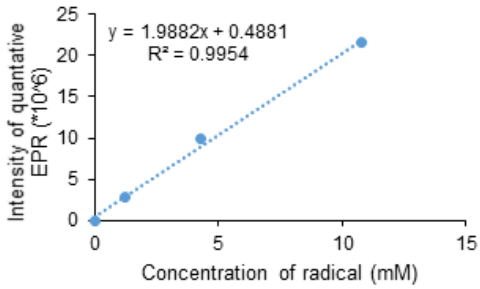

Figure 2-18. Double integral data of quantitative EPR spectra vs the concentration of radical taking into account the mass of G0-Lys(PROXYL)-COOMe (**22**) and the mass of diradical 496.65 g/mol for G1 and G2 derivatives (Table 2-5).

To achieve a better deprotection of the BOC group, we tried to find other deprotecting agents. We made different trials using different conditions reported in the literature such as H_3PO_4,[42] TsOH,[43,44] HCl,[45] or HNO_3[46] (Table 2-6). However, all these agents also produced some dendrimer degradation, which was confirmed by ^{31}P NMR spectra.

Finally, we successfully deprotected BOC group of G1-Lys(BOC)-COOMe (**18**) with $SnCl_4$[47,48] (Scheme 2-30). G1-Lys-COOMe (**24**) dendrimer was characterized by ^{31}P NMR and ^{1}H NMR. The ^{31}P NMR spectrum clearly showed the two phosphorus peaks at 8.4 ppm and 67 ppm, which indicated the dendrimer kept intact during the process. In the corresponding ^{1}H NMR spectrum, there was not the proton peak of BOC group at 1.4 ppm which meant the BOC was removed and the integrals of the proton peaks were in agreement with the theoretical values.

Table 2-6. Different conditions for the deprotection of G1-Lys(BOC)-COOMe (**18**).

Deprotecting reagents	eq	Temperature	time	Solvent	results
TFA	120	r.t.	overnight	$CHCl_3$	degraded
85% H_3PO_4[42]	120	0 ℃	7 h	Toluene	degraded
$TsOH{\cdot}H_2O$[43]	72	r.t.	overnight	MeOH	degraded
$TsOH{\cdot}H_2O$[44]	12	40 ℃ (microwave oven)	30 s	Toluene	No change
2 M HCl[45]	5217	r.t.	30 min	Dioxane	degraded
HNO_3[46]	42	0℃	1 h	CH_2Cl_2	degraded
$SnCl_4$[47,48]	12	r.t.	30 min	CH_2Cl_2	deprotected

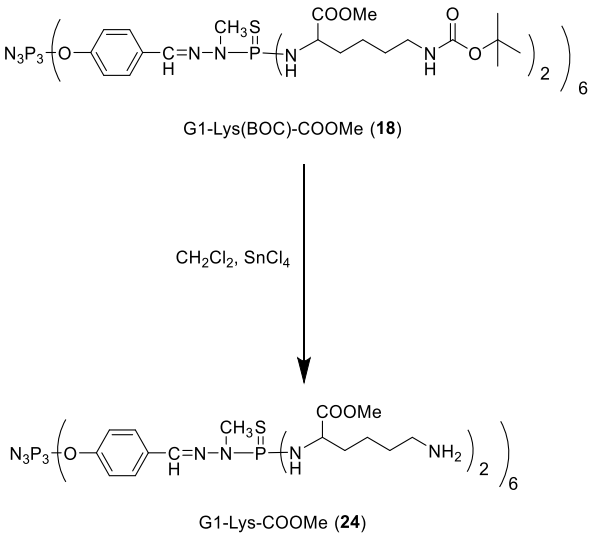

Scheme 2-30. Deprotection of G1-Lys(BOC)-COOMe (**18**) dendrimer with $SnCl_4$ to achieve G1-Lys-COOMe (**24**).

The deprotection reaction with $SnCl_4$ had to be optimized since we found that sometimes the dendrimer also degraded. Given that $SnCl_4$ can easily react with water from the solvent or air, producing hydrochloric acid, we performed the reaction with molecular sieves, which could catch the water. However, the reaction did not afford the good product. Finally, we performed the reaction under strict argon atmosphere with argon flow to protect the $SnCl_4$ from water, and the reaction afforded the product after 30 min as white solid in DCM. Therefore, even when $SnCl_4$ is used as deprotecting agent, it is also important to avoid the generation of acid.

After successful removal of the BOC group, we coupled the PROXYL radical on the surface of dendrimer G1-Lys-COOMe (**24**) with HATU as coupling agent (Scheme 2-31) to obtain G1-Lys(PROXYL)-COOMe (**25**) radical dendrimer. Since G1-Lys-COOMe (**24**) dendrimer has free amine end group, it is soluble in polar solvents, such as DMSO and MeOH. In this step, we performed the reaction in DMSO. After purification by extraction with DCM/H_2O and then by GPC column (Bio-Beads^{TM} S-X1), the product was characterized by ^{31}P NMR and EPR, confirming the successful formation of **25**. The ^{31}P NMR clearly showed the two phosphorus peaks at 8.4 ppm and 66.8 ppm. The EPR spectrum showed a broad single line overlapping the three narrow lines (Figure 2-19), like in G1-Tyr(PROXYL)-COOMe compound, which suggested the radicals were anchored on the surface of the dendrimer interacting among them (intramolecular spin-exchange interaction). In addition, the quantitative EPR study showed the same area (double integral) for G1-Lys(PROXYL)-COOMe (**25**) than for G1-Tyr(PROXYL)-

COOMe and around 12 times more than PROXYL free radical.

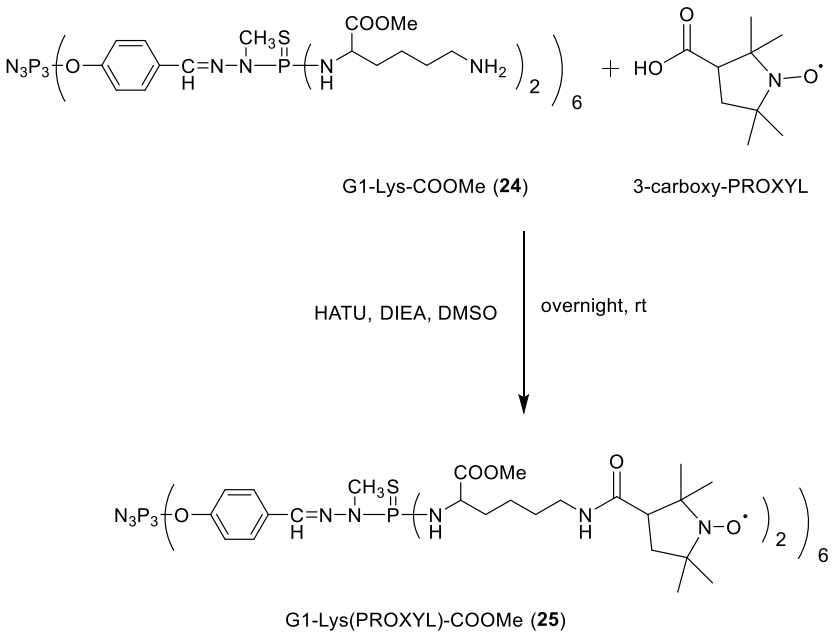

Scheme 2-31. Synthesis of G1-Lys(PROXYL)-COOMe (**25**) radical dendrimer.

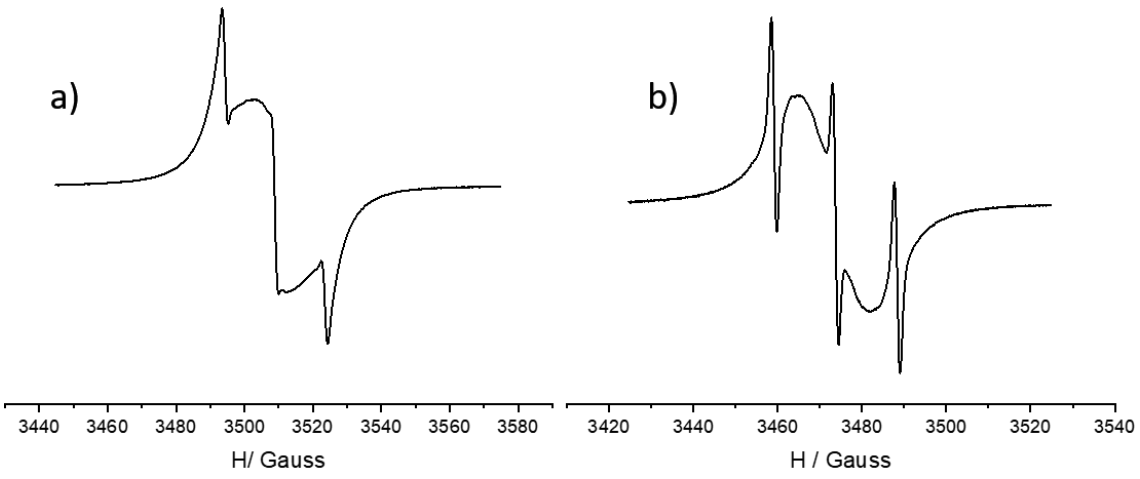

Figure 2-19. EPR spectra of G1-Lys(PROXYL)-COOMe (**25**) (a) and G1-Tyr(PROXYL)-COOMe (b) (CH_2Cl_2, 300 K).

Thus, Gn-Lys(BOC)-COOMe dendrimers from G0 to G3 have been prepared by functionalization of Gn dendrimer with lysine amino acid. After that, G0-Lys(BOC)-COOMe (**17**) dendrimer was deprotected with TFA and coupled with 3-carboxy-PROXYL. The obtained G0-Lys(PROXYL)-COOMe (**22**) radical dendrimer was well characterized by MALDI-TOF, ^{1}H NMR and EPR. However, when the same procedure was applied to G1- or G2-Lys(BOC)-COOMe dendrimers, the dendrimer degraded. Finally, G1-Lys(BOC)-COOMe (**18**) dendrimer was successfully deprotected with Lewis

acid $SnCl_4$, obtaining G1-Lys-COOMe (**24**) dendrimer and then G1-Lys(PROXYL)-COOMe (**25**) radical dendrimer was also successfully obtained after the radical coupling. Finally, G0-Lys(PROXYL)-COOMe (**22**) and G1-Lys(PROXYL)-COOMe (**25**) species were hydrolyzed to obtain their respective water-soluble -COOLi derivatives. In the case of G0 derivative, we could obtain G0-Lys(PROXYL)-COOLi (**23**) and for G1-Lys(PROXYL)-COOLi (**27**) species see Section 2.6.3.

The stability of the dendrimer under acid conditions is essential for its use under physiological conditions. Therefore, we decided to carefully study the stability of our dendrimers in these conditions.

2.6 Study of the stability of Gn-Lys(BOC)-COOMe (n=0,1,3) and G1-Tyr(BOC)-COOMe dendrimers under acid conditions

The deprotection process indicated that while G0 was not affected, the higher generation dendrimers were degraded by protonic acids, most probably through lysine release from P-N bond cleavage. In order to delve into this phenomenon, the stability of these Gn-Lys(BOC)-COOMe dendrimers under acid conditions was carefully checked. In particular, G0-Lys(BOC)-COOMe (**17**), G1-Lys(BOC)-COOMe (**18**) and G3-Lys(BOC)-COOMe (**20**) dendrimers. Besides, G1-Tyr(BOC)-COOMe dendrimer with tyrosine as linker was also studied for comparison purposes. Finally, the stability of G1-Lys(BOC)-COOLi and G1-Lys(PROXYL)-COOLi were investigated in aqueous solution to know at which pH the release occurred.

2.6.1 Stability of Gn-Lys(BOC)-COOMe (n=0,1,3) and G1-Tyr(BOC)-COOMe under acid conditions in organic solution

To study the stability of Gn-Lys(BOC)-COOMe dendrimers under acid conditions, particularly their P-N bond stability, we subjected these compounds to acid conditions in organic solvents, using trifluoroacetic acid (TFA). TFA was added to the different dendrimers in different amounts, namely 1, 5 and 20 equivalents (eq) per branch, in deuterated dichloromethane, and the process was followed by ^{31}P NMR and ^{1}H NMR. In

the case of G0- and G1-Lys(BOC)-COOMe dendrimers it could also be followed by MALDI-TOF and ESI-MS mass spectrometries and in generation G1 derivative by UV-Vis as well. In addition, some theoretical calculations have been started to illustrate the difference between behavior of G0- and G1-Lys(BOC)-COOMe against acid conditions.

In the case of **G0-Lys(BOC)-COOMe** (**17**), after the addition of 1, 5 or 20 eq per branch of TFA in CD_2Cl_2 we obtained the same kind of ^{31}P NMR spectra. In all cases, the ^{31}P NMR spectra showed a shift of the phosphorus peak of the N_3P_3 ring from 15 to 9.5 ppm, after 15 min (Figure 2-20). The maintenance of only one peak in the ^{31}P NMR spectra means that all branches continued fully substituted, with only one kind of functional group, but with different environment. The shift observed could be probably explained due to the protonation of the -NH- amine group connected to the N_3P_3 ring, thus, highly affecting the P chemical shift. The corresponding ^{1}H NMR spectra obtained (Figure 2-21) confirmed such an hypothesis, since the peak of the methyne proton (CH, *a*), the one closest to the -NH- group, shifted from 3.50 to 4.20 ppm. Also, the peak of the methyl ester group shifted from 3.68 to 3.79 ppm. Both spectral changes were well reproduced by simulating the theoretical ^{1}H NMR spectrum after the -NH- group protonation from G0-Lys(BOC)-COOMe (**17**), using the MestReNova software. Other possibility is the protonation of the N of the N_3P_3 ring. On the other hand, the peak of the *g* protons from the BOC group disappeared due to the BOC deprotection only when 5 or 20 equivalents of TFA were added to G0-Lys(BOC)-COOMe (**17**). In fact, with the addition of 1 eq per branch of TFA, the *g* protons from BOC groups were maintained.

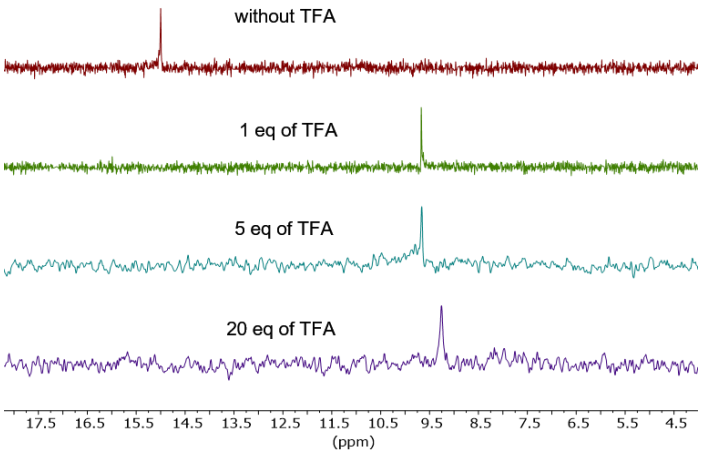

Figure 2-20. ^{31}P NMR of G0-Lys(BOC)-COOMe (**17**) with the different equivalents of TFA, measured after 15 min (CD_2Cl_2, 250 MHz).

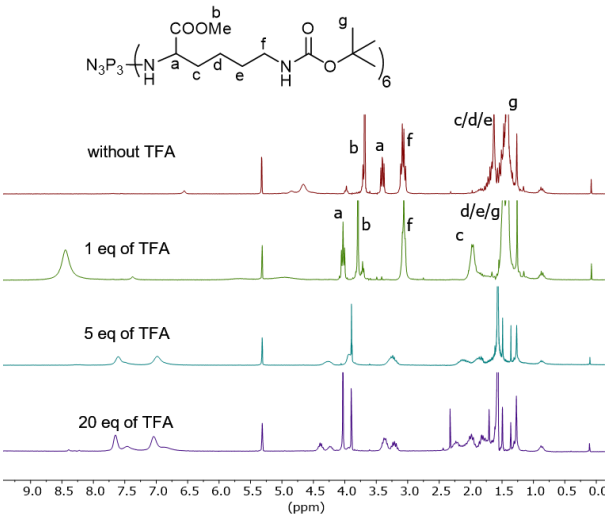

Figure 2-21. ^{1}H NMR of G0-Lys(BOC)-COOMe (**17**) with the different equivalents of TFA, measured after 15 min (CD_2Cl_2, 250 MHz).

We also characterized the G0-Lys(BOC)-COOMe (**17**) dendrimer by MALDI-TOF after the addition of 1 eq of TFA. The result showed the existence of the corresponding molecular ion at 1690 m/z in both mass spectra, before and after the addition of TFA (Figure 2-22).

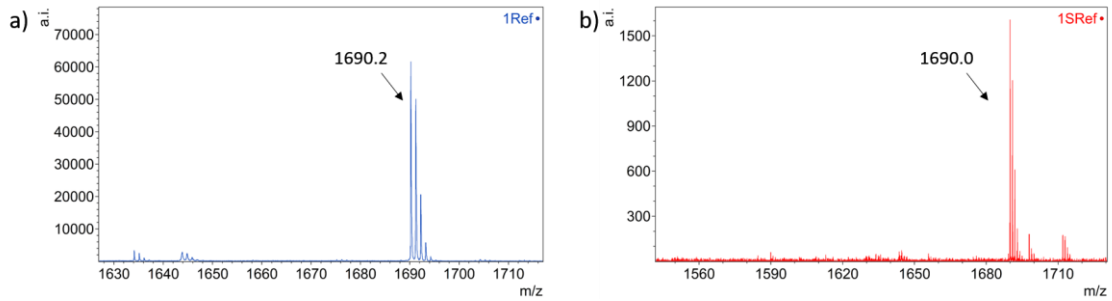

Figure 2-22. MALDI-TOF spectra of G0-Lys(BOC)-COOMe (**17**) without TFA (a) and with 1 eq of TFA (b).

The maintenance of the molecular ion of G0-Lys(BOC)-COOMe (**17**) was also confirmed by ESI-MS spectrometry after the addition of 0.1 % of TFA (36 eq) (Figure 2-23). Furthermore, the ESI-MS spectra of the samples without and with TFA showed practically the same spectral pattern, which means that the molecule analyzed in both cases was the same, and hence presents similar fragments. Therefore, both MALDI-TOF and ESI-MS spectra showed the existence of the molecular ion, after the addition of TFA. Although we have observed that the chemical shift of the phosphorus and protons can be affected under acid conditions for the N protonation, we can say that the G0-Lys(BOC)-COOMe (**17**) dendrimer is not degraded. Also, we have to say that, as it has been

explained in Section 2.5.2, the subsequent full functionalization of this dendrimer with PROXYL radicals was successfully performed (G0-Lys(PROXYL)-COOMe, **22**) which is another proof of the non-degradability of this zero-generation dendrimer.

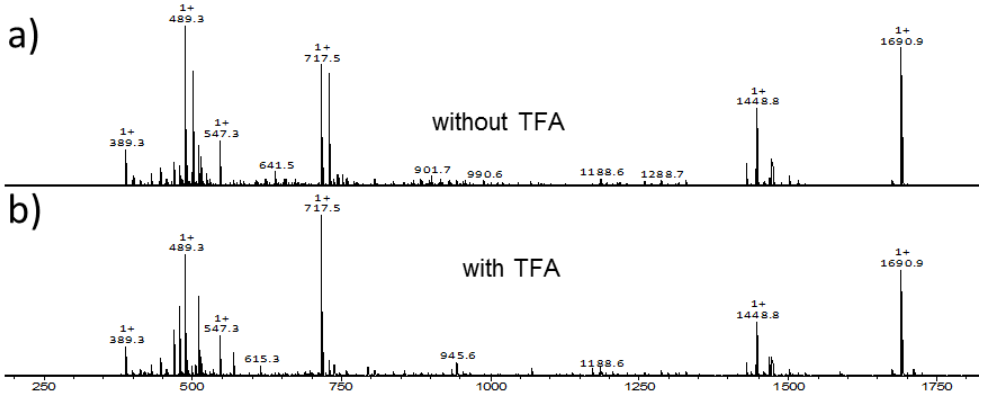

Figure 2-23. ESI-MS spectra of G0-Lys(BOC)-COOMe (**17**) without (a) and with (b) TFA 0.1%.

We proceeded in the same way with **G1-Lys(BOC)-COOMe** (**18**) dendrimer. It was dissolved in CD_2Cl_2 with different equivalents of TFA. Under 1 eq of TFA per branch, the G1-Lys(BOC)-COOMe (**18**) dendrimer was found to be stable for at least 5 h 45 min because the chemical shift of the phosphorus did not change (Figure 2-24(a)). Under 5 eq of TFA per branch, the exterior phosphorus peak from the P(S)NH part of the branches (from the anchoring of the lysine to the dendrimer through P-N bond) at 68 ppm started to disappear and split into two after 15 min, while two new peaks appeared at 59 and 72 ppm due to the cleavage of some P-N bonds (Figure 2-24(b)). After 4.5 hours, the peak at 68 ppm disappeared almost completely while new peaks close to 0 ppm, assigned to inorganic phosphate, and at -9.9 ppm and -22.3 ppm, associated with the formation of degradation products with –P-OH and –P=O moieties, appeared (Figure 2-24 (b)).[49] Instead, the peak from the P of the N_3P_3 core at 8.5 ppm was almost no affected. At higher TFA concentration, 20 eq of TFA, the degradation process was accelerated, as expected. The peak at 68 ppm disappeared completely in 15 minutes instead of taking more than 4.5 hours, and, additionally, the phosphorus peak of the N_3P_3 dendrimer core was also affected (Figure 2-24 (c)), indicating the inner layer of the dendrimer collapsed after the cleavage of P-N bonds from the exterior layer, at this high TFA concentration.

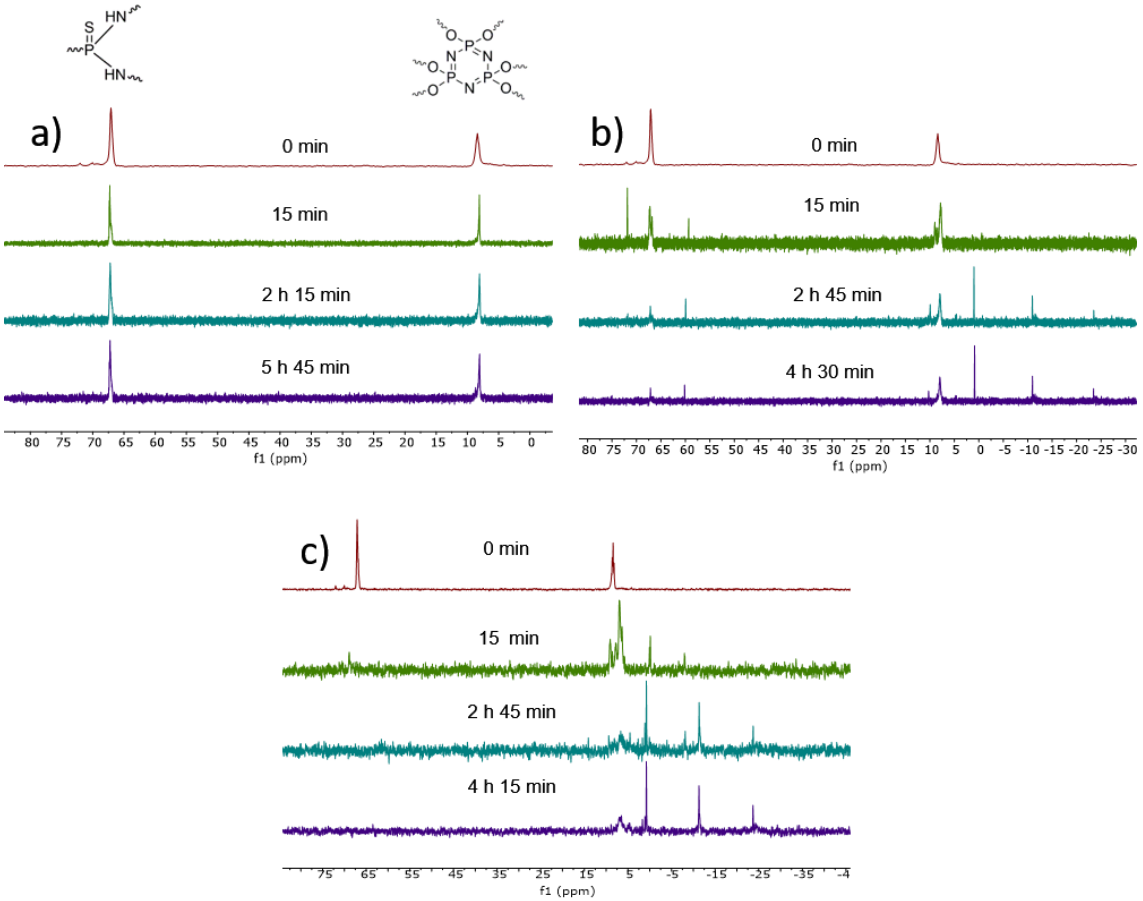

Figure 2-24. ^{31}P NMR spectra of G1-Lys(BOC)-COOMe (**18**) under 1 eq of TFA (a), 5 eq of TFA (b), and 20 eq of TFA (c) (CD_2Cl_2, 250 MHz).

The degradation process was also followed by ^{1}H NMR. When 1 eq of TFA was added, the ^{1}H NMR did not change apparently after 5 h 45 min (Figure 2-25(a)). However, with 5 eq of TFA, the peak of protons of methyl ester shifted from 3.62 to 3.84 ppm (Figure 2-25(b)). The ^{1}H NMR under 20 eq of TFA per branch also showed the chemical shift change of the methyl ester protons (Figure 2-25(c)), but the change was faster (faster degradation rate).

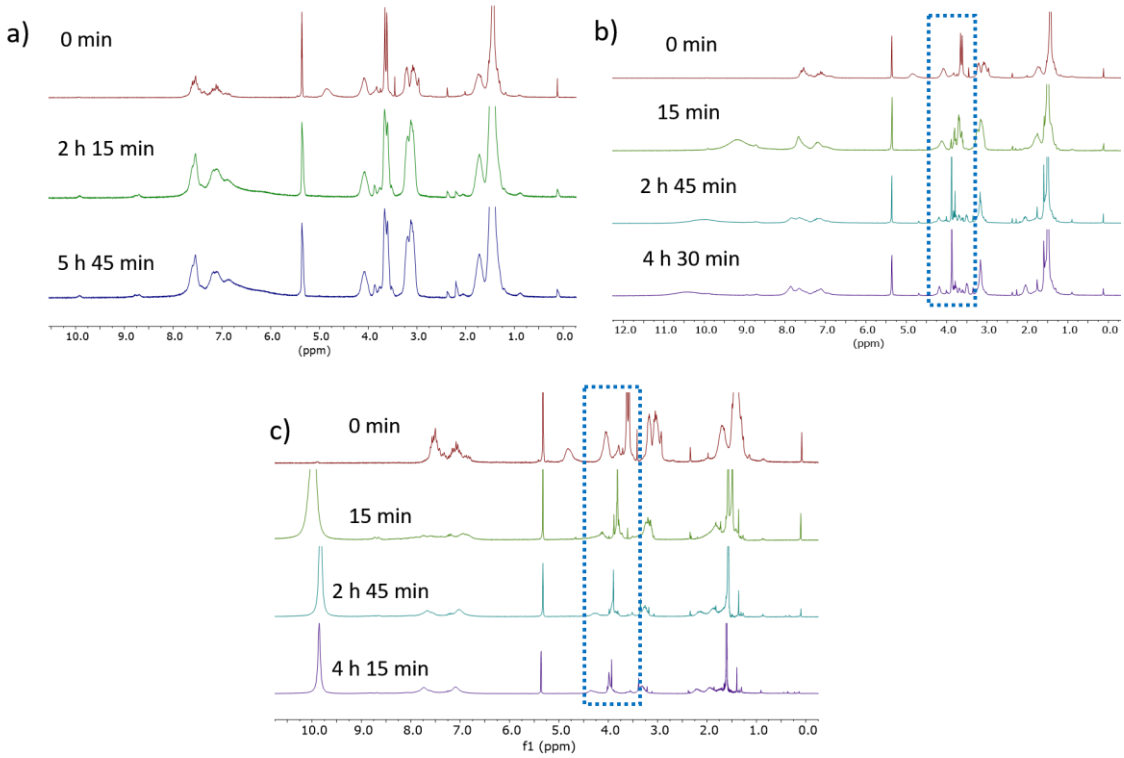

Figure 2-25. ^{1}H NMR spectra of G1-Lys(BOC)-COOMe (**18**) with 1 eq of TFA (a), 5 eq of TFA (b), and 20 eq of TFA (c) (CD_2Cl_2, 250 MHz).

The degradation process of G1-Lys(BOC)-COOMe (**18**) was also confirmed by diffusion-ordered spectroscopy (DOSY) method (Figure 2-26). DOSY seeks to separate the NMR signals of different species according to their diffusion coefficient. In DOSY spectra, chemical shift is along the detected f2 axis and diffusion coefficient is along the other f1 axis. The DOSY spectrum of G1-Lys(BOC)-COOMe (**18**) (Figure 2-26 (a)) presented only one diffusion coefficient, indicating the purity of only this species. However, after the addition of TFA, the DOSY spectrum showed two different diffusion coefficients (Figure 2-26 (b)), indicating the formation of different species from the degradation process due to the action of TFA.

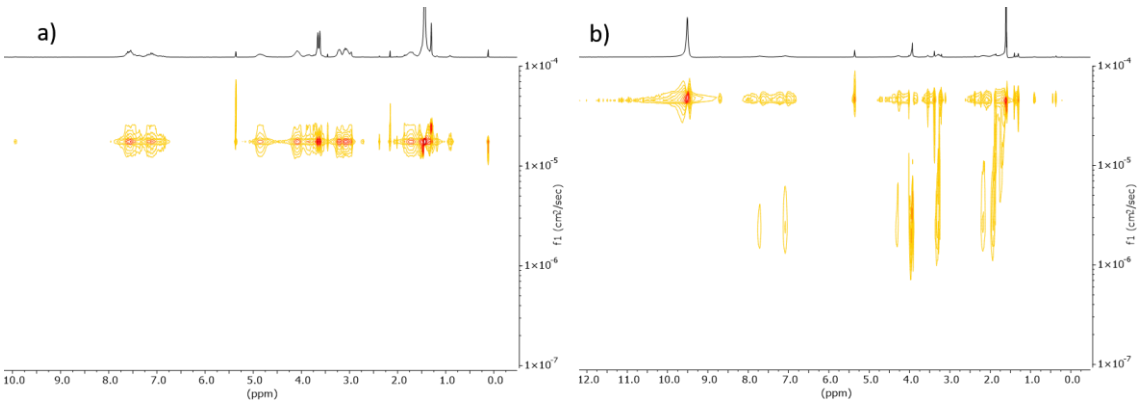

Figure 2-26. DOSY of G1-Lys(BOC)-COOMe (**18**) without TFA (a) and with TFA (b) (CD_2Cl_2, 250 MHz).

MALDI-TOF and ESI-MS mass spectrometries were also used to check the stability of G1-Lys(BOC)COOMe (**18**) dendrimer under acid conditions and to check the possible fragments produced. By MALDI-TOF, we observed the quasi-molecular ion at 4537.9 m/z (Figure 2-27 (a)) before the acid addition, that comes from the adduct of the molecular ion of G1-Lys(BOC)-COOMe (**18**) plus a sodium ion $[M+Na]^+$ = 4537.0, which disappeared after the TFA addition (Figure 2-27 (b)). More obvious, the quasi-molecular ion at 2269.0 m/z, which comes from the adduct of molecular weight of G1-Lys(BOC)-COOMe (**18**) plus a sodium ion and a proton $[M+Na+H]^{2+}$ = 2269.0 also disappeared, confirming the degradation of the dendrimer under these conditions.

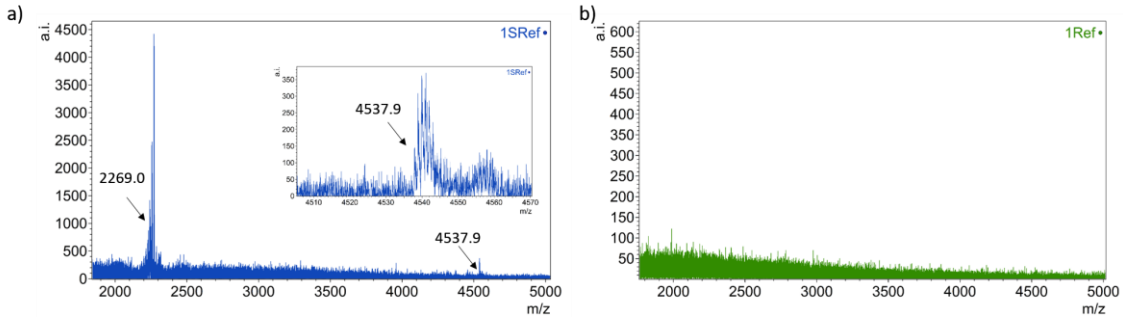

Figure 2-27. MALDI-TOF spectra of G1-Lys(BOC)-COOMe (**18**) without TFA (a) and with 20 eq of TFA (b).

The degradation of G1-Lys(BOC)-COOMe (**18**) is more clearly presented in the ESI-MS spectra (Figure 2-28). Without acid, the quasi-molecular ion peak of G1-Lys(BOC)-COOMe (**18**) dendrimer is reflected in the peak of m/z = 2280.0, that comes from the adduct $[M+Na+Na]^{2+}$. However, with the addition of 0.1% of TFA (50 eq) to G1-Lys(BOC)-COOMe (**18**) dendrimer, the quasi-molecular ion peak disappeared and

new peaks emerged, showing a different spectral pattern than the previous one without acid. This suggests the degradation of G1-Lys(BOC)-COOMe (**18**) dendrimer with the addition of TFA, and the new peaks that do not appear in the spectrum without TFA are likely the degradation products/fragments.

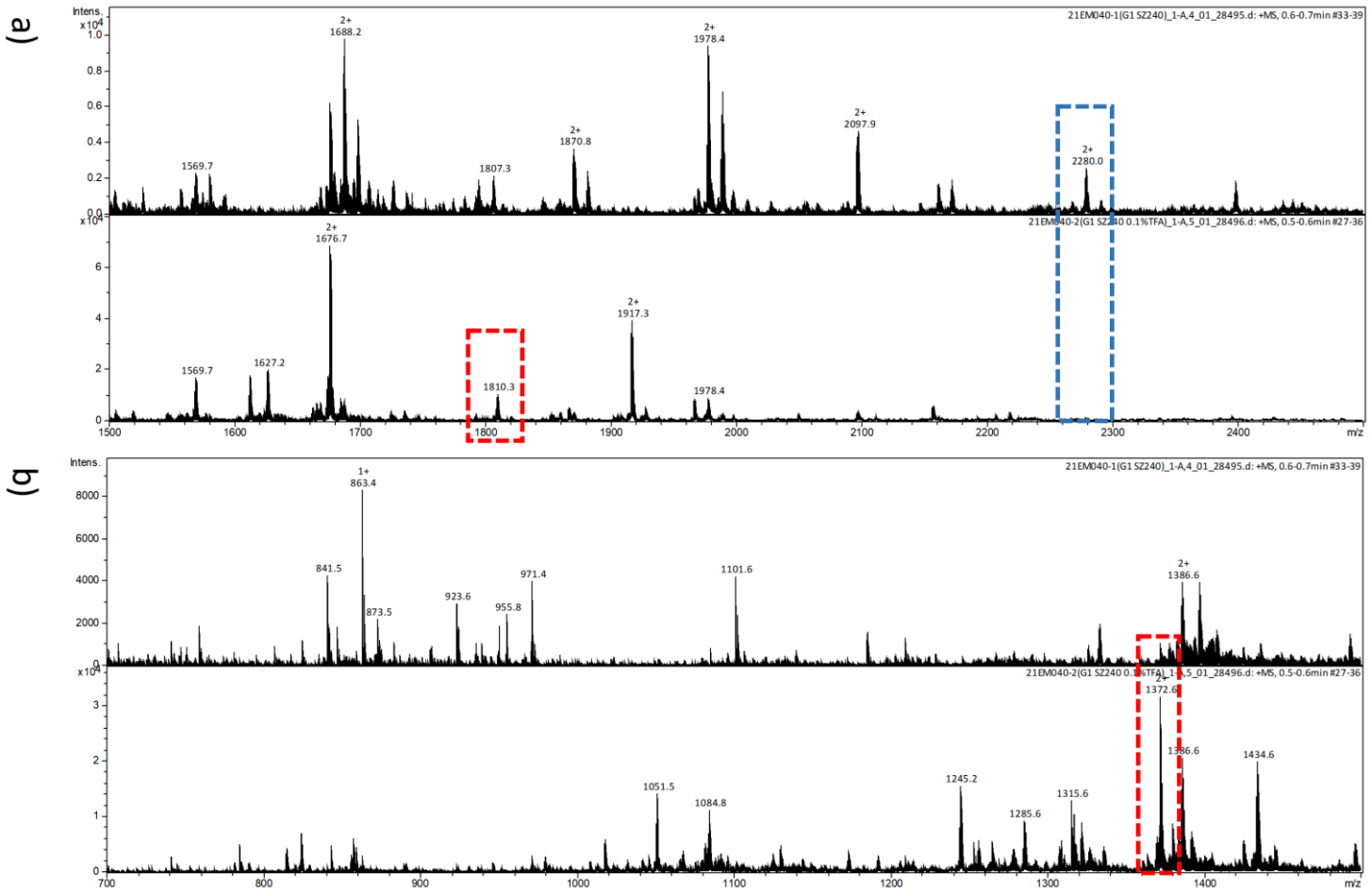

Figure 2-28. ESI-MS spectra of G1-Lys(BOC)-COOMe (**18**) dendrimer without TFA and with 0.1% of TFA (50 eq) in the range 1500-2500 m/z (a) and in the range 700-1500 m/z (b), measured in acetonitrile. In blue is marked the quasi-molecular ion peak adduct and in red two new peaks that we have analysed.

We tried to identify the possible degradation products, taking into account the mass and charge of the new peaks, trying to draw a possible chemical structure related to that m/z and finally checking or confirming the possible chemical structure by using a simulation program (Bruker Compass Data Analysis Version 4.1). We successfully found the chemical structures corresponding to the peaks of m/z = 1810.3 and m/z = 1372.6, which are shown in Scheme 2-32 as structures A and B, respectively, since the simulation matched perfectly with the experimental peaks, in all aspects: in terms of position (mass) and relative intensities (isotopic distribution/pattern). The comparison of the experimental and simulated peaks at m/z = 1810.3 and m/z = 1372.6 is shown in Figure 2-29 and Figure 2-30, respectively. The first one m/z = 1810.3 comes from the adduct of $[M_A+H+Na]^{2+}$, while the second one m/z = 1372.6 comes from the adduct of $[M_B+H+Na]^{2+}$.

The good match verifies/confirms the structures of the degradation products drawn (Scheme 2-32). According to the molecular structures found, we can say that with the addition of TFA to G1-Lys(BOC)-COOMe (**18**) there is some P-N bond cleavage or lysine release (red circles) that leads to phosphoric acid derivatives (from -P(S)-$(NH-R)_2$ group to HO-P(O)-(NH-R)) and hence dendrimer degradation, along with some BOC deprotection to the corresponding NH_2 groups (blue circles). That is, in the chemical structure of m/z = 1810.3 (structure A) there are 2 P-N bonds cleaved as well as 4 groups of BOC deprotected, while in the chemical structure of m/z = 1372.6 (structure B) there are 5 P-N bonds cleaved (5 lysine ligands released) as well as 5 groups of BOC deprotected.

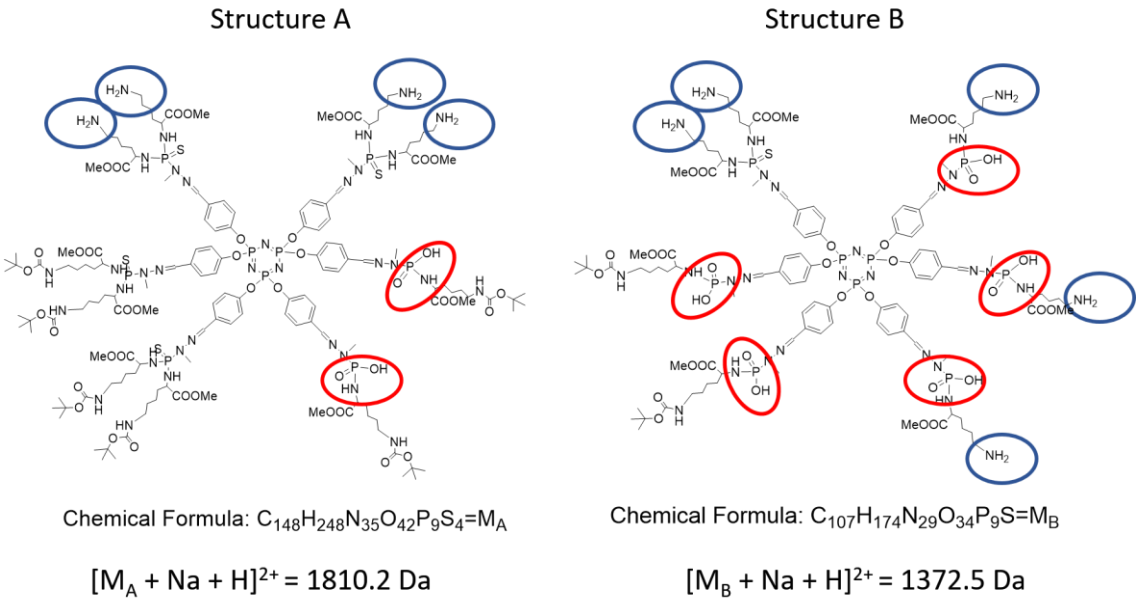

Scheme 2-32. The possible molecular structures corresponding to the peaks of m/z = 1810.3 (structure A) and 1372.6 (structure B) both with one Na^+ and one H^+ in their structure, i.e. $[M_{A/B}+ Na + H]^{2+}$. $[M_{A/B}]$ are the neutral isotopic mass peak of 100% intensity of structure A and B, respectively. In red circles the P-N cleavage of one lysine ligand from -P(S)-$(NH-R)_2$ group to HO-P(O)-(NH-R) and in blue circles the BOC groups deprotected to NH_2 groups.

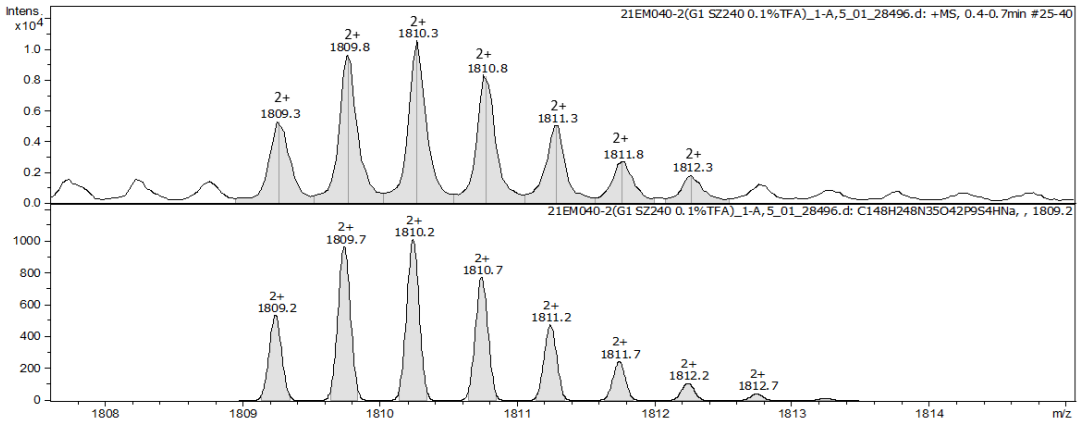

Figure 2-29. Comparison of the isotopic pattern obtained experimentally at m/z = $1810.3^{(2+)}$ (up) and the simulation (down) of the compound with chemical formula $C_{148}H_{248}N_{35}O_{42}P_9S_4HNa$ (structure A).

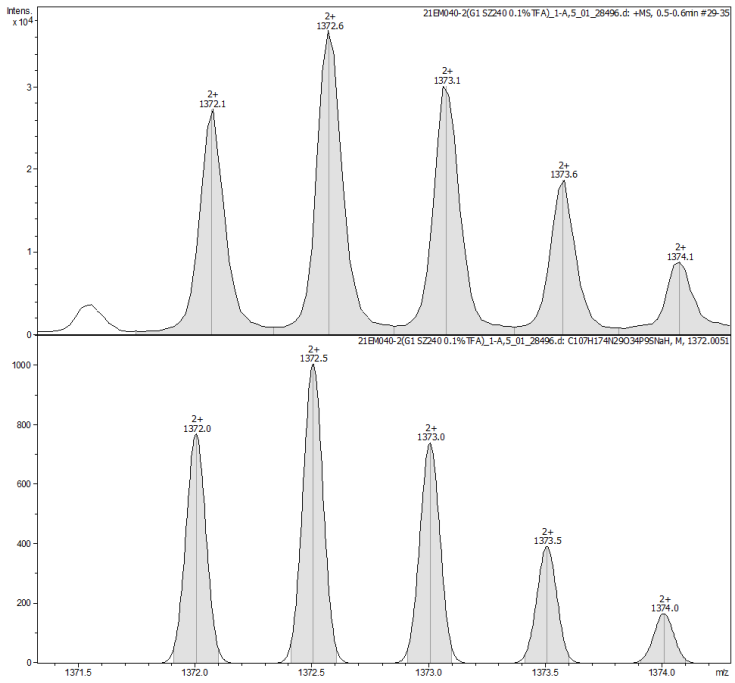

Figure 2-30. Comparison of the peak pattern obtained experimentally at m/z = $1372.6^{(2+)}$ (up) and the simulation (down) of the peak pattern of the compound with chemical formula $C_{107}H_{174}N_{29}O_{34}P_9SHNa$ (structure B).

The degradation process of the G1-Lys(BOC)-COOMe (**18**) was also followed by UV-Vis, under 20 eq of TFA (Figure 2-31 a). The absorbance of the main band of G1-Lys(BOC)-COOMe (**18**) dendrimer decreased along time, accompanied by a blue shift. In addition, an isosbestic point at around 270 nm was clearly observed in the UV-Vis spectra, which means the existence of two species A→B, indicating the gradual release of lysine amino acid. However, when we did the same study in dendrimer G1(**2**) (that does not present any P-N bond) for comparison, it remained intact under the same 20 eq of TFA (Figure 2-31 b), which meant that the G1(**2**) dendrimer was stable and not affected by these conditions. The NMR results also confirmed that G1 (**2**) was stable under acid conditions (Figure 2-32). According to the ^{31}P NMR spectrum of G1 (**2**) dendrimer with 20 eq of TFA, the two phosphorus peaks remained after 27 h 45 min, accompanied by a small shift of the peak corresponding to the dendrimer core from 8.6 to 5.9 ppm, that can be explained by the protonation of the nitrogen of the core (N_3P_3).

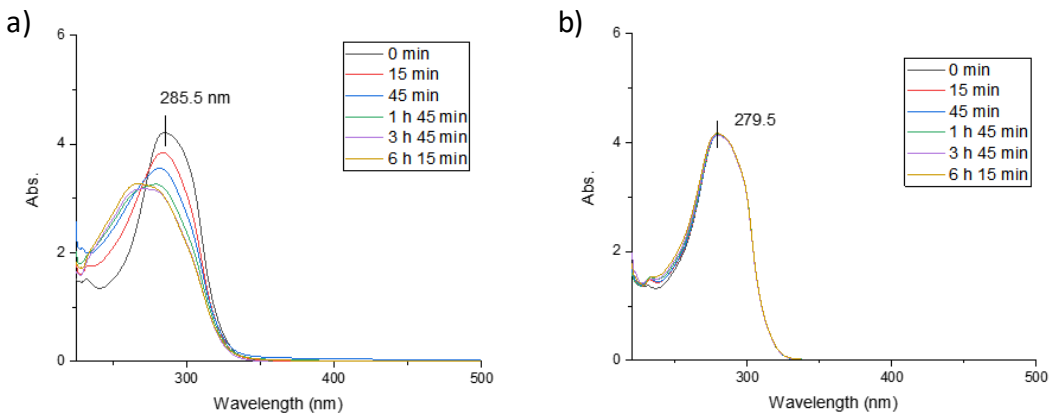

Figure 2-31. UV-Vis spectra of G1-Lys(BOC)-COOMe (**18**) dendrimer with P-N bonds (a) and G1 (**2**) dendrimer without P-N bonds (b) under 20 eq of TFA, along time.

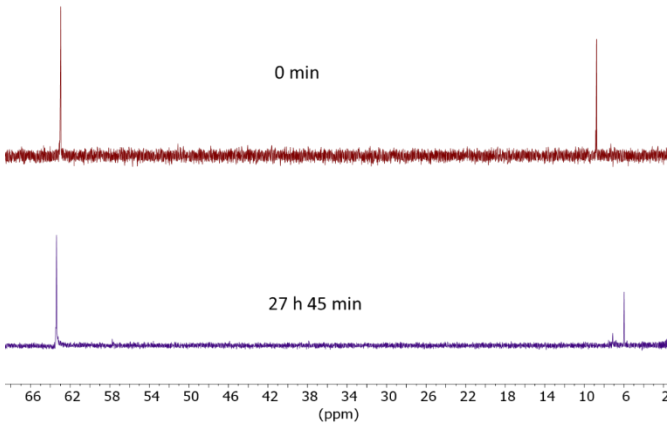

Figure 2-32. ^{31}P NMR of G1 (**2**) dendrimer with 20 eq of TFA, along time (CD_2Cl_2, 250 MHz).

Next, the highest dendrimer generation, **G3-Lys(BOC)-COOMe** (**20**) was also researched under acid conditions, with 5 and 20 eq of TFA in CD_2Cl_2. As showed in the ^{31}P NMR spectra of Figure 2-33a, after the addition of 5 eq of TFA per branch, the phosphorus peak at 67 ppm from the most exterior P (from the anchoring of the lysine to the dendrimer through P-N bond) gradually decreased together with the appearance of only a new peak at 73 ppm associated with very few P-N bond fractures, while the rest of the peaks (the inner P from P-O bonds) were not affected. With the same number of TFA equivalents added (5 eq), G1 dendrimer showed faster change than G3 since it showed almost the complete disappearance of the 68 ppm P peak and more additional peaks from cleavage. This difference could result from the higher density of branches in G3 that could protect the P-N bonds from cleavage. This interesting result provides us another possibility to control the degradation of the PPH dendrimers. The changes observed by ^{1}H NMR (Figure 2-33b) were also small.

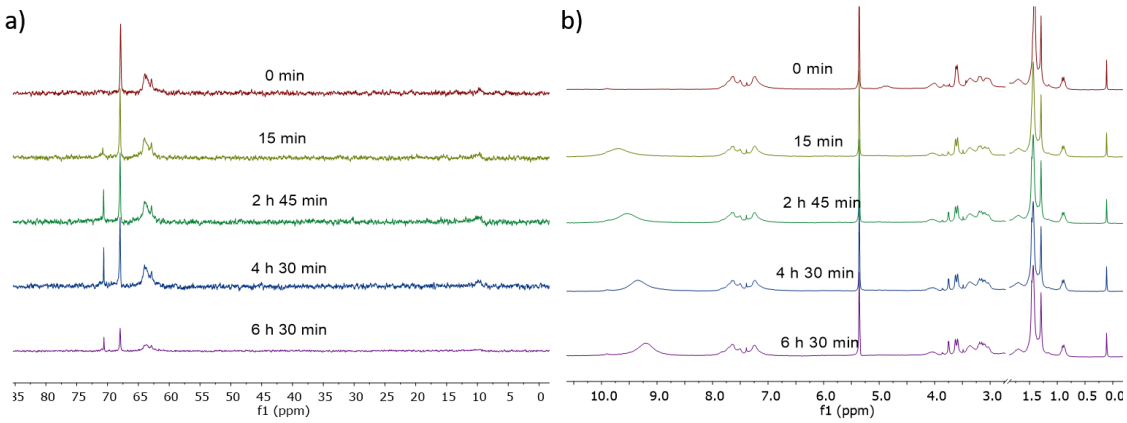

Figure 2-33. a) ^{31}P NMR spectra (LB=3) and b) ^{1}H NMR spectra along time of G3-Lys(BOC)-COOMe (**20**) dendrimer with 5 eq of TFA (CD_2Cl_2, 250 MHz).

Under 20 eq of TFA per branch (Figure 2-34), the dendrimer degraded faster compared with 5 eq of TFA. The peak of phosphorus of the most exterior layer (from P-N bonds) disappeared quickly, after 15 min, while new peaks between 5 and -25 ppm appeared from degradation products with –P-OH and –P=O moieties (Figure 2-34a), like in G1 dendrimer. These results indicate that both G1-Lys(BOC)-COOMe (**18**) and G3-Lys(BOC)-COOMe (**20**) dendrimers have similar degradation mechanisms and produced similar fragments. The corresponding ^{1}H NMR (Figure 2-34b) showed the same tendency than in G1 dendrimer, the methyl ester peak at 3.7 ppm shifted to 3.9 ppm after 15 min. The peak at 10.1 ppm gradually shifted to 9.8 ppm after 5 h 30 min, which can be explained by the complex formed from free amine and trifluoroacetic acid. When the content of amine increased, the formed complex shifted more to higher field. A similar phenomenon was observed in the ^{1}H NMR spectrum of G3-Lys(BOC)-COOMe (**20**) with 5 eq of TFA (Figure 2-33b), and G1-Lys(BOC)-COOMe (**18**) with 20 eq of TFA (Figure 2-25b).

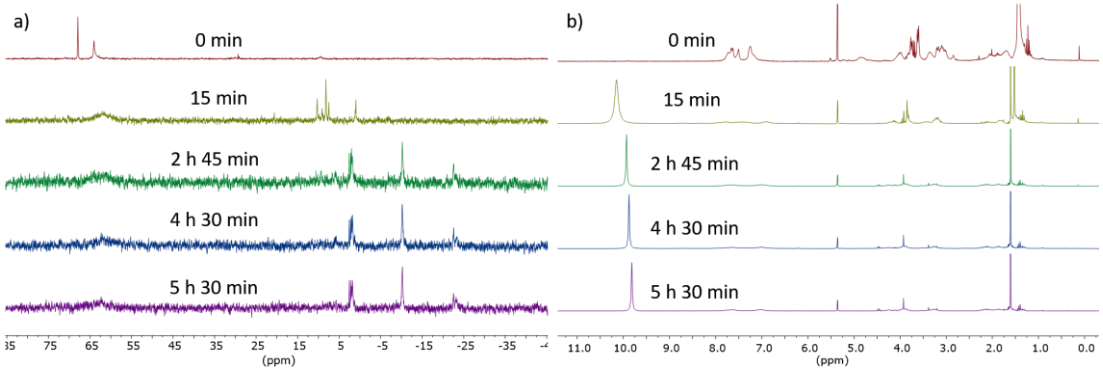

Figure 2-34. ^{31}P NMR (a) and ^{1}H NMR (b) along time of G3-Lys(BOC)-COOMe (**20**) with 20 eq of TFA (CD_2Cl_2, 250 MHz).

From these studies, we can observe that during the degradation process of G3-Lys-(BOC)-COOMe (**20**) dendrimer, the P-N bonds are more easily cleaved than the other phosphorous bonds (the P-O bonds), i.e. the P-O bonds are more stable than the P-N bonds, since the peak of the P-O bond at around 65 ppm could still be observed after the most exterior P-N bond cleaved with the TFA addition of as high as 20 eq per branch (Figure 2-34a). To further check the different stability between the P-N and P-O bonds, the same experiment was performed with G1-Tyr(BOC)-COOMe dendrimer with only P-O bonds in its structure, since the anchoring of tyrosine amino acid is through a P-O bond.

Therefore, we proceeded to add 20 eq of TFA per branch to **G1-Tyr(BOC)-COOMe** dendrimer, in CD_2Cl_2 and followed up by ^{31}P NMR along time (Figure 2-35a). We could see that the two phosphorus peaks (at 65 ppm and 8 ppm) were maintained after 4.5 hours although the ^{31}P NMR spectrum was not as clean as the starting one, because the solubility of the compound changed after BOC group deprotection by TFA, appearing two phases. We used DMSO-d_6 to dissolve the bottom layer to obtain the ^{1}H NMR and ^{31}P NMR spectra and we observed a clean ^{31}P NMR spectrum, with the two phosphorus peaks and the same chemical shift than at beginning (Figure 2-35b). The ^{1}H NMR also confirmed the integrity of the dendrimer, just showing the loss of the BOC group (Figure 2-36). This result showed that the G1-Tyr(BOC)-COOMe dendrimer (with tyrosine coupled through P-O bond) can remain stable even at 20 eq of TFA, on the contrary to G1- or G3-Lys(BOC)-COOMe dendrimers (with lysine coupled through P-N bond), which showed a complete disappearance of the P-N phosphorous peak in only 15 minutes.

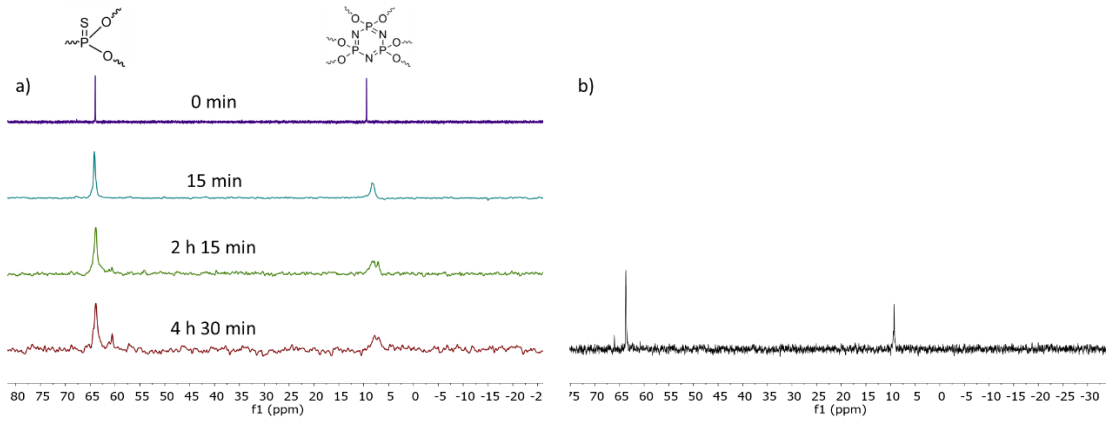

Figure 2-35. ^{31}P NMR spectra of G1-Tyr(BOC)-COOMe with 20 eq of TFA per branch a) along time, in CD_2Cl_2 at 250 MHz and b) in DMSO-d_6 after 4.5 h from the TFA addition.

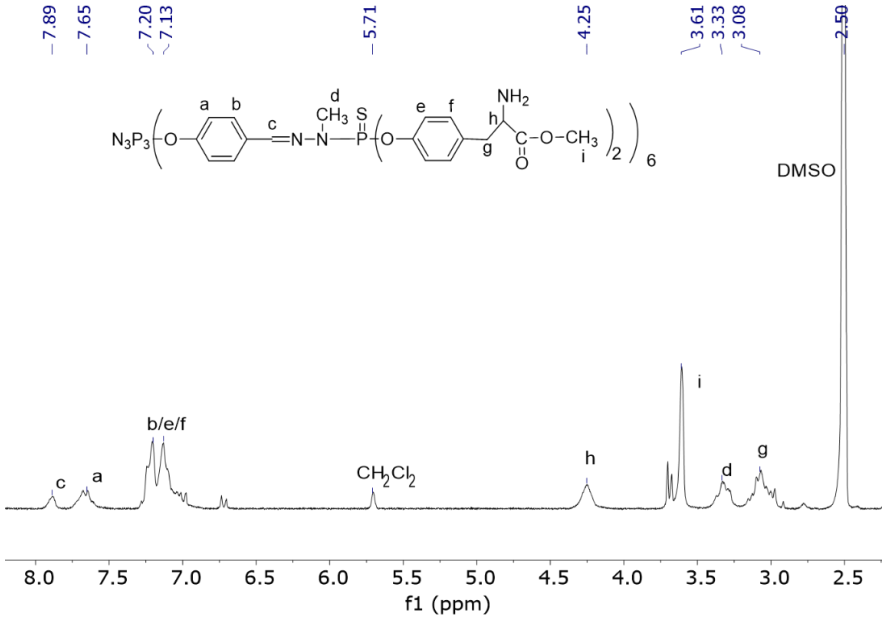

Figure 2-36. ^{1}H NMR of G1-Tyr-COOMe in DMSO-d_6 after addition of 20 eq of TFA.

G0-Lys(BOC)-COOMe (**17**) and G1-Tyr(BOC)-COOMe dendrimers are found to be stable in organic solvent with TFA. However, G1-Lys(BOC)-COOMe (**18**) and G3-Lys(BOC)-COOMe (**20**) dendrimers are not stable with 5 eq and 20 eq of TFA per branch. The different stability comes from the different bond with phosphorous atoms: P-O bonds are more resistant to hydrolysis than P-N bonds.[50]

2.6.2 Stability of G1-Lys(BOC)-COOLi in aqueous solution

After the previous study of dendrimers degradation under acid conditions in organic solutions we would like to know the stability in aqueous solution and at which pH the degradation (P-N bond cleavage) occurred. For this reason, methyl ester groups of G1-Lys(BOC)-COOMe (**18**) dendrimer were hydrolyzed with excess of LiOH (Scheme 2-33). The resulting water-soluble G1-Lys(BOC)-COOLi dendrimer solution was under very basic conditions (pH 14 with the pH indicator test paper, and pH > 12 by the pH-meter). In these conditions, it is important to highlight that G1-Lys(BOC)-COOLi dendrimer was stable according to its ^{31}P NMR spectrum showing its corresponding two characteristic phosphorous peaks (Figure 2-37a). Then, we decreased the pH in two different ways, giving both methods the same result. We used citric acid buffer and citric acid directly to the basic solution to gradually decrease the pH, by one hand, and, also, we carried out a dialysis process to gradually eliminate the excess of LiOH base. When the pH was decreased, the dendrimers presented degradation according to its ^{31}P NMR

(Figure 2-37 b) when the pH value reached 7.7. Also, at this pH there appeared a white solid (see image of Figure 2-37).

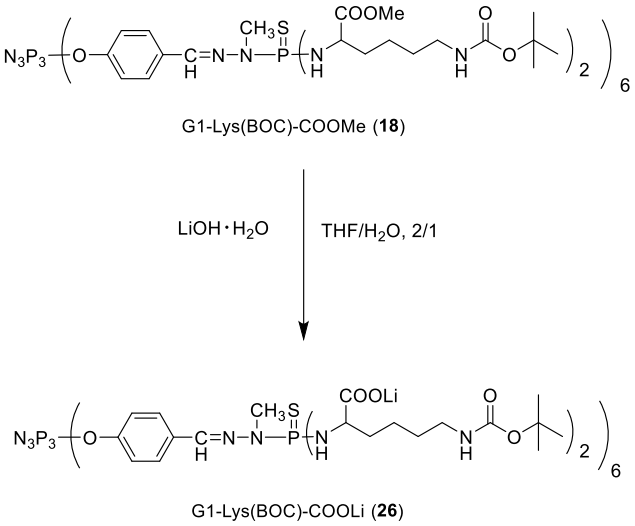

Scheme 2-33. Hydrolysis of G1-Lys(BOC)-COOMe (**18**) dendrimer with LiOH to obtain G1-Lys(BOC)-COOLi (**26**) dendrimer.

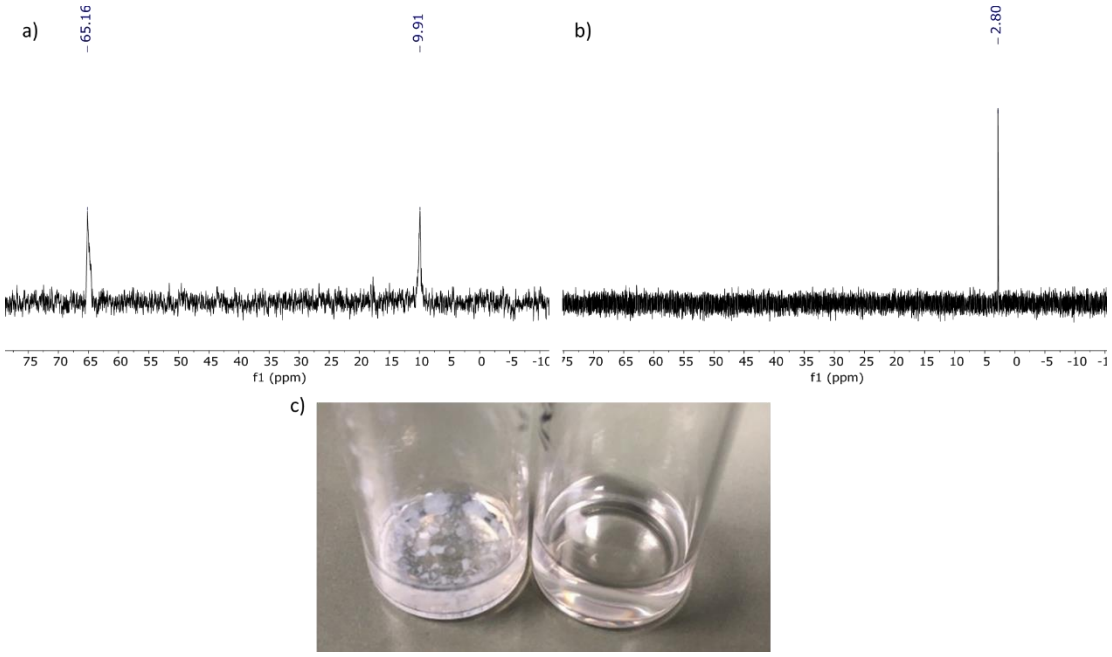

Figure 2-37. ^{31}P NMR spectra of G1-Lys(BOC)-COOLi (**26**) in basic conditions (a) and at pH 7.7 (b), and the image of G1-Lys(BOC)-COOLi (**26**) at different aqueous solutions (c) (left, at pH 7.7; right, in basic conditions).

On the contrary to G1-Tyr(BOC)-COOLi, which was stable in aqueous solutions showing intact ^{31}P NMR spectra, G1-Lys(BOC)-COOLi (**26**) was stable only until pH ca. 7.7 and then degraded.

2.6.3 Stability of G1-Lys(PROXYL)-COOLi in aqueous solution checked by EPR.

We also followed the stability of G1-Lys(PROXYL)-COOMe (**25**) radical dendrimer in aqueous solution by hydrolysis with LiOH to obtain the corresponding water-soluble dendrimer G1-Lys(PROXYL)-COOLi (**27**).

As we have radicals anchored, they can be used as labels to check the integrity of the dendrimer structure by EPR. We can follow the intramolecular spin-exchange interaction among the radicals. This parameter can help us to determine the cleavage of the P-N bonds since if we have the radicals anchored we observed interaction but if they are released from the dendrimer (through lysine-PROXYL release) they are free in solution without the possibility to interact intramolecularly among them.

First, G1-Lys(PROXYL)-COOMe (**25**) radical dendrimer was hydrolyzed with LiOH aqueous solution (0.4 M) and the solution was checked by EPR without further purification. In these conditions, when the aqueous solution was alkaline, we observed broad peaks in the EPR spectrum because of the intramolecular interaction between the radicals (Figure 2-38). Then, the pH of the solution was adjusted to 6 with citrate acid solution (2 M) and citrate buffer (pH 5.0). The EPR spectrum under those conditions did not present spin-exchange interaction between the radicals but only the three-line spectrum, indicating that the lysine-PROXYL radicals were released and were free in solution. In fact, the shape of the EPR spectrum is similar to the spectrum of PROXYL-Lys-COOMe (**11**) ligand (Figure 2-9). The loss of the characteristic broad interaction peaks in the EPR spectrum confirmed that the release occurred above pH = 6.

The stability study of G1-Lys(PROXYL)-COOLi (**27**) confirmed that this lysine functionalized PPH dendrimer was stable in alkaline solution, but it can degrade (P-N bond cleavage and lysine release) when the acidity of the solution increases.

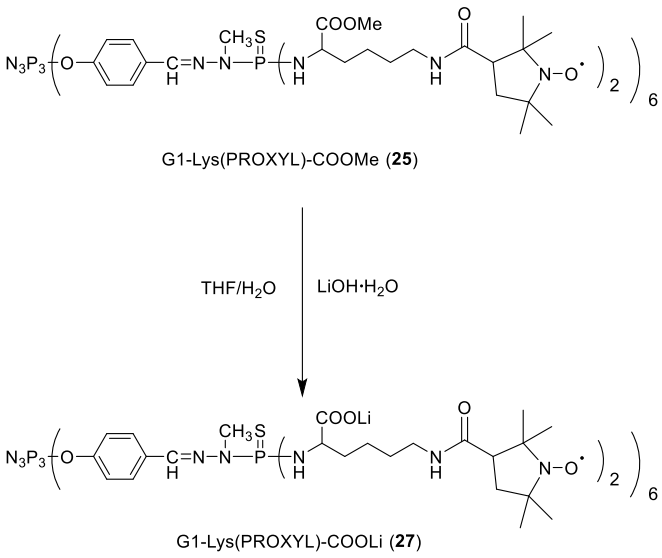

Scheme 2-34. Hydrolysis of G1-Lys(PROXYL)-COOMe (**25**) to afford G1-Lys(PROXYL)-COOLi (**27**).

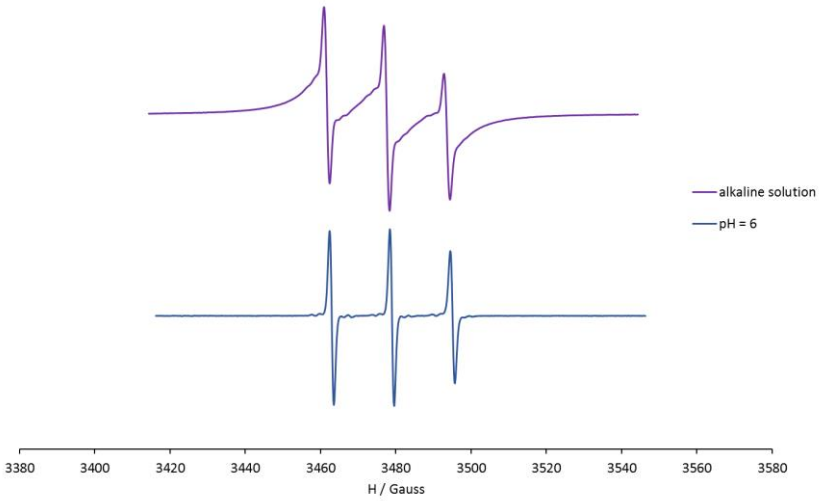

Figure 2-38. EPR spectra of G1-Lys(PROXYL)-COOLi (**27**) in alkaline solution and solution at pH=6.

Therefore, due to the problem of stability in water, these lysine-functionalized PPH dendrimers are not suitable for using as MRI contrast agents. They suffer P-N bond cleavage (lysine release), in particular generation G1 at pH = 7.7. However, this new property can be used to prepare pH controlled degradable dendrimers (or pH controlled release). In fact, if we anchor instead of an organic radical, a different analyte (like a drug) to these lysine-functionalized PPH dendrimers, we may control their release by controlling the pH, opening a new field of research.

We have seen that different amino acid-functionalized PPH dendrimers have different stabilities. Related phenomenon has been researched in polyphosphazene

polymers and cyclotriphosphazene ring. For cyclotriphosphazene ring, the hydrolysis behavior of different aminocyclotriphosphazenes ($(NPR_2)_3$) were researched, where R was = NH_2, $NHCH_3$, $NHCH_2COOC_2H_5$, $NHCH_2CONHCH_3$, $N_2C_3H_3$ (imidazolyl), $NHCH_2CF_3$, $NHCH_2C_6H_5$, NHC_6H_5, NC_4H_4 (pyrrolyl), NC_4H_8 (pyrrolidino), NC_5H_{10} (piperidino) and NC_4H_8O (morpholino). The ease of hydrolysis in aqueous dioxane varied depending on the amino group. A possible mechanism was that one amino group was removed remaining $N_3P_3R_5OH$.[17]

Amino acid substituted polyphosphazenes were also investigated with different poly(amino acid ester)phosphazenes. The hydrolysis experiment showed that the hydrolysis rate was related to the volume of the ester end group and the type of group linked to the α-carbon atom of the amino acid. Three different hydrolysis pathways were proposed for poly(amino acid ester)phosphazenes.[51] Overall, some polyphosphazenes with different side groups have been prepared. However, only few of the side groups promote the sensitivity to hydrolysis of polyphosphazane.[52] Generally, the side groups linked to the phosphorus through oxygen (P-O bonds) are more resistant to hydrolysis than those linked through nitrogen (P-N bonds).[50]

It is important to say that there are some examples of PPH dendrimers substituted with amine derivatives that have showed good stability under acid conditions. For example, amine (ethylenediamine) substituted PPH dendrimers can successfully form ammonium derivatives with acid to promote the water solubility,[18,53,54] without showing degradability. This indicates that the P-N bond degradability also depends on the type of amine anchored. This is the first time that this P-N bond related degradability is researched in PPH dendrimers, opening a possibility to control such release by pH.

2.6.4 Preliminary theoretical calculations

In order to analyze the different behavior between G0- and G1-Lys(BOC)-COOMe in acidic conditions, theoretical calculations on related model systems for these two dendrimers are performed, in collaboration with Prof. Gregori Ujaque from the Department of Chemistry of the Autonomous University of Barcelona. The reaction implies the activation (decomposition) of the phosphine group. Therefore, the phosphine moieties were modelled according to their nature in the dendrimer for G0 and G1, respectively. The model for G0 was selected considering the central aromatic ring N_3P_3 with two out of three P atoms bearing two methylamines and the third P bearing two

aminoesters. Regarding G1, it was modelled by considering the $R_2P(S)(R_1)_2$ system, where R_1 = −NH(CH(CH_3)(COOMe)) and R_2 = −N(CH_3)(NCH_2); see Figure 2-39. Theoretical calculations are based on the DFT framework including solvent effects by means of a continuum model. Acidic conditions are modelled by adding an explicit H_3O^+ molecule; in some cases, one, two or three additional explicit water molecules are also included in the model.

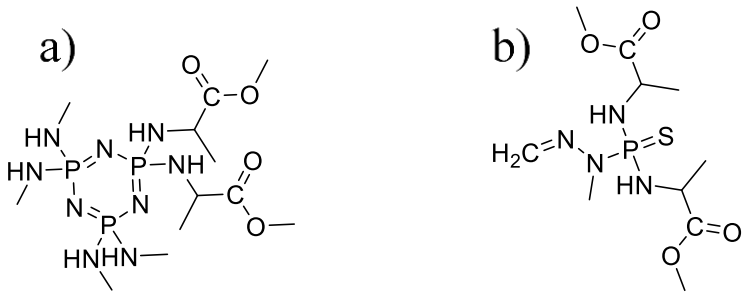

Figure 2-39. Schematic representation of the models employed for DFT calculations for G0 (a) and G1(b) dendrimers, respectively.

A conformational analysis of the system was initially carried out. The best conformer for each of the modelled dendrimers was selected to perform the subsequent mechanistic analysis. Both model dendrimers can be protonated in several places. The first analysis was done to locate the basic site with larger proton affinity (since this must be the first protonated group). For model of G0, it was an aminoester group, whereas for model G1 it was the amine group bonded to the P atom.

The preliminary results for the activation of G0 by water addition to the phosphine under acidic conditions show that the reaction takes place in two steps: water addition and amine release. The Gibbs energy barrier is found to be higher than 40 kcal/mol. Therefore, this is an unfeasible process even at the harsh conditions that the reaction takes place (over 100 ºC). The mechanistic analysis of the model system for G1 shows that there are at least three reactions step involved. Nevertheless, the highest barrier found for this reaction is around 30 kcal/mol; this is a better agreement with the experimental reaction conditions. Additional calculations are needed to have a complete description of the overall processes, but these preliminary results suggest that the activation of the phosphine group of model G1 is much more feasible than that of model G0.

2.7 Conclusions

- The synthesis of five generations of PPH dendrimers (G0 to G4) has been carried out, improving the methodology previously used in the group. All the synthesized dendrimers have been well characterized by NMR (^{1}H, ^{31}P, ^{13}C) and IR.
- Previously, in our group, tyrosine linker had been anchored to four generations of PPH dendrimers through P-O bonds, then they were fully functionalized with PROXYL radicals and finally made them water-soluble (Gn-Tyr(PROXYL)-COOLi, n=0-3) radical dendrimers. We have characterized these compounds by EPR, DLS and TEM and their cytotoxicity and MRI relaxivity have been studied. They are fully soluble in water, do not show cytotoxicity, and their relaxivity per molecule is high, increasing from 1.39 $mM^{-1}s^{-1}$ in G0 to 12.96 $mM^{-1}s^{-1}$ in G3. Remarkably, the relaxivity of G3-Tyr(PROXYL)-COOLi is four times higher than the most widely used Gd-DPTA in clinics (3.2 $mM^{-1}s^{-1}$).
- Lysine has been also chosen as a linker to prepare water-soluble radical dendrimers. Lysine has been properly anchored to four generations of PPH dendrimers through P-N bonds (Gn-Lys(BOC)-COOMe, n=0-3). However, only water-soluble G0-Lys(PROXYL)-COOLi radical dendrimer has been achieved since generations higher than G0 show lysine release through P-N bond cleavage under acid conditions preventing the obtaining of radical dendrimers with this linker in them. We have been also able to prepare G1-Lys(PROXYL)-COOMe radical dendrimer avoiding protonic acids in the deprotection step, however it suffers P-N bond cleavage during the last hydrolysis step, at pH 7.7. Although PPH-Lys based generations higher than G0 cannot be used to prepare water-soluble contrast agents, interestingly, they might be used to prepare pH-controlled degradable dendrimers or dendrimers with pH-controlled release properties, opening a new field of research.
- Through stability studies under acid conditions of lysine and tyrosine functionalized dendrimers: i) G0-Lys generation (P-N bond from P of the N_3P_3 core), ii) G1-/G3-Lys generations (P-N bond from P of the branches) and iii) G1-Tyr generation (with only P-O bonds), we have demonstrated that P-O bonds are more stable and more resistant to hydrolysis than P-N bonds, and that P-N bonds

from P of the core are more stable than P-N bonds from P of the branches. Preliminar theoretical calculations have been performed comparing the different P-N bond stability between G0 and G1-Lys dendrimers, suggesting that the activation of the phosphine group of model G1 is much more feasible than that of model G0.

2.8 References

(1) Launay, N.; Caminade, A. M.; Majoral, J. P. Synthesis of Bowl-Shaped Dendrimers from Generation 1 to Generation 8. *J. Organomet. Chem.* **1997**, *529* (1–2), 51–58.

(2) Turrin, C.-O.; Chiffre, J.; de Montauzon, D.; Daran, J.-C.; Caminade, A.-M.; Manoury, E.; Balavoine, G.; Majoral, J.-P. Phosphorus-Containing Dendrimers with Ferrocenyl Units at the Core, within the Branches, and on the Periphery. *Macromolecules* **2000**, *33* (20), 7328–7336.

(3) Terenziani, F.; Parthasarathy, V.; Pla-Quintana, A.; Maishal, T.; Caminade, A.-M.; Majoral, J.-P.; Blanchard-Desce, M. Cooperative Two-Photon Absorption Enhancement by Through-Space Interactions in Multichromophoric Compounds. *Angew. Chemie* **2009**, *121* (46), 8847–8850.

(4) Pérez-Anes, A.; Spataro, G.; Coppel, Y.; Moog, C.; Blanzat, M.; Turrin, C.-O.; Caminade, A.-M.; Rico-Lattes, I.; Majoral, J.-P. Phosphonate Terminated PPH Dendrimers: Influence of Pendant Alkyl Chains on the in Vitro Anti-HIV-1 Properties. *Org. Biomol. Chem.* **2009**, *7* (17), 3491.

(5) Caminade, A. M.; Majoral, J. P. Multiplurifunctionalized Phosphorus Dendrimers: Selective Functionalization of P(X)CL 2 Terminal Groups. *Phosphorus, Sulfur Silicon Relat. Elem.* **2014**, *189* (X), 1132–1143.

(6) Lartigue, M. L.; Slany, M.; Caminade, A. M.; Majoral, J. P. Phosphorus-Containing Dendrimers: Synthesis of Macromolecules with Multiple Tri- and Tetrafunctionalization. *Chem. - A Eur. J.* **1996**, *2* (11), 1417–1426.

(7) Majoral, J. P.; Caminade, A. M. Dendrimers Containing Heteroatoms (Si, P, B, Ge, or Bi). *Chem. Rev.* **1999**, *99* (3), 845–880.

(8) Prévôté, D.; Caminade, A. M.; Majoral, J. P. Phosphate-, Phosphite-, Ylide-, and Phosphonate-Terminated Dendrimers. *J. Org. Chem.* **1997**, *62* (14), 4834–4841.

(9) Launay, N.; Slany, M.; Caminade, A. M.; Majoral, J. P. Phosphorus-Containing Dendrimers. Easy Access to New Multi-Difunctionalized Macromolecules. *J. Org. Chem.* **1996**, *61* (11), 3799–3805.

(10) Prévôté, D.; Le Roy-Gourvennec, S.; Caminade, A.-M.; Masson, S.; Majoral, J.-P. Application of the Horner-Wadsworth-Emmons Reaction to the

Functionalization of Dendrimers: Synthesis of Amino Acid Terminated Dendrimers. *Synthesis (Stuttg).* **1997**, *1997* (10), 1199–1207.

(11) Lloveras, V.; Liko, F.; Muñoz-Gómez, J. L.; Veciana, J.; Vidal-Gancedo, J. Redox-Active PTM Radical Dendrimers as Promising Multifunctional Molecular Switches. *Chem. Mater.* **2019**, *31* (22), 9400–9412.

(12) Hadad, C.; Majoral, J. P.; Muzart, J.; Caminade, A. M.; Bouquillon, S. First Phosphorous D-Xylose-Derived Glycodendrimers. *Tetrahedron Lett.* **2009**, *50* (17), 1902–1905.

(13) De Jong, E. R.; Deloch, N.; Knoll, W.; Turrin, C. O.; Majoral, J. P.; Caminade, A. M.; Köper, I. Synthesis and Characterization of Bifunctional Dendrimers: Preliminary Use for the Coating of Gold Surfaces and the Proliferation of Human Osteoblasts (HOB). *New J. Chem.* **2015**, *39* (9), 7194–7205.

(14) Caminade, A. M.; Majoral, J. P. Water-Soluble Phosphorus-Containing Dendrimers. *Prog. Polym. Sci.* **2005**, *30* (3–4), 491–505.

(15) Leclaire, J.; Dantras, E.; Lacabanne, C. Surface , Core , and Structure Modifications of Phosphorus- Containing Dendrimers . Influence on the Thermal Stability. **2003**, *59*, 3965–3973.

(16) Allcock, H. R.; Singh, A.; Ambrosio, A. M. A.; Laredo, W. R. Tyrosine-Bearing Polyphosphazenes. *Biomacromolecules* **2003**, *4* (6), 1646–1653.

(17) Allcock, H. R.; Fuller, T. J.; Matsumura, K. Hydrolysis Pathways for Aminophosphazenes. *Inorg. Chem.* **1982**, *21* (2), 515–521.

(18) Loup, C.; Zanta, M.; Caminade, A. Preparation of Water-Soluble Cationic Phosphorus-Containing Dendrimers. *Chem. Eur . J.* **1999**, *5* (12), 3644–3650.

(19) Ledall, J.; Fruchon, S.; Garzoni, M.; Pavan, G. M.; Caminade, A. M.; Turrin, C. O.; Blanzat, M.; Poupot, R. Interaction Studies Reveal Specific Recognition of an Anti-Inflammatory Polyphosphorhydrazone Dendrimer by Human Monocytes. *Nanoscale* **2015**, *7* (42), 17672–17684.

(20) Görgülü, A. O.; Koran, K.; Özen, F.; Tekin, S.; Sandal, S. Synthesis, Structural Characterization and Anti-Carcinogenic Activity of New Cyclotriphosphazenes Containing Dioxybiphenyl and Chalcone Groups. *J. Mol. Struct.* **2015**, *1087*, 1–10.

(21) El Brahmi, N.; El Kazzouli, S.; Mignani, S. M.; Essassi, E. M.;

Aubert, G.; Laurent, R.; Caminade, A. M.; Bousmina, M. M.; Cresteil, T.; Majoral, J. P. Original Multivalent Copper(II)-Conjugated Phosphorus Dendrimers and Corresponding Mononuclear Copper(II) Complexes with Antitumoral Activities. *Mol. Pharm.* **2013**, *10* (4), 1459–1464.

(22) Zhu, J.; Gale, E. M.; Atanasova, I.; Rietz, T. A.; Caravan, P. Hexameric Mn II Dendrimer as MRI Contrast Agent. *Chem. - A Eur. J.* **2014**, *20* (44), 14507–14513.

(23) Badetti, E.; Lloveras, V.; Muñoz-Gómez, J. L.; Sebastián, R. M.; Caminade, A. M.; Majoral, J. P.; Veciana, J.; Vidal-Gancedo, J. Radical Dendrimers: A Family of Five Generations of Phosphorus Dendrimers Functionalized with TEMPO Radicals. *Macromolecules* **2014**, *47* (22), 7717–7724.

(24) Badetti, E.; Lloveras, V.; Wurst, K.; Sebastián, R. M.; Caminade, A. M.; Majoral, J. P.; Veciana, J.; Vidal-Gancedo, J. Synthesis and Structural Characterization of a Dendrimer Model Compound Based on a Cyclotriphosphazene Core with TEMPO Radicals as Substituents. *Org. Lett.* **2013**, *15* (14), 3490–3493.

(25) Lloveras, V.; Vidal-Gancedo, J. Polyphosphorhydrazone-Based Radical Dendrimers. *Molecules* **2021**, *26* (5), 1230.

(26) Hadad, C.; Majoral, J. P.; Muzart, J.; Caminade, A. M.; Bouquillon, S. First Phosphorous D-Xylose-Derived Glycodendrimers. *Tetrahedron Lett.* **2009**, *50* (17), 1902–1905.

(27) Sebastián, R. M.; Magro, G.; Caminade, A. M.; Majoral, J. P. Dendrimers with N,N-Disubstituted Hydrazines as End Groups, Useful Precursors for the Synthesis of Water-Soluble Dendrimers Capped with Carbohydrate, Carboxylic or Boronic Acid Derivatives. *Tetrahedron* **2000**, *56* (34), 6269–6277.

(28) Jain, K.; Kesharwani, P.; Gupta, U.; Jain, N. K. Dendrimer Toxicity: Let's Meet the Challenge. *Int. J. Pharm.* **2010**, *394* (1–2), 122–142.

(29) Pinto, L. F.; Lloveras, V.; Zhang, S.; Liko, F.; Veciana, J.; Muñoz-Gómez, J. L.; Vidal-Gancedo, J. Fully Water-Soluble Polyphosphorhydrazone-Based Radical Dendrimers Functionalized with Tyr-PROXYL Radicals as Metal-Free MRI T1 Contrast Agents. *ACS Appl. Bio Mater.* **2020**, *3* (1), 369–376.

(30) Bhattacharjee, S. DLS and Zeta Potential - What They Are and What They Are Not? *J. Control. Release* **2016**, *235*, 337–351.

(31) Amaral, S. P.; Tawara, M. H.; Fernandez-Villamarin, M.; Borrajo, E.; Martínez-Costas, J.; Vidal, A.; Riguera, R.; Fernandez-Megia, E. Tuning the Size of Nanoassembles: A Hierarchical Transfer of Information from Dendrimers to Polyion Complexes. *Angew. Chemie - Int. Ed.* **2018**, *57* (19), 5273–5277.

(32) Liu, K.; Zhang, X.; Tao, X.; Yan, J.; Kuang, G.; Li, W.; Zhang, A. Lysine-Based Dendronized Polymers with Preferred Chirality. *Polym. Chem.* **2012**, *3* (10), 2708–2711.

(33) Sosnovsky, G. A Critical Evaluation of the Present Status of Toxicity of Aminoxyl Radicals. *J. Pharm. Sci.* **1992**, *81* (6), 496–499.

(34) Ankel, E. G.; Lai, C.-S.; Hopwood, L. E.; Zivkovic, Z. Cytotoxicity of Commonly Used Nitroxide Radical Spin Probes. *Life Sci.* **1987**, *40* (5), 495–498.

(35) Krishnamurthy, S. S.; Sau, A. C.; Woods, M. Cyclophosphazenes; 1978; pp 41–112.

(36) Lee, S. B.; Song, S.-C.; Jin, J.-I.; Sohn, Y. S. Thermosensitive Cyclotriphosphazenes. *J. Am. Chem. Soc.* **2000**, *122* (34), 8315–8316.

(37) Allen, C. W. Regio- and Stereochemical Control in Substitution Reactions of Cyclophosphazenes. *Chem. Rev.* **1991**, *91* (2), 119–135.

(38) Bobbitt, J. M.; Eddy, N. A.; Cady, C. X.; Jin, J.; Gascon, J. A.; Gelpí-Dominguez, S.; Zakrzewski, J.; Morton, M. D. Preparation of Some Homologous TEMPO Nitroxides and Oxoammonium Salts; Notes on the NMR Spectroscopy of Nitroxide Free Radicals; Observed Radical Nature of Oxoammonium Salt Solutions Containing Trace Amounts of Corresponding Nitroxides in an Equilibrium R. *J. Org. Chem.* **2017**, *82* (18), 9279–9290.

(39) Sen, V. D.; Tikhonov, I. V.; Borodin, L. I.; Pliss, E. M.; Golubev, V. A.; Syroeshkin, M. A.; Rusakov, A. I. Kinetics and Thermodynamics of Reversible Disproportionation-Comproportionation in Redox Triad Oxoammonium Cations - Nitroxyl Radicals - Hydroxylamines. *J. Phys. Org. Chem.* **2015**, *28* (1), 17–24.

(40) Tikhonov, I. V.; Sen', V. D.; Borodin, L. I.; Pliss, E. M.; Golubev, V. A.; Rusakov, A. I. Effect of the Structure of Nitroxyl Radicals on the Kinetics of Their Acid-Catalyzed Disproportionation. *J. Phys. Org. Chem.* **2014**, *27* (2), 114–120.

(41) Allcock, H. R. Recent Advances in Phosphazene (Phosphonitrilic)

Chemistry. *Chem. Rev.* **1972**, *72* (4), 315–356.

(42) Li, B.; Berliner, M.; Buzon, R.; Chiu, C. K. F.; Colgan, S. T.; Kaneko, T.; Keene, N.; Kissel, W.; Le, T.; Leeman, K. R.; Marquez, B.; Morris, R.; Newell, L.; Wunderwald, S.; Witt, M.; Weaver, J.; Zhang, Z.; Zhang, Z. Aqueous Phosphoric Acid as a Mild Reagent for Deprotection of Tert-Butyl Carbamates, Esters, and Ethers. *J. Org. Chem.* **2006**, *71* (24), 9045–9050.

(43) Ray Banerjee, S.; Pullambhatla, M.; Foss, C. A.; Falk, A.; Byun, Y.; Nimmagadda, S.; Mease, R. C.; Pomper, M. G. Effect of Chelators on the Pharmacokinetics of 99mTc-Labeled Imaging Agents for the Prostate-Specific Membrane Antigen (PSMA). *J. Med. Chem.* **2013**, *56* (15), 6108–6121.

(44) Suresh Babu, V. V.; Patil, B. S.; Vasanthakumar, G. R. MW-Enhanced High-Speed Deprotection of Boc Group Using p-TsOH and Concommitant Formation of N-Me-Amino Acid Benzyl Ester p-TsOH Salts. *Synth. Commun.* **2005**, *35* (13), 1795–1802.

(45) Han, G.; Tamaki, M.; Hruby, V. J. Fast, Efficient and Selective Deprotection of the Tert-butoxycarbonyl (Boc) Group Using HCl/Dioxane (4 M). *J. Pept. Res.* **2001**, *58* (4), 338–341.

(46) Strazzolini, P.; Melloni, T.; Giumanini, A. G. Selective Nitrolytic Deprotection of N-BOC-Amines and N-BOC-Amino Acids Derivatives. *Tetrahedron* **2001**, *57* (43), 9033–9043.

(47) Miel, H.; Rault, S. Total Deprotection of N , N ’ -Bis (Tert-Butoxycarbonyl) Guanidines Using SnCI4. **1997**, *38* (45), 7865–7866.

(48) Frank, R.; Schutkowski, M. Extremely Mild Reagent for Boc Deprotection Applicable to the Synthesis of Peptides with Thioamide Linkages. *Chem. Commun.* **1996**, No. 22, 2509–2510.

(49) Uslu, A.; Mutlu Balcı, C.; Yuksel, F.; Özcan, E.; Dural, S.; Beşli, S. The Investigation of Thermosensitive Properties of Phosphazene Derivatives Bearing Amino Acid Ester Groups. *J. Mol. Struct.* **2017**, *1136*, 90–99.

(50) Mack, L. L.; Fitzpatrick, R. J.; Allcock, H. R. Langmuir− Adam Trough Studies of Hydrophobicity, Hydrophilicity, and Amphilicity in Small-Molecule and High-Polymeric Phosphazenes. *Langmuir* **1997**, *13* (7), 2123–2132.

(51) Allcock, H. R.; Pucher, S. R.; Scopelianos, A. G. Poly[(Amino Acid Ester)Phosphazenes]: Synthesis, Crystallinity, and Hydrolytic Sensitivity in Solution and the Solid State. *Macromolecules* **1994**, *27* (5), 1071–1075.

(52) Allcock, H. R.; Morozowich, N. L. Bioerodible Polyphosphazenes and Their Medical Potential. *Polym. Chem.* **2012**, *3* (3), 578–590.

(53) Leclaire, J.; Coppel, Y.; Caminade, A. M.; Majoral, J. P. Nanometric Sponges Made of Water-Soluble Hydrophobic Dendrimers. *J. Am. Chem. Soc.* **2004**, *126* (8), 2304–2305.

(54) Shcharbin, D.; Dzmitruk, V.; Shakhbazau, A.; Goncharova, N.; Seviaryn, I.; Kosmacheva, S.; Potapnev, M.; Pedziwiatr-Werbicka, E.; Bryszewska, M.; Talabaev, M.; Chernov, A.; Kulchitsky, V.; Caminade, A. M.; Majoral, J. P. Fourth Generation Phosphorus-Containing Dendrimers: Prospective Drug and Gene Delivery Carrier. *Pharmaceutics* **2011**, *3* (3), 458–473.

Chapter 3 Radical dendrimers based on oligoethylene glycol dendrimers

3.1 Introduction

In the previous Chapter we have used a strategy to increase the water solubility of radical dendrimers that consists in using an amino acid as a linker between the dendrimer branches and the organic radicals, which provided an available amino group for radical coupling, and a methyl ester group to afford negative charges via hydrolysis. This strategy can produce high water-soluble systems due to the hydrophilic carboxylic salt. However, this way normally needs multiple synthetic steps.

A strategy commonly used to overcome such a lack of water solubility in organic systems is including water-solubilizing groups such as poly(ethylene glycol) (PEG) chains. Particularly in dendritic systems, for example Rajca[1] and Katayama[2] groups anchored PEG chains on the surface of the dendrimer in some of the end groups positions while the other anchoring positions were used to anchor the organic radicals. However, in that way, the total number of organic radical units anchored on the dendrimer's surface, by one hand, does not correspond to the maximum anchoring positions of the dendrimer, so that the number of anchored radicals decrease and hence the molecular relaxivity should be lower than with a fully radicals covered surface. On the other hand, the number of radical units anchored is not well controlled but only statistically known.

In this chapter, we propose another way to obtain fully water-soluble radical dendrimers, allowing at the same time the full functionalization of their branches with radicals. It consists of the use of dendrimers containing water-soluble branches themselves. Two generations of DTPA (diethylenetriaminepentaacetic acid)-core based dendrimers containing five and twenty equivalent oligoethylene glycol (OEG) branches (particularly triethylene glycol like ones) synthesized in collaboration with Miriam Royo's group have been used. The chemical structures of the two generations of dendrimers are shown in (Scheme 3-1). The amine functional groups at the end of the branches allowed the complete functionalization of both generations with PROXYL radical units.

G0 dendrimer (G0-OEG-NH_2) was prepared as previously described[3] by acylation of commercially available DTPA dianhydride with amine protected BOC-OEG

derivative, and by subsequent BOC removal.

The preparation of G1 dendrimer (G1-OEG-NH_2) was more complex and involved more steps, and it was prepared as new compound for this work.[4] The DTPA dianhydride was acylated using another DTPA core previously functionalized by one NH_2-OEG and four BOC-OEG branches. Then, the total 20 BOC groups were deprotected by HCl, giving rise to G1 dendrimer with 20 amine end groups.

In fact, the versatile synthetic strategy can be used to synthesize dendrimers with different end groups, from mono- to pentamodal functionalization patterns.[3] It is important to highlight that such OEG dendrimers used as scaffolds are biocompatible.[5] The fact that OEG dendrimers are biocompatible and that their small size minimizes their unwanted accumulation in the body gives the possibility to obtain contrast agents which improve the properties of Gd-based CA. Moreover, the control over the size of the dendrimers opens the opportunity to modulate their distribution profile in the body, which is impossible in the case of Gd(III) chelates.

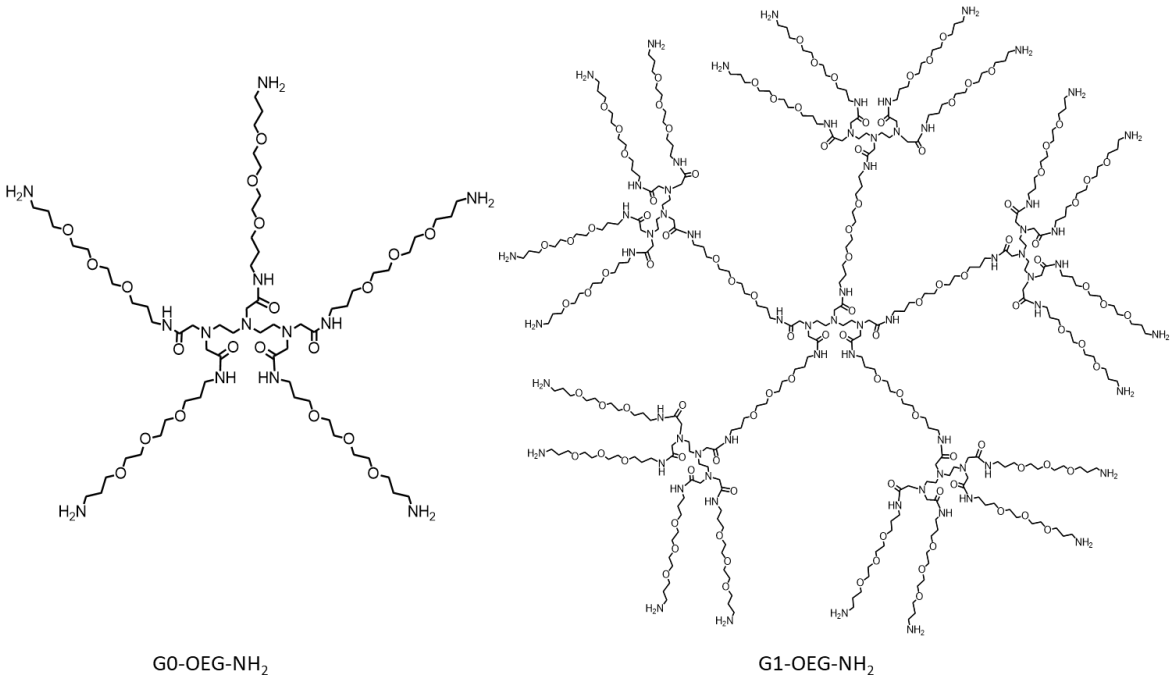

Scheme 3-1. Structures of Gn-OEG-NH_2 dendrimers, n=0,1.

3.2 Synthesis of radical dendrimers based on oligoethylene glycol dendrimers

3.2.1 Synthesis and characterization of G0- and G1-OEG-PROXYL radical dendrimers

The synthesis of G0- and G1-OEG-PROXYL radical dendrimers were conducted in a similar way (Scheme 3-2).

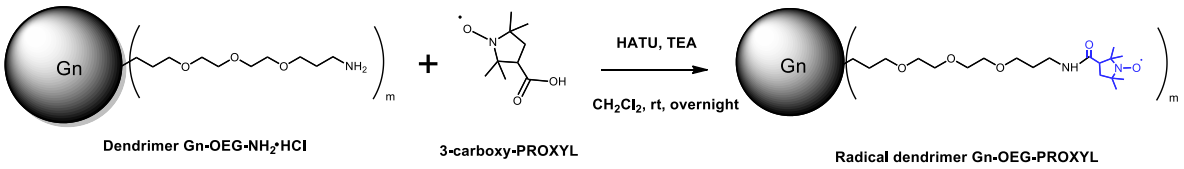

Scheme 3-2. Synthesis of radical dendrimers Gn-OEG-PROXYL, n=0,1 (m=5 and m=20, respectively).

The amine groups of G0-/G1-OEG-NH_2 dendrimers were coupled with the carboxylic acid functional groups of 3-carboxy-PROXYL radicals using HATU as coupling reagent and triethylamine as base, in anhydrous CH_2Cl_2 to obtain the corresponding radical dendrimers Gn-OEG-PROXYL, n=0,1 with amide linkers. Triethylamine was used in excess both, for the correct activation of carboxylic acid group by HATU, and to neutralize the hydrochloric acid terminated -NH_2•HCl end groups of Gn-OEG dendrimers. The purification of both radical dendrimers was performed by ultrafiltration .

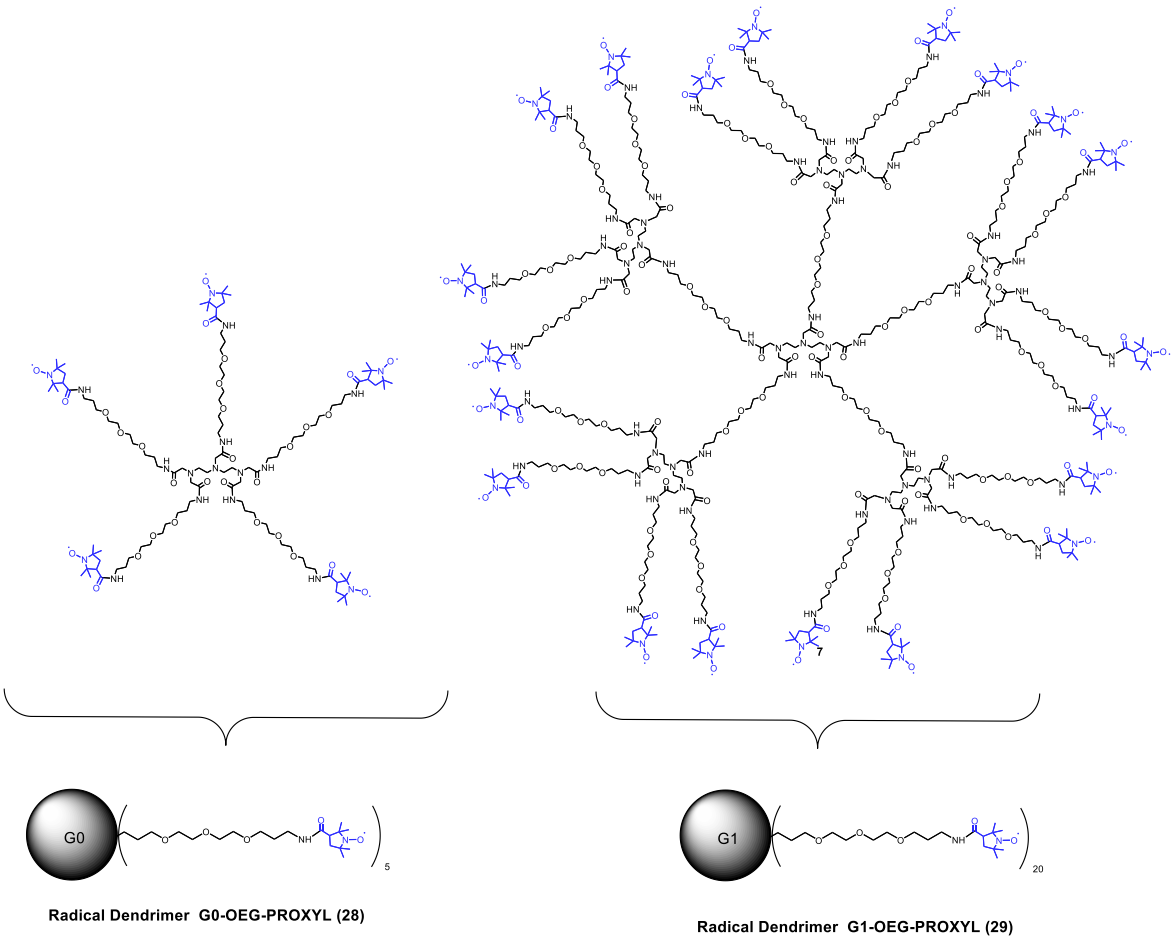

Scheme 3-3. Structures of Gn-OEG-PROXYL radical dendrimers, n=0,1.

The purity of the radical dendrimers was verified by SEC-GPC, using water (with 0.25 mM LiCl) as eluent (Figure 3-1). G1-OEG-PROXYL (**29**) with bigger hydrodynamic volume eluted at lower retention time (11.91 min.) than G0-OEG-PROXYL (**28**) (12.39 min.).

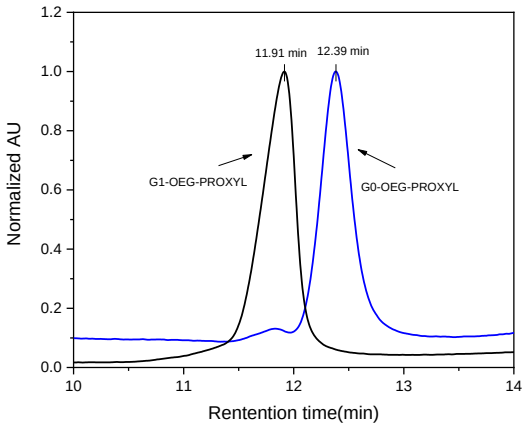

Figure 3-1. SEC-GPC of G0-OEG-PROXYL (**28**) and G1-OEG-PROXYL (**29**).

DLS particle size distribution of Gn-OEG-PROXYL, n=0,1 dendrimers determined

in the same conditions revealed a single distribution in each sample, with a mean hydrodynamic diameter of 0.84 and 3.62 nm, respectively (Figure 3-2).

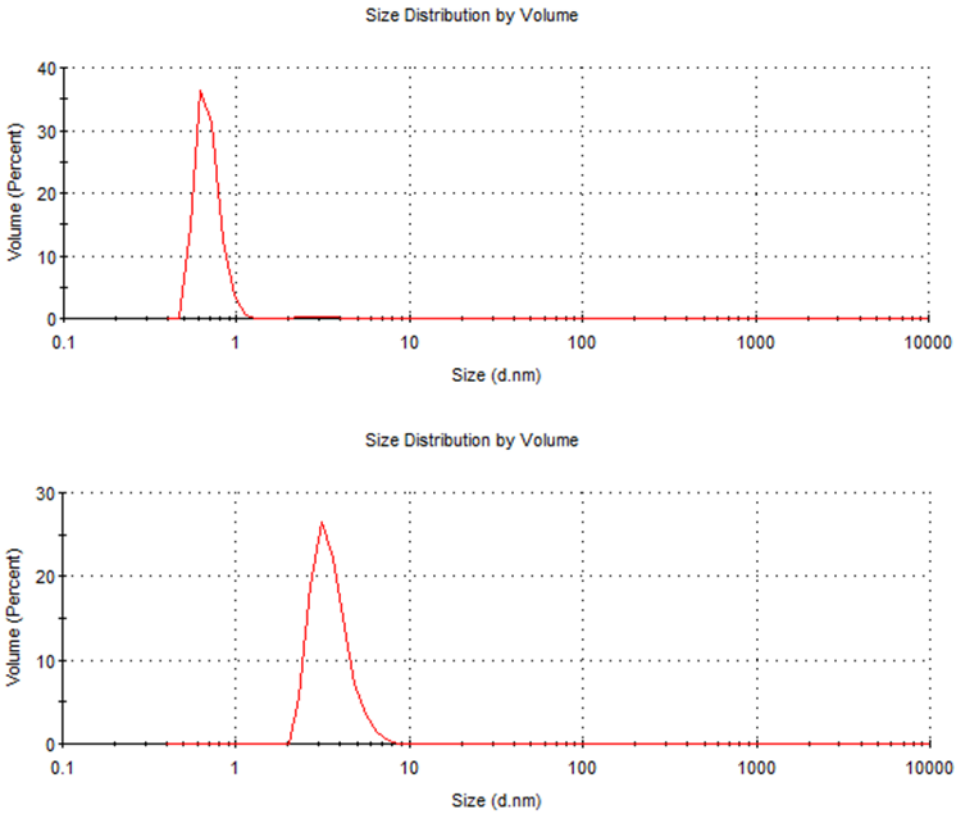

Figure 3-2. Mean diameters of G0-OEG-PROXYL (**28**) (up) and G1-OEG-PROXYL (**29**) (down) determined by DLS, from the volume particle size distribution, at 25ºC in PBS.

By FT-IR (Figure 3-3) we observed the carbonyl stretching vibrational band from the amide group at 1650 cm^{-1} as well as the corresponding N-H stretching band at 3303 cm^{-1}. The bands from PROXYL radical can be found at 1364 cm^{-1} and 1290 cm^{-1}, assigned to the N-O$^{\bullet}$ stretching[6] and -CH- bending, respectively. The band of the ether from the dendrimer branches can be found at 1100 cm^{-1}.

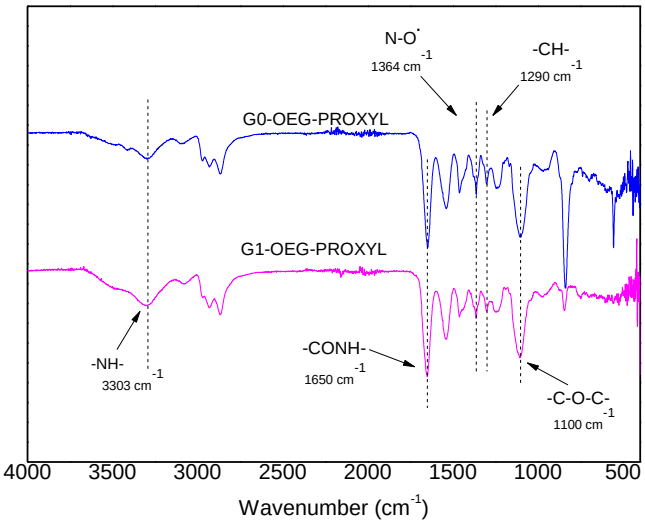

Figure 3-3. FT-IR (ATR) spectra of G0-OEG-PROXYL (**28**) and G1-OEG-PROXYL (**29**) radical dendrimers.

By MALDI-TOF it was possible to analyze radical dendrimer of zero generation G0-OEG-PROXYL (**28**) using dithranol as matrix, obtaining the corresponding molecular ion peak (Figure 3-4). The quasi-molecular ion peaks $[M+Na]^+$ and $[M+K]^+$ can also be observed (Figure 3-4a), as well as $[M+2Na]^{2+}$ adduct that is present at 1145.46 m/z (Figure 3-4b). However, it was not possible to analyze with this technique the dendrimer of the first generation G1-OEG-PROXYL (**29**) with 20 radicals in its periphery, as it is common for these types of compounds.[7,8]

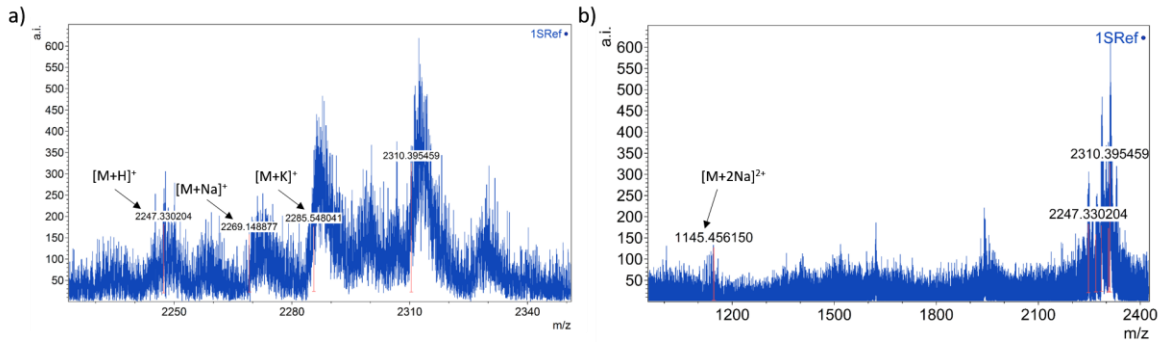

Figure 3-4. MALDI-TOF of G0-OEG-PROXYL (**28**) using dithranol matrix. a) the range between 2230 and 2350 m/z, b) the range between 1000 and 2400 m/z.

In addition, G0-OEG-PROXYL (**28**) radical dendrimer was treated with ascorbic acid to reduce the PROXYL radical units to their corresponding hydroxylamines, to eliminate their radical character and characterize it by ^{1}H NMR (Scheme 3-4). The ^{1}H

NMR spectrum lines of G0-OEG-PROXYL-H in $CDCl_3$ appeared quite broad, indicating that the radical character was not completely eliminated. However, even in this situation, we could differentiate the different groups of protons of the structure (Figure 3-5). A new group of protons signal that did not exist in the initial dendrimer spectrum clearly appeared in the G0-OEG-PROXYL-H spectrum between 0.8 and 1.5 ppm, which corresponded to the protons of PROXYL units. Moreover, the relative integrals of the ^1H resonances of PROXYL protons and the other groups of protons were consistent with the corresponding theoretical number of protons of the structure (Figure 3-6).

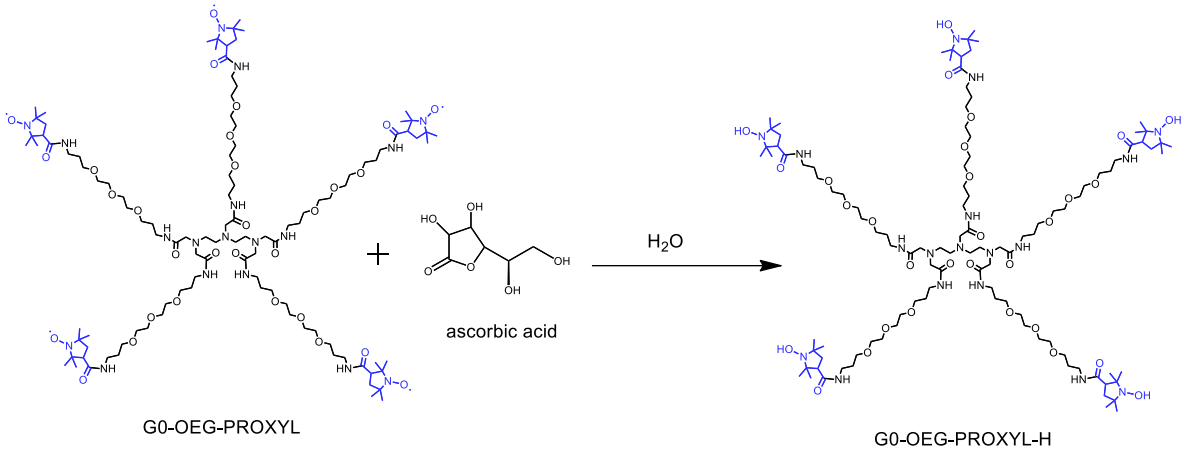

Scheme 3-4. Reaction of G0-OEG-PROXYL (**28**) with ascorbic acid.

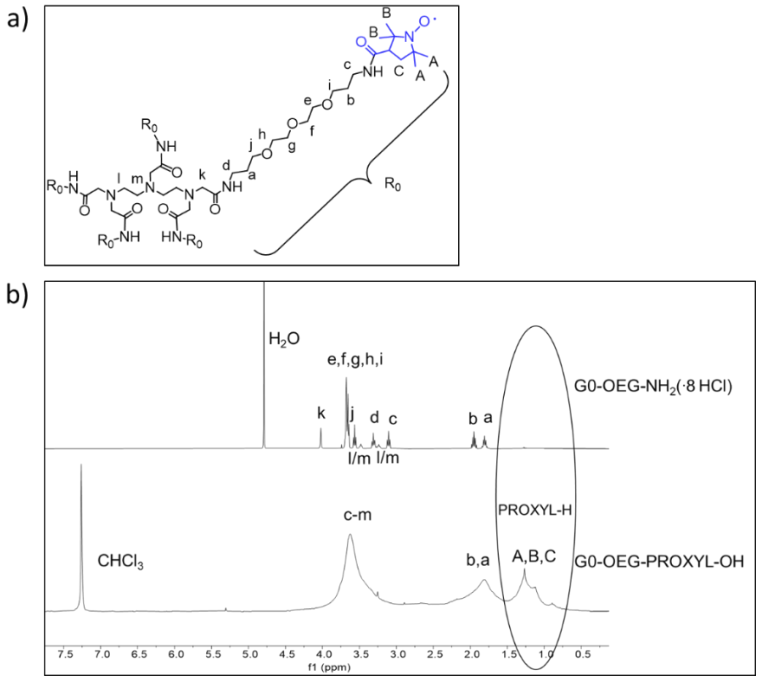

Figure 3-5. a) Structure of G0-OEG-PROXYL (**28**) with the protons labelling. b) ^1H NMR spectra of G0-OEG-NH_2(·8 HCl) dendrimer (up) and G0-OEG-PROXYL-H dendrimer (down) with their corresponding peaks assignment.

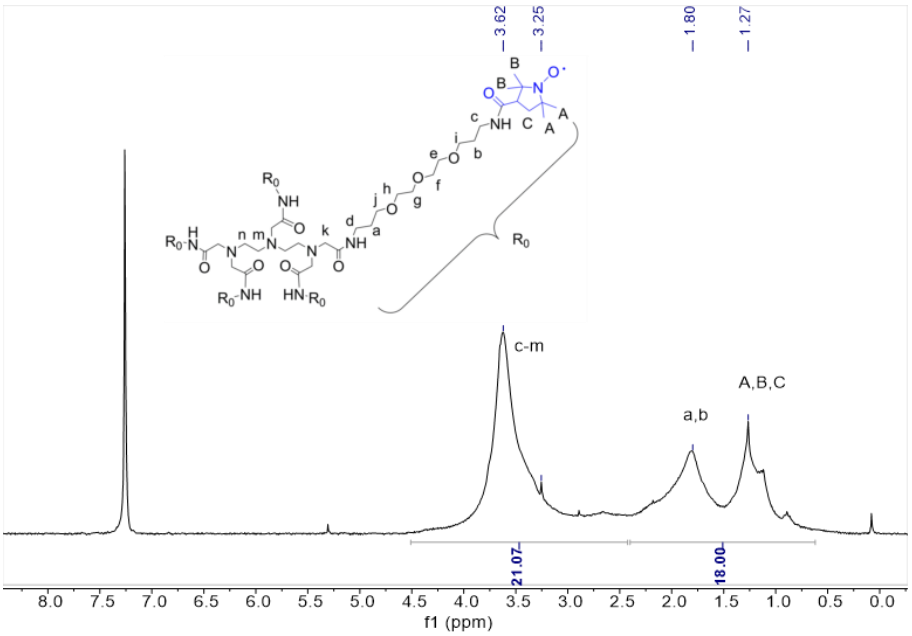

Figure 3-6. ^{1}H NMR spectrum of G0-OEG-PROXYL-H dendrimer with their corresponding peaks assignment and relative integral values. The relative integral value for the group of protons (A,B,C + a,b) was found to be 18 and for the group of protons (c-m) 21.1, the same than the theoretical one 18: 22.

3.2.2 EPR study of G0-OEG-PROXYL and G1-OEG-PROXYL

The EPR spectrum of PROXYL free radical presents the typical nitroxide three-line spectrum pattern from the coupling of the unpaired electron with the ^{14}N atom of the N-O$^{\bullet}$ unit, with hyperfine coupling constant a_N *ca.* 14.5 G in organic solvent.

However, the EPR spectrum of G0-OEG-PROXYL (**28**) at 300 K showed 11 lines separated by *ca.* 3.0 G with alternating linewidth effect: three narrow lines (1st, 6th and 11th) and in between them two groups of 4 broad lines (marked with asterisks in Figure 3-7). This spectral pattern fits with a spectrum generated by strong spin exchange interaction ($|J| >> |a_N|$) between five nitroxide units (because in the case of two, three or four interacting nitroxide units it would give rise to 5-, 7- and 9-line hyperfine pattern, respectively). In fact, in the case of a flexible polyradical containing five nitroxide radicals with only a through-space spin exchange mechanism between them, we may have two limit cases. When radicals are too far and therefore not interacting among them ($|J| << |a_N|$), the spectrum would be similar to that of five independent monoradicals exhibiting three lines separated by a_N; whereas when radicals are closer and thereby $|J| >> |a_N|$, it would give rise to an eleven-line hyperfine pattern with a separation of 1/5 a_N, as it is our case. Therefore, the fact of observing 11 lines in the EPR spectrum is an evidence of the full functionalization of G0 dendrimer with 5 nitroxide units. However,

the relative EPR lines intensities observed do not correspond to the theoretical ones expected for 5 equivalent nitroxyl radicals, since there exists spin exchange dynamics modulated by the temperature. In fact, *J* may be not constant in solution because the radical units could be in movement and consequently, the EPR spectra should be dependent on the conformation and mobility of the dendrimer branches (i.e. on the frequency of collisions of the spin-bearing groups) that depends on the temperature (Figure 3-8) and solvent nature. At high temperature, the frequency of collisions is higher but as the temperature is gradually lowered (Figure 3-8), the alternate lines broaden[9] and disappear (leading to three main lines) since the frequency of collisions decreases and the spectra are less affected by spin exchange interaction.

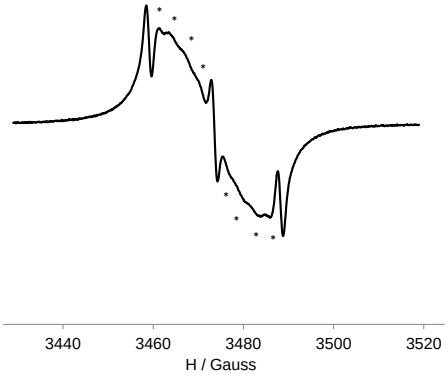

Figure 3-7. EPR spectrum of G0-OEG-PROXYL (**28**) at 300 K in CH_2Cl_2 with the eight broad alternate lines marked with asterisks.

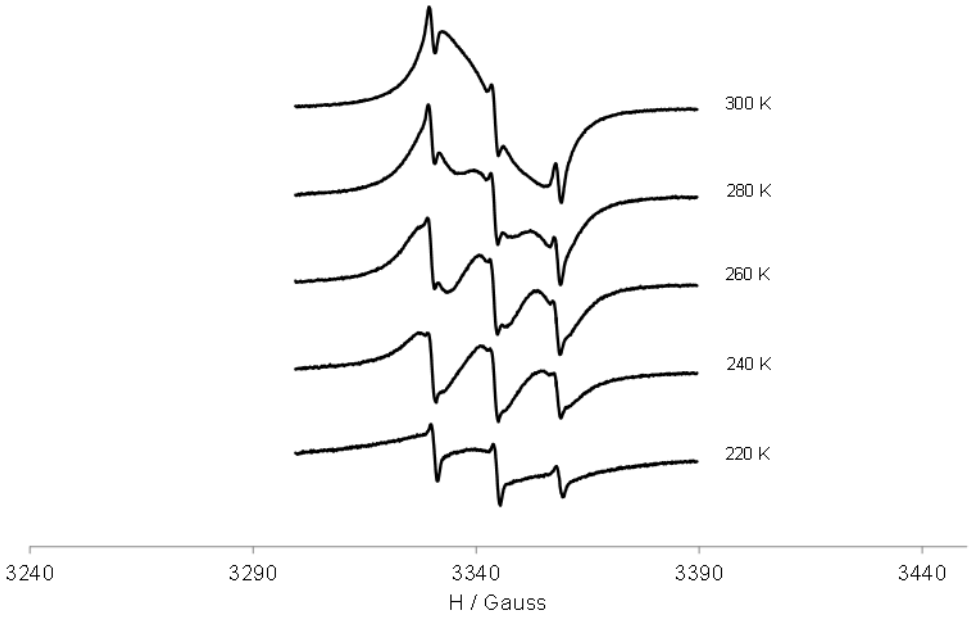

Figure 3-8. Variable temperature EPR spectra of G0-OEG-PROXYL (**28**) from 300 to 220 K in CH_2Cl_2.

On the other hand, the EPR spectral pattern of G1-OEG-PROXYL (**29**) at 300 K (Figure 3-9) is dominated by a non-resolved, single, intense broad line overlapping three narrow lines. This broad line results from spin exchange and dipole-dipole interactions between several nitroxide units anchored on the dendrimer surface, averaged over different interaction distances. In fact, only for compound G0-OEG-PROXYL (**28**) the spectral resolution allows us to determine the number of interacting PROXYL radicals. However, with 20 radical units the spectral resolution does not allow the observation of the ever decreasing spacing between the various hyperfine transitions (decrease of the splitting value a_N/n and increase of the number of lines 2n + 1). We also observed alternating linewidth effect upon cooling from 300 to 220 K (Figure 3-10) because of the modulation of the spin exchange interaction with the temperature. As the temperature goes down the single broad line intensity starts to decrease meanwhile the three main lines are maintained, as in the zero generation. In addition, the EPR intensity of G1-OEG-PROXYL (**29**) (measured in terms of area, i.e. double integral of the EPR signal) was exactly 4 times higher than that of G0-OEG-PROXYL (**28**) in quantitative conditions, confirming the ratio of 20 to 5 PROXYL radical units between both radical dendrimers, respectively (

Table 3-1, Figure 3-9).

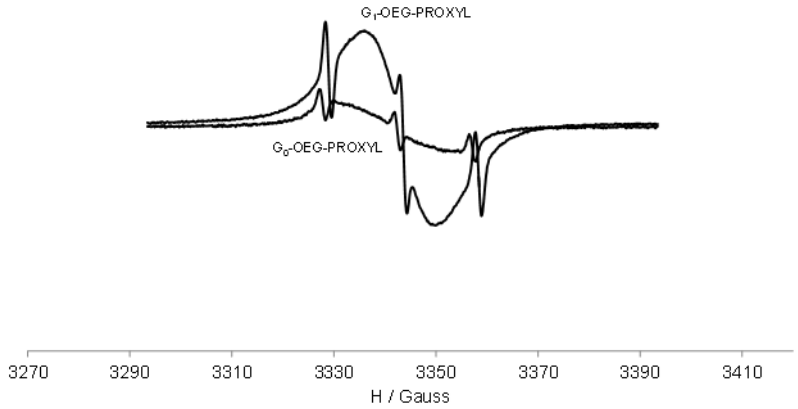

Figure 3-9. EPR spectra of G0-OEG-PROXYL (**28**) and G1-OEG-PROXYL (**29**) at 300 K in CH_2Cl_2, at the same concentration 10^{-4} M and in quantitative conditions.

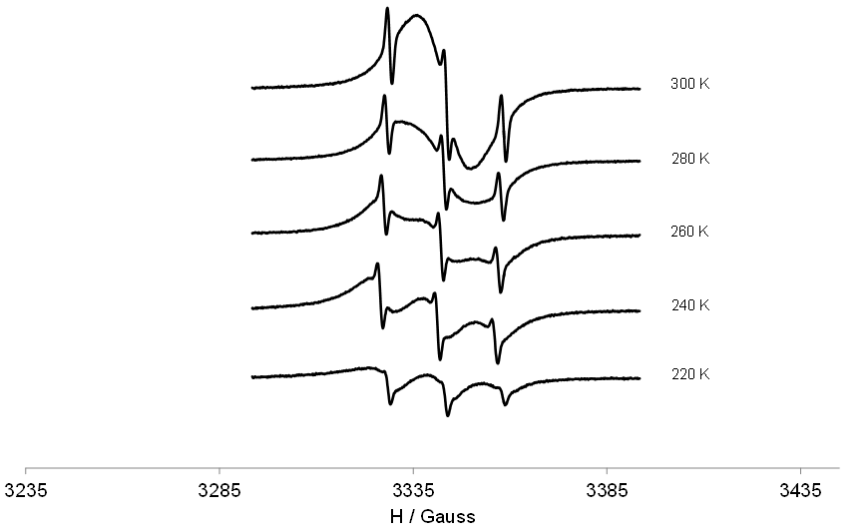

Figure 3-10. Variable temperature EPR spectra of G1-OEG-PROXYL (**29**) from 300 to 220 K in CH_2Cl_2.

Table 3-1. Ratio between the relative double integral values of G1 and G0 from their corresponding spectra obtained at 300 and 120 K in quantitative conditions.

Dendrimer	Area (double integral) Spectra at 300 K[a]	Ratio G1/G0	Area (double integral) Spectra at 120 K[a]	Ratio G1/G0
G0-OEG-PROXYL (**28**)	$1.83x10^5$	3.96	$1.23x10^6$	4.08
G1-OEG-PROXYL (**29**)	$7.25x10^5$		$5.03x10^6$	

a) The acquisition EPR parameters are the same at each temperature but not between the different temperatures.

In frozen solution (120 K), the shape of the spectra changes completely as we are under anisotropic conditions (Figure 3-11). In such conditions, the EPR spectrum is sensitive to the intramolecular dipole-dipole interaction between neighboring nitroxides which substantially alters the shape of the spectrum. This effect could be estimated by the empirical ratio of peak heights d_1/d.[9,10] This parameter is shown to be sensitive to the distance between adjacent nitroxides and hence a convenient measure of the strength of the dipole-dipole interactions (e. g., the higher the ratio, the shorter the distance between the radical centers and hence the higher the radical interactions). The d_1/d parameter for G0 and G1-OEG-PROXYL was 0.71 and 0.87, respectively, whereas for free nitroxide is only 0.53.[11] Thus, both radical dendrimers showed significant contribution of intramolecular dipole-dipole interactions among adjacent spin labels, but, as expected, G1 shows much higher d_1/d ratio than G0, since the presence of four times more radicals should make them be closer. Also in frozen solution we observed that the intensity of G1

(double integral) was 4 times higher than that in G0, measured in quantitative conditions (

Table 3-1 and Figure 3-11).

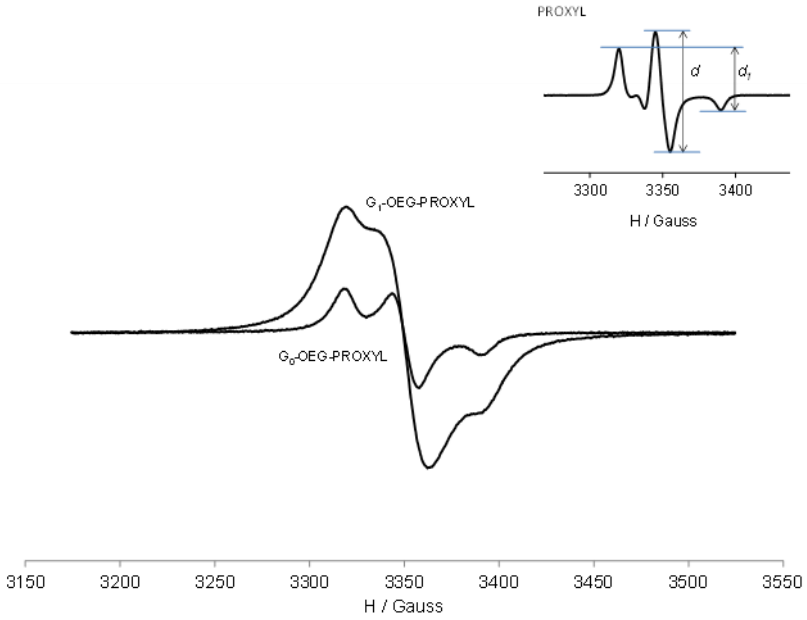

Figure 3-11. EPR spectra of G0-OEG-PROXYL (**28**) and G1-OEG-PROXYL (**29**) at 120 K in CH_2Cl_2, at the same concentration 10^{-4} M and in quantitative conditions. Inset: free PROXYL at 120 K with *d* and d_1 representation.

In addition, under frozen conditions we also observed an $|\Delta m_s| = 2$ transition at half-field in both generations, in dilution conditions to ensure the study of the intramolecular interactions present in the dendrimers (Figure 3-12). This forbidden transition is characteristic of dipolar coupled spins and gives direct evidence of the presence of a high-spin state.

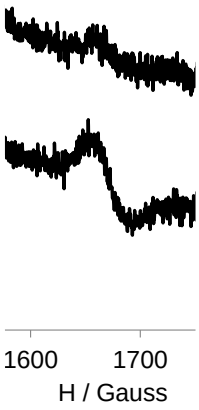

Figure 3-12. EPR spectra of $|\Delta m_s| = 2$ transition at half-field for the same concentration 10^{-4} M of G0-OEG-

PROXYL (**28**) and G1-OEG-PROXYL (**29**) at 120 K in CH_2Cl_2.

The EPR spectra of Gn-OEG-PROXYL (n=0,1) radical dendrimers in water showed similar spectral pattern than in organic solvents, but with a higher alternating linewidth effect due to the increase of the solvent polarity.[12]

3.3 Relaxivity measurements and cytotoxicity

Imaging experiments of 3-carboxy-PROXYL and Gn-OEG-PROXYL n=0,1 radical dendrimers were performed at 7 T and room temperature in 30 mM phosphate buffer pH 7.4. In Table 3-2 r_1 and r_2 relaxivity constants per molecule and per unit of nitroxyl radical, calculated from relaxation times measurements from the imaging experiments, are presented. The plots of proton relaxation rates ^{1}H $R_{1,2}$ ($R_{1,2}$ = 1/ $T_{1,2}$) of water molecules versus the nitroxyl units concentration were linear for all agents, over the concentration range studied (see Table 3-2 and Figure 3-13).

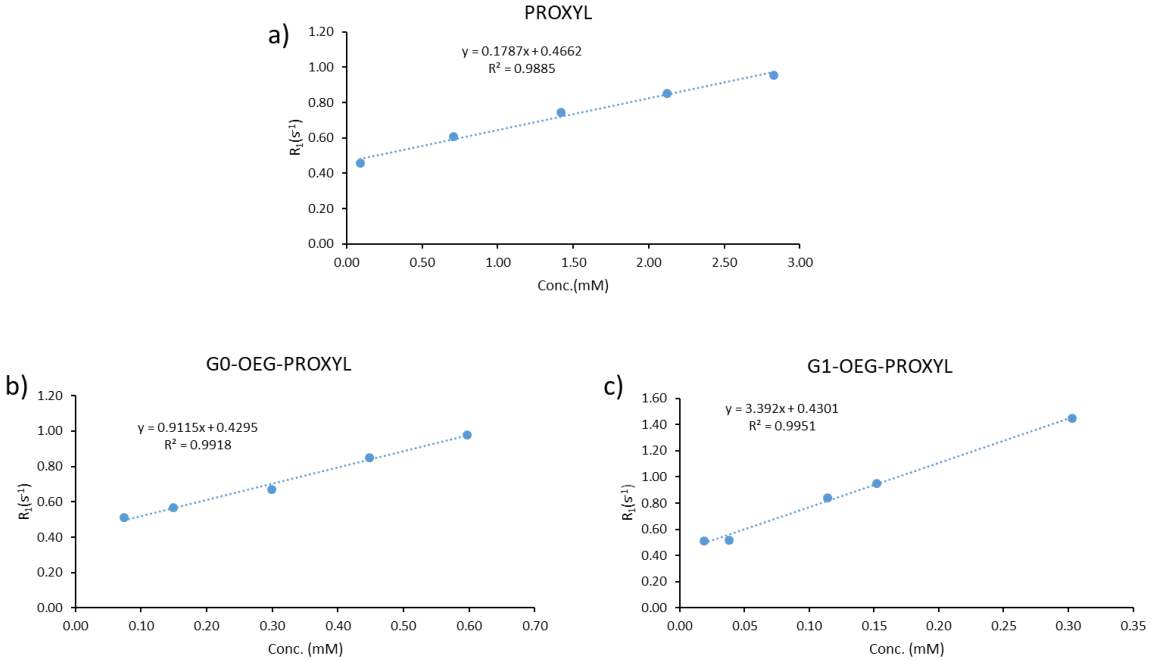

Figure 3-13. Plots of R_1 ($1/T_1$) of water molecules versus the molecular concentration of a) PROXYL, b) G0-OEG-PROXYL (**28**) and c) G1-OEG-PROXYL (**29**).

The presence of a high number of paramagnetic nitroxides in the dendrimers periphery, resulted in high molecular relaxivities. The relaxivity per unit of nitroxyl radical was maintained constant from the free PROXYL. The molecular r_1 relaxivity

obtained for G0-OEG-PROXYL (**28**) (Table 3-2) was 0.91 $mM^{-1}s^{-1}$ while for G1-OEG-PROXYL (**29**) was 3.4 $mM^{-1}s^{-1}$.

Table 3-2. Longitudinal r_1 relaxivity constants per molecule and per unit of nitroxyl radical of G0- and G1-OEG-PROXYL radical dendrimers compared with 3-carboxy-PROXYL, determined at 7T in 30 mM phosphate buffer pH 7.4, 300 K.

Compound	r_1^{7T} ($mM^{-1}s^{-1}$) per molecule	r_1^{7T} ($mM^{-1}s^{-1}$) per unit of radical	r_2^{7T} ($mM^{-1}s^{-1}$) per molecule	r_2^{7T} ($mM^{-1}s^{-1}$) per unit of radical
3-carboxy PROXYL	0.18	0.18	0.20	0.20
G0-OEG-PROXYL (28)	0.91	0.18	0.95	0.19
G1-OEG-PROXYL (29)	3.39	0.17	4.02	0.19

It is worth highlighting that G1-OEG-PROXYL (**29**) presents practically the same relaxivity (3.4 $mM^{-1}s^{-1}$) than the most widely used Gd contrast agent in clinics (Gd-DTPA, 3.2 $mM^{-1}s^{-1}$ or Gd-DOTA, 2.8 $mM^{-1}s^{-1}$) in the same conditions (r.t., 7T). Moreover, we have achieved this optimal relaxivity with an entirely organic metal-free molecule. The absence of Gd in the radical dendrimer avoids the risks associated with its unwanted accumulation in the body and the derived health problems. Furthermore, the control over the size of the dendrimers, opens the opportunity to modulate their distribution profile in the body, which is impossible in the case of Gd chelates.

Another important thing to highlight is the biocompatible essence of OEG dendrimers, in contrast to Gd(III) based contrast agents, which make them very interesting for many applications. In addition, nitroxides have been shown minimal in vivo toxicity.[13,14] To really assess the toxicity of G0- and G1-OEG-PROXYL dendrimers, in vitro cell viability assays were conducted with African green monkey kidney (Vero) cell line. In these assays, the cells were incubated with G0- (**28**) and G1-OEG-PROXYL (**29**) radical dendrimer at different concentrations ranging from 0.0625 to 2 mM per radical unit, for 24 and 48 h, by XTT assay. The XTT assay is used to measure cellular metabolic activity as an indicator of cell viability, proliferation and cytotoxicity. This colorimetric assay is based on the reduction of a yellow tetrazolium salt (XTT) to an orange formazan dye by metabolically active cells. As a result, neither the G0- (**28**) nor the G1-OEG-PROXYL (**29**) dendrimers showed any cytotoxicity *in vitro*, in the tested concentration range, as can be observed in Figure 3-14.

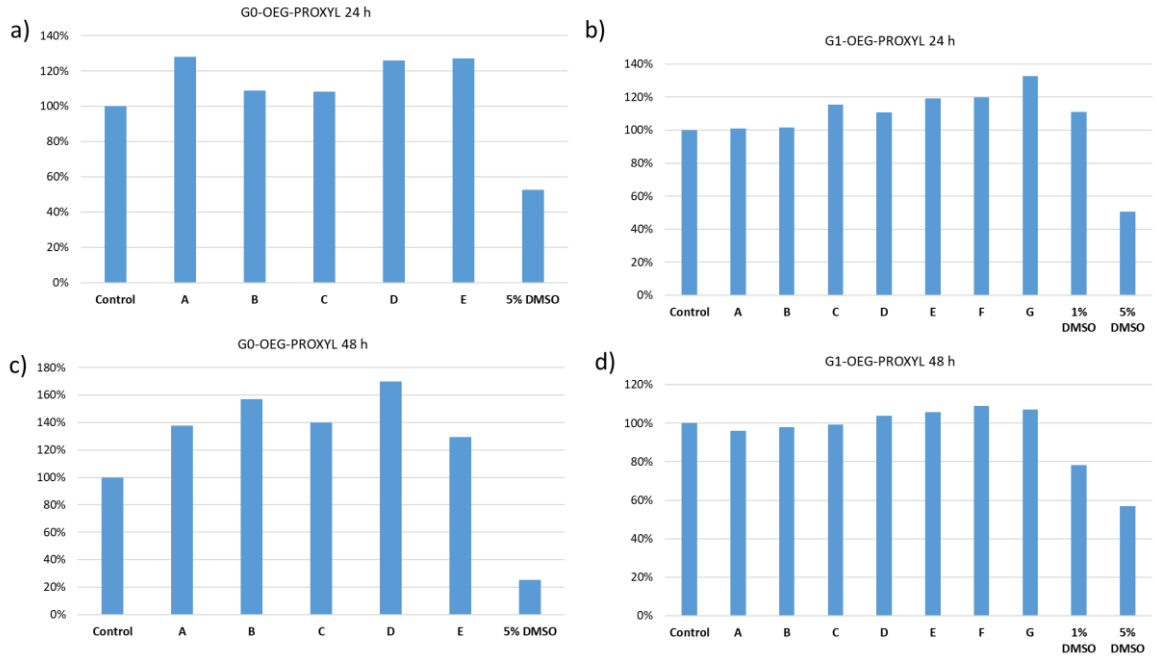

Figure 3-14. In vitro XTT cell viability assays conducted with African green monkey kidney (Vero) cells incubated with G0-OEG-PROXYL (**28**) (a, c) and G1-OEG-PROXYL (**29**) (b,d) dendrimers in a concentration of A) and B) 2mM per radical unit, C) 1mM, D) 0.5 mM, E) 0.25 mM, F) 0.125 mM, G) 0.0625 mM, for 24 and 48 h.

As previously mentioned, there are very few reported works based on dendrimers fully functionalized with nitroxides for MRI applications. However, authors have described water-phase aggregation problems in such nitroxide-based dendrimers, especially in large generation dendrimers. By our strategy of using dendrimers with water-soluble branches themselves we have overcome such water solubility issues and at the same time we have been able to fully functionalize all dendrimer branches with nitroxides.

In general, the optimal characteristics in a contrast agent are to be highly soluble in physiological pH, to present high ^{1}H water relaxivities, to not be toxic and to not accumulate in the body. Our radical dendrimers would fulfill such conditions as they are fully water soluble, present the same relaxivity than the golden standard used in clinics and they are entirely organic and biocompatible non-cytotoxic molecules. All this makes these radical dendrimers excellent candidates to be used as contrast agents for MRI. They are shown as potential candidates to be studied as alternatives to Gd-based contrast agents widely used in many current MRI applications such as diagnosis and follow-up of infectious diseases.

3.4 Conclusions

- Two generations of water-soluble oligoethylele glycol (OEG) dendrimers fully functionalized with 5 and 20 PROXYL organic radicals, respectively, have been synthesized and characterized (G0-OEG-PROXYL (**28**) and G1-OEG-PROXYL (**29**)). The resulting radical dendrimers are soluble in water, non-cytotoxic and present a good relaxivity.

- G1-OEG-PROXYL (**29**) radical dendrimer presents a r_1 relaxivity value (3.4 $mM^{-1}s^{-1}$) similar than the most widely used Gd contrast agent in clinics (Gd-DTPA, 3.2 $mM^{-1}s^{-1}$ or Gd-DOTA, 2.8 $mM^{-1}s^{-1}$), without concerns over long-term tissue accumulation of metals.

These radical dendrimers are shown as potential candidates to be studied as alternatives to Gd-based contrast agents.

3.5 References

(1) Rajca, A.; Wang, Y.; Boska, M.; Paletta, J. T.; Olankitwanit, A.; Swanson, M. A.; Mitchell, D. G.; Eaton, S. S.; Eaton, G. R.; Rajca, S. Organic Radical Contrast Agents for Magnetic Resonance Imaging. *J. Am. Chem. Soc.* **2012**, *134* (38), 15724–15727.

(2) Niidome, T.; Gokuden, R.; Watanabe, K.; Mori, T.; Naganuma, T.; Utsumi, H.; Ichikawa, K.; Katayama, Y. Nitroxyl Radicals-Modified Dendritic Poly(l -Lysine) as a Contrast Agent for Overhauser-Enhanced MRI. *J. Biomater. Sci. Polym. Ed.* **2014**, *25* (13), 1425–1439.

(3) Pulido, D.; Albericio, F.; Royo, M. Controlling Multivalency and Multimodality: Up to Pentamodal Dendritic Platforms Based on Diethylenetriaminepentaacetic Acid Cores. *Org. Lett.* **2014**, *16* (5), 1318–1321.

(4) Zhang, S.; Lloveras, V.; Pulido, D.; Liko, F.; Pinto, L. F.; Albericio, F.; Royo, M.; Vidal-Gancedo, J. Radical Dendrimers Based on Biocompatible Oligoethylene Glycol Dendrimers as Contrast Agents for MRI. *Pharmaceutics* **2020**, *12* (8), 1–15.

(5) Simón-Gracia, L.; Pulido, D.; Sevrin, C.; Grandfils, C.; Albericio, F.; Royo, M. Biocompatible, Multifunctional, and Well-Defined OEG-Based Dendritic Platforms for Biomedical Applications. *Org. Biomol. Chem.* **2013**, *11* (24), 4109–4121.

(6) Kunz, T. K.; Wolf, M. O. Electrodeposition and Properties of TEMPO Functionalized Polythiophene Thin Films. *Polym. Chem.* **2011**, *2* (3), 640–644.

(7) Badetti, E.; Caminade, A. M.; Majoral, J. P.; Moreno-Mañas, M.; Sebastián, R. M. Palladium(0) Nanoparticles Stabilized by Phosphorus Dendrimers Containing Coordinating 15-Membered Triolefinic Macrocycles in Periphery. *Langmuir* **2008**, *24* (5), 2090–2101.

(8) Blais, J. C.; Turrin, C. O.; Caminade, A. M.; Majoral, J. P. MALDI TOF Mass Spectrometry for the Characterization of Phosphorus-Containing Dendrimers. Scope and Limitations. *Anal. Chem.* **2000**, *72* (20), 5097–5105.

(9) Likhtenshteĭn, G. I. *Spin Labeling Methods in Molecular Biology*; Wiley, 1976.

(10) Likhtenshtein, G. I.; Lihtenštejn, G. I.; Gertz, L. *Biophysical Labeling Methods in Molecular Biology*; Cambridge University Press, 1993.

(11) Badetti, E.; Lloveras, V.; Muñoz-Gómez, J. L.; Sebastián, R. M.; Caminade, A. M.; Majoral, J. P.; Veciana, J.; Vidal-Gancedo, J. Radical Dendrimers: A Family of Five Generations of Phosphorus Dendrimers

Functionalized with TEMPO Radicals. *Macromolecules* **2014**, *47* (22), 7717–7724.

(12) Lloveras, V.; Badetti, E.; Wurst, K.; Chechik, V.; Veciana, J.; Vidal-Gancedo, J. Magnetic and Electrochemical Properties of a TEMPO-Substituted Disulfide Diradical in Solution, in the Crystal, and on a Surface. *Chem. - A Eur. J.* **2016**, *22* (5), 1805–1815.

(13) Afzal, V.; Brasch, R. C.; Nitecki, D. E.; Wolff, S. Nitroxyl Spin Label Contrast Enhancers for Magnetic Resonance Imaging. Studies of Acute Toxicity and Mutagenesis. *Invest. Radiol.* **1984**, *19* (6), 549–552.

(14) Samuni, Y.; Gamson, J.; Samuni, A.; Yamada, K.; Russo, A.; Krishna, M. C.; Mitchell, J. B. Factors Influencing Nitroxide Reduction and Cytotoxicity in Vitro. *Antioxidants Redox Signal.* **2004**, *6* (3), 587–595.

Chapter 4 Nanoparticles based on bis-MPA radical dendritic structures

4.1 Introduction

We have used different strategies to prepare water-soluble radical dendrimers, including the incorporation of anions in the radical dendrimers structure or the use of water-soluble dendrimers themselves. However, sometimes it is not easy to find water-soluble dendrimers or anchor ionic groups in the dendrimers structure. One possible strategy is the incorporation of polyethylene glycol (PEG) chains in the macromolecular structure to obtain amphiphilic polymers. These systems have been widely used to prepare self-assembling supramolecular structures such as micelles, liposomes, nanofibers, or nanoparticles.

These amphiphilic polymers contain a hydrophobic and hydrophilic part. Due to the attractive hydrophobic interaction of the segments with the participation sometimes of hydrogen bonding, π-π stacking, etc., they can form aggregates in an aqueous solution with the hydrophobic segments as the core, and the hydrophilic segments as coronas or shell. The morphologies of the aggregates can be spherical micelles, lamellae, vesicles, tubules, etc., which depend on the composition of these polymers, the temperature or the concentration, among others.[1] These hierarchical aggregates have an intrinsic advantage as nanocarriers. The hydrophilic periphery surface can be used to anchor antibodies to achieve target function to specific cells.[2] The interior cavity can be used for the encapsulation of hydrophobic drugs.[3] Furthermore, the nanometric size of the aggregates is helpful to increase the accumulation in the damage tissues due to the enhanced permeability and retention (EPR) effect.[4] These kinds of self-assembly structures can be designed to be controlled release systems. Once the nanoparticles are sent to the target position, the drug in the interior cave can be released under specific stimuli such as pH,[5] temperature,[6] etc., leading to improve treatment efficacy.

Compared with linear copolymers, linear–dendritic polymers architectures, which combine dendrimers with linear polymers, have more end functionalities, which makes the formed supramolecular structures more likely to tune their functions by anchoring different small molecules such as drugs or imaging agents.[7,8] These kinds of linear-dendritic hybrids were first proposed by the Fréchet group.[9] According to the different

topological structures of linear-dendritic hybrids, the linear-dendritic polymers are divided into linear-dendritic (L-D) copolymers, dendritic-linear-dendritic (L-D-L) copolymers, statistical, alternating structure, etc[10] (Figure 4-1). The self-assembly structures based on these linear-dendritic copolymers combine the advantages of dendrimers and linear polymers. The traditional perfect dendrimers have well-defined end groups distribution and relatively rigid structures, while linear polymers are one-dimensional linear structures and have relatively high flexibilities. Moreover, the hydrophilic–lipophilic balance can be adjusted by the composition of the linear–dendritic polymers. Based on this fact, the assembly of these polymers has attracted plenty of attention in drug conjugates[11] or drug delivery.[12]

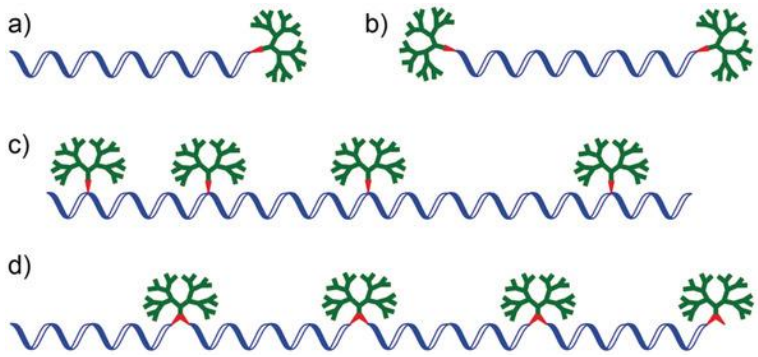

Figure 4-1. Schematic illustrations of linear-dendritic (L-D) copolymers with a) LD-type, b) DLD-type, c) statistical, and d) alternating structures.[10]

When it comes to MRI contrast agents, there have been some reports about self-assembled nanostructures prepared with radical-containing polymers as contrast agents. However, most of them are based on linear polymers,[13–20] or hyperbranched polymers.[21–28] The disadvantage of the self-assembly with linear polymers or high hyperbranched polymers is the limited or uncertain quantity of organic radical anchored in each compound, which might result in low relaxivities or difficulty in the calculation of relaxivities for the MRI contrast agents. The linear–dendritic polymers can provide exact number of radicals on their periphery according to the end groups of the dendrons. In addition, the self-assembled nanostructures formed by linear-dendritic polymers might be helpful to improve their relaxivities, due to the less rotational correlation time of radicals in the relatively big and rigid self-assembled structures.

In this chapter, we have used dendritic-linear-dendritic polymers to prepare, first, radical dendritic systems and then nanoparticles based on them. These kinds of polymers have 2,2-bis(hydroxymethyl)propionic acid (bis-MPA) based dendrons at the end of a

poly(ethylene glycol) chain. These linear-dendritic polymers have been widely used due to their biocompatibility, non-immunogenicity and degradability.[29–32] The PEG linear chain acts as a hydrophilic part, and the dendrons based on bis-MPA as the hydrophobic part. It is well known that the poly(ethylene glycol) segment can prevent the nanoparticles to be cleared by the reticuloendothelial system,[33] which leads to an increase in the circulation time of nanoparticles in the body. Another advantage of this compound is that the hydrophobic parts are at the end of the linear part, therefore, once the nanoparticles are formed, the radical should be in the interior cavities of the nanoparticles (Figure 4-2), which can protect the radicals from being reduced in the body.

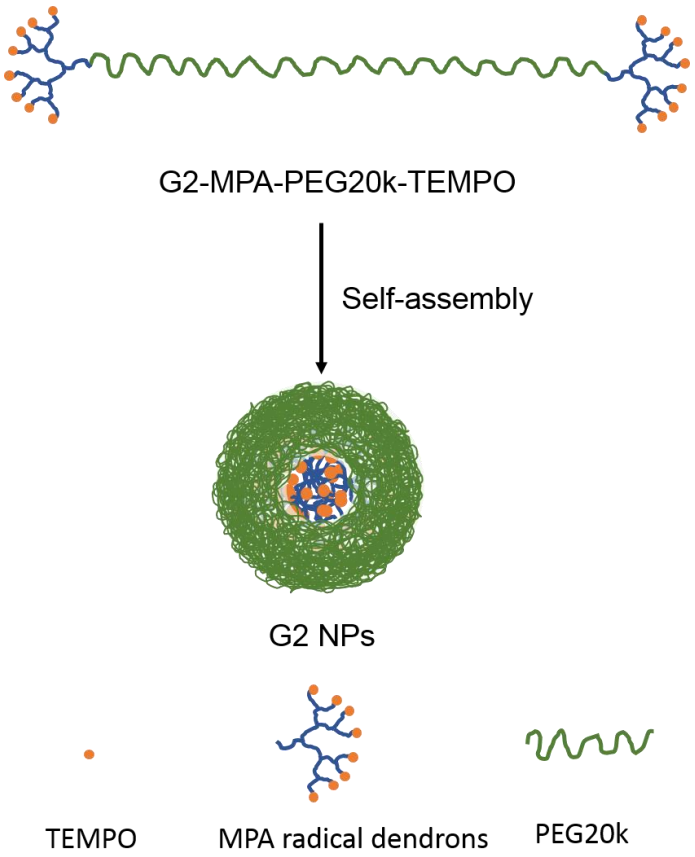

Figure 4-2. Schematic representation of the formation of nanoparticles from bis-MPA dendrons structures. The orange balls represent the organic radicals and the green chain represents the PEG linear chain of the system.

The chemical structures of the dendritic-linear-dendritic polymers we have chosen for this work are shown in Scheme 4-1. They are commercial polymers and are named Gn-MPA-PEG20k-alkyne in this chapter. We chose PEG 20k and not PEG 5k or 10k since it might be more helpful to give our compound water solubility. The alkyne end groups can easily react with commercial azide-TEMPO by copper(I)-catalyzed Huisgen

1,3-dipolar cycloaddition, termed “click chemistry”, producing fully TEMPO functionalized radical polymers. In this way, we can get a series of amphiphilic dendritic-linear-dendritic polymers containing 4, 8 or 16 TEMPO radical units. Furthermore, these amphiphilic polymers can be used to form nanoparticles and study their relaxivities as MRI contrast agents.

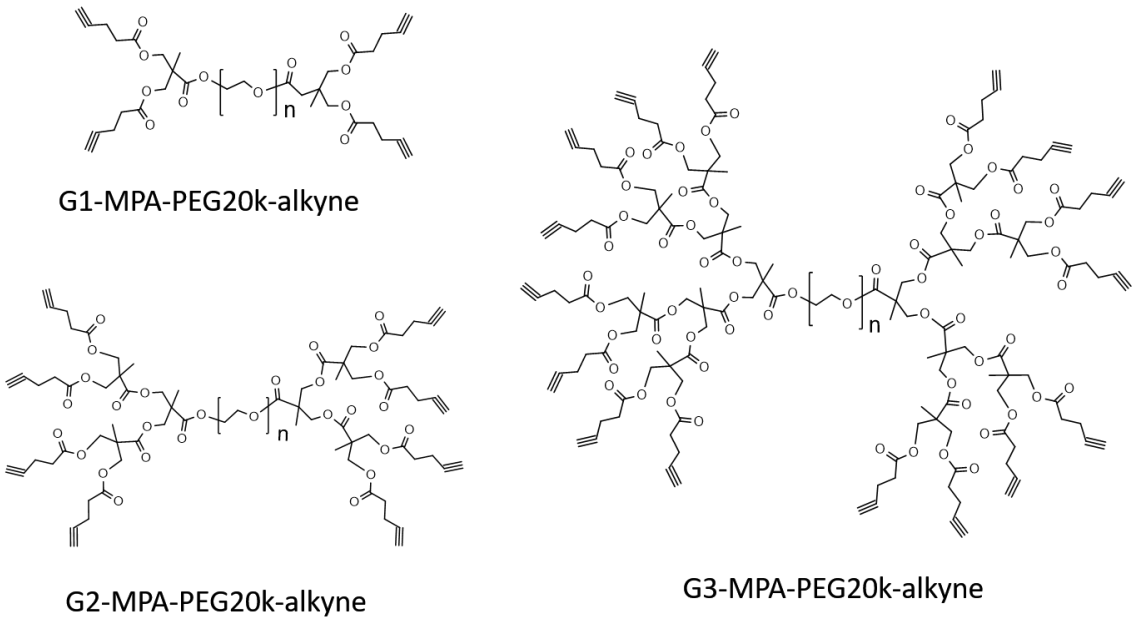

Scheme 4-1. Chemical structure of Gn-MPA-PEG20k-alkyne dendritic-linear-dendritic polymer (n=1, 2, 3).

4.2 Synthesis and characterization of Gn-MPA-PEG20k-TEMPO radical dendritic structures

4.2.1 Synthesis of Gn-MPA-PEG20k-TEMPO (n=1,2,3)

First of all, we synthesized a family of radical dendritic systems anchoring TEMPO-N_3 radicals on such bis-MPA-based polymers with alkyne as end groups by click chemistry (Scheme 4-2). The synthesis of these three-generation dendrimers was conducted in similar conditions, with CuI as catalyst and DIEA as base. After overnight reaction at room temperature in a mixture of solvents of THF and MeCN, the CuI was removed by filtration, and the products were purified by dialysis. Finally, we obtained three “radical dendrimers” G1-MPA-PEG20k-TEMPO (**30**), G2-MPA-PEG20k-TEMPO (**31**) and G3-MPA-PEG20k-TEMPO (**32**) with very high yields, with molecular weight

21359, 22933 and 26081 g/mol, respectively.

We have to say that the solubility in water of these radical dendritic structures decreased with increasing generation, since more precipitation was observed during the dialysis process of G3-MPA-PEG20k-TEMPO (**32**) than G2-MPA-PEG20k-TEMPO (**31**), while G1-MPA-PEG20k-TEMPO (**30**) was soluble during this process at a roughly similar concentration. We have checked the solubility of them in water being G1 ≥ 10 mg/mL, G2 ≥ 3 mg/mL and G3 < 0.1 mg/mL. This phenomenon probably stems from the big hydrophobic dendron part in high generation radical structures. Due to the amphiphilic segments in this structure, it was possible to prepare nanoparticles in water.

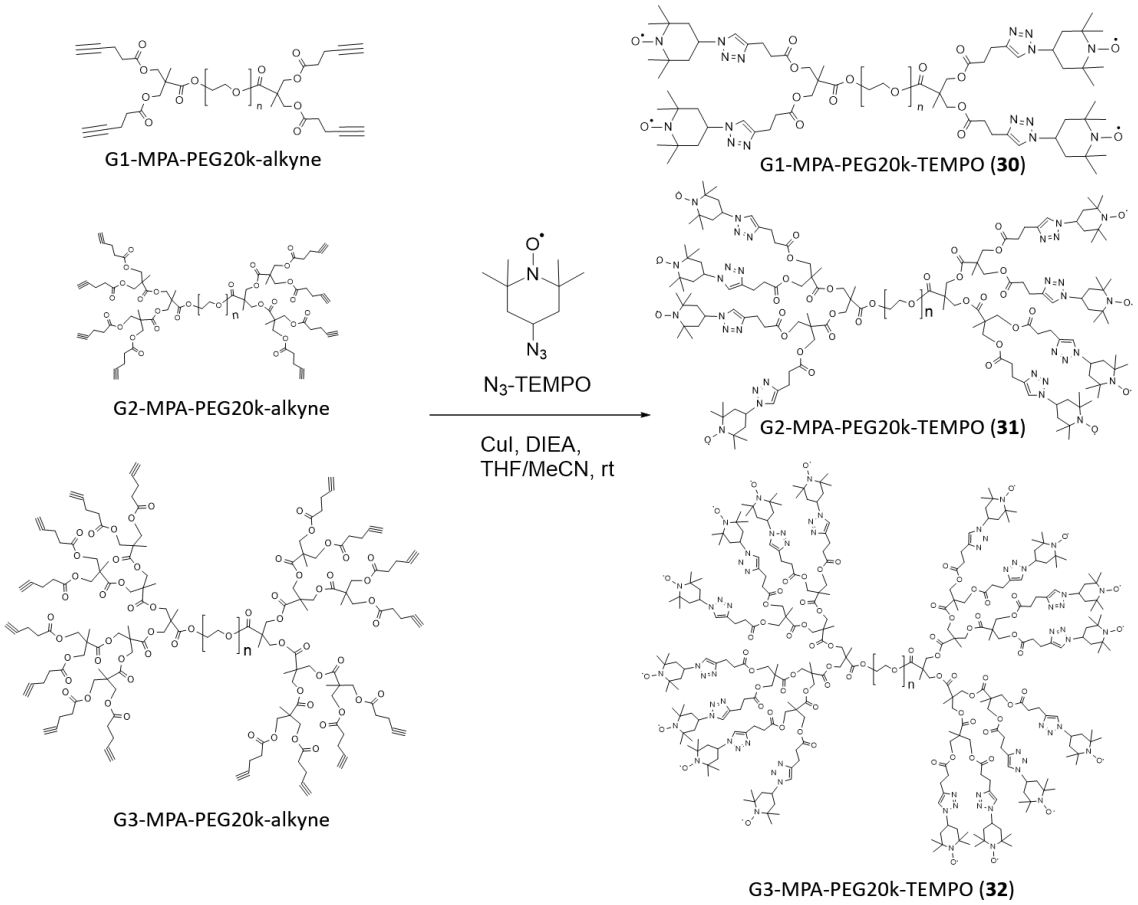

Scheme 4-2. Synthesis of Gn-MPA-PEG20k-TEMPO radical dendritic structures (n=1, 2, 3).

4.2.2 Characterization of Gn-MPA-PEG20k-TEMPO (n=1,2,3)

The characterization of Gn-MPA-PEG20k-TEMPO (n=1,2,3) species by IR was not possible, since we only observed the intense band of the PEG chain. Fortunately, we can use ^{1}H NMR to characterize the products, after the reduction of TEMPO radicals to the

corresponding diamagnetic hydroxylamine derivative by phenylhydrazine.[34] According to the ^{1}H NMR spectra (Figure 4-3 to Figure 4-5), we can see the peaks of TEMPO units between 1.1 and 2.1 ppm, as well as the peaks of the dendrons and the PEG chain, labelled in the corresponding ^{1}H NMR spectra.

Specifically, in the ^{1}H NMR spectrum of G1-MPA-PEG20k-TEMPO (**30**) (Figure 4-3), the peaks of the TEMPO-OH are located at 1.1 ppm (*a*), 1.9 ppm (*b*) and 4.79 ppm (*c*). And the protons from the dendrons can also be recognized at ca. 2.7 ppm (*e,f*) and 4.1 ppm (*g*). The protons from the PEG chain are at 3.51 ppm. Since the ^{1}H NMR spectrum of G1-MPA-PEG20k-TEMPO (**30**) was made in DMSO-d_6 as deuterated solvent, the proton from the triazole (*d*) can also be found at 8.0 ppm. The number of TEMPO units anchored to the dendrons can be obtained according to the relationship between the relative integrals of peaks *a* and *h*, which was in agreement with the theoretical number of 4.

The ^{1}H NMR spectra of G2-MPA-PEG20k-TEMPO (**31**) and G3-MPA-PEG20k-TEMPO (**32**) are given in Figure 4-4 and Figure 4-5, and the ^{1}H NMR spectrum of G2-MPA-PEG20k-alkyne is also shown in Figure 4-4 for comparison. The ^{1}H NMR spectra of G2-MPA-PEG20k-TEMPO (**31**) and G3-MPA-PEG20k-TEMPO (**32**) presented similar chemical shifts of the corresponding protons. Importantly, the chemical shift of peaks from the alkyne groups at 1.99 ppm disappeared in both spectra. The peaks of the protons from the methyl groups of TEMPO-OH are overlapped with the peaks of the methyl groups from the dendrons part, and they are located between 1.20 and 1.40 ppm (*a*, *h*, *j* / *l*). The protons of methylene (CH_2) of TEMPO-OH (*b*) are located between 2.0 and 2.1 ppm, and those from the methine group (CH) of TEMPO-OH (*c*) can be found between 5.0 and 5.2 ppm. The protons of PEG are at ca. 3.6 ppm, and the protons of the dendrons can be found at 2.76, 3.0 ppm (*e,f*) and 4.2 ppm (*g*, *i* / *k*). It is important to remark that the shift of the *e,f* protons of the dendrons chains between G2-MPA-PEG20k-alkyne and G2-MPA-PEG20k-TEMPO (**31**) species (Figure 4-4) is an evidence of the successful anchoring of the TEMPO radicals to the dendrons part. In these two compounds we have used $CDCl_3$ as deuterated solvent, for this reason, the protons from the triazole (*d*) can only be barely observed. Regarding the number of radical units in G2-MPA-PEG20k-TEMPO (**31**) can be obtained from the relationship between the relative integrals of the peaks (*a*, *h*, *j*) and the peak (*g*, *i*) while in G3-MPA-PEG20k-TEMPO (**32**) can be obtained from the relationship between the relative integral values of the peak (*c*) and the peak (*g*, *i*, *k*), in agreement with the theoretical numbers of 8 and 16.

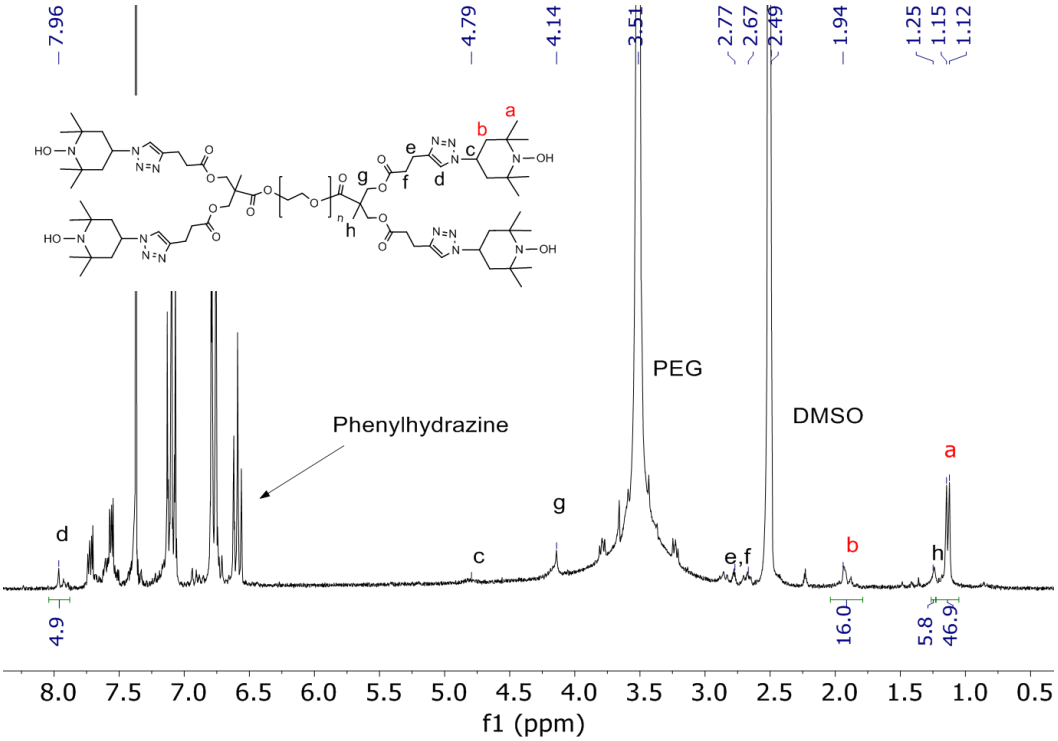

Figure 4-3. ^{1}H NMR spectrum of G1-MPA-PEG20k-TEMPO (**30**) after being reduced with phenylhydrazine (DMSO-d_6, 250 MHz).

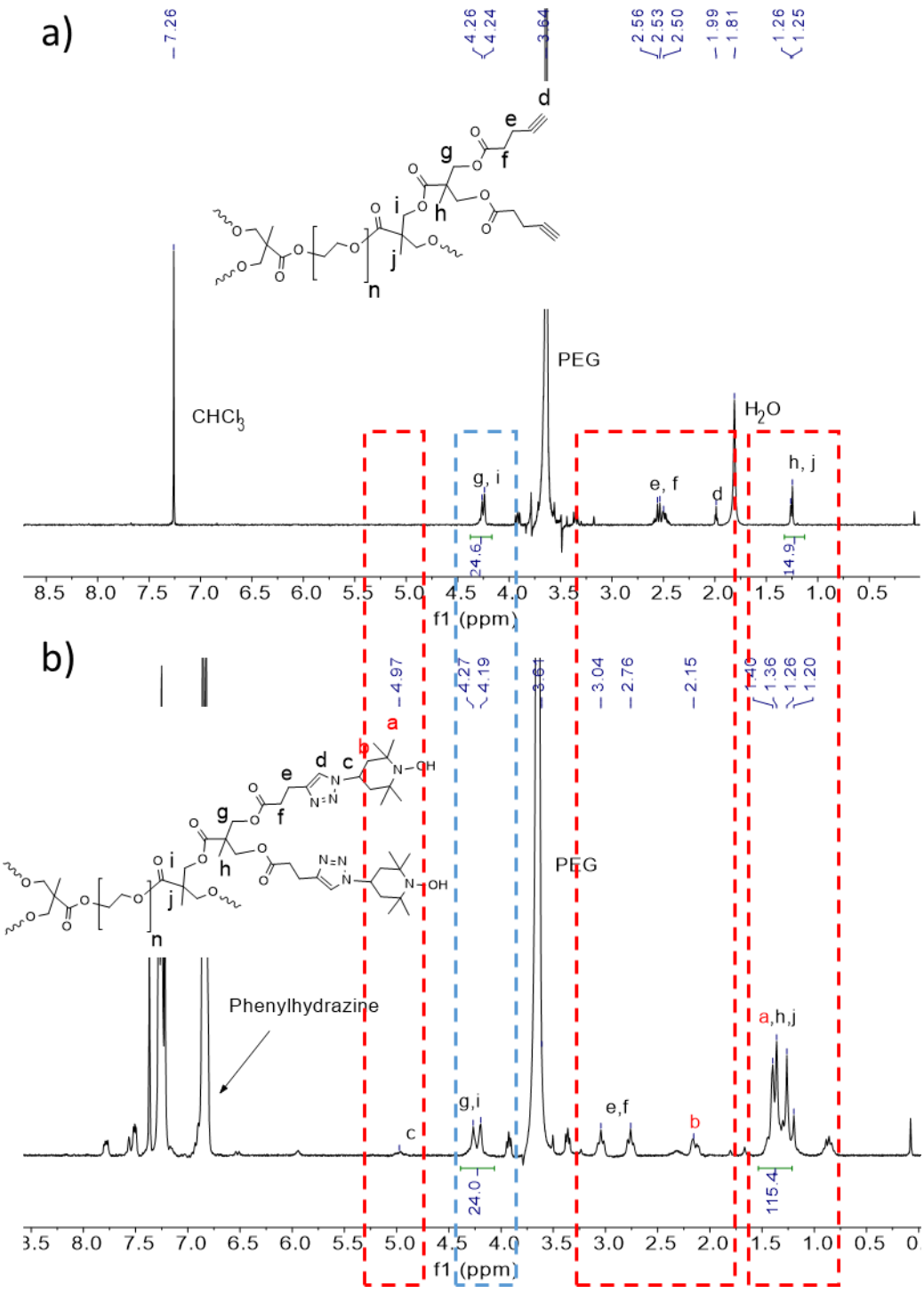

Figure 4-4. ^{1}H NMR spectra of G2-MPA-PEG20k-alkyne (up) and G2-MPA-PEG20k-TEMPO (**31**) (down) after being reduced with phenylhydrazine ($CDCl_3$, 250 MHz).

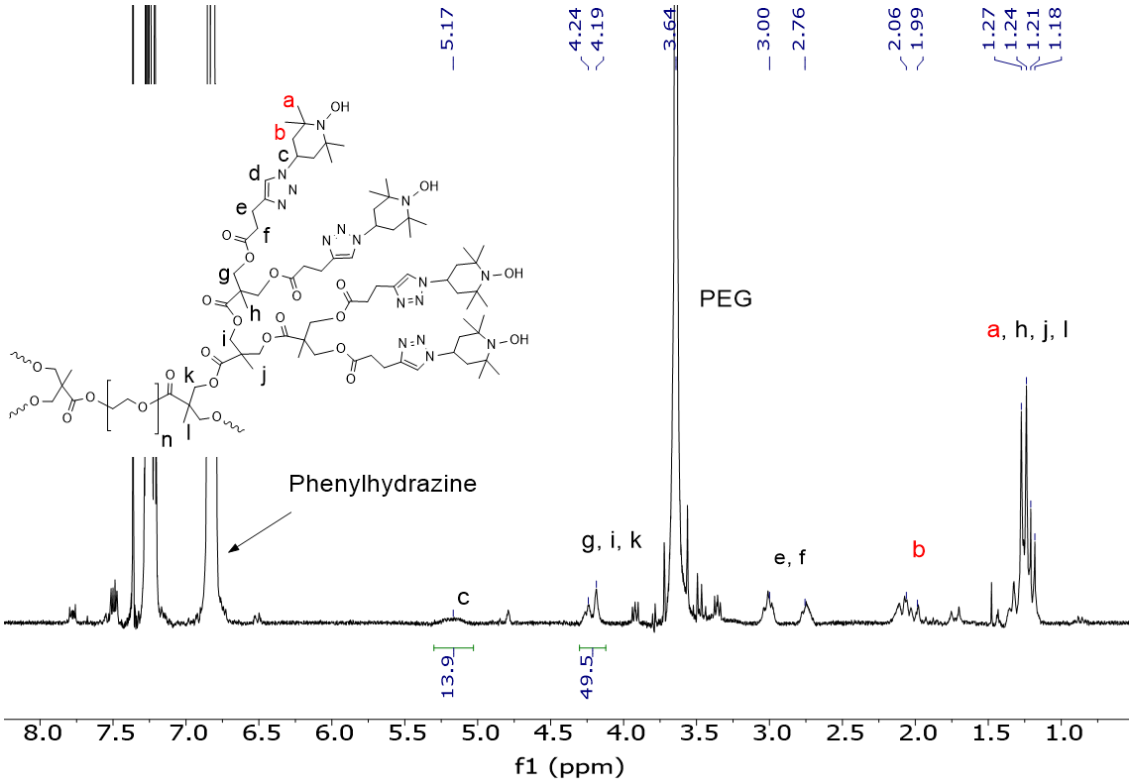

Figure 4-5. ^{1}H NMR spectrum of G3-MPA-PEG20k-TEMPO (**32**) after being reduced with phenylhydrazine ($CDCl_3$, 250 MHz).

The UV-Vis was also used to characterize G1, G2 and G3-MPA-PEG20k-TEMPO. The radical TEMPO has two characteristic absorbance bands at around 240 nm and 450 nm, which are ascribed to π- π* and n-π* transitions, respectively. The absorption band at ca. 450 nm shows additive properties and is normally isolated, but in this series of compounds these bands were not properly observed (Figure 4-6a). However, the band at 240 nm also showed good additive properties [35] and the corresponding absorbances (and molar absorptivities ε) were proportional to the number of TEMPO units (in 0.05 mM solutions of these compounds in CH_2Cl_2) (Figure 4-6b). The data of the UV-Vis are summarized in Table 4-1.

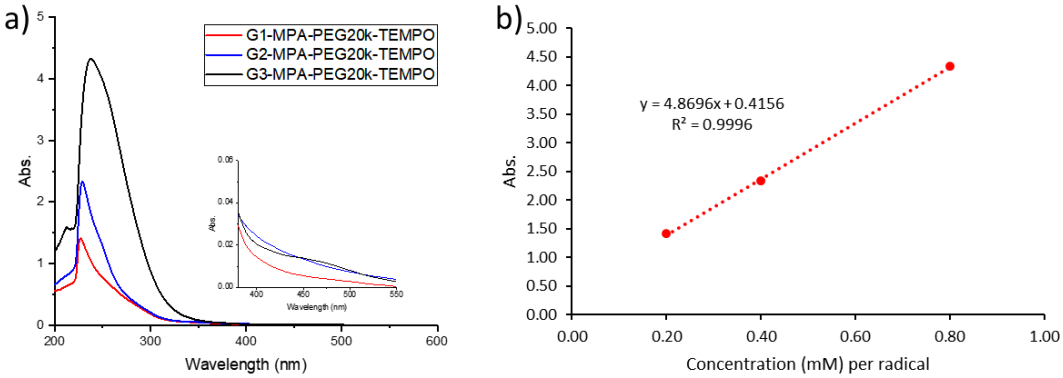

Figure 4-6. a) UV-Vis spectra of G1, G2 and G3-MPA-PEG20k-TEMPO at 0.05 mM in CH_2Cl_2, with the concentration per TEMPO unit ranging from 0.2 mM to 0.8 mM. b) Plot of absorbance versus concentration per radical unit for the different compounds solutions.

Table 4-1. UV-Vis data of G1, G2 and G3-MPA-PEG20k-TEMPO compounds.

Compound	λ_{max}	Abs.	Con. (mM) per molecule	Con. (mM) per radical
G3-MPA-PEG20k-TEMPO (**32**)	238	4.32	0.05	0.8
G2-MPA-PEG20k-TEMPO (**31**)	228.5	2.33	0.05	0.4
G1-MPA-PEG20k-TEMPO (**30**)	227	1.41	0.05	0.2

4.3 EPR study of Gn-MPA-PEG20k-TEMPO

EPR was also used to study the obtained G1-, G2- and G3-MPA-PEG20k-TEMPO "radical dendrimers" (Figure 4-7). Due to the different solubility, the EPR spectra of G1- and G2-MPA-PEG20k-TEMPO were obtained in H_2O, while the spectrum of G3-MPA-PEG20k-TEMPO (**32**) was obtained in DMSO. All of these EPR spectra showed spin-exchange interaction between TEMPO radicals. This interaction in the highest generation G3-MPA-PEG20k-TEMPO (**32**) is stronger than in G2 and G1, which results from the higher number of radicals in higher generations. These results also confirmed that the radicals were anchored onto the surface of the dendrons.

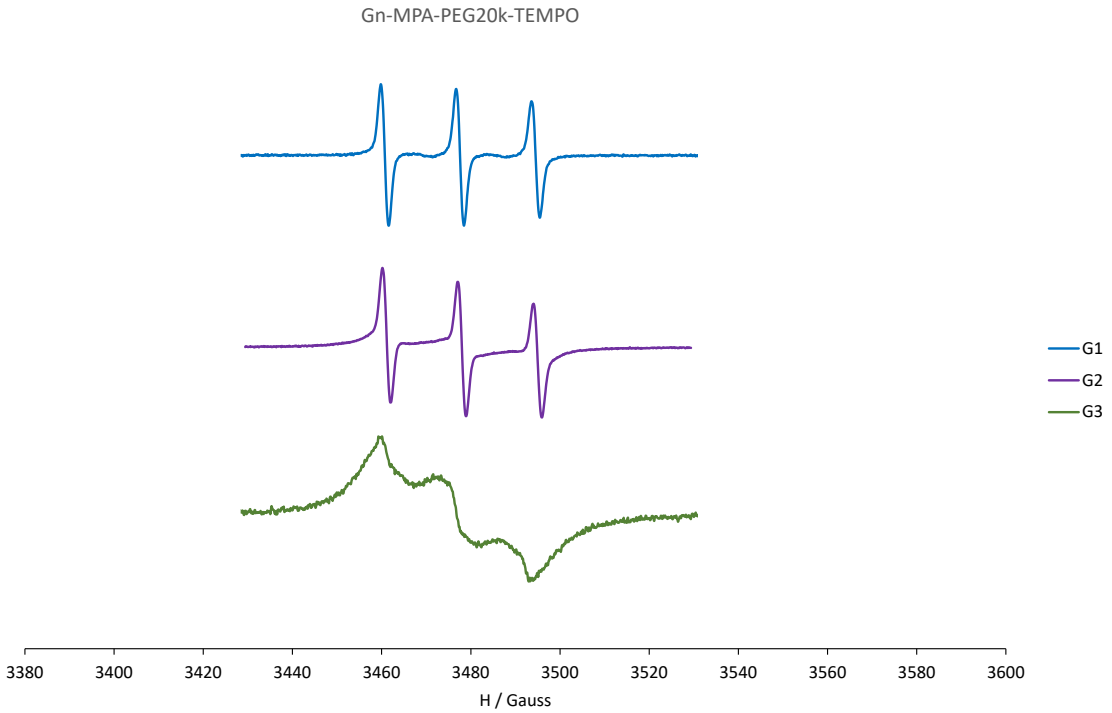

Figure 4-7. EPR spectra of Gn-MPA-PEG20k-TEMPO compounds (G1 and G2 measured in H_2O, G3 measured in DMSO).

Also, the EPR characterization as well as a quantitative study of G1, G2 and G3-MPA-PEG20k-TEMPO dendritic systems was made in CH_2Cl_2. The quantitative EPR study showed a good linear regression between the area of the EPR signal (double integral) and the corresponding number of nitroxides in the structure (Figure 4-8).

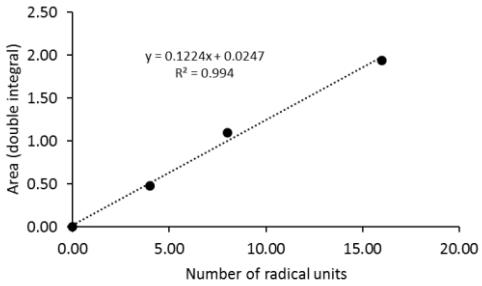

Figure 4-8. Regression line between the EPR signal area (double integral) and the number of TEMPO radicals of G1, G2 and G3-MPA-PEG20k-TEMPO dendrimers, at 0.05 mM and 300 K.

In Figure 4-9, we can observe the spectra of the three compounds in CH_2Cl_2 at 300 K. As explained in Chapter 3, the EPR spectrum of a free nitroxyl radical presents a three-line spectral pattern from the coupling of the unpaired electron with the ^{14}N atom of the N-O$^{\bullet}$ unit, with hyperfine coupling constant a_N *ca.* 15.6 G in organic solvents. The number of lines in the EPR spectra of radical species in which the unpaired electron is

coupled with *n* number of equivalent N atoms (nuclear spin I =1) is $2n + 1$. The spectrum of G1-MPA-PEG20k-TEMPO (**30**) dendrimer shows 5 lines separated by *ca.* 7.8 G ($a_N/2$) while the spectrum of G2-MPA-PEG20k-TEMPO (**31**) shows 9 lines separated by *ca.* 3.9 G ($a_N/4$), both with alternating linewidth effect: three narrow lines and in between them two groups of 1 or 3 broad lines, respectively (marked with asterisks in Figure 4-9). The alternating linewidth effect is due to a dynamic process of the radicals (see below). In the case of G3-MPA-PEG20k-TEMPO (**32**), we observed a single broad line pattern between the three principal lines instead of resolved lines. The G1 spectral pattern indicates strong spin exchange interaction ($|J| >> |a_N|$) between 2 nitroxide units (2 N) which leads to 5 lines separated by $a_N/2$ while the G2 spectral pattern indicates strong spin exchange interaction between 4 nitroxide units (4 N) which leads to 9 lines separated by $a_N/4$. The spectral pattern of G3 indicates spin exchange interactions between several nitroxide units. In fact, in this case, the spectral resolution does not allow to determine the number of interacting TEMPO radicals.

With the decrease of temperature from 300 to 260 K, we observed a decrease of the broad lines/bands of the spectra (Figure 4-10 a,b,c) which means the spin exchange is weaker and slower at lower temperature. This is a typical behaviour of flexible polyradical species that show spin exchange dynamics modulated by temperature. The EPR spectrum shape is dependent on the conformation and mobility of the dendritic branches (i.e. on the frequency of collisions of the spin-bearing groups) that depends on the temperature and solvent nature; at lower temperature lower frequency of collisions among the radicals and weaker spin exchange interaction among them.

Therefore, from the EPR analysis, we can say that the three radical dendritic species are flexible and present spin exchange interaction among some of the radical units. In G1-MPA-PEG20k-TEMPO (**30**) dendrimer (with 4 TEMPO radicals) there are two groups of 2 interacting nitroxides, that are independent from each other, since we only observe 5 lines (in the case of interaction among the 4 radicals the spectrum would present 9 lines). This means that the two groups of 2 nitroxides are well separated by the 20k PEG chain and that the PEG chain is not bent or not bent enough to bring the two groups close together. Similarly, in G2-MPA-PEG20k-TEMPO (**31**) (with 8 TEMPO radicals) there are two groups of 4 nitroxide units at the ends of the PEG chain, which are not interacting between them, since we observe 9 lines (in the case of interaction between the 8 radicals the spectrum would present 17 lines). By extrapolation, the same should happen with G3 compound, having two groups of 8 interacting TEMPO radicals at the end of the PEG

chain.

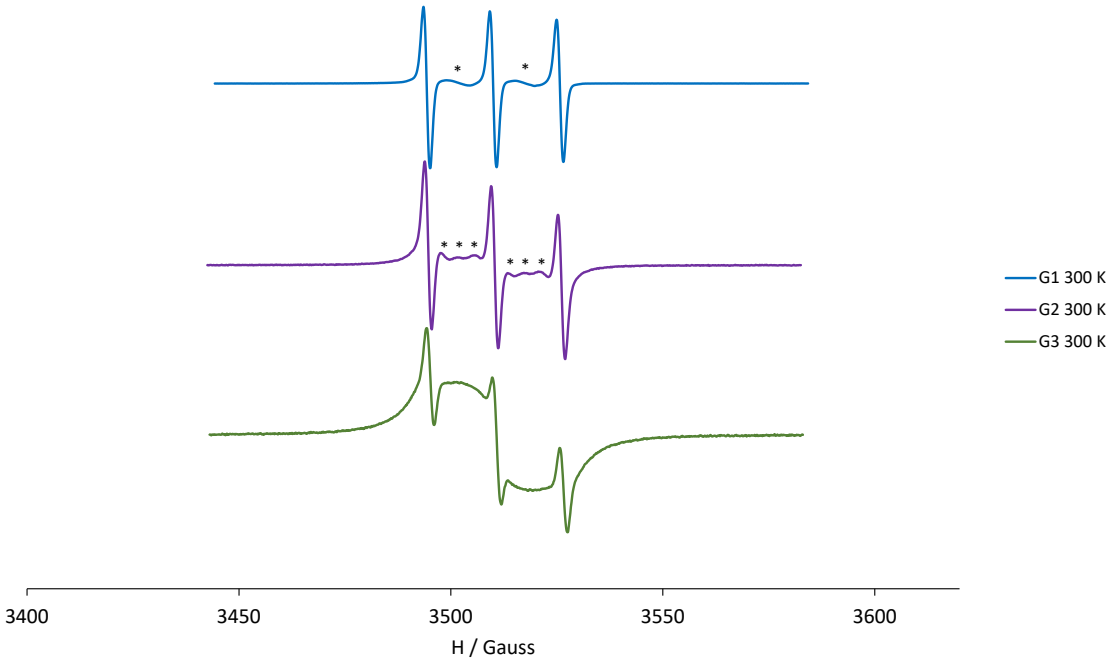

Figure 4-9. EPR spectra of G1, G2 and G3-MPA-PEG20k-TEMPO species in CH_2Cl_2 at 300 K, with normalized intensities.

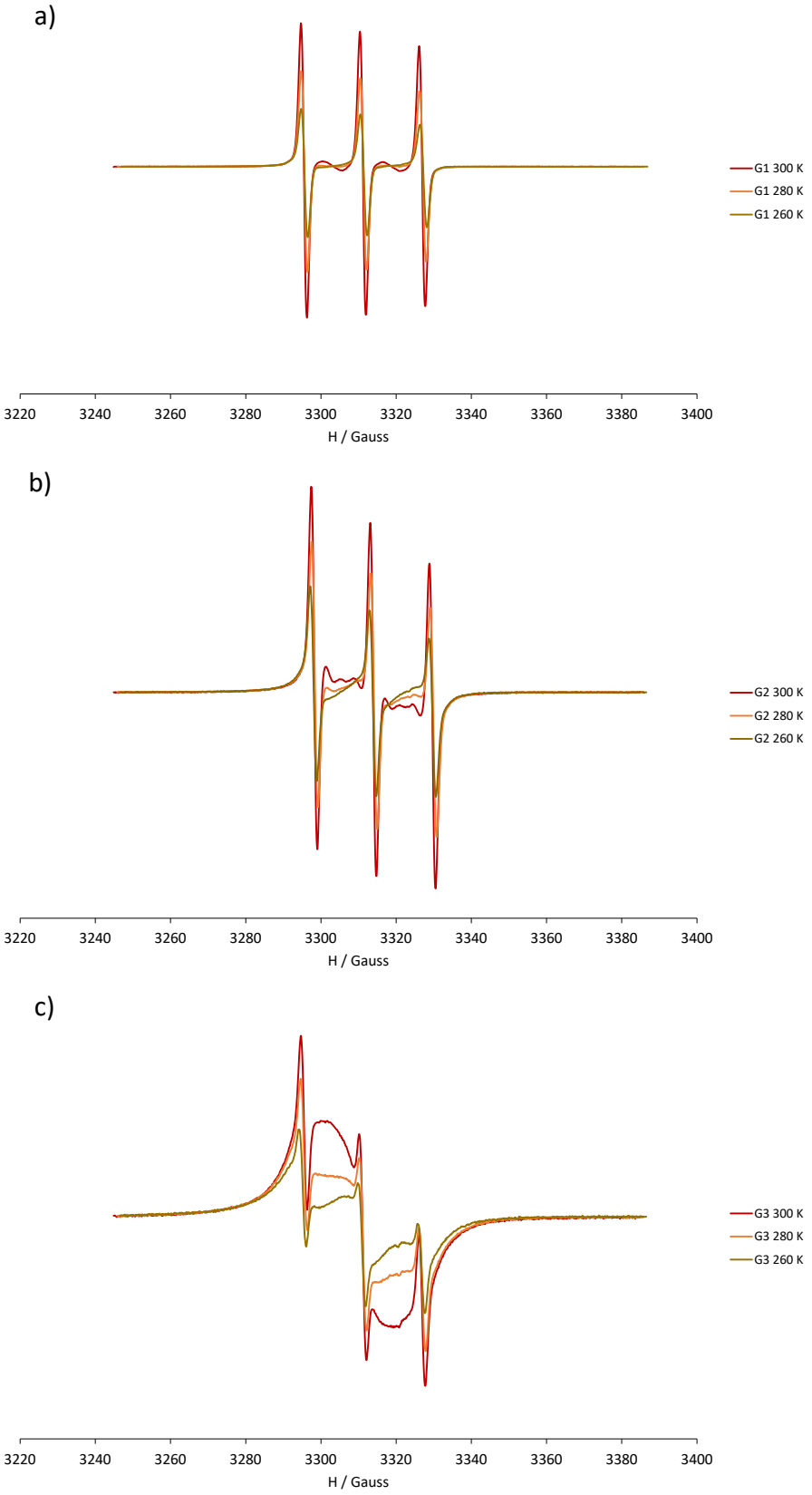

Figure 4-10. EPR spectra of a) G1-MPA-PEG20k-TEMPO (**30**), b) G2-MPA-PEG20k-TEMPO (**31**) and c) G3-MPA-PEG20k-TEMPO (**32**) species at 0.05 mM in CH_2Cl_2 at 300 K-260 K temperature range.

The corresponding EPR spectra in frozen solution (125 K) is shown in Figure 4-11. As explained in Chapter 3, in frozen solution the EPR spectrum is sensitive to the intramolecular dipole-dipole interaction between neighboring nitroxides which substantially alters the shape of the spectrum. This effect could be estimated by the empirical ratio of peak heights d_1/d (Chapter 3, Figure 4-11) which is shown to be sensitive to the distance between adjacent nitroxides (the shorter the distance among nitroxides, the higher the dipolar interactions and hence the higher the d_1/d parameter). As expected, the d_1/d parameter for G2 dendrimer (0.79) was higher than for G1 (0.69), and higher than that for the free nitroxide (0.53),[36] while in G3 the strongest dipolar interactions are translated into broader bands leading to low resolution, not allowing us to calculate properly the d_1/d parameter. Thus, by increasing generation, there are more nitroxides close together, making increase the intramolecular dipolar interactions among them.

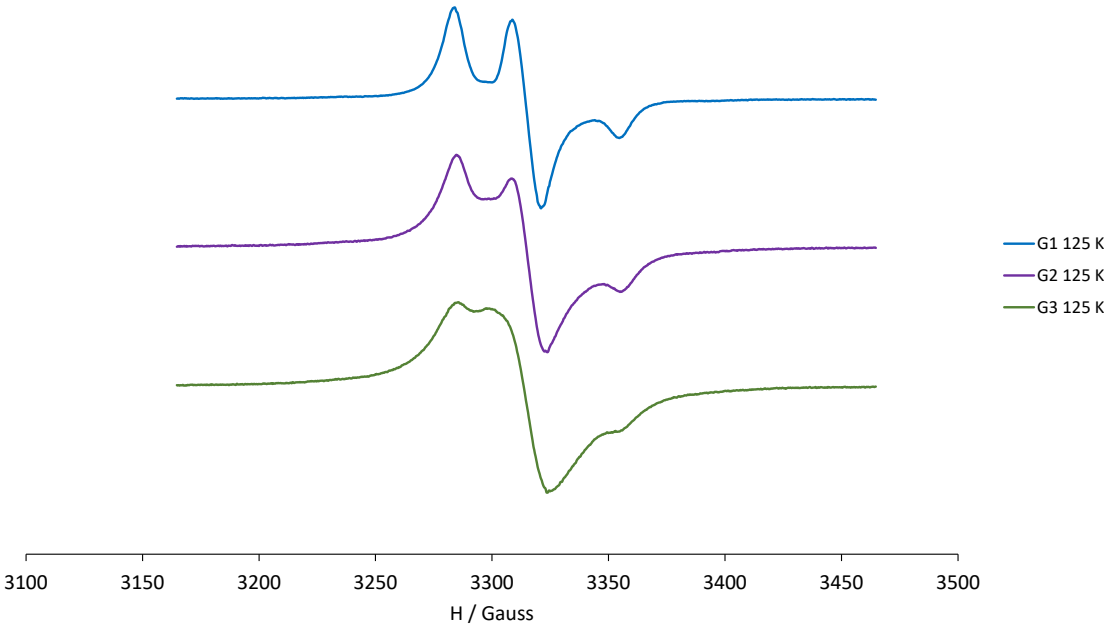

Figure 4-11. EPR spectra of G1, G2 and G3-MPA-PEG20k-TEMPO radical dendritic species in CH_2Cl_2 at 125 K, with normalized intensities.

Under these frozen conditions, we also observed an $|\Delta m_s| = 2$ transition at half-field in the three generations (Figure 4-12), characteristic of dipolar coupled spins and indicating the presence of a high-spin state. The intensity of such a forbidden transition increases with increasing generation.

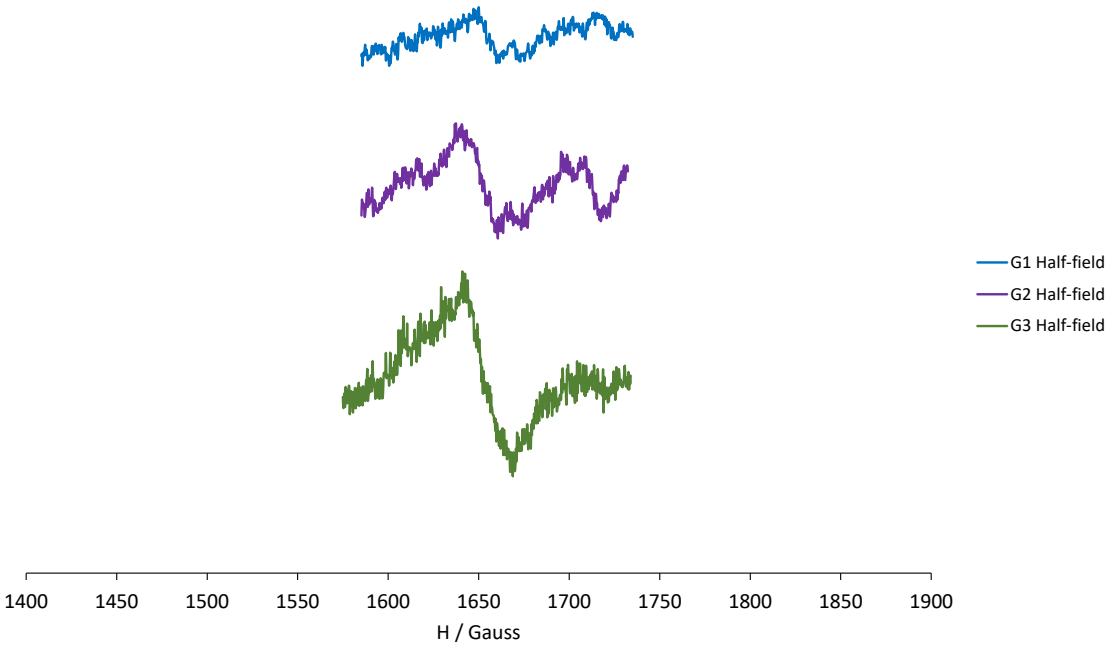

Figure 4-12. EPR spectra of $|\Delta m_s| = 2$ transition at half-field of G1, G2 and G3-MPA-PEG20k-TEMPO dendrimers at the same concentration (0.05 mM), in CH_2Cl_2 at 125 K.

4.4 Preparation and characterization of nanoparticles

After the obtaining and proper characterization of these radical dendritic systems, we tried to prepare nanoparticles with these kinds of compounds. Since G3-MPA-PEG20k-TEMPO (**32**) has more radicals (16) than G1 and G2-MPA-PEG20k-TEMPO, we started with G3-MPA-PEG20k-TEMPO (**32**) compounds. In general, the method of preparation of organic nanoparticles consists in adding the polymer solution into an aqueous solution, followed by dialysis to remove the organic solvent, as shown in Figure 4-13. We prepared organic nanoparticles under different conditions by controlling different parameters, such as the injection speed, the stirring speed, the amount of the compounds, and the sequence of injection (polymer organic solution into water or water into polymer organic solution) as shown in Table 4-2 (entries 1-7) since all of these parameters likely influence the formation of nanoparticles.[37]

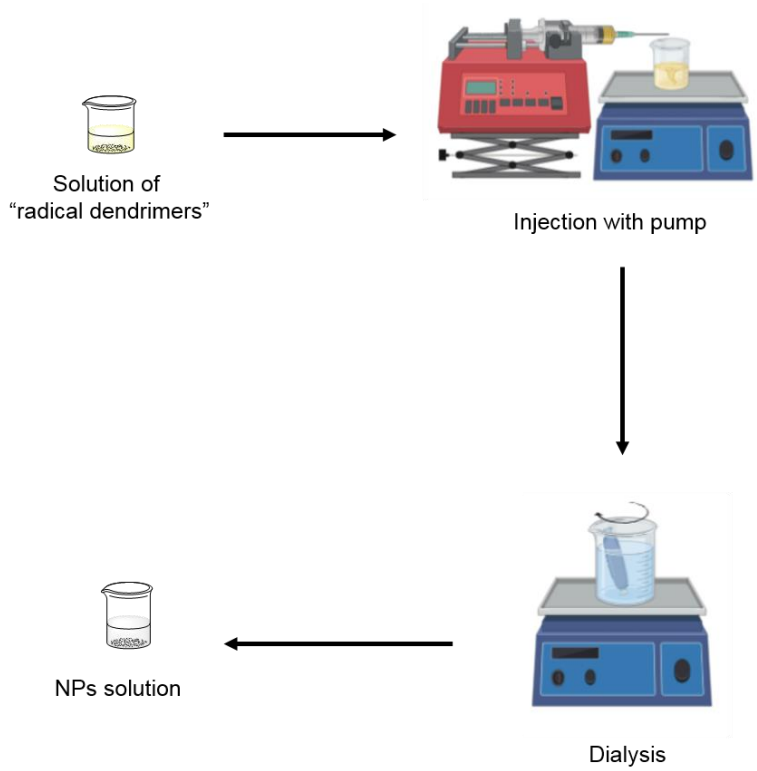

Figure 4-13. The steps to prepare organic nanoparticles with radical dendritic structures.

The injection speed was carefully controlled by an injection pump. We used 5 mg of G3-MPA-PEG20k-TEMPO (**32**) compound dissolved in different organic solvents like DMSO, acetone, methanol or THF, injection speed from 0.5 to 6 mL/h, 3 or 5 mL of water and stirring speed ranging from 180 to 700 rpm (entries 1-7, Table 4-2). However, although some nanoparticles were obtained (see below), in all trials we always saw a white precipitate during these processes. We also tried to form the nanoparticles directly in water using ultrasonication (entry 8, Table 4-2): 0.3 mg of G3-MPA-PEG20k-TEMPO (**32**) were directly dissolved in 3 mL of water with ultrasonication. However, even after 5 hours, the compound was still observed in water. Thus, unfortunately, we did not obtain homogeneous system after some trials. Nevertheless, we characterized the sample from entry 1, Table 4-2, by TEM and DLS, after the precipitate part was removed by centrifugation. Interestingly, we observed that NPs were formed (G3 NPs). TEM images showed that the formed G3 NPs presented homogeneous size distribution and spherical shape, with a mean size of 34±6.4 nm (Figure 4-14b and c).

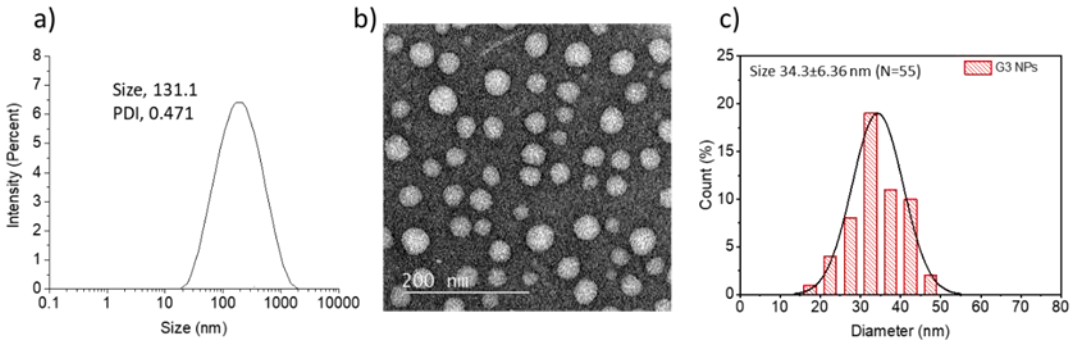

Figure 4-14. DLS and TEM characterization of G3 NPs prepared prepared under the condition from entry 1 of Table 4-2. a) Size distribution by intensity obtained by DLS measurements, b) TEM image using negative stain method with uranyl acetate and c) size distribution histogram.

By DLS, we obtained a monodisperse size distribution of G3 NPs with a z-average size of 131 nm and a quite high polydispersity index PDI = 0.471. Between DLS and TEM characterization there is a big difference in size: 131 nm by DLS (intensity) and 34 nm by TEM. This difference in size comes from the different nature of the size which differs as measured by DLS and TEM. DLS transforms the measured diffusion coefficient to an equivalent hydrodynamic size, which is the size of the nanoparticle plus the liquid layer around the particle and it takes into account any protecting (surfactant, steric layer) or stabilizing layer that may surround the particle (Figure 4-15a). Moreover, in NPs with PEG chains, the higher PEG chain coverage the NPs have, the more hydrodynamic diameter they present (Figure 4-15b). On the other hand, size measured by TEM electron microscopy responds to the electron-dense part of the particle and gives a more real size of the nanoparticle. The size measured by DLS is an estimate but provides complementary information to the TEM.

Taking this into account, this difference in size in our G3 NPs might be due to the high density of PEG chains surrounding the NPs core which leads to obtaining a much larger hydrodynamic diameter than the size obtained by TEM, supporting the schematic drawing that we have made to represent them in Figure 4-2.

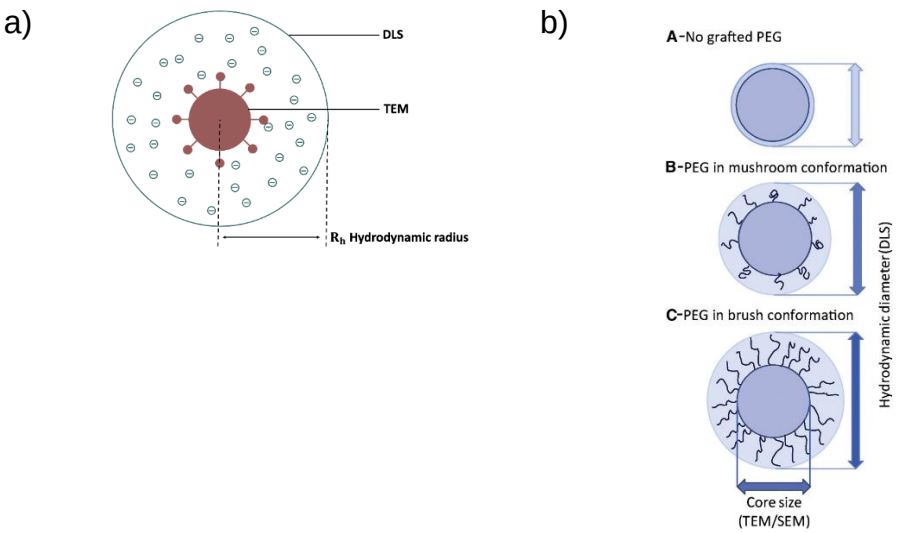

Figure 4-15. Schematic representation of a) the different sizes of a nanoparticle measured by DLS and TEM techniques, and b) the influence of the higher PEG coverage of the NPs in their hydrodynamic diameter size.

The EPR spectrum of G3 NPs presented two types of spectral components: an immobile/slow component represented by a broad anisotropic spectral pattern (indicated by arrows in Figure 4-16) and a mobile/fast component represented by the narrow three-line spectral pattern. The immobile/slow component represents the TEMPO radicals that have restricted movement in the structure (probably those located more in the interior of the NPS, in the dense core) while the mobile/fast component represents the TEMPO radicals anchored on the structure that have much faster mobility (i.e. faster tumbling), probably located farther from the core, a bit closer to the exterior part of the NP structure.

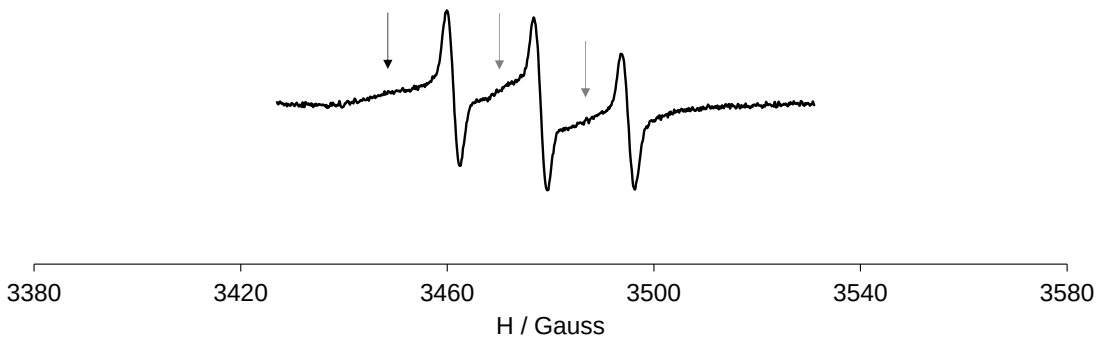

Figure 4-16. EPR spectrum of G3 NPs in H_2O.

Table 4-2. Different parameters used for the preparation of nanoparticles with G3-MPA-PEG20k-TEMPO.

entry	quantity of radical dendrimers	organic solvent	volume of water	injection speed	stiring speed (rpm)	method
1	5.0 mg	0.5 mL of DMSO	3 mL	6 mL/h	250-400	water into organic solvent
2	5.0 mg	0.5 mL of DMSO	3 mL	6 mL/h	250	water into organic solvent
3	5.0 mg	0.5 mL of DMSO	3 mL	6 mL/h	700	water into organic solvent
4	5.0 mg	0.5 mL of DMSO	3 mL	1 mL/h	500	organic solvent into water
5	5.0 mg	0.85 mL of Acetone	5 mL	1 mL/h	200	organic solvent into water
6	5.0 mg	0.8 mL of MeOH	5 mL	1 mL/h	200	organic solvent into water
7	5.0 mg	0.9 mL of THF	5 mL	0.5 mL/h	180	organic solvent into water
8	0.3 mg	no	3 mL	no	no	ultrasonication for 5 hours

Table 4-3. Different parameters for the preparation of nanoparticles with G2-MPA-PEG20k-TEMPO.

entry	quantity of radical dendrimers	organic solvent	volume of water	injection speed	stiring speed (rpm)	method
1	5.3 mg	0.5 mL of EtOH and 0.5 mL of MeOH	5 mL	2 mL/h	250	organic solvent into water
2	4.6 mg	1 mL of acetone	5 mL	1 mL/h	200	organic solvent into water

However, although we successfully obtained nanoparticles with G3-MPA-PEG20k-TEMPO (**32**), precipitation avoids calculating their relaxivity properly, because we need to know the concentration of the active paramagnetic species precisely when they are to be used as contrast agents.

For this reason, we moved to prepare nanoparticles with G2-MPA-PEG20k-TEMPO (**31**) species. At first, we dissolved the compound in a solvent mixture of MeOH and EtOH and injected it into water, but there was some precipitation and it did not disappear overnight (entry 1, Table 4-3). Next, we changed the organic solvent to acetone. The compound solution in acetone was injected into water at 1 mL/h injection speed and the stirring speed was 200 rpm (entry 2, Table 4-3). Then, the colloidal system was allowed to evaporate overnight in the fume hood. Finally, the colloid was dialyzed to remove the small amount of residual acetone. In this case, we got nanoparticles in a stable colloidal suspension (labeled as G2 NPs), without any precipitation.

The colloid was stored at 4 °C and it was characterized by DLS, TEM, and EPR techniques. Moreover, the stability with time was also studied by DLS for 28 days, following the hydrodynamic size, PDI and zeta potential evolution of the obtained nanoparticles (Figure 4-17). These nanoparticles showed unimodal or monodisperse size distribution both at the beginning and after 28 days, with a low polydispersity index (PDI). It was 0.233 at day 0, decreased to 0.111 after 1 day and then it was maintained until the last day. The corresponding hydrodynamic diameter decreased slightly from 210.9 nm to 180 nm after 1 day, but then it also stabilized at this value until the last day. On the other hand, zeta potential also decreased from +11.7 mV to around +4 mV the first day, and then maintained at around this value, in a similar trend to size and PDI values. Thus, it seems that G2 NPs nanoparticles need 24 h to stabilize but then, they are really stable for at least up to about a month. NPs having zeta potential values ranging from −10 to +10 mV are considered to be neutral.[38] The zeta potential with values from −10 to +10 mV are normally considered as a parameter indicating low stability. However, the zeta potential is not the only parameter to indicate the stability of the nanoparticles, and it is not uncommon to encounter stable colloids systems with low zeta potential. For example, it is well known that PEGylation can facilitate the stability of nanoparticles while decreasing the zeta potential.[39,40] The reason for that can be that PEG chains decrease the attraction between nanoparticles by increasing the steric distance and increasing the hydrophilicity via forming hydrogen bonds with solvent.[41] After 28 days at 4 °C, the colloidal suspension was characterized by TEM. The G2 NPs were spherical in shape and

homogeneous, as shown in the TEM image (Figure 4-18a) with a mean diameter of 35±10.1 nm. This difference in size between both techniques, similarly to G3 NPs, seems to support that the NPs have a denser core with mainly the dendritic radical part, and this is highly covered by a PEG shell, leading, hence, to obtain a much larger hydrodynamic diameter (Figure 4-15b). This fact also supports the nanoparticles structure schematized in Figure 4-2.

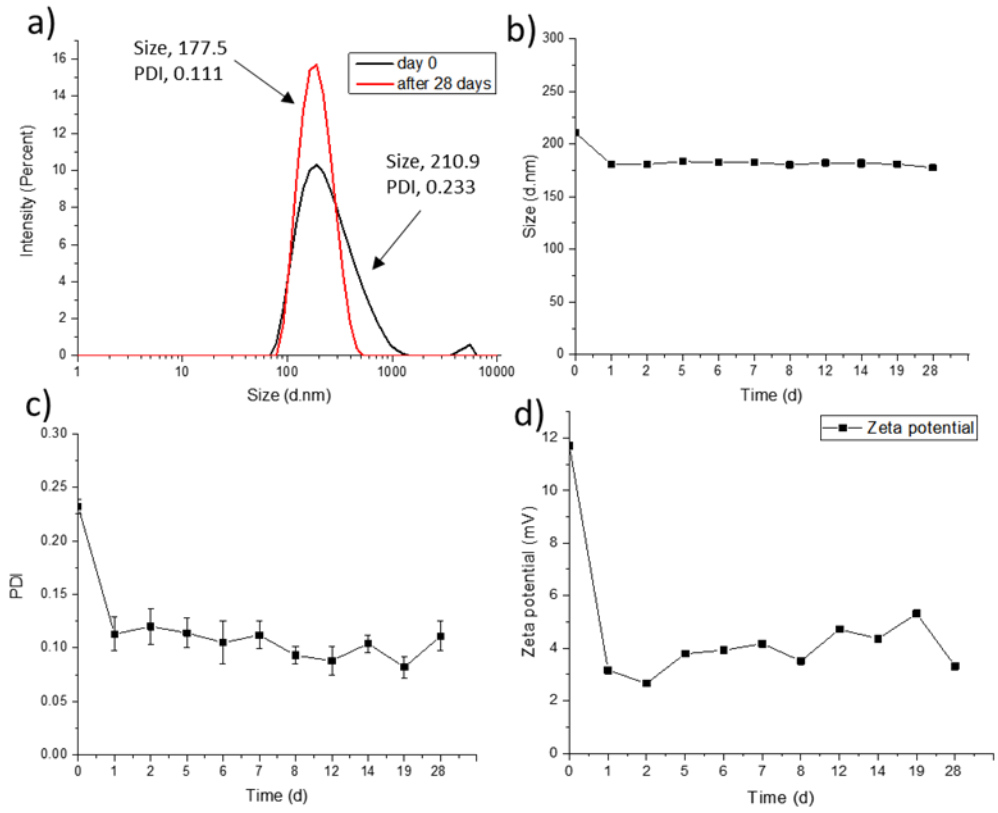

Figure 4-17. a) DLS results of G2 NPs at day 0 and after 28 days. Study of the colloidal stability of G2 NPs along 28 days characterized by b) size (hydrodynamic diameter) c) PDI and d) zeta potential.

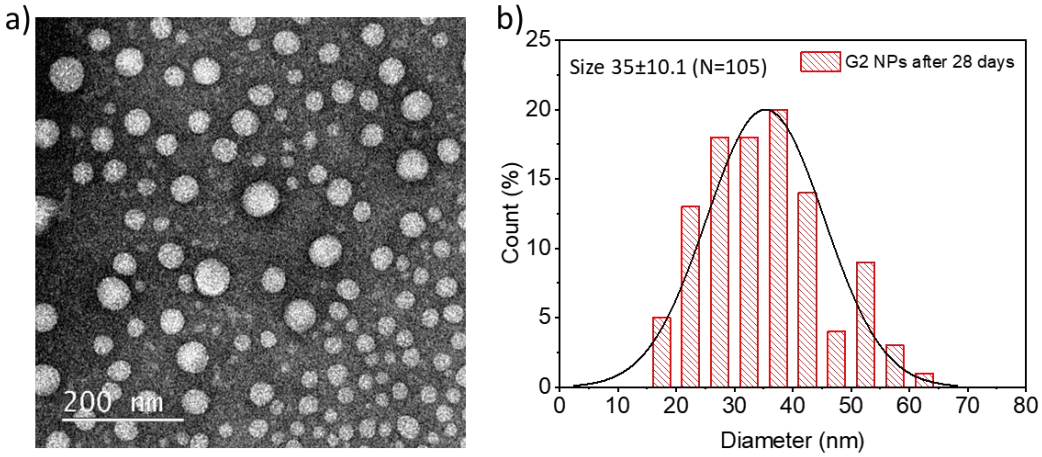

Figure 4-18. a) TEM image and b) size distribution histogram of G2 nanoparticles prepared under the conditions from entry 2 of Table 4-3, measured using negative stain method with uranyl acetate.

To further characterize such a system, we studied the behavior of G2 NPs against dilution by DLS and TEM and compared it with the same study but using G2-MPA-PEG20k-TEMPO (**31**) species directly in water, this is, without preparing NPs. By one hand, we wanted to check the size and morphology of G2 NPs with dilution, and hence, their stability, and, on the other hand, to know and compare the size and shape of the dendritic system as-synthesized without being forced to make nanoparticles, at the same concentrations than the nanoparticles system.

We dissolved the G2-MPA-PEG20k-TEMPO (**31**) polymer directly in water at the same concentration than for G2 NPs. Due to the high molecular weight of this polymer, it took few hours to swell. Finally, it was completely dissolved at the same concentration than the G2 NPs (1 mM per TEMPO radical unit) and we got the solution of this compound (labeled as G2 from now on).

The two systems (G2 and G2 NPs) were characterized by DLS at 1 mM per TEMPO radical unit concentration and after different dilutions. As shown in Figure 4-19, at 1 mM concentration the G2 NPs colloid presented a unimodal distribution size with very low PDI (0.070) while the G2 solution presented some polydispersity (PDI 0.4). Then, these two solutions were diluted to different concentrations, 0.1 mM, 0.01 mM and 0.001 mM (in the case of G2 NPs). As can be observed in Figure 4-19 and Table 4-4, the G2 NPs systems kept the unimodal size distribution (even after dilution to 0.001 mM), similar size and low PDI (only at 1000 times dilution, the PDI slightly increases). However, the G2 solutions presented multimodal size distribution in all the concentrations studied and an increase of size and PDI during dilution. This result points out that, under dilution

conditions, G2 NPs are quite stable since they are maintained with similar size, monodisperse size distribution and low PDI, in contrast to G2 compound behavior.

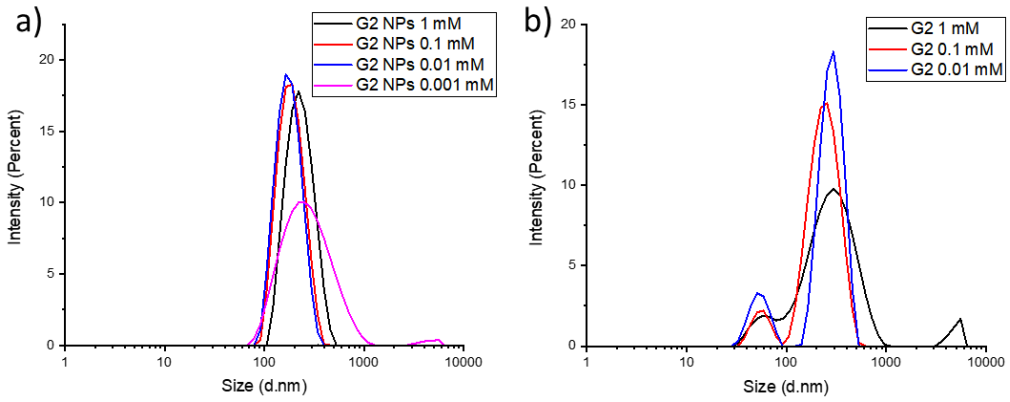

Figure 4-19. DLS results of G2 NPs (a) and G2 solution (b) at different concentrations. The concentration is measured per radical unit.

Table 4-4. Size and PDI data of G2 NPs and G2 solutions after dilution to different concentrations.

Sample	Concentration	Size	PDI
G2	1 mM	218.0±1.970	0.399±0.014
	0.1 mM	224.2±3.487	0.417±0.046
	0.01 mM	530.1±198.8	0.488±0.124
G2 NPs	1 mM	214.7±2.055	0.070±0.023
	0.1 mM	177.9±0.4583	0.108±0.025
	0.01 mM	175.7±5.859	0.182±0.073
	0.001 mM	225.7±18.23	0.292±0.041

G2 NPs colloids and G2 solution were also characterized by TEM at concentrations 1 and 0.1 mM (Figure 4-20). G2 NPs showed spherical nanoparticles both at 1 mM and 0.1 mM, thus, maintaining the spherical shape after dilution. On the other hand, the behavior of G2 solution was interesting. At 0.1 mM, the G2-MPA-PEG20k-TEMPO (**31**) species are structured forming mainly fibers, that is, unidirectional structures, while at a higher concentration, 1 mM, some spherical nanoparticles of very different sizes are formed, coexisting with still some fibers. Thus, in G2 species there is a morphological transition from fibers to spheres with the increase in concentration, while G2 NPs are maintained spherical, indicating better stability of G2 NPs than G2 species, which is consistent with the DLS results.

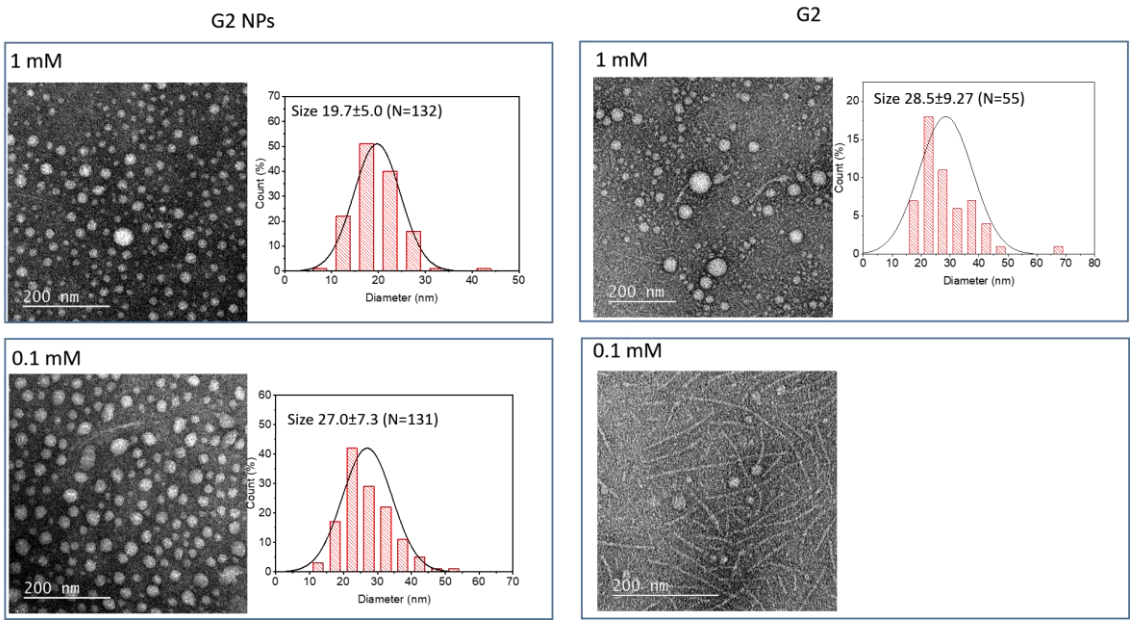

Figure 4-20. TEM images and size distribution histograms of G2 NPs and G2 solution in water, at 1 and 0.1 mM per radical unit, measured using negative stain method with uranyl acetate.

The EPR spectrum of G2 NPs (Figure 4-21) also presented the two types of spectral components mentioned in the EPR of G3 NPs. However, G2 NPs presented a smaller portion of the immobile/slow component (mainly seen in its lower magnetic field band marked by a black arrow in Figure 4-21) compared with G3 NPs, probably due to the lower number of radicals present onto the G2 dendritic structure. In this case, most TEMPO radicals present fast mobility, as shown by the three main narrow lines.

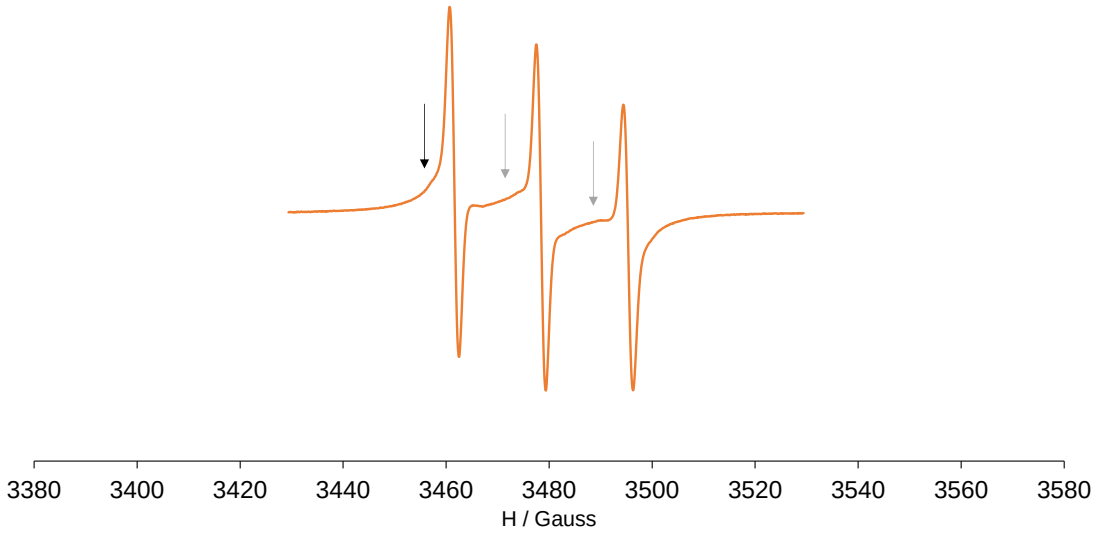

Figure 4-21. EPR spectrum of G2 NPs in H_2O.

On the other hand, if we compare the EPR spectrum of G2 NPs with that obtained

for G2, we can observe that the differences between them are very small (Figure 4-22a). In fact, as we have observed by TEM, G2 macromolecules can also form some nanoparticles themselves only by dissolving them in H_2O, although to a lesser extent and with higher polydispersity than if we force to prepare them with optimal procedure. Nevertheless, although the differences are subtle, they can help us to explain or understand the small differences between these two systems.

In the case of G2 NPs, the portion of immobile/slow component is slightly higher than in G2 (mainly observed in the higher intensity of the spectral pattern between the three lines indicated by grey arrows in Figure 4-22a). This means a slightly higher amount of radicals immobilized in G2 NPs than in G2, which agrees with the fact that in linear fibers like in linear polymers the rigidity is lower than in NPs.

The small difference between their coupling constants a_N (Figure 4-22b and Table 4-5), being lower in G2 NPs, is explained in terms that radicals are slightly less exposed to the polarity of the solvent, i.e. more embedded in the interior part of the NP than in G2, since the isotropic hyperfine constant a_N of nitroxides is sensitive to the polarity of the local nitroxide environment, being lower in solvents with low polarity and higher in polar solvents.[42]

The linewidth of G2 NPs spectrum is also a little bit higher than in G2 (Figure 4-22c and Table 4-5), which means higher intramolecular spin exchange interaction among radicals as well as that radicals are anchored to bigger size structures. Therefore, although the differences between the two systems (G2 and G2 NPs) are subtle, they have helped us to explain the small differences between them.

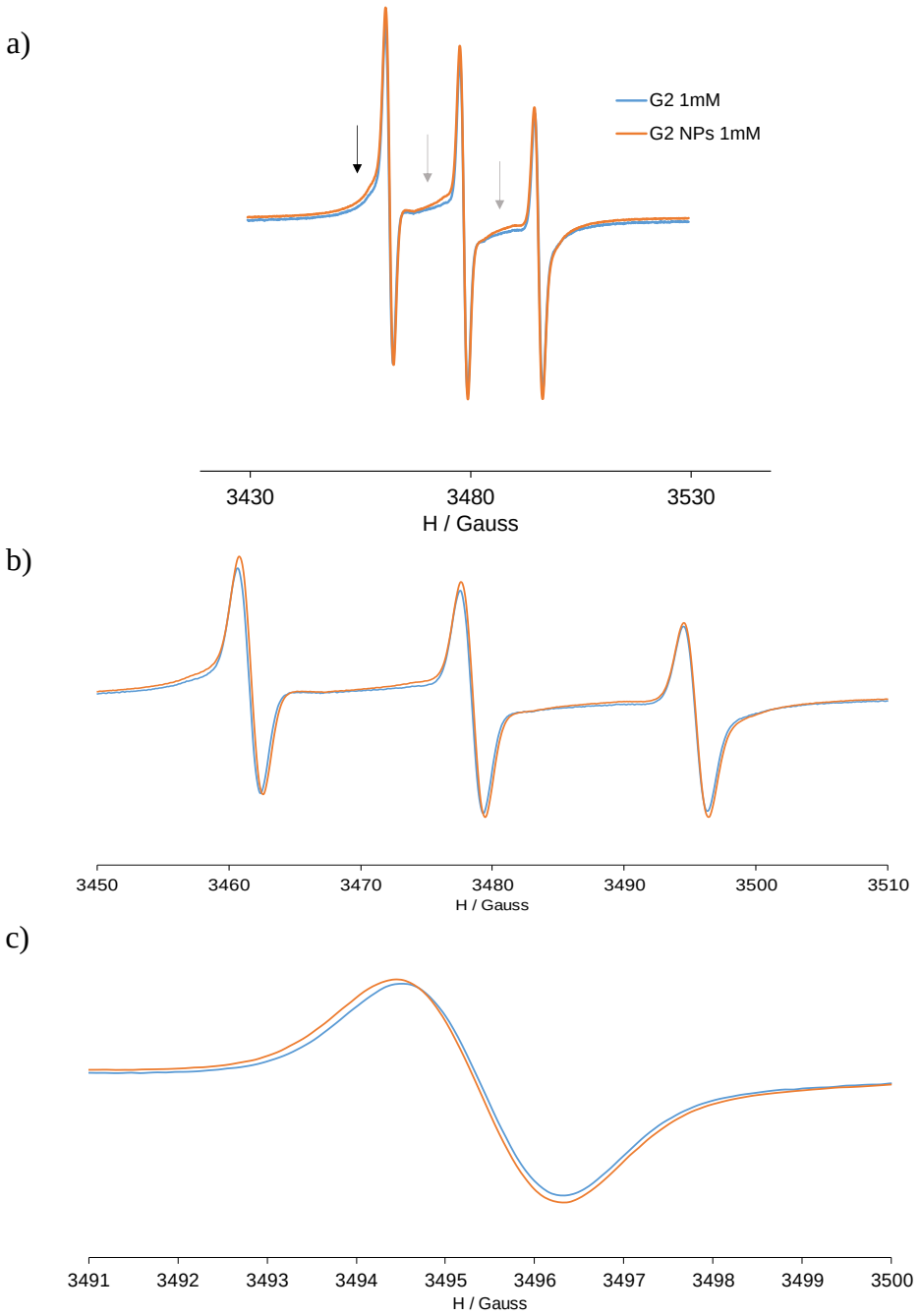

Figure 4-22. Normalized EPR spectra of G2 dendritic structure (blue) and G2 NPs (orange) in H_2O. a) in the normal range b) enlarged spectra and c) enlarge of the higher magnetic field line.

Table 4-5. g, a_N and ΔHpp of G2 and G2 NPs measured under the same conditions by EPR.

Compound	g	a_N (G)	ΔHpp (G)
G2	2.0048	16.91	1.73
G2 NPs	2.0053	16.79	1.81

4.5 MRI measurement of G2 nanoparticles

Since the nanoparticles obtained with G2-MPA-PEG20k-TEMPO (**31**) compound were homogeneous and showed good stability, we performed the phantom experiments to measure their relaxivity. An important question of this strategy that we would like to answer is whether the radicals that are contained inside the nanoparticles core can effectively relax the water protons nearby. In addition, we considered interesting to compare the G2 NPs relaxivity result with the one obtained from the as-synthesized G2-MPA-PEG20k-TEMPO (G2) compound in the same concentration range to check the possible influence of the different morphology (only spheres in G2 NPs, and mainly fibers in G2 species). TEMPO free radical was also measured as a reference.

In both cases, the concentration of G2 compound ranged from 0.012 to 0.13 mM and the concentration per TEMPO unit ranged from 0.1 to 1 mM. The relaxivities were obtained from the plots of the R_1 ($1/T_1$) versus the concentration of each compound (Figure 4-23) and the data are shown in Table 4-6. First of all, it is worth mentioning that the regression line obtained in both cases presented a very good correlation coefficient (as well as for free TEMPO). The relaxivities obtained for G2 and G2 NPs were 1.88 and 2.06 $mM^{-1}s^{-1}$ per molecule, respectively, while the relaxivities per radical unit were 0.236 and 0.258 $mM^{-1}s^{-1}$, respectively, since this compound has 8 radicals in its structure. First of all, it is worth mentioning that it has been demonstrated that the radicals that are contained inside the nanoparticles can effectively relax the water protons nearby since G2 NPs present high relaxivity. Then, analyzing the results obtained we can say that in both cases (G2 and G2 NPs) the relaxivities per radical unit are significantly higher than in the free TEMPO radical which presents a relaxivity of 0.181 $mM^{-1}s^{-1}$ under the same conditions, due to the high molecular weight of G2 compound, i.e. big size, which induces a slow rotational correlation time of the anchored radicals. More interesting is the fact that colloidal dispersions of G2 NPs present higher relaxivities than G2 solutions. Considering the different morphology of nanoparticles, it can be concluded that the formation of stable homogeneous spherical nanoparticles is helpful to improve the relaxivities compared with linear structures probably because the movement of radicals in the sphere could be more restricted than in the more flexible fibers, making increase the rotational correlation time. This result points out the importance not only of the size but also the rigidity of the structures that support the radicals to improve the relaxivity

values. Finally, if we think in the relaxivity per unit of nanoparticle, we can consider that a nanoparticle should be composed of more than one G2 compound, which therefore leads to a relaxivity value per nanoparticle > 2.0603 $mM^{-1}s^{-1}$.

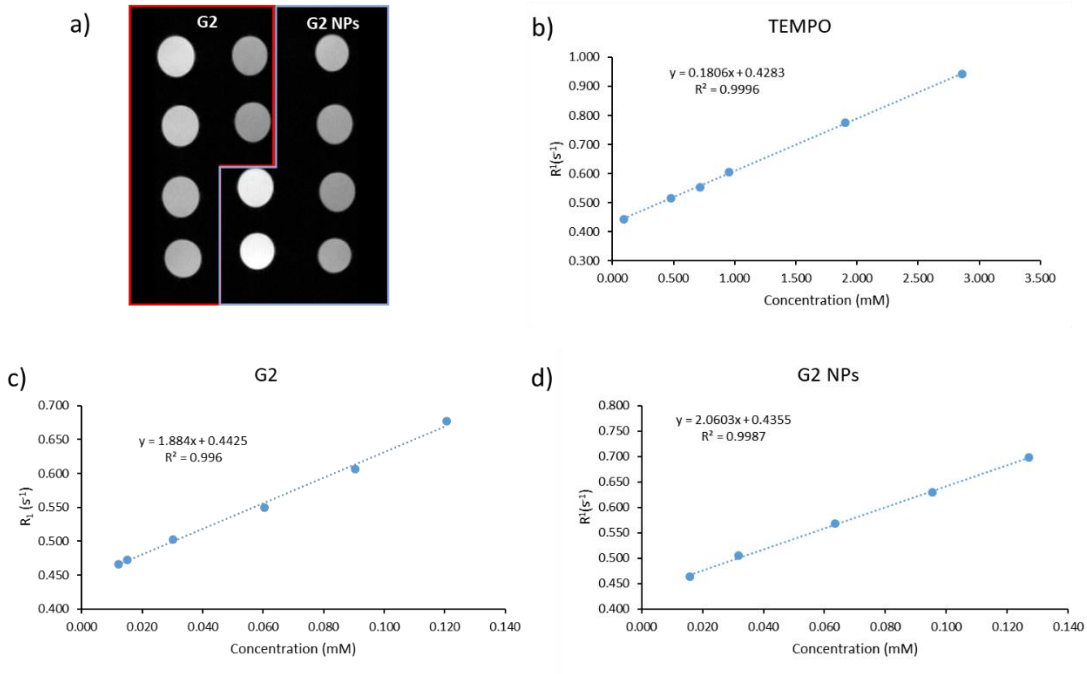

Figure 4-23.T_1 weighted images in a phantom experiment for G2 and G2 NPs and the plots of R_1 (1/ T_1) versus concentration for TEMPO, G2 and G2 NPs. The slope corresponds to r_1.

Table 4-6. Relaxivity values of TEMPO, G2 and G2 NPs in water.

sample	r_1 ($mM^{-1}s^{-1}$) per molecule	r_1 ($mM^{-1}s^{-1}$) per radical
TEMPO	0.1806	0.1806
G2	1.884	0.2355
G2 NPs	2.0603	0.2575
G2 NPs per NP unit > 2.0603*		

* We consider that a nanoparticle should be composed with more than one G2 compound.

4.6 Cytotoxicity

In vitro cell viability was carried out to assess the cytoxicity of G2-MPA-PEG20k-TEMPO with African green monkey kidney (Vero) cell line. As described in Chapter 3, the cells were incubated with G2-MPA-PEG20K-TEMPO (**31**) at different concentrations ranging from 0.13 mM to 1 mM per radical unit, and the cell viability was checked by XTT assay at 24 h and 48 h. As a result, this species did not show cytotoxicity *in vitro* in

the tested concentration range, as indicated by the high cell viability after 24 and 48 h (Figure 4-24).

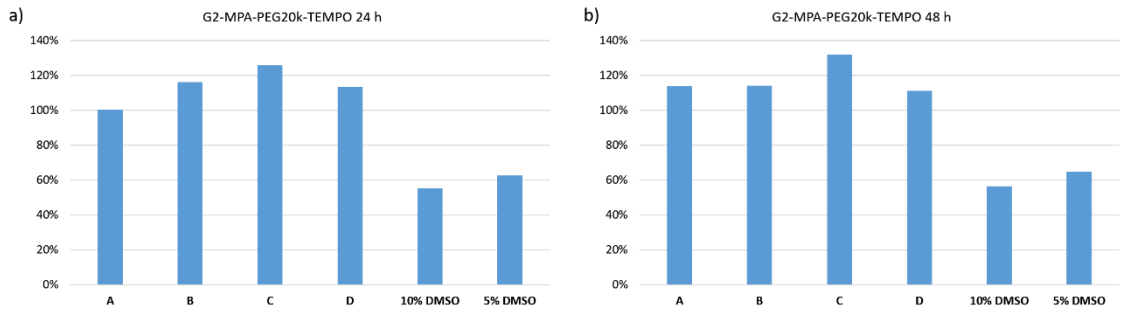

Figure 4-24. *In vitro* XTT cell viability assays conducted with African green monkey kidney (Vero) cells incubated with G2-MPA-PEG20K-TEMPO (**31**) in a concentration per radical unit of A) 1 mM, B) 0.5 mM, C) 0.25 mM, E) 0.13 mM, for 24 (a) and 48 h (b).

4.7 Conclusions

In this chapter, we have proposed the preparation of nanoparticles using radical functionalized dendritic-linear-dendritic polymers based on bis-MPA dendrons at the ends of a PEG chain, as MRI contrast agents.

- Three different generations of radical dendritic systems have been synthesized by click chemistry (G1-, G2- and G3-MPA-PEG20k-TEMPO species) and well-characterized by ^{1}H NMR, EPR and UV-Vis spectroscopies.

- The obtained compounds have been used to prepare nanoparticles. While with G3-MPA-PEG20k-TEMPO (**32**) species we have obtained some nanoparticles in a non-homogeneous system, with G2-MPA-PEG20k-TEMPO (G2) species we have obtained homogeneous nanoparticles dispersion (G2 NPs).

- The size and stability along time and under dilution conditions of G2 NPs have been studied by DLS and TEM and compared with G2 species. The results showed that the same compound likely presents different supramolecular structure morphologies and stabilities due to the different preparation processes. The nanoparticles prepared with organic solvents were more stable and homogeneous than directly the G2 compound dissolved in water, showing the former spherical nanoparticles shape and the latter organized forming mostly fibers.

- The r_1 relaxivities in water of G2 and G2 NPs have been obtained, showing both systems higher relaxivities than the free radical. Interestingly, the different nanostructures formed seem to affect the relaxivity. It seems that the formation of stable homogeneous spherical nanoparticles is beneficial for the improvement of relaxivity compared with the more flexible linear structures organizations, probably due to the higher rigidity of nanoparticles.

- G2-MPA-PEG20k-TEMPO species have not been shown to be cytotoxic.

4.8 References

(1) Mai, Y.; Eisenberg, A. Self-Assembly of Block Copolymerswz. *Chem. Soc. Rev* **2012**, *41*, 5969–5985.

(2) Pang, Z.; Lu, W.; Gao, H.; Hu, K.; Chen, J.; Zhang, C.; Gao, X.; Jiang, X.; Zhu, C. Preparation and Brain Delivery Property of Biodegradable Polymersomes Conjugated with OX26. *J. Control. Release* **2008**, *128* (2), 120–127.

(3) Pustulka, K. M.; Wohl, A. R.; Lee, H. S.; Michel, A. R.; Han, J.; Hoye, T. R.; McCormick, A. V.; Panyam, J.; Macosko, C. W. Flash Nanoprecipitation: Particle Structure and Stability. *Mol. Pharm.* **2013**, *10* (11), 4367–4377.

(4) Kalyane, D.; Raval, N.; Maheshwari, R.; Tambe, V.; Kalia, K.; Tekade, R. K. Employment of Enhanced Permeability and Retention Effect (EPR): Nanoparticle-Based Precision Tools for Targeting of Therapeutic and Diagnostic Agent in Cancer. *Mater. Sci. Eng. C* **2019**, *98* (August 2018), 1252–1276.

(5) Yu, S.; Azzam, T.; Rouiller, I.; Eisenberg, A. " Breathing " Vesicles. **2009**, No. 32, 10557–10566.

(6) Li, Y.; Lokitz, B. S.; McCormick, C. L. Thermally Responsive Vesicles and Their Structural "Locking" through Polyelectrolyte Complex Formation. *Angew. Chemie - Int. Ed.* **2006**, *45* (35), 5792–5795.

(7) Gheybi, H.; Adeli, M. Supramolecular Anticancer Drug Delivery Systems Based on Linear-Dendritic Copolymers. *Polym. Chem.* **2015**, *6* (14), 2580–2615.

(8) Whitton, G.; Gillies, E. R. Functional Aqueous Assemblies of Linear-Dendron Hybrids. *J. Polym. Sci. Part A Polym. Chem.* **2015**, *53* (2), 148–172.

(9) Gitsov, I.; Wooley, K. L.; Hawker, C. J.; Fréchet, J. M. J. Synthesis and Solution Properties of Polystyrenes with Dendritic End Groups. In *ABSTRACTS OF PAPERS OF THE AMERICAN CHEMICAL SOCIETY*; AMER CHEMICAL SOC 1155 16TH ST, NW, WASHINGTON, DC 20036, 1991; Vol. 202, pp 322-POLY.

(10) Sun, H.; Haque, F. M.; Zhang, Y.; Commisso, A.; Mohamed, M.

A.; Tsianou, M.; Cui, H.; Grayson, S. M.; Cheng, C. Linear-Dendritic Alternating Copolymers. *Angew. Chemie - Int. Ed.* **2019**, *58* (31), 10572–10576.

(11) Stover, T. C.; Kim, Y. S.; Lowe, T. L.; Kester, M. Thermoresponsive and Biodegradable Linear-Dendritic Nanoparticles for Targeted and Sustained Release of a pro-Apoptotic Drug. *Biomaterials* **2008**, *29* (3), 359–369.

(12) Li, Y.; Xiao, K.; Luo, J.; Xiao, W.; Lee, J. S.; Gonik, A. M.; Kato, J.; Dong, T. A.; Lam, K. S. Well-Defined, Reversible Disulfide Cross-Linked Micelles for on-Demand Paclitaxel Delivery. *Biomaterials* **2011**, *32* (27), 6633–6645.

(13) Nagura, K.; Takemoto, Y.; Moronaga, S.; Uchida, Y.; Shimono, S.; Shiino, A.; Tanigaki, K.; Amano, T.; Yoshino, F.; Noda, Y.; Koizumi, S.; Komatsu, N.; Kato, T.; Yamauchi, J.; Tamura, R. Preparation of Robust Metal-Free Magnetic Nanoemulsions Encapsulating Low-Molecular-Weight Nitroxide Radicals and Hydrophobic Drugs Directed Toward MRI-Visible Targeted Delivery. *Chem. - A Eur. J.* **2017**, *23* (62), 15713–15720.

(14) Morishita, K.; Ueki, S.; Fuchi, Y.; Murayama, S.; Kaneko, T.; Narita, N.; Kobayashi, S.; Hirai, G.; Aoki, I.; Karasawa, S. Self-Assembled Biradical Ureabenzene Nanoparticles for Magnetic Resonance Imaging. *ACS Appl. Nano Mater.* **2018**, *1* (12), 6967–6975.

(15) Shiraishi, R.; Matsumoto, S.; Fuchi, Y.; Naganuma, T.; Yoshihara, D.; Usui, K.; Yamada, K. I.; Karasawa, S. Characterization and Water-Proton Longitudinal Relaxivities of Liposome-Type Radical Nanoparticles Prepared via a Supramolecular Approach. *Langmuir* **2020**, *36* (19), 5280–5286.

(16) Nagura, K.; Takemoto, Y.; Yoshino, F.; Bogdanov, A.; Chumakova, N.; Vorobiev, A. K.; Imai, H.; Matsuda, T.; Shimono, S.; Kato, T.; Komatsu, N.; Tamura, R. Magnetic Mixed Micelles Composed of a Non-Ionic Surfactant and Nitroxide Radicals Containing a D-Glucosamine Unit: Preparation, Stability, and Biomedical Application. *Pharmaceutics* **2019**, *11* (1), 1–7.

(17) Garmendia, S.; Mantione, D.; Alonso-De Castro, S.; Jehanno, C.; Lezama, L.; Hedrick, J. L.; Mecerreyes, D.; Salassa, L.; Sardon, H. Polyurethane Based Organic Macromolecular Contrast Agents (PU-ORCAs) for Magnetic Resonance Imaging. *Polym. Chem.* **2017**, *8* (17), 2693–2701.

(18) Huang, L.; Yan, C.; Cui, D.; Yan, Y.; Liu, X.; Lu, X.; Tan, X.; Lu,

X.; Xu, J.; Xu, Y.; Liu, R. Organic Radical Contrast Agents Based on Polyacetylenes Containing 2,2,6,6-Tetramethylpiperidine 1-Oxyl (TEMPO): Targeted Magnetic Resonance (MR)/Optical Bimodal Imaging of Folate Receptor Expressing HeLa Tumors *in Vitro* and in Vivoa. *Macromol. Biosci.* **2015**, *15* (6), 788–798.

(19) Chan, J. M. W.; Wojtecki, R. J.; Sardon, H.; Lee, A. L. Z.; Smith, C. E.; Shkumatov, A.; Gao, S.; Kong, H.; Yang, Y. Y.; Hedrick, J. L. Self-Assembled, Biodegradable Magnetic Resonance Imaging Agents: Organic Radical-Functionalized Diblock Copolymers. *ACS Macro Lett.* **2017**, *6* (2), 176–180.

(20) Hou, M.; Lu, X.; Zhang, Z.; Xia, Q.; Yan, C.; Yu, Z.; Xu, Y.; Liu, R. Conjugated Polymer Containing Organic Radical for Optical/MR Dual-Modality Bioimaging. *ACS Appl. Mater. Interfaces* **2017**, *9* (51), 44316–44323.

(21) Morishita, K.; Murayama, S.; Araki, T.; Aoki, I.; Karasawa, S. Thermal- and PH-Dependent Size Variable Radical Nanoparticles and Its Water Proton Relaxivity for Metal-Free MRI Functional Contrast Agents. *J. Org. Chem.* **2016**, *81* (18), 8351–8362.

(22) Guo, S.; Wang, X.; Dai, Y.; Dai, X.; Li, Z.; Luo, Q.; Zheng, X.; Gu, Z.; Zhang, H.; Gong, Q.; Luo, K. Enhancing the Efficacy of Metal-Free MRI Contrast Agents via Conjugating Nitroxides onto PEGylated Cross-Linked Poly(Carboxylate Ester). *Adv. Sci.* **2020**, *7* (14).

(23) Sowers, M. A.; Mccombs, J. R.; Wang, Y.; Paletta, J. T.; Morton, S. W.; Dreaden, E. C.; Boska, M. D.; Francesca Ottaviani, M.; Hammond, P. T.; Rajca, A.; Johnson, J. A. Redox-Responsive Branched-Bottlebrush Polymers for in Vivo MRI and Fluorescence Imaging. *Nat. Commun.* **2014**, *5* (1), 1–9.

(24) Saatchi, K.; Soema, P.; Gelder, N.; Misri, R.; McPhee, K.; Baker, J. H. E.; Reinsberg, S. A.; Brooks, D. E.; Häfeli, U. O. Hyperbranched Polyglycerols as Trimodal Imaging Agents: Design, Biocompatibility, and Tumor Uptake. *Bioconjug. Chem.* **2012**, *23* (3), 372–381.

(25) Zhou, X.; Ren, L. Building a Better Magnetic Resonance Imaging Contrast Agent Using Macromolecular Architecture. *ACS Cent. Sci.* **2017**, *3* (8), 820–822.

(26) Jing, X.; Zhi, Z.; Jin, L.; Wang, F.; Wu, Y.; Wang, D.; Yan, K.; Shao, Y.; Meng, L. PH/Redox Dual-Stimuli-Responsive Cross-Linked

Polyphosphazene Nanoparticles for Multimodal Imaging-Guided Chemo-Photodynamic Therapy. *Nanoscale* **2019**, *11* (19), 9457–9467.

(27) Morishita, K.; Okamoto, Y.; Murayama, S.; Usui, K.; Ohashi, E.; Hirai, G.; Aoki, I.; Karasawa, S. Water-Proton Relaxivities of Radical Nanoparticles Self-Assembled via Hydration or Dehydration Processes. *Langmuir* **2017**, *33* (31), 7810–7817.

(28) Alvaradejo, G. G.; Nguyen, H. V. T.; Harvey, P.; Gallagher, N. M.; Le, D.; Ottaviani, M. F.; Jasanoff, A.; Delaittre, G.; Johnson, J. A. Polyoxazoline-Based Bottlebrush and Brush-Arm Star Polymers via ROMP: Syntheses and Applications as Organic Radical Contrast Agents. *ACS Macro Lett.* **2019**, *8* (4), 473–478.

(29) Del Barrios, J.; Oriol, L.; Sánchez, C.; Luis Serrano, J.; Di Cicco, A.; Keller, P.; Li, M. H. Self-Assembly of Linear-Dendritic Diblock Copolymers: From Nanofibers to Polymersomes. *J. Am. Chem. Soc.* **2010**, *132* (11), 3762–3769.

(30) Hed, Y.; Zhang, Y.; Andrén, O. C. J.; Zeng, X.; Nyström, A. M.; Malkoch, M. Side-by-Side Comparison of Dendritic-Linear Hybrids and Their Hyperbranched Analogs as Micellar Carriers of Chemotherapeutics. *J. Polym. Sci. Part A Polym. Chem.* **2013**, *51* (19), 3992–3996.

(31) Andrén, O. C. J.; Zhang, Y.; Lundberg, P.; Hawker, C. J.; Nyström, A. M.; Malkoch, M. Therapeutic Nanocarriers via Cholesterol Directed Self-Assembly of Well-Defined Linear-Dendritic Polymeric Amphiphiles. *Chem. Mater.* **2017**, *29* (9), 3891–3898.

(32) Zheng, X.; Pan, D.; Chen, M.; Dai, X.; Cai, H.; Zhang, H.; Gong, Q.; Gu, Z.; Luo, K. Tunable Hydrophile–Lipophile Balance for Manipulating Structural Stability and Tumor Retention of Amphiphilic Nanoparticles. *Adv. Mater.* **2019**, *31* (35).

(33) Alexis, F.; Pridgen, E.; Molnar, L. K.; Farokhzad, O. C. Factors Affecting the Clearance and Biodistribution of Polymeric Nanoparticles. *Mol. Pharm.* **2008**, *5* (4), 505–515.

(34) Lee, T. D.; Keana, J. F. W. In Situ Reduction of Nitroxide Spin Labels with Phenylhydrazine in Deuteriochloroform Solution. A Convenient Method for Obtaining Structural Information on Nitroxides Using Nuclear Magnetic Resonance Spectroscopy. *J. Org. Chem.* **1975**, *40* (21), 3145–3147.

(35) Zhang, J.; Shen, H.; Song, W.; Wang, G. Synthesis and

Characterization of Novel Copolymers with Different Topological Structures and TEMPO Radical Distributions. *Macromolecules* **2017**, *50* (7), 2683–2695.

(36) Badetti, E.; Lloveras, V.; Muñoz-Gómez, J. L.; Sebastián, R. M.; Caminade, A. M.; Majoral, J. P.; Veciana, J.; Vidal-Gancedo, J. Radical Dendrimers: A Family of Five Generations of Phosphorus Dendrimers Functionalized with TEMPO Radicals. *Macromolecules* **2014**, *47* (22), 7717–7724.

(37) Rao J P, G. K. E. Polymer Nanoparticles: Preparation Techniques and Size-Control Parameters. *Prog. Polym. Sci.* **2011**, *36* (7), 887–913.

(38) Clogston, J. D.; Patri, A. K. Zeta Potential Measurement. In *Methods in molecular biology (Clifton, N.J.)*; 2011; Vol. 697, pp 63–70.

(39) Bhattacharjee, S. DLS and Zeta Potential - What They Are and What They Are Not? *J. Control. Release* **2016**, *235*, 337–351.

(40) Kouchakzadeh, H.; Shojaosadati, S. A.; Maghsoudi, A.; Vasheghani Farahani, E. Optimization of PEGylation Conditions for BSA Nanoparticles Using Response Surface Methodology. *AAPS PharmSciTech* **2010**, *11* (3), 1206–1211.

(41) Jokerst, J. V; Lobovkina, T.; Zare, R. N.; Gambhir, S. S. Nanoparticle PEGylation for Imaging and Therapy. *Nanomedicine* **2011**, *6* (4), 715–728.

(42) Campestrini, S.; Corvaja, C.; De Nardi, M.; Ducati, C.; Franco, L.; Maggini, M.; Meneghetti, M.; Menna, E.; Ruaro, G. Investigation of the Inner Environment of Carbon Nanotubes with a Fullerene-Nitroxide Probe. *Small* **2008**, *4* (3), 350–356.

Chapter 5 Bimodal fluorescent magnetic radical dendrimers

5.1 Introduction

Dual- or multimodal imaging probes have emerged as powerful tools that improve detection sensitivity and accuracy, important in disease diagnosis and treatment. Multimodal imaging probes are designed to overcome inherent drawbacks of each imaging modality and take advantage of the complementary information they provide. A single probe, which integrates dual or multiple imaging properties is preferred over employing a cocktail approach by using a mixture of various contrast agents.

As explained in the Introduction, there exists some imaging modalities apart from magnetic resonance imaging (MRI) such as X-ray computed tomography (CT), positron emission tomography (PET), single-photon emission computed tomography (SPECT) or optical fluorescence imaging (OFI), with different characteristics and complementary information. In this chapter, we have tried to prepare compounds with two potential imaging modalities that present complementary information and that do not use ionizing radiation: MRI and OFI. Thus, trying to join in the same compound two different properties, magnetic and fluorescence properties, for potential MRI and OFI applications.

Fluorescence imaging, is widely used in histologic examination of cells, and has gained clinical interest and potential application in intraoperative use like in imaging-guided surgery.[1] OFI has the main advantage of high sensitivity compared with MRI, however, due to photon scattering and light attenuation of biological tissue, fluorescence imaging is limited by depth penetration, and present lower spatial resolution *in vivo*.[2] MRI has the advantage of high spatial resolution and unlimited depth penetration, but the drawback of its low sensitivity. By combining these two imaging techniques the imaging result can be substantially improved. In addition, fluorescence can be useful to monitor biodistribution in animal models.

Fluorescence imaging are used with fluorophores emitting in the visible region (400-650 nm) as well as in the near-infrared fluorescence region (NIRF) of 650-900 nm, being the latter more used for *in vivo* imaging applications due to lower background tissue absorption and deeper penetration depth.[3] In addition, NIRF imaging in the range of 1000-1400 nm, called as the second biological window and also named over-thousand near-

infrared (OTN) imaging, has attracted significant attention in *in vivo* imaging applications due to its even deeper tissue penetration, higher image contrast, and reduced phototoxicity and photobleaching.[4]

There are several reports on dual modality MRI/OFI imaging probes in the literature, using different fluorophores and mostly Gd-based contrast agents as MRI contrast agents, although the use of Fe_3O_4 or ^{19}F, among others, has also been reported.[2,5–7] Recently, a bimodal fluorescence-magnetic resonance probe was synthesized based on DOTA-Gd(III) chelate as MRI contrast agent and tetraphenylethylene as the aggregation-induced emission luminogen (AIEgen), for apoptosis imaging. These two functional agents are connected to a DEVD peptide, which is a substrate for caspase-3/7. Caspases (cysteine-aspartic proteases) are a family of protease enzymes that play an essential role in cell death. The caspases are inactive in normal cells but they can be activated when apoptosis happens in cancer cells. In response to caspase-3/7, the DEVD peptide is cleaved and then the remaining Gd(III)-AIEgen conjugate aggregates leading to increased FL-MR signals.[8]

When bimodal MRI/OFI contrast agents are prepared on the basis of organic radicals, the interaction between the radical and the fluorophore can give the contrast agent special properties. For example, nitroxides can quench fluorescence but fluorescence can be recovered after the radical deactivation. Different mechanisms of fluorescence quenching by nitroxides have been proposed such as exchange-induced relaxation processes,[9] intersystem crossing[10], energy transfer interactions[11] or electron transfer.[12] When the nitroxide is close to the fluorophore, the fluorescence is quenched, but once the nitroxide is trapped by another radical or participates in a redox process, the fluorescence can be recovered. The term profluorescent nitroxides has been proposed for these fluorophore-nitroxide couples[13] and this special property has been exploited to monitor polymer degradation,[14,15] and some other radical-based chemical processes.

Very few examples have been reported on bimodal MRI/OFI imaging probes using organic radicals as MRI contrast agents, and they have used polymers as scaffolds.[16–18] Rajca and Johnson group prepared bimodal MRI and fluorescence contrast agents based on organic radicals (nitroxides) and Cy5.5 fluorophores. On branched-bottlebrush polymers, the fluorescence was quenched but once the nitroxide was reduced by ascorbate, the fluorescence intensity increased by 2 to 3.5 times.[17] The same group prepared polymeric nanoparticles with the same active agents. In that case, it can be achieved simultaneously MRI and NIRF imaging *in vivo*, due to the large distance between the fluorophore and the nitroxides.[18]

In this chapter, we have tried to combine magnetic and fluorescent properties in the same dendrimer scaffold. Organic radicals have been anchored to the dendrimers branches. On the other hand, to give fluorescent properties to the dendrimers, there are mainly two different strategies, the incorporation/anchoring of fluorescent dyes to the dendrimers, or using dendrimers that are themselves fluorescent. This last option avoids additional synthetic steps and is therefore not time-consuming while at the same time leaves all the anchoring positions at the end of the dendrimer branches free (for full functionalization with organic radicals), resulting in a more optimal strategy. For this reason, we have used oligo(styryl)benzene (OSB) dendrimers that present fluorescent properties by their own, synthesized by the group of Joaquín C. García from the "Química Inorgánica, Orgánica y Bioquímica" department of the Castilla-La Mancha University. In this chapter, we have synthesized new radical dendrimers based on oligo(styryl)benzene and explored the possibility of preparing MRI/OFI bimodal imaging contrast agents with them.

The chemical structures of the oligo(styryl)benzene derivatives used in this work are shown in Scheme 5-1. They form rigid structures, and present three or four branches with acid or aldehyde end groups, named in this chapter as tri- and tetra-acid, and tri- and tetra-aldehyde. In the dendrimers with three branches, these are slightly inclined like the propellers of a fan and the three double bonds rotate in the same direction (Figure 5-1, a), while in the dendrimers with four branches, the double bonds go in the same direction two by two, and one pair slopes up and the other pair down (Figure 5-1, b).[19]

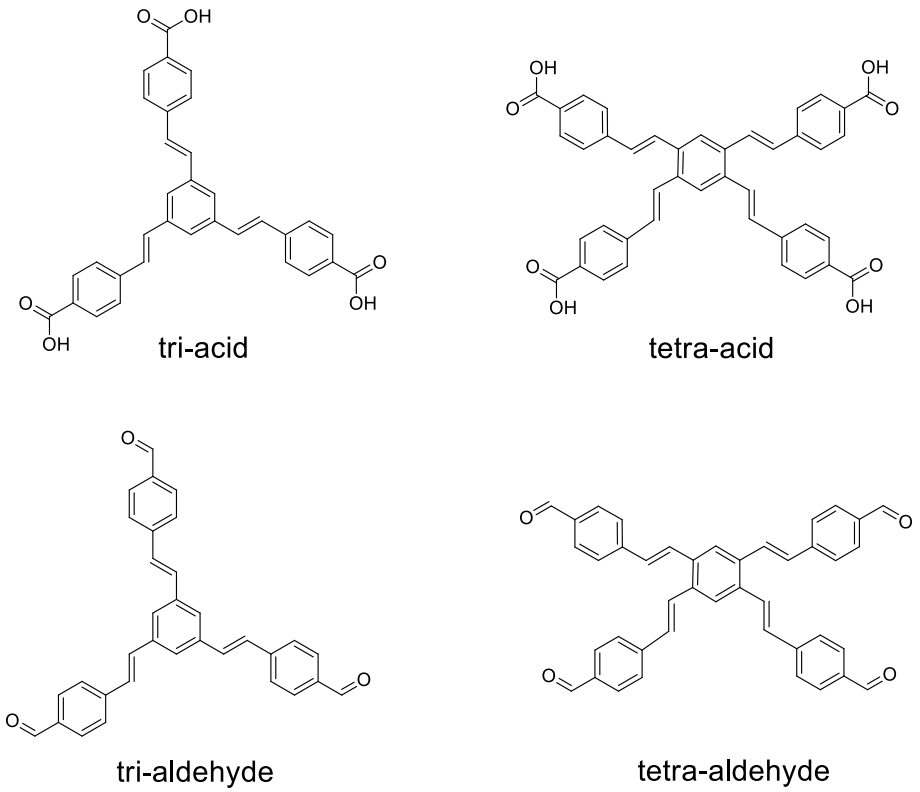

Scheme 5-1. Chemical structures of oligo(styryl)benzene dendrimers (tri-acid, tetra-acid, tri-aldehyde and tetra-aldehyde) derivatives.

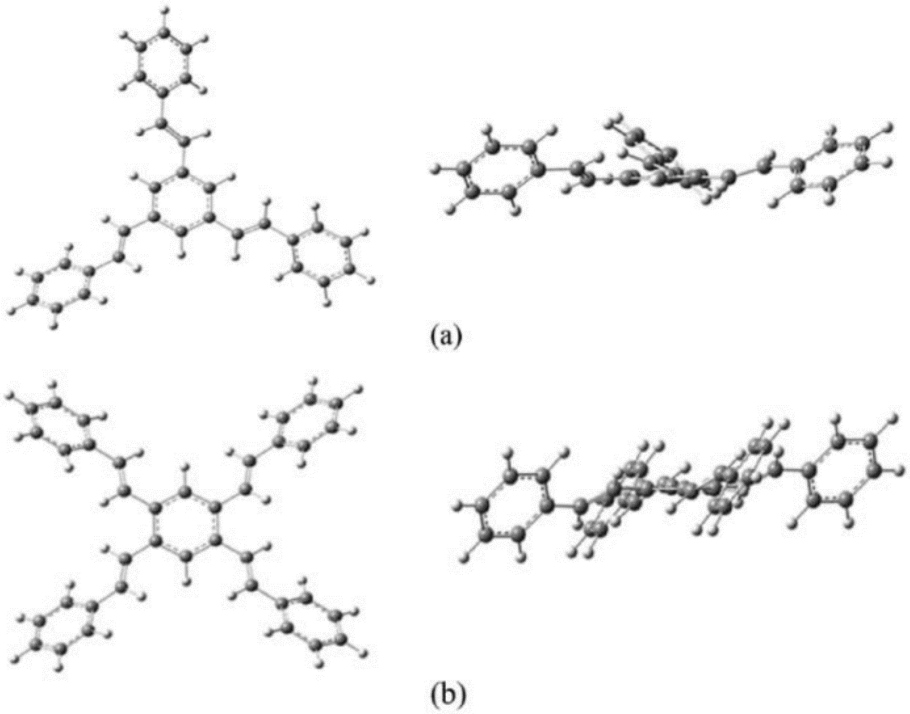

Figure 5-1. Selected view of (styryl)benzenes with three (a) and four (b) branches showing the changes in the dihedral angles, calculated at the M06-2X/6-31G∗ level of theory in the gas phase by the group of Joaquín C. García.[19]

5.2 Synthesis and characterization of radical dendrimers based on oligo(styryl)benzenes

We have synthesized a series of radical dendrimers by coupling the amine of 4-amino-TEMPO to the carboxyl or aldehyde groups of the oligo(styryl)benzenes dendrimers tri-, tetra-acid and tri-, tetra-aldehyde. Thus, we have obtained two different linking bonds, amido and imino ones, respectively. The radical dendrimers obtained are named (tri- or tetra-)-amido-TEMPO radical dendrimers and (tri- or tetra-)-imino-TEMPO radical dendrimers. In addition, the imine group formed between aldehyde and primary amine of the free radical can be reduced to a secondary amine which is a more stable linker. For this reason, we also prepared amino radical dendrimers derivatives from the imino ones to gain stability.

5.2.1 Synthesis and characterization of amido radical dendrimers derivatives

The synthesis of tri- and tetra-amido-TEMPO derivatives was carried out coupling the amine group of 4-amino-TEMPO to the carboxyl acid group of tri- and tetra-acid OSB, using HATU/DIEA as coupling agent, as shown in Scheme 5-2. The synthesis of tri-amido-TEMPO was performed in THF, while to obtain tetra-amido-TEMPO, a small amount of DMSO was added to make tetra-acid soluble in the reaction system. After overnight reaction at room temperature, the products were firstly extracted in DCM/water and then purified by column chromatography on silica gel in DCM/EtOH. The obtained yields were 88 and 53%, for tri-amido-TEMPO (**33**) and tetra-amido-TEMPO (**34**), respectively.

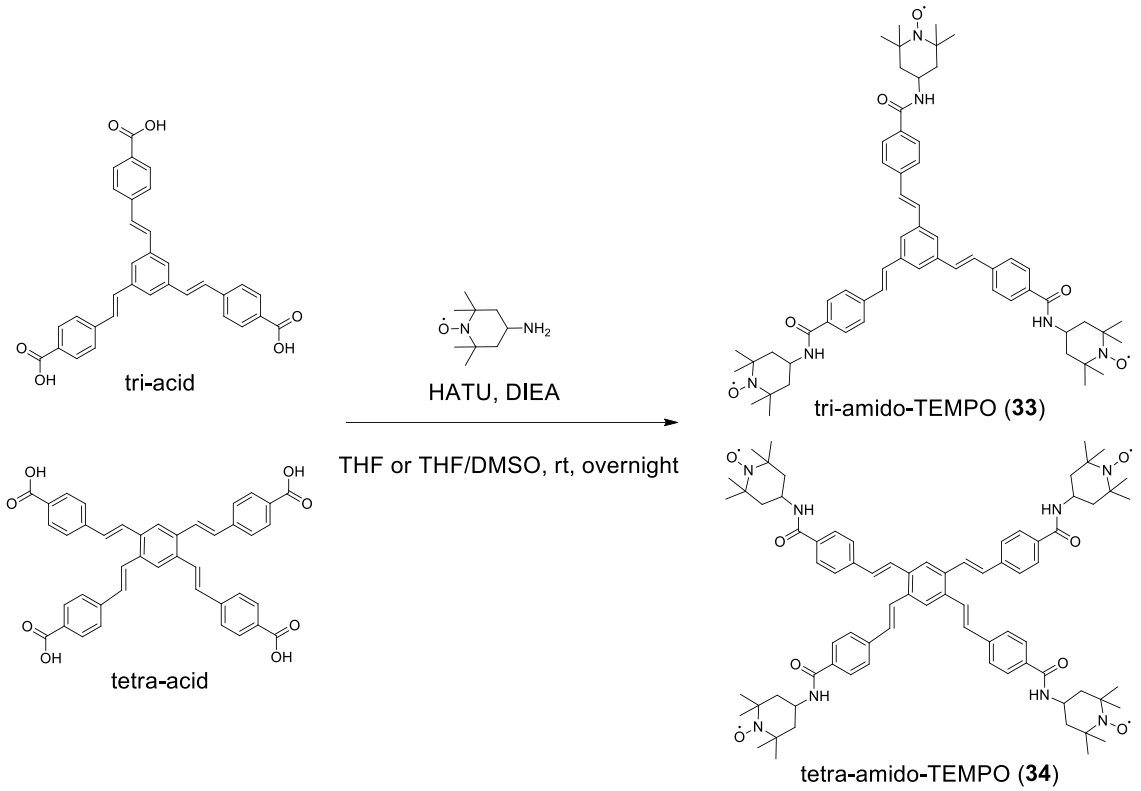

Scheme 5-2. Synthesis of tri-amido-TEMPO (**33**) and tetra-amido-TEMPO (**34**).

The obtained products tri-amido-TEMPO (**33**) and tetra-amido-TEMPO (**34**) were characterized by IR, ^{1}H NMR, UV-Vis, MALDI-TOF, SEC and EPR. Also, fluorescence and MRI studies have been performed.

The IR spectra of tri-acid, tri-amido-TEMPO (**33**) and tetra-amido-TEMPO (**34**) are shown in Figure 5-2. In the case of the formation of these two compounds we have followed-up the reaction by IR, by the shift of the C=O stretching band of -COOH from 1674 cm^{-1} to 1632 cm^{-1} from the new -CONH amide group for both compounds, as well as by the disappearance of the very broad OH stretching band at 3250-2500 cm^{-1} from the -COOH groups, and the appearance of the corresponding NH stretching band from the amide group at 3299 and 3297 cm^{-1} (for **33** and **34**, respectively). In addition, we can observe the -CH stretching bands of $-CH_3$ and $-CH_2-$ groups of TEMPO radicals at the range ca. 2854-2971 cm^{-1}. Moreover, at 1364 and 1362 cm^{-1} there appeared a band assigned to the N-O$^{\bullet}$ stretching of the TEMPO radical in tri-amido-TEMPO (**33**) and tetra-amido-TEMPO (**34**), respectively.[20,21]

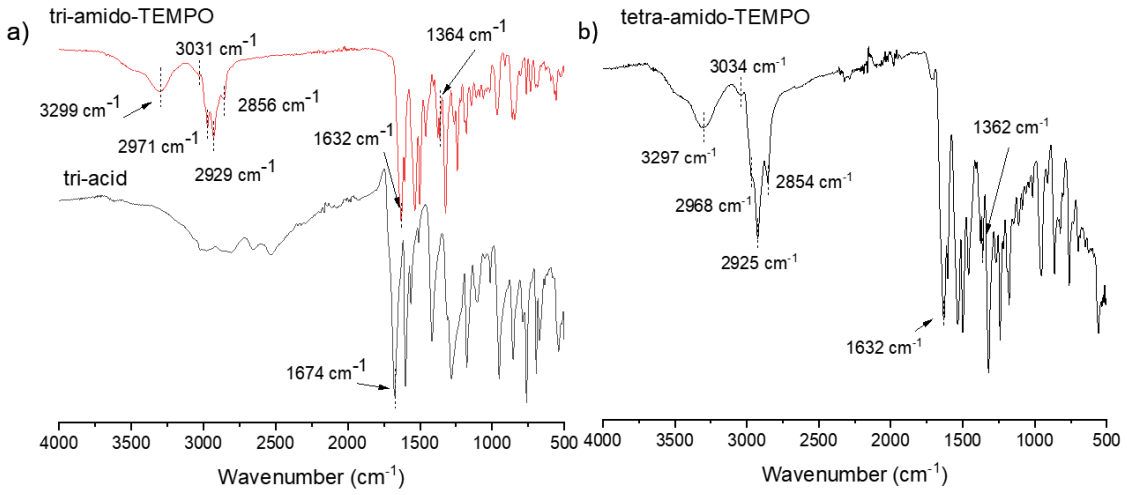

Figure 5-2. IR spectra of a) tri-acid and tri-amido-TEMPO (**33**) and b) tetra-amido-TEMPO (**34**).

Phenylhydrazine was used to reduce the nitroxyl radicals (TEMPO) to the corresponding diamagnetic hydroxylamine (Scheme 5-3), in order to characterize by ^{1}H NMR such structures (see Materials and methods section). With this method, the synthesized tri-amido-TEMPO (**33**) and tetra-amido-TEMPO (**34**) were well characterized by ^{1}H NMR, as shown in Figure 5-3 and Figure 5-4, respectively, with the corresponding peak labeling. The peaks of the TEMPO protons can be found in the range 1-1.73 ppm (*a* and *b*) and at 4.22 ppm (*c*). The protons of the dendrimer structure (*d*,*e*,*f*,*g*,*h*) can be found between 7.47 and 8.17 ppm. Moreover, the relative integral values of the ^{1}H resonances were in agreement with the theoretical ones, confirming the number of TEMPO radicals anchored on their structures (3 and 4, respectively).

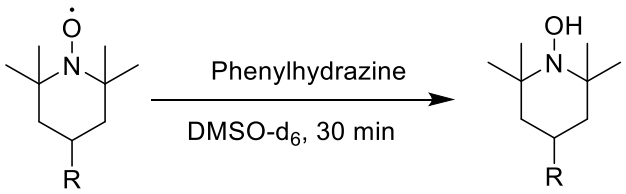

Scheme 5-3. Reduction of TEMPO radical to hydroxylamine with phenylhydrazine.

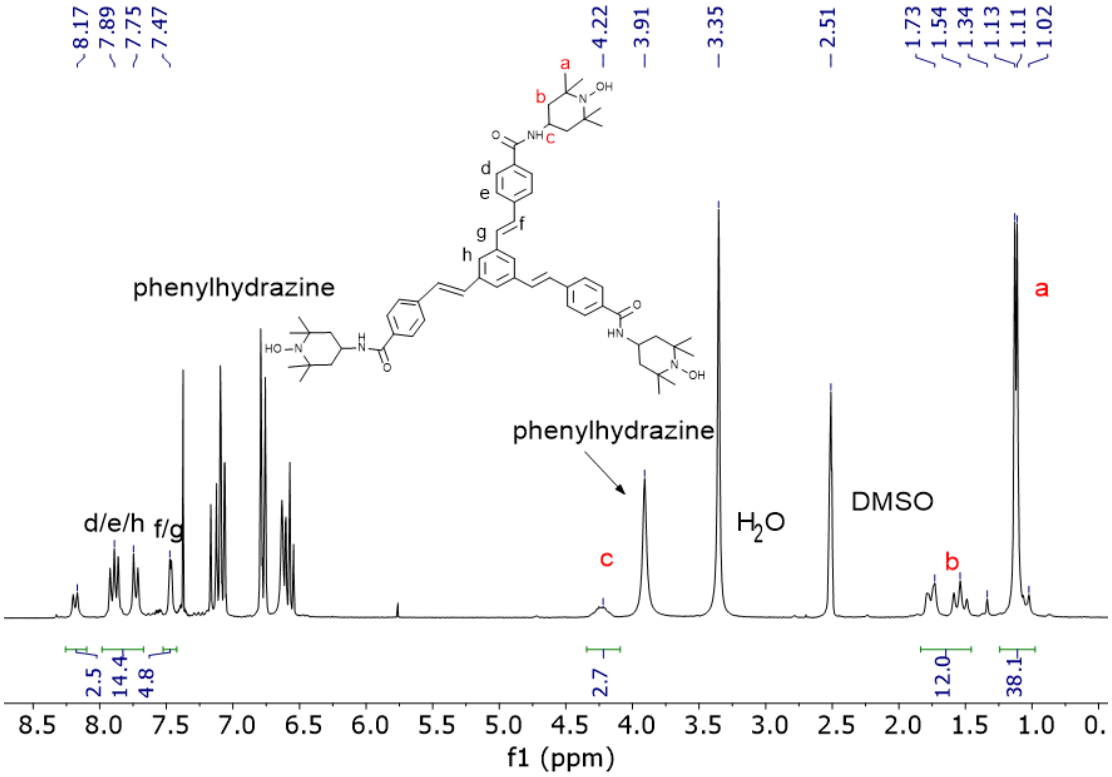

Figure 5-3. ^{1}H NMR spectrum of tri-amido-TEMPO (**33**) after being reduced with phenylhydrazine (DMSO-d_6, 250 MHz).

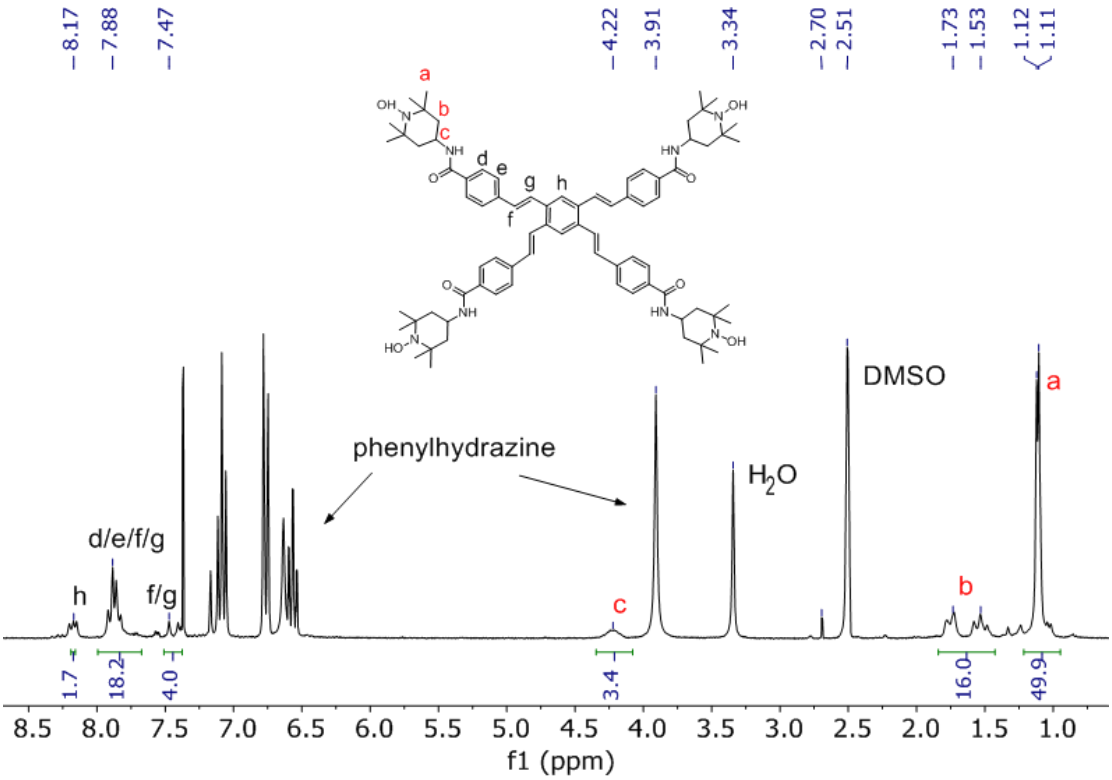

Figure 5-4. ^{1}H NMR spectrum of tetra-amido-TEMPO (**34**) after being reduced with phenylhydrazine (DMSO-d_6, 250 MHz).

Tri-amido-TEMPO (**33**) and tetra-amido-TEMPO (**34**) were also characterized by UV-Vis spectroscopy. The UV-Vis spectrum of TEMPO radical shows two typical absorption bands: an intense band at 240 nm (Figure 5-5a) and a very low intense band at ca. 450 nm (Figure 5-5b). By UV-Vis spectroscopy, we can characterize the radical dendrimer compounds by one hand, and on the other hand, we can also quantify the number of TEMPO radical units anchored to the dendrimers, as the low intense n-π^* transition absorption band at ca. 450 nm is known to be additive. For this reason, the number of TEMPO units anchored to the dendrimers can be calculated, comparing the molar extinction coefficient of the ca. 450 nm absorption band of the radical dendrimers with the TEMPO free radical one, through the Lambert-Beer law $A = \varepsilon * l * c$, where A is the absorbance (no units), ε is the molar extinction coefficient (in $M^{-1}cm^{-1}$), l is the optical path length (in cm) and c is the concentration (in M). The molar extinction coefficient of the ca. 450 nm band of TEMPO radical is around 10 $M^{-1}cm^{-1}$ with small variations depending on the solvent used.[22] For this reason, we calculated first the ε of TEMPO free radical in CH_2Cl_2, in which the radical dendrimers are soluble. We prepared five different concentrations, from 1 to 0.1 mM, and measured the maximum absorbance of the corresponding 452 nm band. The regression line obtained from the plot of A vs c gave a good regression coefficient R^2 (Figure 5-5c). From the slope of the regression line, we took the ε value for TEMPO in CH_2Cl_2, being 11.1 $M^{-1}cm^{-1}$.

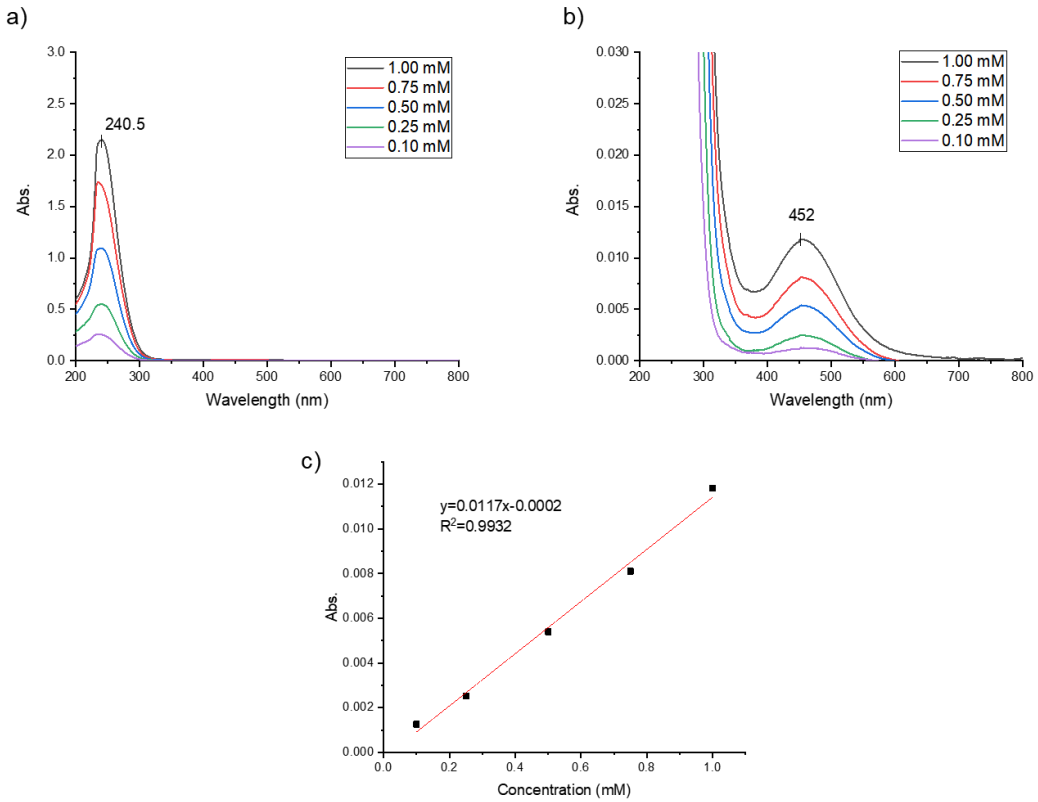

Figure 5-5. UV-Vis spectra of TEMPO free radical at different concentrations in DCM (1, 0.75, 0.5, 0.25, and 0.1 mM) a) the complete spectra, b) enlargement to see the 450 nm absorption band and c) absorbance versus concentration plot for the different concentrations.

The UV-Vis spectra of tri-amido-TEMPO (**33**) are shown in Figure 5-6. The ε value of the band at 450 nm was 30.6 $M^{-1}cm^{-1}$ indicating 3 times higher coefficient than the free TEMPO, confirming that 3 radicals were coupled to the dendrimer. It was not possible to observe this band in tetra-amido-TEMPO (**34**) since the band of the dendrimer overlapped the radical band (Figure 5-7).

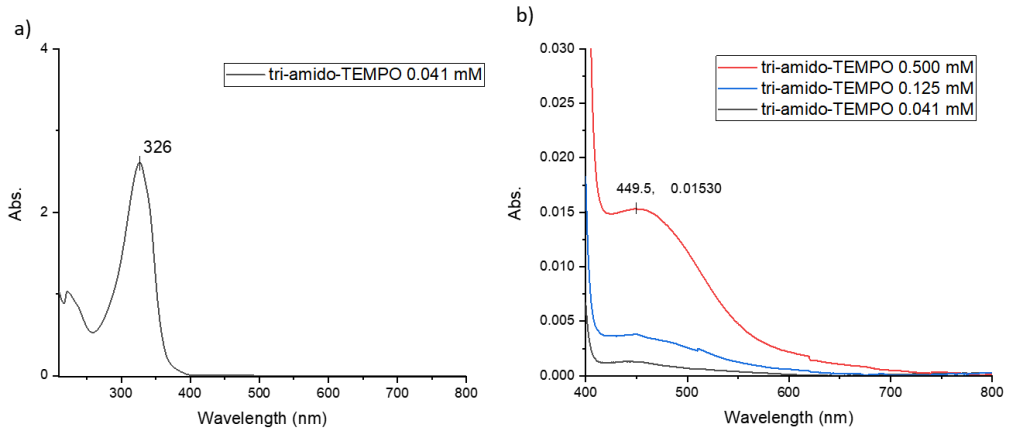

Figure 5-6. UV-Vis spectra of tri-amido-TEMPO (**33**) in DCM, a) the complete spectra at 0.041 mM, b) enlargement to see the 450 nm TEMPO radical absorption band at different concentration (0.500, 0.125 and 0.041 mM).

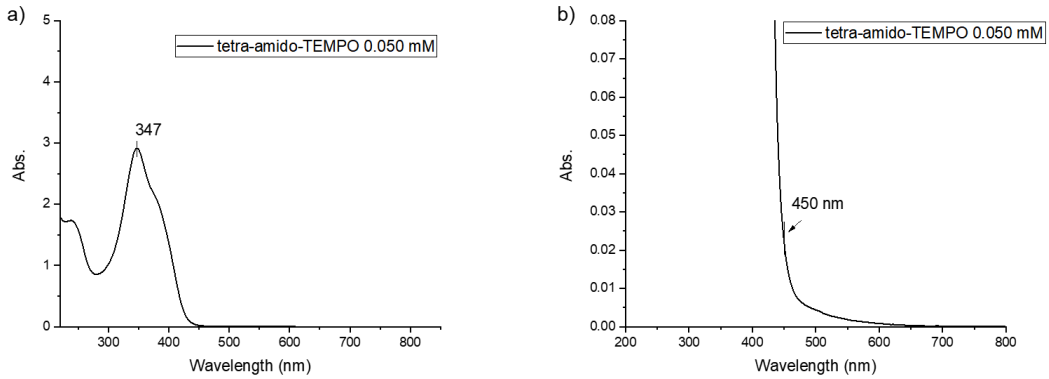

Figure 5-7. UV-Vis spectra of tetra-amido-TEMPO (**34**) in DCM at 0.050 mM, a) the complete spectra, b) enlargement to see the 450 nm TEMPO radical absorption band.

MALDI-TOF mass spectrometry was also used to characterize the radical dendrimers tri-amido-TEMPO (**33**) and tetra-amido-TEMPO (**34**). The molecular ion peaks $[M+H]^+$ of tri- and tetra-amido-TEMPO can be found at m/z = 977.2 and 1277.2, respectively, which are in agreement with the theoretical molecular weight (976.30 and 1275.69 g/mol, respectively), as well as a $[M+Na]^+$ cluster in both cases.

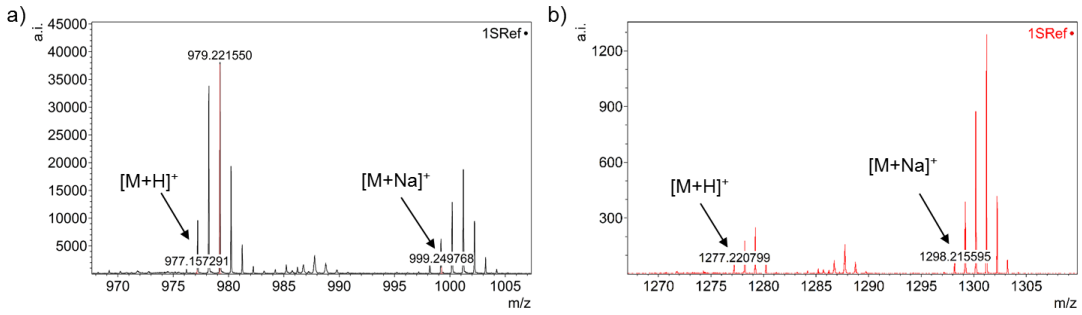

Figure 5-8. MALDI-TOF mass spectra of a) tri-amido-TEMPO (**33**) and b) tetra-amido-TEMPO (**34**) (matrix, positive mode).

Size exclusive chromatography (SEC) was used to check the purity of both tri-amido-TEMPO (**33**) and tetra-amido-TEMPO (**34**). These two compounds showed only one peak with narrow signal distribution, which confirmed their purities. The slightly lower retention time obtained for tetra-amido-TEMPO (**34**) is in agreement with the slightly larger size than tri-amido-TEMPO (**33**).

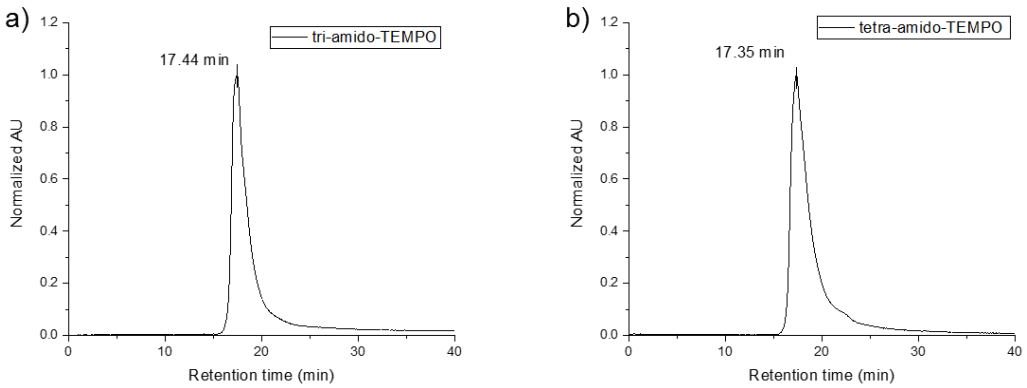

Figure 5-9. SEC chromatograms of a) tri-amido-TEMPO (**33**) and b) tetra-amido-TEMPO (**34**) radical dendrimers.

5.2.2 Synthesis and characterization of imino radical dendrimers derivatives

In the case of the coupling of 4-amino-TEMPO radical to the aldehyde terminal groups of the dendrimers (tri- and tetra-aldehyde), we followed the conditions already reported for the condensation of 4-amino-TEMPO to other derivatives with aldehyde terminal groups, using Al_2O_3, in THF (Scheme 5-4).[23,24] The reaction completion was also followed-up by IR. Briefly, aldehyde derivatives were subjected to sonification in

the presence of alumina gel with excess of 4-amino-TEMPO in THF. The reactions were stopped when the IR showed that the band of aldehyde disappeared. The alumina gel was removed by filtration, and the resulting product precipitated from the reaction mixture by the addition of *n*-pentane. We obtained radical dendrimers tri-imino-TEMPO (**35**) and tetra-imino-TEMPO (**36**) in 63 % and 85% yields, respectively.

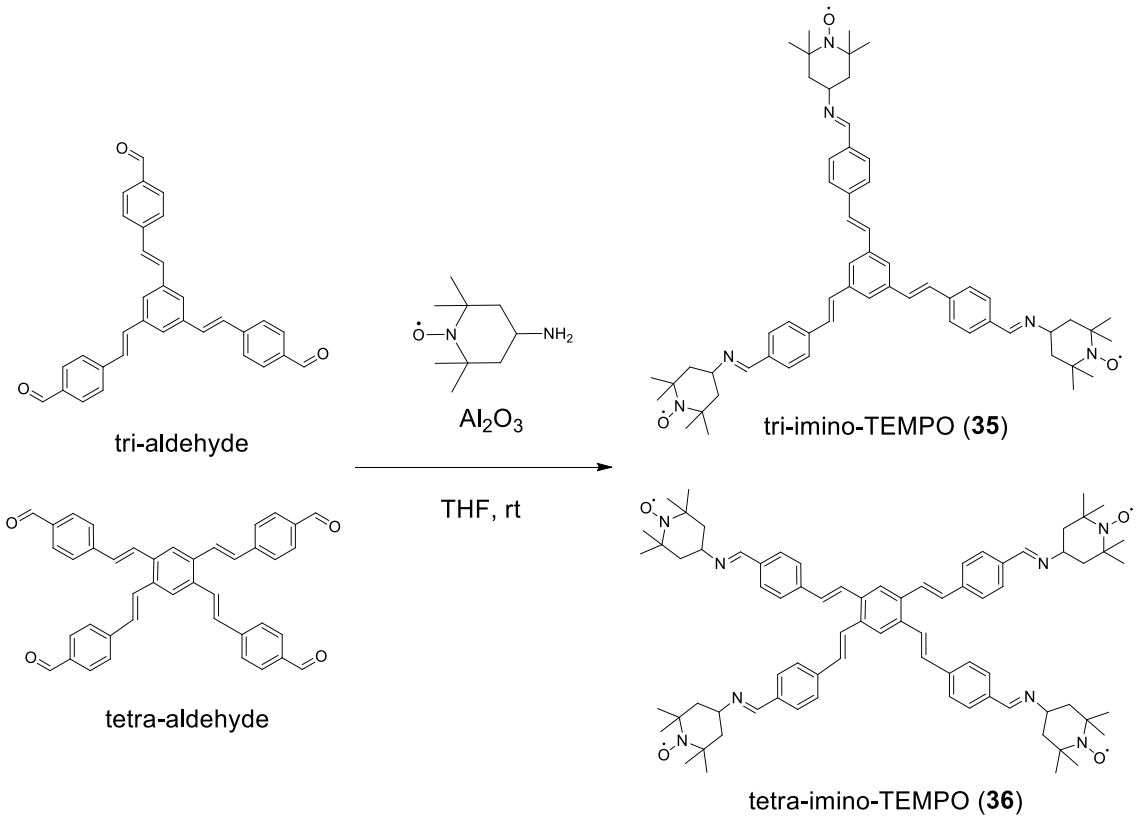

Scheme 5-4. Synthesis of tri-imino-TEMPO (**35**) and tetra-imino-TEMPO (**36**) radical dendrimers.

The IR spectra of the imino radical dendrimer derivatives (tri-imino-TEMPO (**35**) and tetra-imino-TEMPO (**36**)) are shown in Figure 5-10 together with the tri-aldehyde one, for comparison. We have followed the disappearance of the C=O stretching bands from the −CHO group at 1690 cm^{-1} of tri- and tetra-aldehyde, and the appearance of the CH=N band of the new imine group at 1637 cm^{-1} for both tri-imino-TEMPO (**35**) and tetra-imino-TEMPO (**36**) compounds. In addition, we can also observe the -CH stretching bands of $-CH_3$ and $-CH_2-$ groups of TEMPO radicals at the range ca. 2857-2972 cm^{-1}. Besides, we can also observe the bands at 1360 cm^{-1} in both cases assigned to the N-O• stretching of the TEMPO radicals.

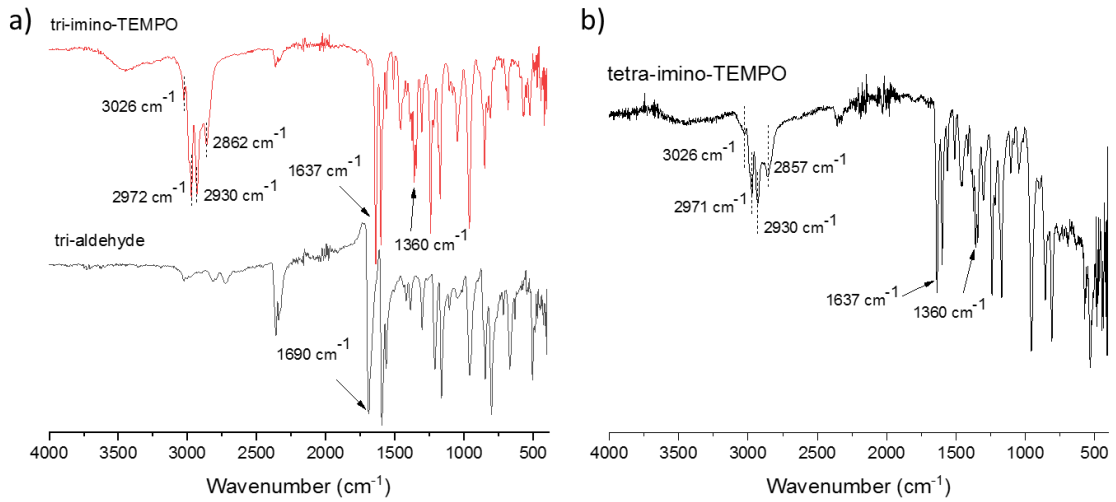

Figure 5-10. IR spectra of a) tri-aldehyde and tri-imino-TEMPO (**35**), and b) tetra-imino-TEMPO (**36**).

The ^{1}H NMR spectra of tri-imino-TEMPO (**35**) and tetra-imino-TEMPO (**36**) were also obtained by using phenylhydrazine as a reducing agent, shown in Figure 5-11 and Figure 5-12 with the corresponding peak labeling. The characteristic peaks of TEMPO protons can be found between 1.13-1.64 ppm (*a*, *b*) and 3.64 or 3.65 ppm (*c*) for TEMPO radicals, while the proton peaks of the dendrimer structure (*d*, *e*, *f*, *g*, *h*, *i*) can be found between 7.42 and 8.47 ppm. Importantly, the peak of aldehyde groups at 9.8 ppm disappeared in the ^{1}H NMR spectra of tri-imino-TEMPO (**35**) and tetra-imino-TEMPO (**36**), which confirmed all the aldehyde groups reacted with 4-amino-TEMPO. The peaks of the new imine groups can be found at around 8.5 ppm. Besides, the relative integral values of the ^{1}H resonances were in agreement with the theoretical ones, confirming the number of TEMPO radicals anchored on their structures (3 and 4, respectively).

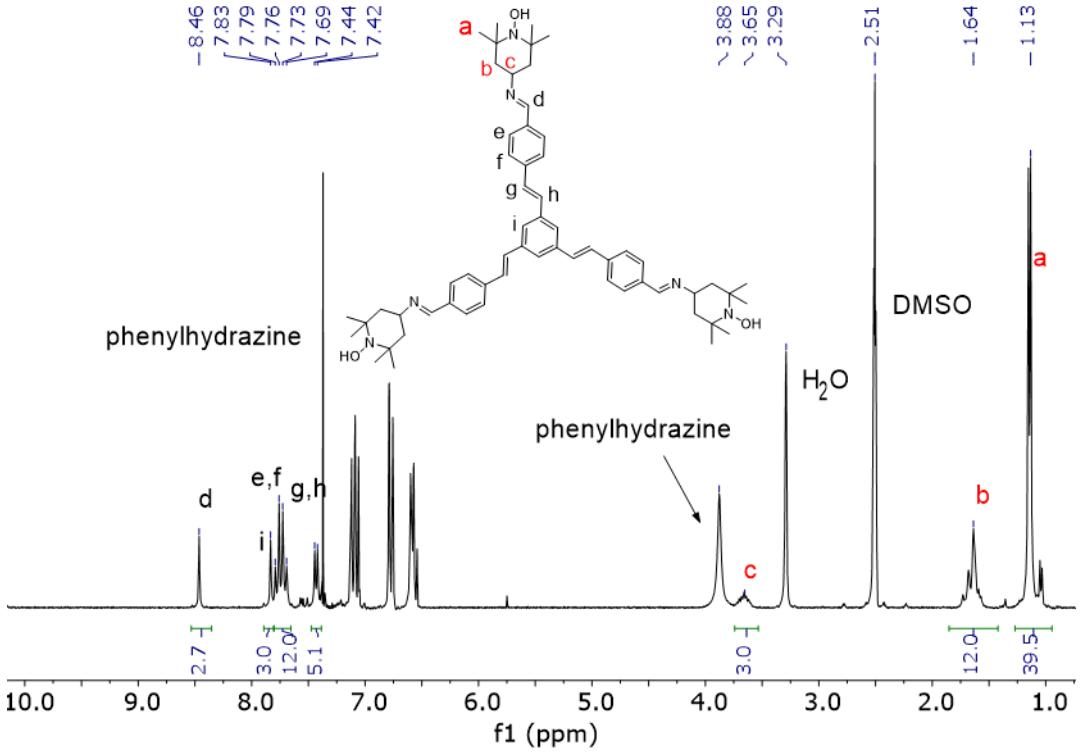

Figure 5-11. ^{1}H NMR spectrum of tri-imino-TEMPO (**35**) after being reduced with phenylhydrazine (DMSO-d_6, 250 MHz).

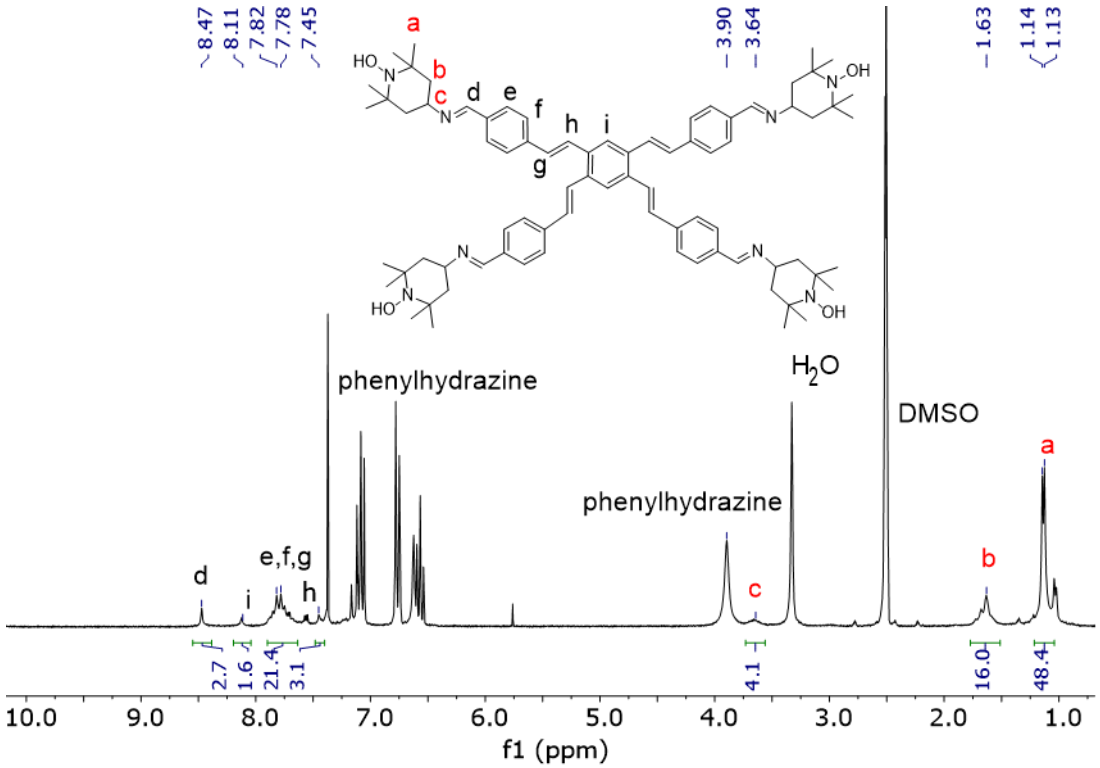

Figure 5-12. ^{1}H NMR spectrum of tetra-imino-TEMPO (**36**) after being reduced with phenylhydrazine (DMSO-d_6, 250 MHz).

The obtained tri-imino-TEMPO (**35**) and tetra-imino-TEMPO (**36**) were also

characterized by UV-Vis spectroscopy. However, the absorption band of the radical at around 450 nm was overlapped by the band of the OSB dendrimer in both cases. The UV-Vis spectrum of tri-imino-TEMPO (**35**) is shown in Figure 5-13.

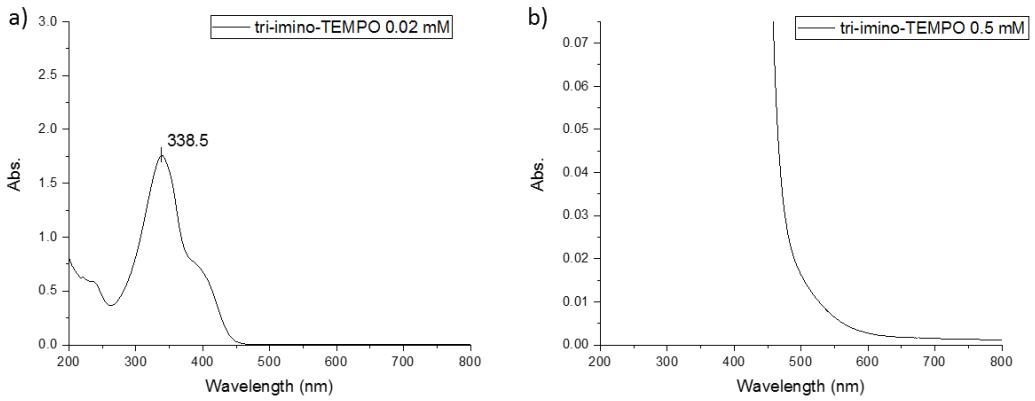

Figure 5-13. UV-Vis spectra of tri-imino-TEMPO (**35**) in DCM, a) the complete spectrum at 0.02 mM, b) enlargement to see the 450 nm TEMPO radical absorption band at 0.5 mM.

The MALDI-TOF mass spectra of tri-imino-TEMPO (**35**) and tetra-imino-TEMPO (**36**) presented the corresponding molecular ion peak $[M+H]^+$ at m/z = 929.2 and 1213.2 respectively, in agreement with the theoretical molecular weight (928.30 g/mol and 1211.69 g/mol, respectively), confirming the formation of the two radical dendrimers (Figure 5-14).

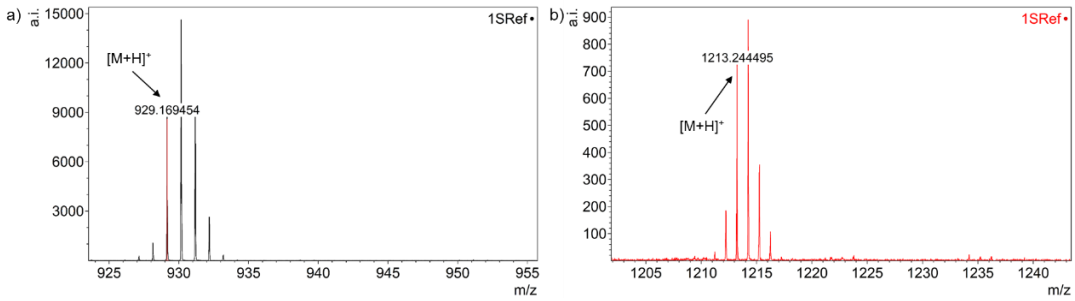

Figure 5-14. MALDI-TOF mass spectra of a) tri-imino-TEMPO (**35**) and b) tetra-imino-TEMPO (**36**) (matrix, positive mode).

Tri-imino-TEMPO (**35**) and tetra-imino-TEMPO (**36**) radical dendrimers were also characterized by SEC (Figure 5-15). As expected, the retention time of tri-imino-TEMPO (**35**) was slightly larger than tetra-imino-TEMPO (**36**). The single signal distribution confirmed the purity of these two compounds.

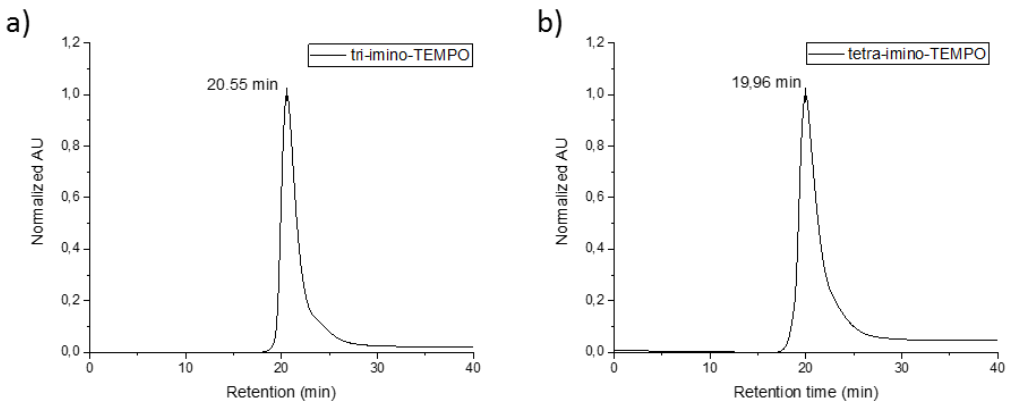

Figure 5-15. SEC chromatograms of a) tri-imino-TEMPO (**35**) and b) tetra-imino-TEMPO (**36**) radical dendrimers.

5.2.3 Synthesis and characterization of amino radical dendrimers derivatives

The synthesis of tri-amino-TEMPO (**37**) and tetra-amino-TEMPO (**38**) was performed by reduction of tri-imino-TEMPO (**35**) and tetra-imino-TEMPO (**36**) with $NaBH_4$, as shown in Scheme 5-5. These two compounds were synthesized in a similar way. After the reaction of tri-imino-TEMPO (**35**) and tetra-imino-TEMPO (**36**) with $NaBH_4$ overnight in methanol and chloroform, the reaction mixture was extracted with DCM/water three times, and, the products tri-amino-TEMPO (**37**) and tetra-amino-TEMPO (**38**) were obtained in 97% and 95% yield, respectively.

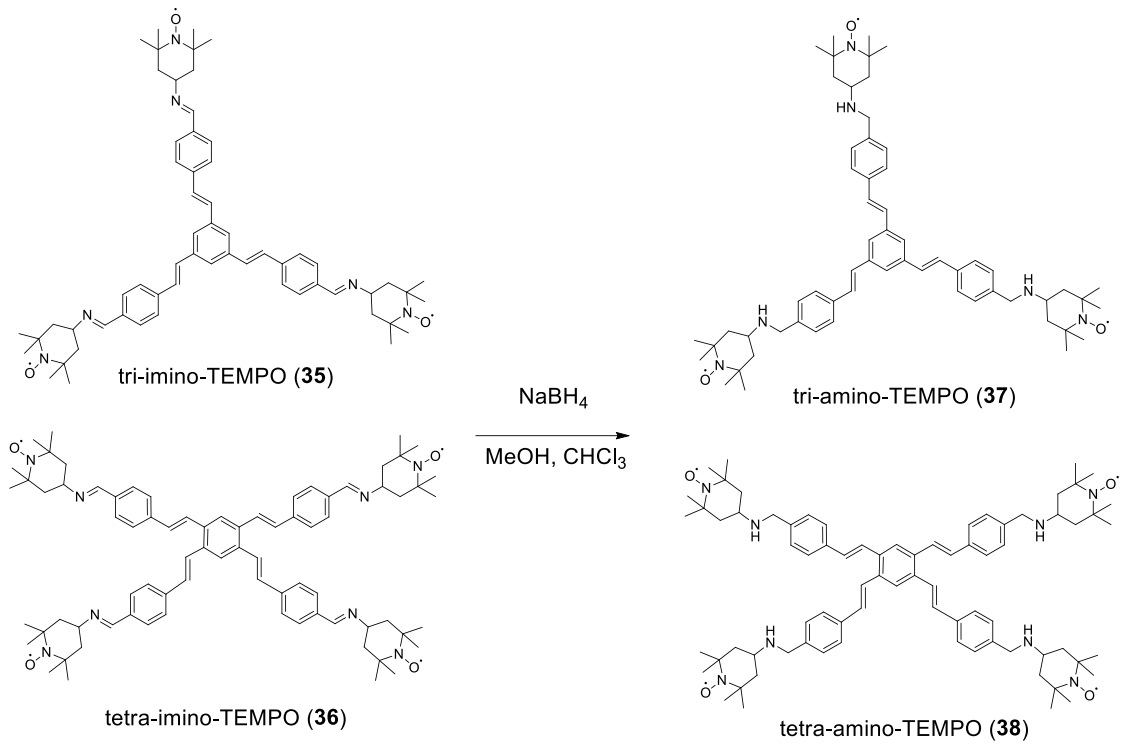

Scheme 5-5. Synthesis of tri-amino-TEMPO (**37**) and tetra-amino-TEMPO (**38**) radical dendrimers.

The IR spectra of tri-amino-TEMPO (**37**) and tetra-amino-TEMPO (**38**) are shown in Figure 5-16. In the IR spectra of both compounds, it is clear that the bands at 1637 cm^{-1} of the imine (C=N) bond disappeared completely, and the new bands at 3300 cm^{-1} corresponding to the formed amine group appeared. The bands of -CH_2 and -CH_3 of TEMPO can be found between 2854 and 2970 cm^{-1}, and the N-O• stretching bands at 1360 cm^{-1} in both compounds. These results confirm that the imino-TEMPO radical dendrimers were reduced to the corresponding amino derivatives.

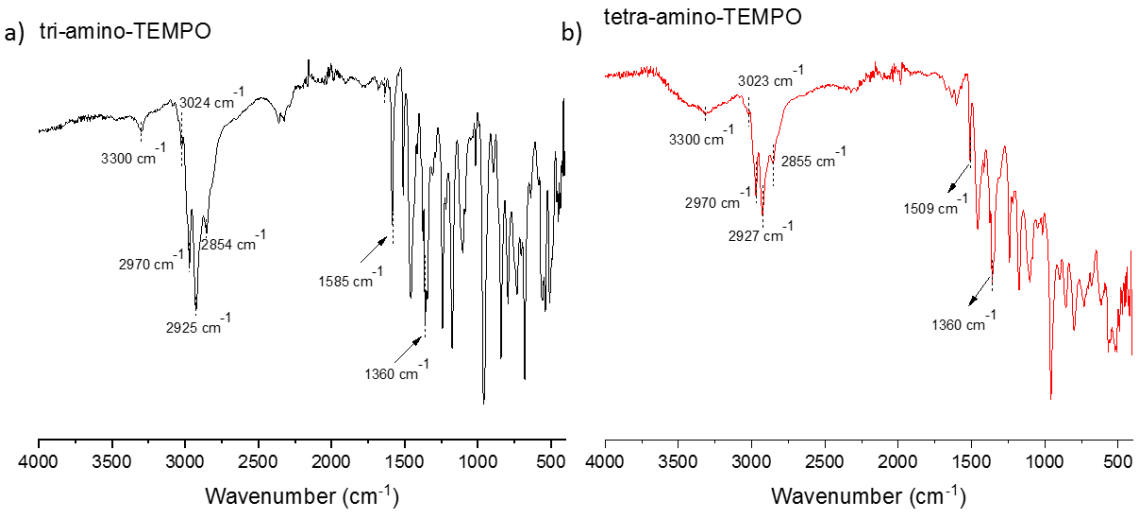

Figure 5-16. IR spectra of a) tri-amino-TEMPO (**37**) and b) tetra-amino-TEMPO (**38**) radical dendrimers.

With phenylhydrazine as a reducing agent, we also characterized the amino-radical dendrimers by ^{1}H NMR. As shown in Figure 5-17 and Figure 5-18, the peaks of the imine groups at 8.5 ppm of the imino radical dendrimers **37** and **38** disappeared, while the new peaks at 3.7 ppm corresponding to the new formed methylene groups (-CH_2-) appeared. Meanwhile, the chemical shift of the methine (-CH-) groups of TEMPO changed from 3.6 ppm to 2.8 ppm, due to the close imine group changed to an amine group. In both cases, the number of radical units obtained by the relative integral values of ^{1}H resonances was well consistent with the theoretical values, confirming the number of anchored TEMPO radical units was 3 and 4, respectively.

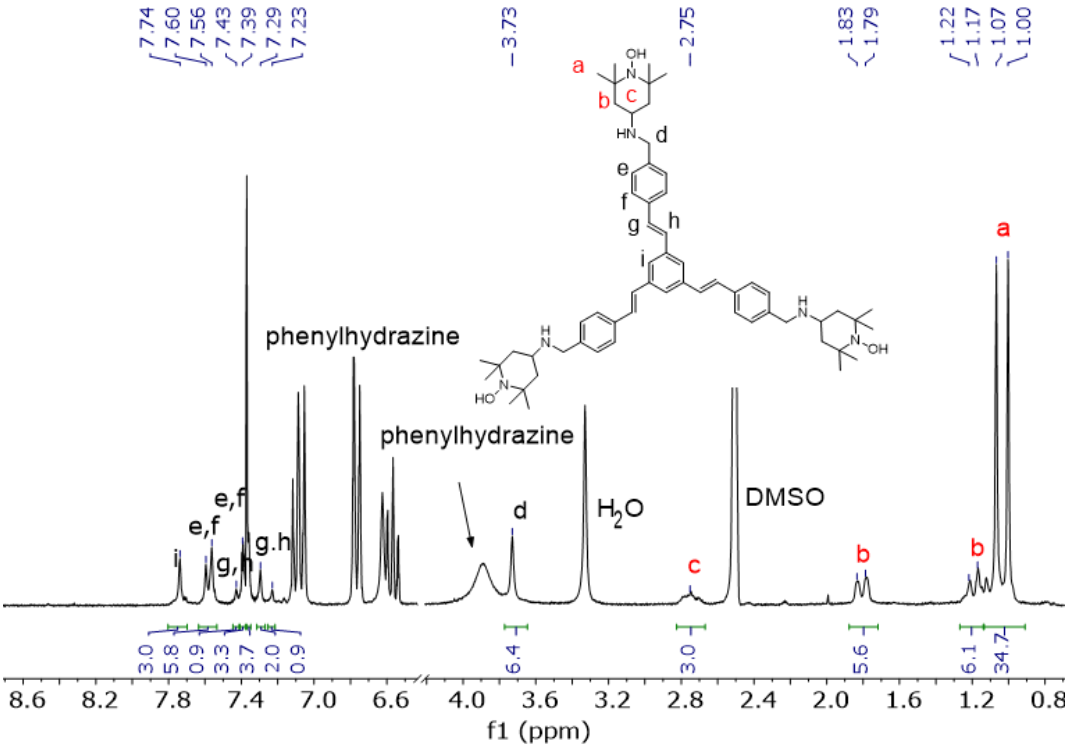

Figure 5-17. ^{1}H NMR spectrum of tri-amino-TEMPO (**37**) after being reduced with phenylhydrazine (DMSO-d_6, 250 MHz).

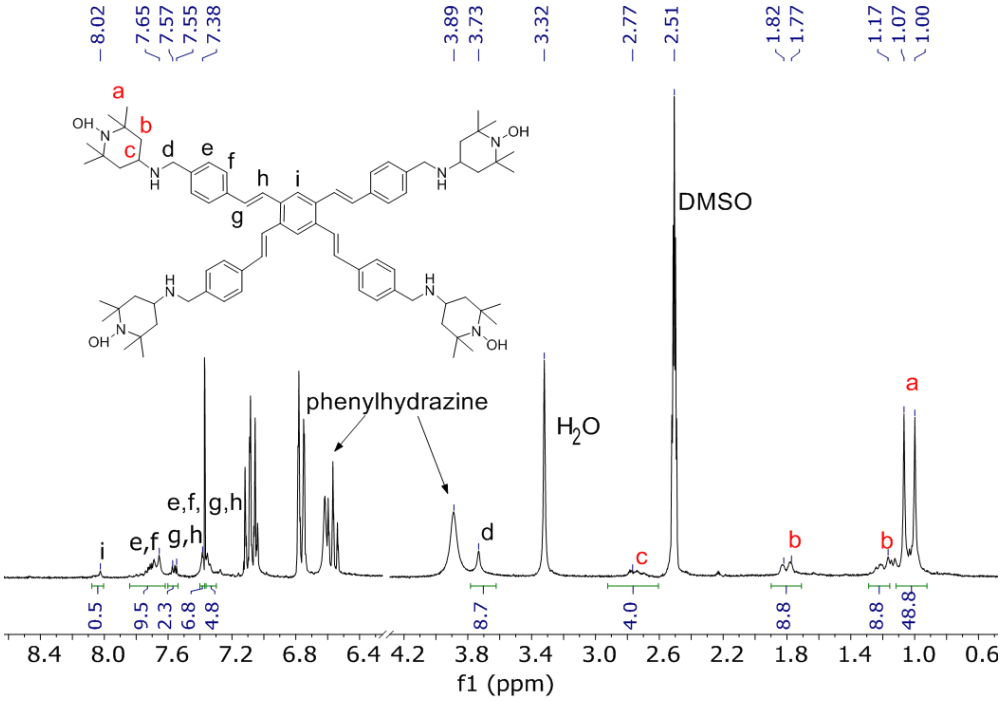

Figure 5-18. ^{1}H NMR spectrum of tetra-amino-TEMPO (**38**) after being reduced with phenylhydrazine (DMSO-d_6, 250 MHz).

The UV-Vis spectrum of tri-amino-TEMPO (**37**) is shown in Figure 5-19. The characteristic absorption band of the nitroxide radical can be observed at 470 nm and the number of radicals can be obtained according to the extinction coefficient of such a band. The extinction coefficient obtained for tri-amino-TEMPO was 30.98 $M^{-1}cm^{-1}$, which is 3 times that of the free radical TEMPO. Since the UV-Vis of tri-amino-TEMPO (**37**) shows that it contains three radicals, this also confirms in turn that tri-imino-TEMPO (**35**) presented three radicals, as it was obtained by reduction of the latter. In tetra-amino-TEMPO (**38**), the characteristic band of the nitroxide was overlapped by the OSB dendrimers band, so it was not possible to observe it.

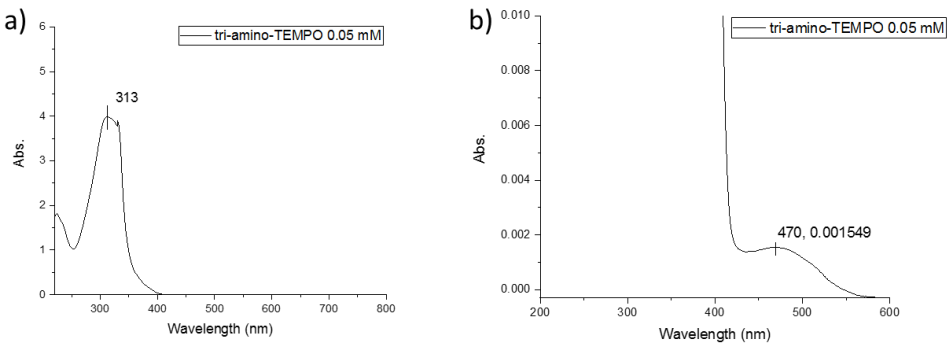

Figure 5-19. UV-Vis spectra of tri-amino-TEMPO (**37**) in DCM at 0.05 mM a) the complete spectrum, b) enlargement to see the TEMPO radical absorption band.

The MALDI-TOF mass spectrometry of tri-amino-TEMPO (**37**) and tetra-amino-TEMPO (**38**) are shown in Figure 5-20. The molecular ion peak $[M+H]^+$ of tri- and tetra-amino-TEMPO can be found at 935.1 and 1220.3 m/z, respectively, which are in agreement with the theoretical molecular weight (934.35 g/mol and 1219.76 g/mol, respectively).

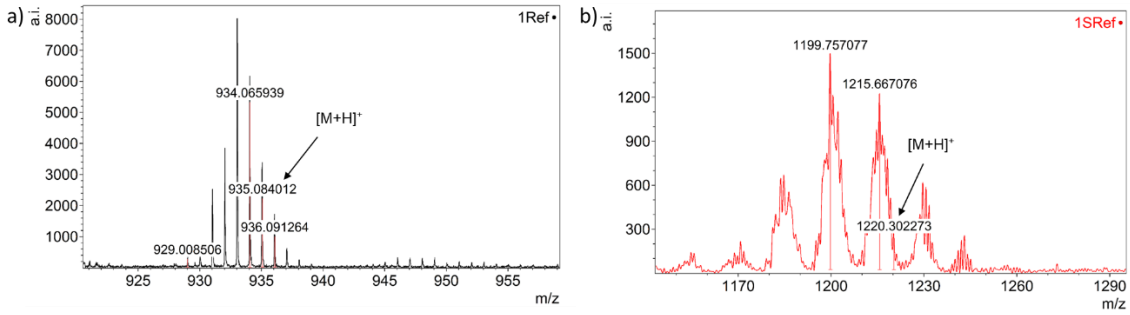

Figure 5-20. MALDI-TOF mass spectra of a) tri-amino-TEMPO (**37**), and b) tetra-amino-TEMPO (**38**), (matrix, positive mode).

We also did the SEC analysis of these two compounds but we obtained low intensity of the peaks. However, even we had more error the retention time was: 17.04 and 16.96 min for tri-amino-TEMPO (**37**) and tetra-amino-TEMPO (**38**), respectively.

5.3 EPR study of the radical dendrimers

We have done the EPR spectra of TEMPO free radical and the six radical dendrimers synthesized (**33**-**38**) at 300 K (isotropic conditions) and at 120 K (frozen solution, anisotropic conditions).

At 300 K, we first obtained the EPR spectrum of TEMPO free radical for comparison. It showed the typical 3 lines with the same relative intensities 1:1:1, with a coupling constant with the ^{14}N atom of a_N = 15.7 G, at g = 2.0061 and ΔHpp=1.20 G (Figure 5-21). The EPR obtained for the radical dendrimers **33**-**38** at 300 K also showed three lines, thus, they showed negligible spin exchange interaction between their radical units, probably because of the rigidity of the structures that do not allow radicals to approach each other. They presented similar a_N and g factor than TEMPO free radical, the typical ones of nitroxyl radicals in organic solvents (a_N ~ 15.4/15.5 G and g between 2.0053 and 2.0064, Figure 5-21,Table 5-2). However, the line width of their spectral lines was slightly broader (~1.60 G) than for TEMPO free radical (1.20 G) and they presented

a selective decrease of the high-field line. These two things are due to the hindered motion of the radicals when they are attached to a big molecule, confirming, thus, the anchoring of the radicals to the dendrimer.

On the other hand, the EPR signal intensity (measured in terms of area obtained from the double integral) of the tri- compounds were three times higher than the TEMPO free radical, while the tetra- derivatives showed four times more EPR area (see Table 5-1).

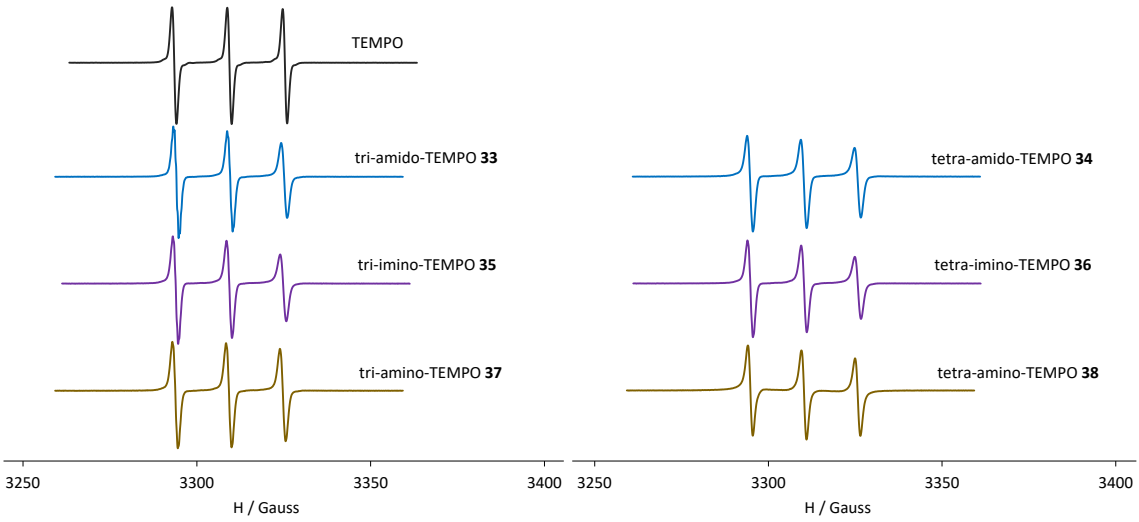

Figure 5-21. EPR spectra of TEMPO, tri-amido-TEMPO (**33**), tetra-amido-TEMPO (**34**), tri-imino-TEMPO (**35**), tetra-imino-TEMPO (**36**), tri-amino-TEMPO (**37**) and tetra-amino-TEMPO (**38**) radical dendrimers in THF at 300 K.

Table 5-2. EPR data of TEMPO and **33**-**38** species at 300 K and at 120 K, in THF.

Compound	300 K			120 K	
	g	a_N (G)	ΔH_{pp} (G)	d_1/d	Area (a.u.)
TEMPO	2.0061	15.7	1.20	0.53	2.47×10^5
tri-amido-TEMPO (**33**)	2.0059	15.5	1.61	0.66	7.22×10^5
tri-imino-TEMPO (**35**)	2.0060	15.4	1.59	0.63	7.12×10^5
tri-amino-TEMPO (**37**)	2.0057	15.4	1.62	0.60	7.31×10^5
tetra-amido-TEMPO (**34**)	2.0064	15.5	1.64	0.80	9.49×10^5
tetra-imino-TEMPO (**36**)	2.0053	15.4	1.56	0.79	9.61×10^5
tetra-amino-TEMPO (**38**)	2.0057	15.4	1.40	0.75	9.52×10^5

In frozen solution, 120 K (Figure 5-22), the EPR spectra shape of radical dendrimers **33**, **35** and **37** with three radical units was similar to the obtained with the TEMPO free radical, i.e. showing weak dipole-dipole interactions among the TEMPO radicals. In fact,

the d_1/d parameter values (see EPR Appendix C) obtained for them were only slightly higher than for TEMPO free radical (see Table 5-2). However, in tetra- compounds derivatives (**34**, **36** and **38**) these interactions were a bit higher than in the compounds with three radical units, which means radicals are closer in those structures (see Table 5-2).

In addition, under these conditions, all compounds showed a $|\Delta m_s| = 2$ transition at half-field (Figure 5-23), characteristic of dipolar coupled spins that gives direct evidence of the presence of a high-spin state. This signal was more intense in compounds **34**, **36** and **38** with four radical units than in the tri- derivative ones **33**, **35** and **37**.

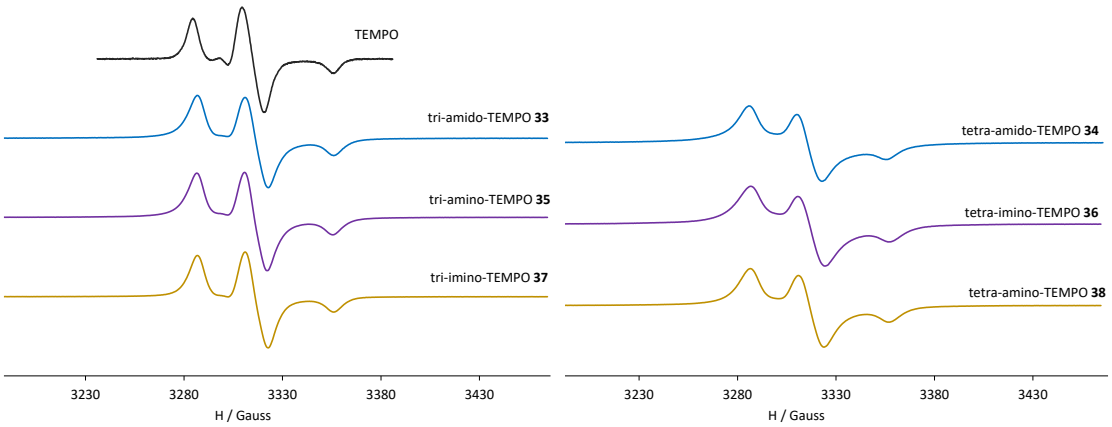

Figure 5-22. EPR spectra of TEMPO, tri-amido-TEMPO (**33**), tetra-amido-TEMPO (**34**), tri-imino-TEMPO (**35**), tetra-imino-TEMPO (**36**), tri-amino-TEMPO (**37**) and tetra-amino-TEMPO (**38**) radical dendrimers in THF at 120 K.

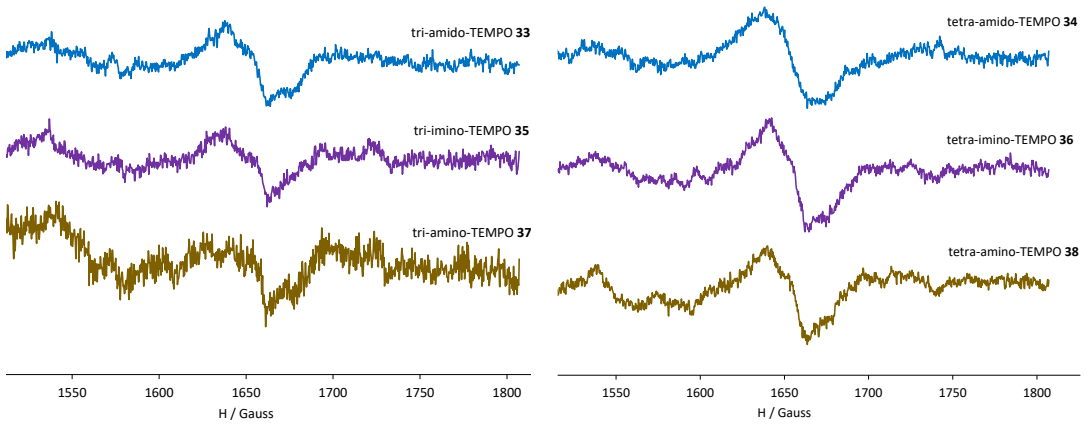

Figure 5-23. EPR spectra of $|\Delta m_s| = 2$ transition at half-field of tri-amido-TEMPO (**33**), tetra-amido-TEMPO (**34**), tri-imino-TEMPO (**35**), tetra-imino-TEMPO (**36**), tri-amino-TEMPO (**37**) and tetra-amino-TEMPO (**38**) radical dendrimers in THF at 120 K.

5.4 Fluorimetry study of the radical dendrimers

As explained in the Introduction, the oligo(styryl)benzenes dendrimers used in this work present fluorescent properties. When the nitroxide radicals are anchored to a fluorophore, they can quench the fluorescence intensity. For this work, it was very important to study the fluorescence of the resulting radical dendrimers to check if the dendrimer fluorescence was maintained, quenched, or disappeared after their coupling with 4-amino-TEMPO radical, as one of the properties we are looking for in this chapter is to obtain not only dendrimers with paramagnetic properties but also with fluorescent ones, i.e. bimodal magnetic-fluorescent molecules.

The fluorescence process can be depicted by Jablonski diagram (Figure 5-24). The singlet ground, first, and second electronic states was labeled by S_0, S_1, and S_2. First, the fluorophore is excited to higher vibrational level S_1 or S_2. In liquid or solid, the molecules in S_2 state quickly relax to the lowest vibrational state of S_1, and this process is called internal conversion (IC). When the molecule returns to S_0 state, the emission spectrum is obtained. Molecules in the S_1 state can also experience intersystem crossing (ISC), by undergoing a spin conversion from the first excited state S_1 to the first triplet sate T_1. The return from T_1 to S_0 give the phosphorescence spectrum. Since the existence of the internal conversion and the intersystem crossing (ISC), the fluorescence quantum yield QY can be defined by the ratio of the number of photons emitted to the number absorbed. i.e.

$$QY = \frac{n_{emitted\ photos}}{n_{absorbed\ photos}} \qquad (5\text{-}1)$$

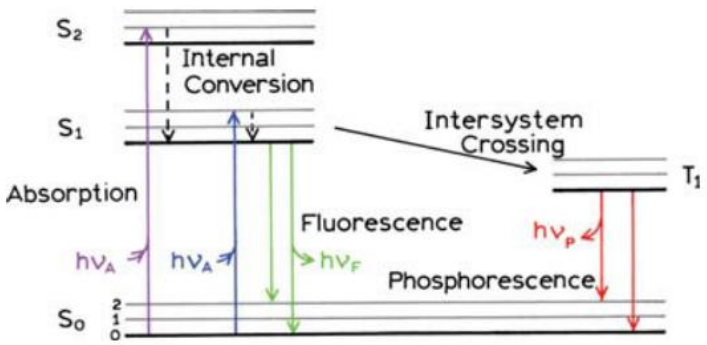

Figure 5-24. One form of a Jablonski diagram.[25]

To measure the quantum yield, first, we have to prepare a diluted solution of the

compound and do the corresponding UV-Vis spectrum to get the wavelength of the maximum absorption band (that will be the wavelength of excitation to obtain the emission spectra, $\lambda_{exc.}$), and then make some dilutions until obtaining a concentration in which the value of the absorbance of such a band is slightly below 0.1 (typically it corresponds to solutions at 10^{-6} or 10^{-7} M). With this sample, we can do the fluorescence emission spectrum selecting the λ_{exc} from the UV-Vis and a range of emission wavelength after the $\lambda_{exc.}$ We also have to measure a blank of only the solvent of the sample. Finally, to calculate the fluorescence quantum yield, we have to measure a reference with a similar excitation wavelength, in the same way as the samples. The most commonly used fluorescence standards are quinine sulfate and rhodamine derivatives, for lower and higher $\lambda_{exc.}$, respectively. The best standard for us was quinine sulfate as it has similar $\lambda_{exc.}$ than our radical dendrimers. The equation to calculate the quantum yield is

$$QY = \frac{F_s \times A_r \times R_s^2 \times QY_r}{F_r \times A_s \times R_r^2} \quad (5\text{-}2)$$

where:

F_s: Fluorescence peak area of the sample

A_r: Absorbance of the reference

R_s: Refraction index of the solvent used to dissolve the sample

QY_r: QY of the reference

F_r: Fluorescence peak area of the reference

A_s: Absorbance of the sample

R_r: Refraction index of the solvent used to dissolve the reference

We prepared diluted solutions of 1) quinine sulfate in H_2SO_4 (0.1 M), 2) tri-acid dendrimer, 3) tri-amido-TEMPO (**33**) radical dendrimer, 4) tetra-acid dendrimer, 5) tetra-amido-TEMPO (**34**) radical dendrimer, 6) tri-aldehyde dendrimer, 7) tri-imino-TEMPO (**35**) radical dendrimer, 8) tri-amino-TEMPO (**37**) radical dendrimer, 9) tetra-aldehyde dendrimer, 10) tetra-imino-TEMPO (**36**) radical dendrimer and 11) tetra-amino-TEMPO (**38**) radical dendrimer, all of them in THF as some dendrimers were not soluble in dichloromethane. Hence, all the measurements could be done in the same solvent for proper comparison. We also measured Mili-Q water as the blank for quinine sulfate and THF as the blank for the other samples. We proceeded following the procedure explained above, doing first the UV-Vis of very diluted samples and then the corresponding fluorescence spectra.

The UV-Vis spectrum and the fluorescence emission spectrum of the standard quinine sulfate are shown in Figure 5-25. The UV-Vis spectra of the other compounds are shown in Figure 5-26 and the corresponding fluorescence emission spectra are shown in Figure 5-27. The quantum yield was calculated by using the equation 5-2. The results of the quantum yield are shown in Table 5-3. The $\lambda_{exc.}$ and $\lambda_{em.}$ values are shown in Table 5-4.

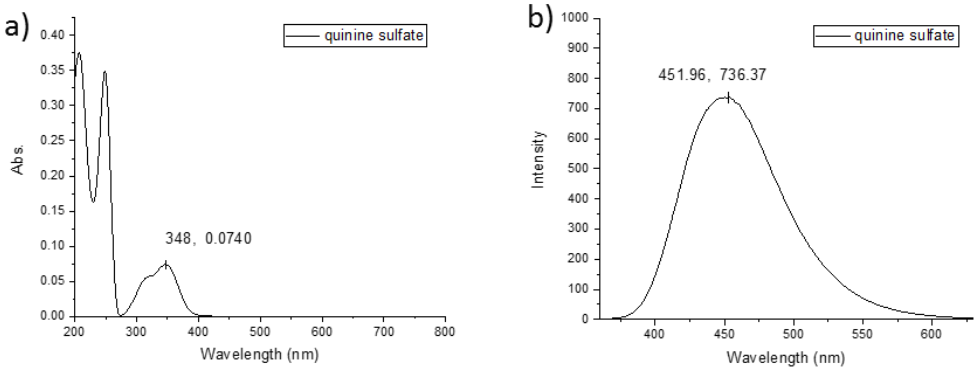

Figure 5-25. a) UV-Vis spectrum and b) fluorescence emission spectrum of the standard quinine sulfate.

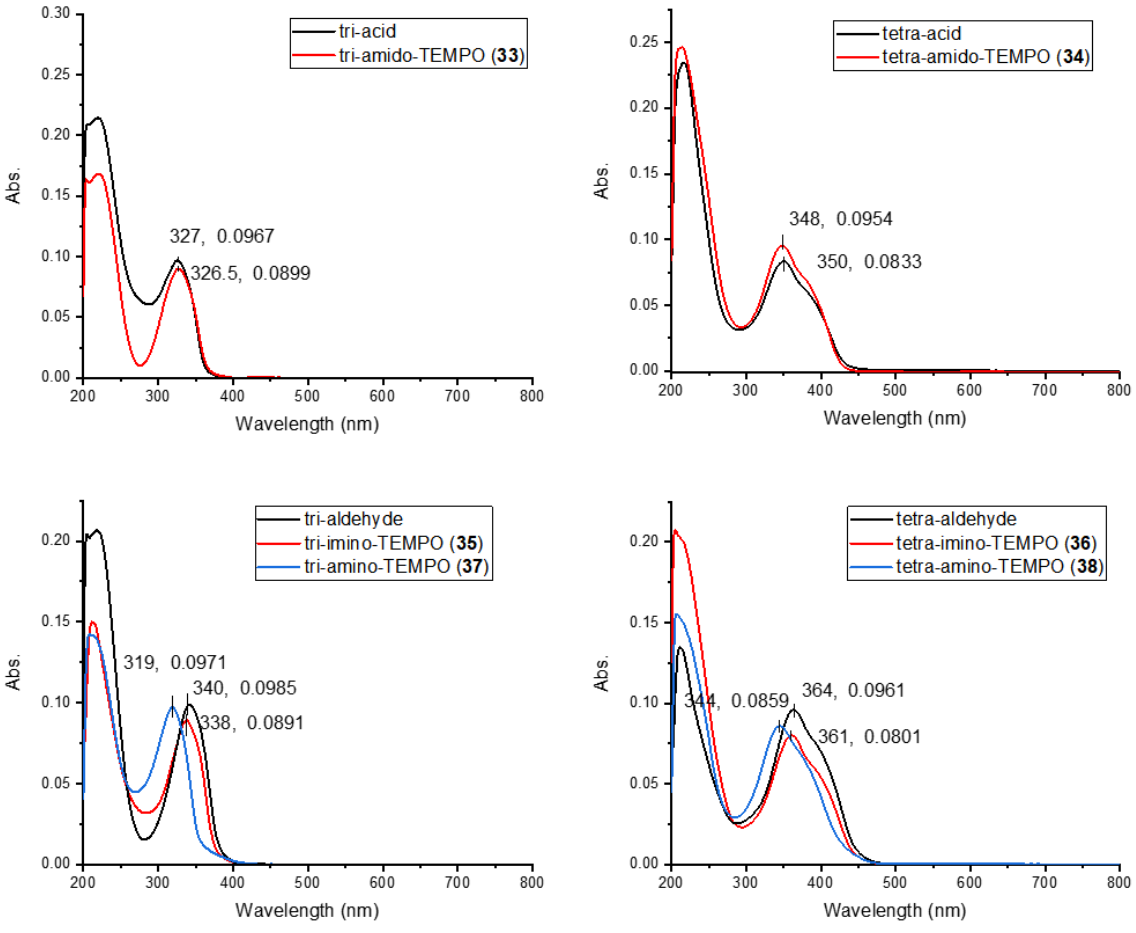

Figure 5-26. UV-Vis spectra of amido-, imino- and amino- radical dendrimers derivatives **33**-**38** in THF.

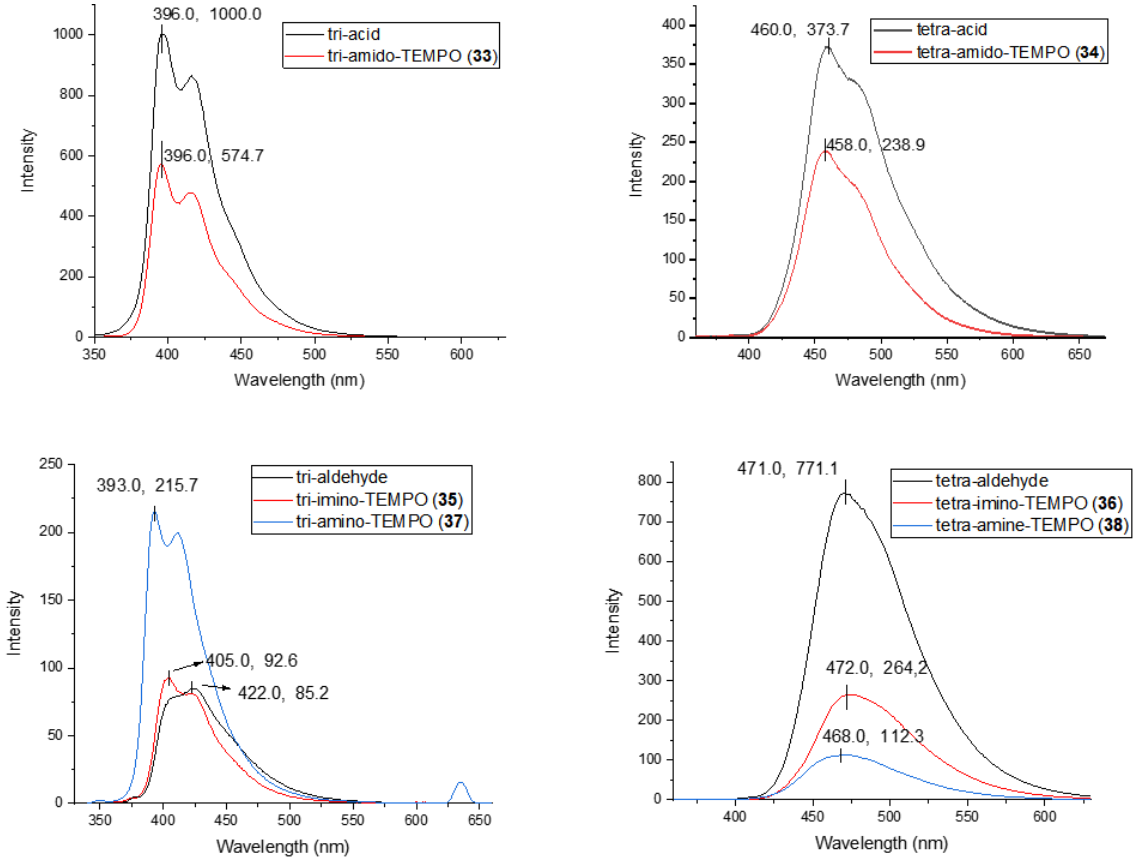

Figure 5-27. Fluorescence emission spectra of amido-, imino- and amino- radical dendrimers derivatives **33-38** in THF.

Table 5-3. $\lambda_{exc.}$ and $\lambda_{em.}$ values for quinine sulfate, dendrimers and radical dendrimers **33-38**.

Compound	$\lambda_{exc.}$ (nm)	$\lambda_{em.}$ (nm)
quinine sulfate	348	452
tri-acid	326.5	396
tri-amido-TEMPO (**33**)	327	396
tetra-acid	350	460
tetra-amido-TEMPO (**34**)	338	458
tri-aldehyde	340	422
tri-imino-TEMPO (**35**)	338	405
tri-amino-TEMPO (**37**)	319	393
tetra-aldehyde	364	471
tetra-imino-TEMPO (**36**)	361	472
tetra-amino-TEMPO (**38**)	344	468

Table 5-4. Calculated quantum yield of quinine sulfate, dendrimers and radical dendrimers **33**-**38**.

Compound	Abs. (A)	FL area (F)	Refraction Index (R)	Quantum Yield
quinine sulfate	0.074	65192.32	1.33	0.540
tri-acid	0.0899	52371.05	1.4072	0.400
tri-amido-TEMPO (**33**)	0.0967	28274.02	1.4072	0.201
tetra-acid	0.0833	30086.73	1.4072	0.248
tetra-amido-TEMPO (**34**)	0.0954	16902.84	1.4072	0.122
tri-aldehyde	0.0985	5922.78	1.4072	0.041
tri-imino-TEMPO (**35**)	0.0891	5171.24	1.4072	0.040
tri-amino-TEMPO (**37**)	0.0971	12236.02	1.4072	0.086
tetra-aldehyde	0.0961	59755.09	1.4072	0.427
tetra-imino-TEMPO (**36**)	0.0801	21039.81	1.4072	0.180
tetra-amino-TEMPO (**38**)	0.0859	9150.83	1.4072	0.073

According to the spectroscopic results obtained and shown in Figure 5-26 and Table 5-3, it is observed that the **absorption** occurs mainly on the part of the oligo(styryl)benzene units since both the absorbance maximum and the shape of the bands between the precursor dendrimers and the radical dendrimers are coincident. The optical properties of OSBs are highly dependent on their peripheral substituents[26–28]. Specifically, for the tri-acid and tri-aldehyde compounds, a previous study indicates that these absorptions correspond mainly to various contributions from $S_0 \rightarrow S_1$ and $S_0 \rightarrow S_2$ transitions and the attached functional groups participate in these transitions by stabilizing or destabilizing the HOMO or LUMO[29]. The tetra-substituted derivatives show more red-shifted absorbances. When comparing the tri-amido-TEMPO (**33**) and tetra-amido-TEMPO (**34**) derivatives with the starting precursors, tri-acid and tetra-acid respectively, it is observed that there is no substantial variation in the absorbance maximum for each of them. This is because the electronic characteristics of the OSB do not change substantially since the differences between the electronic properties of the acid group and the amido group are not large enough to modify the OSB, since both are electrowithdrawing groups. However, when comparing the imino- and amino- radical dendrimers with the tri-aldehyde and tetra-aldehyde precursors, it is observed that the formation of the imine does not produce a change in the electronics of the OSB but its reduction to form the amino. The reduction transforms a sp^2 carbon of the imine into a sp^3 carbon which interrupts the communication between the amino group and the OSB. This results in a hypsochromic shift (or blue shift) of the absorption band. The

electroattracting groups such as aldehyde or imine remove electron density from the HOMO, destabilizing it, increasing its energy and reducing the gap between HOMO and LUMO, leading to absorption bands at 340 nm for tri-substituted and at 360 nm for tetra-substituted. However, when this interaction between the functional group and the OSB is broken (due to the amine group formation), the HOMO stabilizes (i.e. the HOMO-LUMO gap increases), and the observed absorption is slowed blue shifted (319 nm for the tri-amino-TEMPO **37** and 344 nm for the tetra-amino-TEMPO **38**).

This effect is less important at the **emission** wavelength, where the fluorescence of each radical dendrimer is very similar to that of the precursor OSB. This indicates that the excited state from which the emission starts is very similar in both the radical dendrimer and the precursor and is mainly centered on the OSB backbone. It is important to remark that all the radical dendrimers synthesized (**33**, **34**, **35**, **36**, **37** and **38**) show fluorescence, and they emit at $\lambda_{em.}$ between 393 and 472 nm with a quantum yield between 4.0 and 20.1 % (see Figure 5-27 and Table 5-4). Previous work on OSB indicates that tri-substituted acidic compounds exhibit better quantum yields than their four-branched analogues. This is because increasing the number of stilbene units increases the vibrational and rotational motions in a so-called restriction of intramolecular motions (RIM) mechanism,[30] all responsible for the non-radiative relaxations of the absorbed light from the molecule. In the case of aldehyde derivatives, the 3-branched compound presents worse quantum yields because it undergoes a cis/trans photoisomerization process that is not possible in the 4-branched compound due to steric hindrance. The incorporation of radicals into OSB scaffolds leads, in most cases, to a decrease in fluorescence, although they are still acceptable quantum yields in general. Tri-amido-TEMPO (**33**) and tetra-amido-TEMPO (**34**) the quantum yield decreases to the half, approximately, with respect to tri-acid and tetra-acid, respectively. In the case of tetra-imino-TEMPO (**36**) and tetra-amino-TEMPO (**38**), their fluorescence quantum yield is quenched with respect to tetra-aldehyde dendrimer until also approximately the half in the former and 1/5, in the latter. On the other hand, the quantum yield of tri-imino-TEMPO (**35**), around 4 % (0.04), is similar to its corresponding tri-aldehyde dendrimer (0.041), i.e. in this case the anchoring of radicals does not quench the fluorescence. However, the quantum yield of tri-amino-TEMPO (**37**) is double (0.073) from that of the tri-aldehyde dendrimer (0.041). In this case, the fluorescence values are very low, both in the precursor molecule and in the radical dendrimer, so that any changes may appear to greatly affect the quantum yields.

It is true that it has been described how amines not directly bound to chromophore systems can give rise to special fluorescence phenomena called photoinduced electron transfer (PET) effect and that cannot be ruled out in this system. In any case, the radical dendrimers studied show good fluorescent properties that allow them to be used as fluorescent probes.[31]

5.5 MRI experiments

As explained in the introduction, contrast agents are paramagnetic compounds that allow improving the contrast of the images obtained in MRI by modifying the relaxation time of the solvent protons (typically water protons). The relaxivity (r) is the degree to which the contrast agent can affect the longitudinal T_1 or transversal T_2 solvent protons relaxation rate constant ($R_1 = 1/ T_1$ or $R_2 = T_2$) normalized to the concentration of the contrast agent ($mM^{-1}s^{-1}$ units).

The capacity of decreasing the relaxation time T_1 of the protons of the solvent, and hence their capacity to act as a contrast agent, has been evaluated *in vitro* in organic solvents, as a probe of concept, for tri-amido-TEMPO (**33**), tetra-amido-TEMPO (**34**), tri-imino-TEMPO (**35**) and tri-amino-TEMPO (**37**) derivatives, as well as for TEMPO radical, used as a reference. The requirement for the solvent to perform this MRI evaluation is that it presents only one NMR signal for the protons of its structure, that is, one type of equivalent protons, and the samples must be soluble in it. DMSO and dichloromethane were the solvents of choice.

For tri-amido-TEMPO (**33**), tri-imino-TEMPO (**35**) and tri-amino-TEMPO (**37**) derivatives, we chose dichloromethane as both requirements were accomplished. For each compound, we prepared six solutions covering a big range of concentrations, from 10 to 0.625 mM per TEMPO radical unit concentration, and placed them in 1.5 mL Eppendorfs. The values of T_1 were obtained for each concentration and we plotted R_1 values ($R_1=1/ T_1$) versus the concentration to obtain the relaxivity r_1 of each compound, which was compared with the r_1 of TEMPO free radical in the same solvent (see Figure 5-28). The relaxivities r_1 of these compounds are listed in Table 5-5. The three compounds present similar relaxivities ranging from 0.316 to 0.339 $mM^{-1}s^{-1}$. When we consider the relaxivities per radical, their relaxivities are higher than free TEMPO, which possibly results from the higher molecular weights (bigger size) and high rigidity of these radical

dendrimers,[32] slowing down the rotational correlation time.

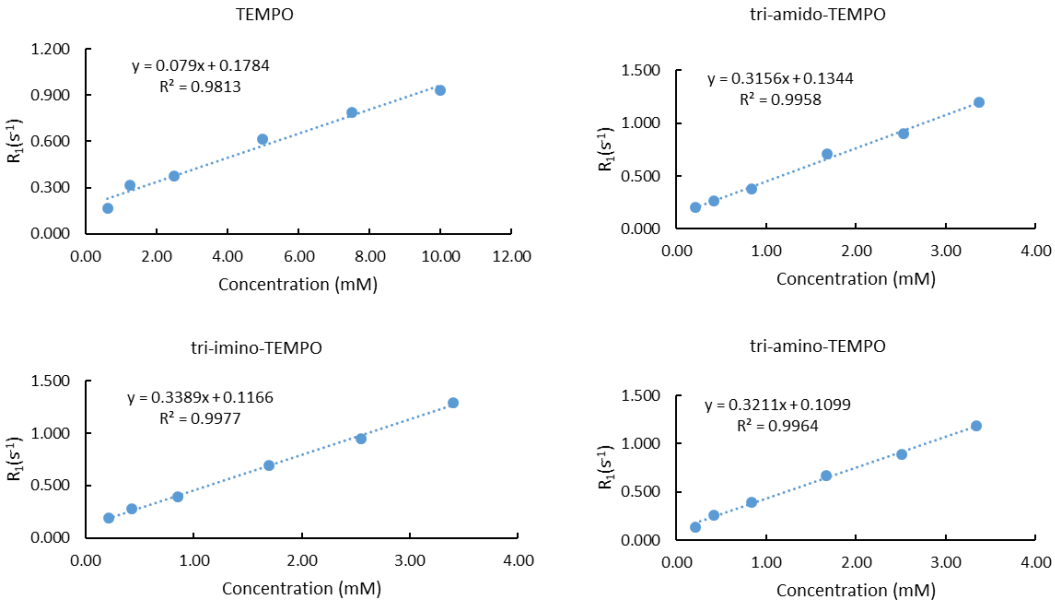

Figure 5-28. Plots of R_1 (1/ T_1) versus concentration for different concentrations of free TEMPO, tri-amido-TEMPO (**33**), tri-imino-TEMPO (**35**) and tri-amino-TEMPO (**37**) in dichloromethane.

Table 5-5. Relaxivity values (r_1) for free TEMPO, tri-amido-TEMPO (**33**), tri-imino-TEMPO (**35**) and tri-imino-TEMPO (**37**) in dichloromethane.

Compound	r_1 (mM^{-1} s^{-1}) per molecule	r_1 (mM^{-1} s^{-1}) per radical
TEMPO	0.079	0.079
tri-amido-TEMPO (**33**)	0.316	0.105
tri-imino-TEMPO (**35**)	0.339	0.113
tri-amino-TEMPO (**37**)	0.321	0.107

The relaxivities of free TEMPO, tri-amido-TEMPO (**33**) and tetra-amido-TEMPO (**34**) radical dendrimers were obtained in DMSO which also presents only one proton signal and the radical dendrimers were completely soluble in it at these concentrations. Similarly, we plotted R_1 values (R_1=1/ T_1) versus the concentration to obtain the relaxivity r_1 of each compound (Figure 5-29). The relaxivities of these three compounds are listed in Table 5-6. The relaxivities of tri-amido-TEMPO (**33**) and tetra-amido-TEMPO (**34**) are 0.530 and 0.828 mM^{-1} s^{-1}, respectively. The relaxivities of these two compounds per radical are significantly higher than the free TEMPO, which confirmed that the high molecular weight and rigidity is beneficial to increase the relaxivities.

The other compounds tetra-imino-TEMPO (**36**) and tetra-amino-TEMPO (**38**)

showed not full solubility in dichloromethane or DMSO at high concentrations, for this reason, we could not do the MRI *in vitro* in such solvents and they are not shown in this work.

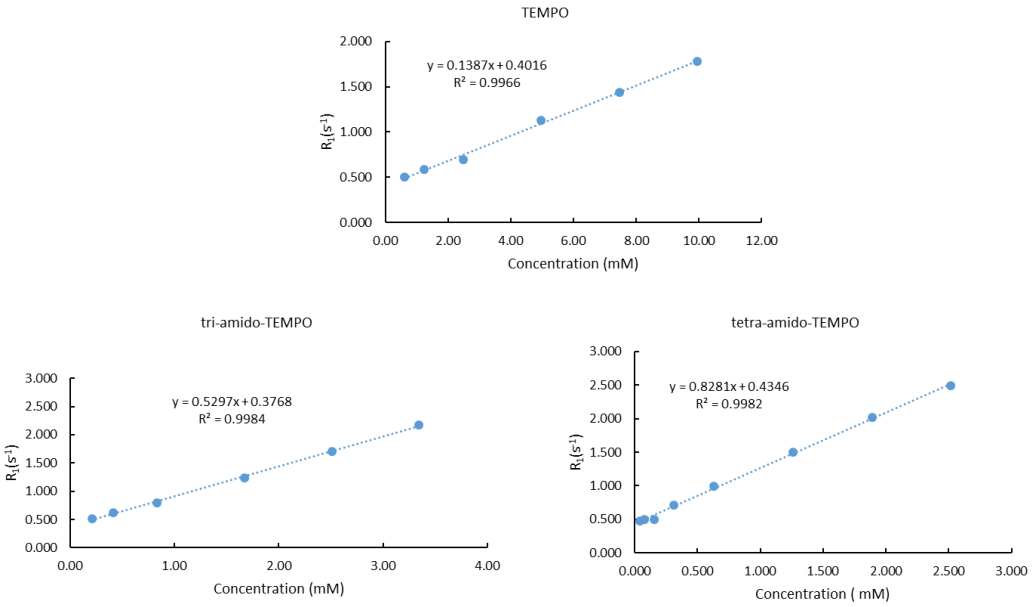

Figure 5-29. Plots of R_1 (1/ T_1) versus concentration for different concentrations of TEMPO, tri-amido-TEMPO (**33**) and tetra-amino-TEMPO (**34**) in DMSO.

Table 5-6. Relaxivity values (r_1) for free TEMPO, tri-amido-TEMPO (**33**) and tetra-amido-TEMPO (**34**) in DMSO.

Compound	r_1 (mM^{-1} s^{-1}) per molecule	r_1 (mM^{-1} s^{-1}) per radical
TEMPO	0.139	0.139
tri-amido-TEMPO (**33**)	0.530	0.177
tetra-amido-TEMPO (**34**)	0.828	0.207

5.6 Preparation of micelles containing fluorescent radical dendrimers

Until now, we have obtained oligo(styryl)benzene based radical dendrimers showing at the same time fluorescence properties and the capacity of decreasing the relaxation time T_1 of the protons of the surrounding solvent. However, these studies have been carried out in organic solvents, where they are soluble. With the aim of application as bimodal fluorescence-magnetic imaging contrast agents, the next question is to address

the problem of water solubility. To achieve this goal, different strategies can be carried out. We can take advantage of hydrophilic groups or chains, such as anions or poly(ethylene glycol) (PEG), for example following the "aminoacid linker strategy" used in Chapter 2 or by anchoring PEG chains to the dendrimers. However, these strategies need several synthetic steps. Another strategy is to impart the solubility to these hydrophobic radical dendrimers by micellar encapsulation in aqueous medium using a surfactant such as cetyltrimethylammonium bromide (CTAB). In contrast to the first strategies which are time-consuming, this other method is simpler and it has been tested by other groups [33]. Although the first two options may be carried out by the group in the future, in this Thesis we have explored the micelle formation strategy, which represents another strategy to achieve water-soluble radical dendrimer systems.

We chose radical dendrimer tetra-amido-TEMPO (**34**) as an example for this pilot experiment. We used the thin film hydration process to obtain the micellar systems. In short, the hydrophobic compound **34** was dissolved in ethanol together with the CTAB, the solvent was allowed to evaporate in air for one week, and finally the dry compounds were hydrated with water, then heated at 50 ºC for 10 minutes and shaken. After one day, we filtered all of them by a 0.2 μm porous size filter and we allowed them to stabilize one day more. After that, the samples were analysed.

At first, we tried to encapsulate the radical dendrimer in 100 mM CTAB solution, from 0.01 mM to 1.6 mM of dendrimer concentrations. It was observed that only the 0.01 mM micellar dispersion was homogeneous since in the other dispersions there appeared some precipitate at the bottom of the vials. Furthermore, after 15 days, we noticed that there was some precipitated or crystallized CTAB in some vials, even in the first one at a concentration of 0.01 mM (Figure 5-30), which we attributed to the high concentration of CTAB. Consequently, we decreased the CTAB concentration to 5 mM.

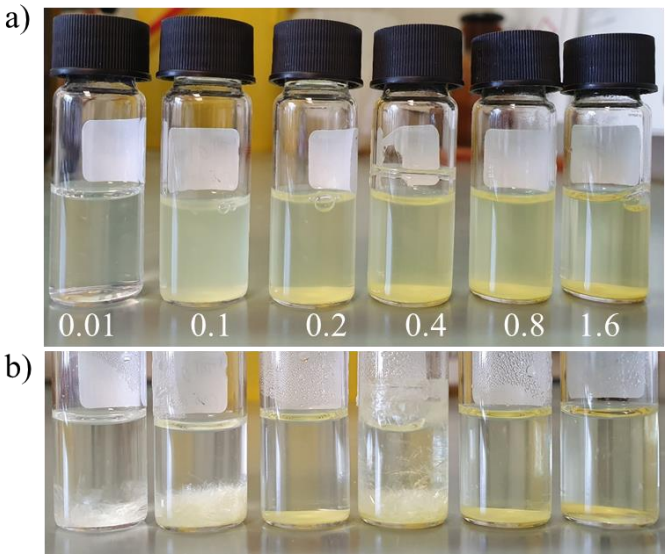

Figure 5-30. Photos of the different micellar dispersion with CTAB concentration at 100 mM and tetra-amido-TEMPO (**34**) concentrations at 0.01, 0.1, 0.2, 0.4, 0.8 and 1.6 mM a) overnight and b) after 15 days of being formed.

Next, we carried out the encapsulation of the radical dendrimer in 5 mM CTAB, to avoid the precipitation of CTAB. The concentration of tetra-amido-TEMPO (**34**) was from 2.5 to 200 μM. In this case, we obtained homogeneous systems in the six first dispersions prepared (0, 2.5, 5, 10, 20 and 50 μM concentrations of **34**) according to the transparency of the media (Figure 5-31a). In addition, when the micellar dispersions were under an ultraviolet light of 254 nm, we could observe fluorescence emission in them that was more intense at a high concentration of radical dendrimer, confirming the increasing amount of radical dendrimer encapsulated in the micelles (Figure 5-31b).

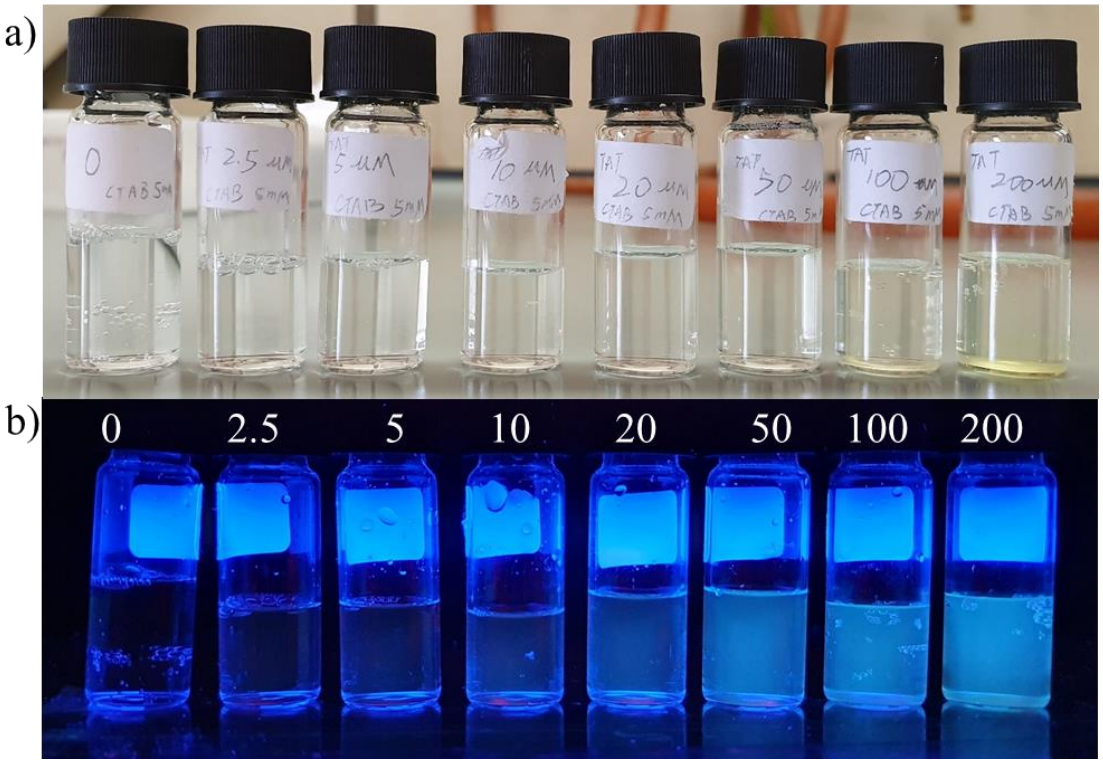

Figure 5-31. Photo of the different micellar dispersions with CTAB concentration at 5 mM and tetra-amido-TEMPO (**34**) concentration at 0, 2.5, 5, 10, 20, 50, 100 and 200 μM. a) under ambient light, b) under a 254 nm lamp.

The different micellar dispersions were characterized by UV-Vis, fluorescence and EPR spectroscopy, DLS and TEM.

The UV-Vis spectra of the different micellar systems are shown in Figure 5-32a. They show similar shape of the absorption bands compared with the spectrum of the same compound **34** in DCM or THF, but with the maximum absorption band blue shifted (from ca. 348 nm to ca. 310 nm) since the increase of the polarity of the solvent (H_2O). The shoulder at higher wavelength (ca. 340 nm) increases in intensity with respect to the band at 310 nm in the 100 and 200 μM samples, which can be explained in terms of increase of aggregation of the species inside the micelles.[33,34] The absorbance of the bands increased with the increasing concentration of **34** (Figure 5-32a), but only in the range of concentrations from 2.5 μM to 50 μM the relationship between the concentration and absorbance showed good linearity (Figure 5-32b). This indicates that the concentration of radical dendrimer encapsulated in the micelles can be as high as 50 μM in these conditions (CTAB at 5 mM), i.e. Above this concentration, the system becomes supersaturated and begins to precipitate, for this reason the last two micellar dispersions with a concentration of 100 and 200 μM of **34** presented some precipitate at the bottom

of the vials.

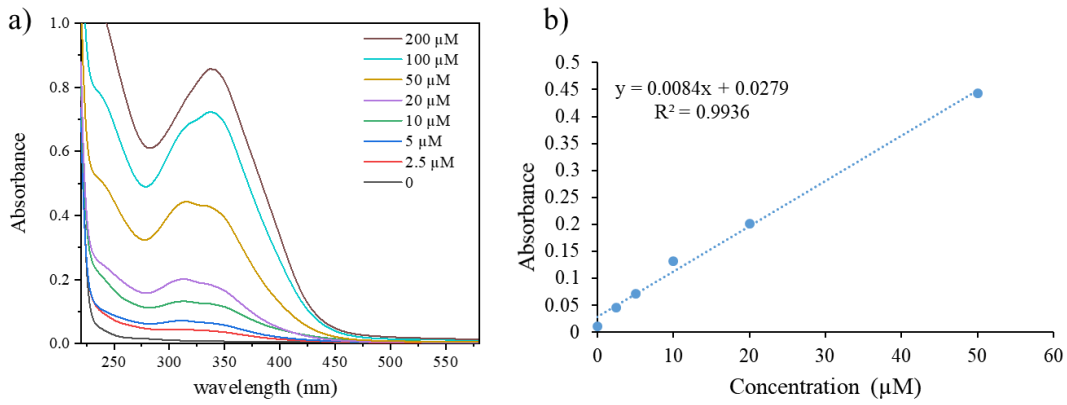

Figure 5-32. a) UV−Vis spectra of CTAB micellar dispersions with different concentrations of tetra-amido-TEMPO (**34**) from 0 to 200 µM; b) plot of the UV-Vis Absorbance versus the concentration of **34** from 0 to 50 µM.

The micellar systems were also studied by fluorescence spectroscopy. The fluorescence emission spectra showed a emission band at ca. $\lambda_{em.}$ 453 nm (Figure 5-33), which is close to the value of **34** in THF. To calculate the corresponding quantum yield, we took the data from the micellar system with the concentration of radical dendrimer **34** at 5 µM, since the corresponding UV-Vis spectrum showed an absorption band slightly below 0.1 Abs. We used the equation (5-2) with quinine sulfate as a standard and the QY obtained was 2% (Table 5-7), which is lower than the corresponding QY for **34** in THF solution (12.2 %). The lower quantum yield obtained in micellar aqueous system than in THF is possibly caused by quenching of luminescence due to molecular aggregation (aggregation-caused quenching (ACQ)).[28] Also, the different solvent can affect.

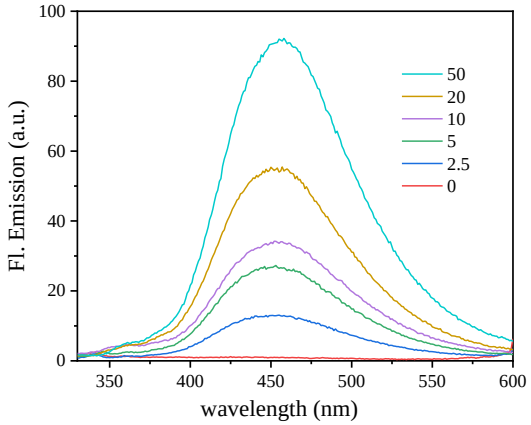

Figure 5-33. Emission spectra of the micellar dispersions with 0, 2.5, 5, 10, 20 and 50 µM concentration of **34** and CTAB concentration at 5 mM, obtained at the excitation wavelength 310 nm.

Table 5-7. Calculated quantum yield of quinine sulfate and micellar dispersion with 5 μM concentration of tetra-amido-TEMPO (**34**) in CTAB at 5 mM.

Compound	Abs. (A)	FL area (F)	Refraction Index (R)	Quantum Yield
quinine sulfate	0.074	65192.32	1.33	0.540
tetra-amido-TEMPO (**34**) (5 μM)	0.072	2485.3	1.33	0.0199

The prepared CTAB micellar dispersions were also characterized by DLS (Figure 5-34). All the micellar systems from 2.5 μM to 200 μM concentration of **34** presented a narrow unimodal distribution of size with quite low polydispersion index (being the lowest PDI 0.15 for the 200 μM system (Figure 5-34), and the hydrodynamic size ranged from 93 nm to 144 nm (Table 5-8).

The TEM was also used to effectively observe the micelles and study their morphology or shape. We studied the micellar dispersion with concentration of tetra-amido-TEMPO **34** at 10 μM and we observed that the micelles presented spherical shape with size 54.34 ± 16.37 nm (Figure 5-35).

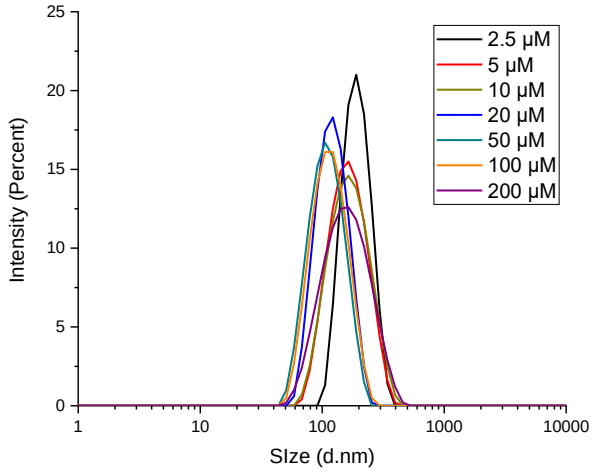

Figure 5-34. Size distribution by intensity measured by DLS of the CTAB micellar dispersions with tetra-amido-TEMPO (**34**) encapsulated at concentrations 2.5, 5, 10, 20, 50, 100 and 200 μM.

Table 5-8 Size and PDI measured by DLS for the micellar dispersions at different concentrations of tetra-amido-TEMPO **34** and CTAB at 5 mM.

Sample	Concentration	Size	PDI
Tetra-amido-TEMPO (**34**)	2.5 μM	140.4±28.53	0.263±0.059
	5 μM	125.7±23.40	0.266±0.18
	10 μM	145.6±0.72	0.189±0.009
	20 μM	96.88±3.049	0.283±0.015
	50 μM	93.28±2.378	0.210±0.025
	100 μM	99.57±3.099	0.195±0.018
	200 μM	144.1±4.504	0.150±0.019

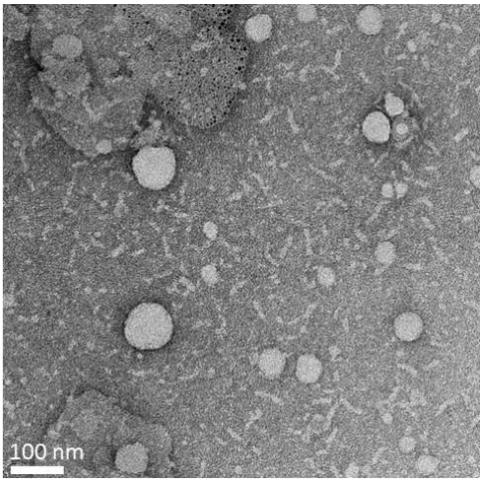

Figure 5-35. TEM image of CTAB micelles with concentration of tetra-amido-TEMPO **34** at 10 μM, using negative stain method with uranyl acetate.

The micellar dispersions were also characterized by EPR, showing all of them the same kind of EPR spectrum. As an example, we show in Figure 5-36, the EPR spectrum of the micellar system at 50 μM concentration of **34**. The spectral shape obtained was a bit different than the corresponding to **34** free in solution. On the other hand, while the line with was similar (around 1.60 G), the *g* factor and a_N were different than in **34** due to the new polar solvent environment. The coupling constant a_N in the micellar system was higher (16.9 G) than in **34** in THF (15.5 G), due to the a_N is sensitive to the polarity of the solvent. In more polar solvents, the a_N is higher. The *g* factor in the micellar system was 2.0051 versus 2.0064 in **34**.

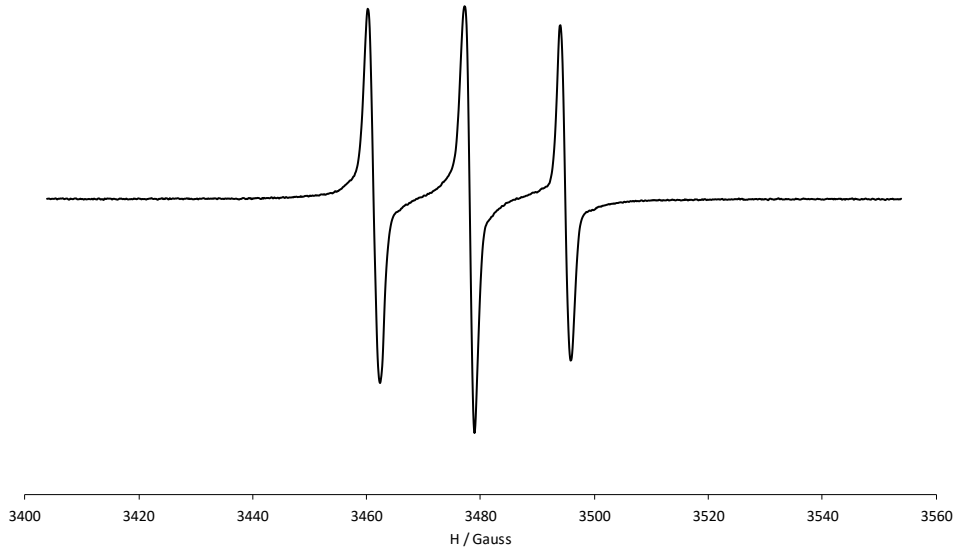

Figure 5-36. EPR spectrum of CTAB micelles with a concentration of tetra-amido-TEMPO **34** at 50 μM.

5.7 Conclusions

- We have synthesized six radical dendrimers based on fluorescent oligo(styryl)benzenes, with different linking bonds between the radicals and the dendrimers (amido, imino and amino linkers). IR, ^{1}H NMR, UV-Vis, MALDI-TOF, SEC and EPR confirmed that the dendrimers were fully substituted with TEMPO radicals.

- It is important to remark that all the synthesized radical dendrimers maintain fluorescent properties after the radical coupling, although the fluorescence has been quenched in almost all cases with respect to their corresponding dendrimer precursors.

- *In vitro* MRI studies of tri-amido-TEMPO (**33**), tetra-amido-TEMPO (**34**), tri-imino-TEMPO (**35**) and tri-amino-TEMPO (**37**) have shown that they have the capacity to decrease the relaxation time T_1 of DMSO and/or dichloromethane protons, showing a relaxivity r_1 per unit of radical higher than the TEMPO free radical. Thus, we have obtained bimodal fluorescent-magnetic species.

- In order to prepare aqueous solutions of the radical dendrimers, CTAB micelles have been chosen as a carrier to encapsulate tetra-amido-TEMPO (**34**). With a concentration of CTAB at 5 mM, the maximum concentration of tetra-amido-TEMPO (**34**) encapsulated can be 50 μM. Such systems, with the radical dendrimers inside, maintain both magnetic and fluorescent properties.

5.8 References

(1) Van Dam, G. M.; Themelis, G.; Crane, L. M. A.; Harlaar, N. J.; Pleijhuis, R. G.; Kelder, W.; Sarantopoulos, A.; De Jong, J. S.; Arts, H. J. G.; Van Der Zee, A. G. J. Intraoperative Tumor-Specific Fluorescence Imaging in Ovarian Cancer by Folate Receptor-α Targeting: First in-Human Results. *Nat. Med.* **2011**, *17* (10), 1315–1319.

(2) Zhao, J.; Chen, J.; Ma, S.; Liu, Q.; Huang, L.; Chen, X.; Lou, K.; Wang, W. Recent Developments in Multimodality Fluorescence Imaging Probes. *Acta Pharm. Sin. B* **2018**, *8* (3), 320–338.

(3) Tong, H.; Lou, K.; Wang, W. Near-Infrared Fluorescent Probes for Imaging of Amyloid Plaques in Alzheimer′ s Disease. *Acta Pharm. Sin. B* **2015**, *5* (1), 25–33.

(4) Hemmer, E.; Benayas, A.; Légaré, F.; Vetrone, F. Exploiting the Biological Windows: Current Perspectives on Fluorescent Bioprobes Emitting above 1000 Nm. *Nanoscale Horizons* **2016**, *1* (3), 168–184.

(5) Guo, K.; Berezin, M. Y.; Zheng, J.; Akers, W.; Lin, F.; Teng, B.; Vasalatiy, O.; Gandjbakhche, A.; Griffiths, G. L.; Achilefu, S. Near Infrared-Fluorescent and Magnetic Resonance Imaging Molecular Probe with High T1 Relaxivity for in Vivo Multimodal Imaging. *Chem. Commun.* **2010**, *46* (21), 3705–3707.

(6) Harrison, V. S. R.; Carney, C. E.; MacRenaris, K. W.; Waters, E. A.; Meade, T. J. Multimeric Near IR-MR Contrast Agent for Multimodal in Vivo Imaging. *J. Am. Chem. Soc.* **2015**, *137* (28), 9108–9116.

(7) Dong, D.; Jing, X.; Zhang, X.; Hu, X.; Wu, Y.; Duan, C. Gadolinium(III)-Fluorescein Complex as a Dual Modal Probe for MRI and Fluorescence Zinc Sensing. *Tetrahedron* **2012**, *68* (1), 306–310.

(8) Li, H.; Parigi, G.; Luchinat, C.; Meade, T. J. Bimodal Fluorescence-Magnetic Resonance Contrast Agent for Apoptosis Imaging. *J. Am. Chem. Soc.* **2019**, *141* (15), 6224–6233.

(9) Watkins, A. R. Solvent Effects on Triplet State Quenching by Tetramethylpiperidcme-N-Oxide. *Chem. Phys. Lett.* **1980**, *70* (2), 262–265.

(10) Wang, Z.; Gao, Y.; Hussain, M.; Kundu, S.; Rane, V.; Hayvali, M.;

Yildiz, E. A.; Zhao, J.; Yaglioglu, H. G.; Das, R.; Luo, L.; Li, J. Efficient Radical-Enhanced Intersystem Crossing in an NDI-TEMPO Dyad: Photophysics, Electron Spin Polarization, and Application in Photodynamic Therapy. *Chem. - A Eur. J.* **2018**, *24* (70), 18663–18675.

(11) Kohtani, S.; Murata, M.; Itoh, M. Resonance Energy Transfer from the Excited Singlet State of Dye Molecules to a Stable Free Radical. *Chem. Phys. Lett.* **1995**, *247* (3), 293–298.

(12) Samanta, A.; Kamat, P. V. Qenching of Fullerene Triplets by Stable Nitroxide Radicals. *Chem. Phys. Lett.* **1992**, *199* (6), 635–639.

(13) Blinco, J. P.; Fairfull-Smith, K. E.; Morrow, B. J.; Bottle, S. E. Profluorescent Nitroxides as Sensitive Probes of Oxidative Change and Free Radical Reactions. *Aust. J. Chem.* **2011**, *64* (4), 373–389.

(14) Lussini, V. C.; Colwell, J. M.; Fairfull-Smith, K. E.; Bottle, S. E. Profluorescent Nitroxide Sensors for Monitoring Photo-Induced Degradation in Polymer Films. *Sensors Actuators, B Chem.* **2017**, *241*, 199–209.

(15) Lussini, V. C.; Blinco, J. P.; Fairfull-Smith, K. E.; Bottle, S. E.; Colwell, J. M. Profluorescent Nitroxide Sensors for Monitoring the Natural Aging of Polymer Materials. *Polym. Degrad. Stab.* **2020**, *174*, 109091.

(16) Hou, M.; Lu, X.; Zhang, Z.; Xia, Q.; Yan, C.; Yu, Z.; Xu, Y.; Liu, R. Conjugated Polymer Containing Organic Radical for Optical/MR Dual-Modality Bioimaging. *ACS Appl. Mater. Interfaces* **2017**, *9* (51), 44316–44323.

(17) Sowers, M. A.; Mccombs, J. R.; Wang, Y.; Paletta, J. T.; Morton, S. W.; Dreaden, E. C.; Boska, M. D.; Francesca Ottaviani, M.; Hammond, P. T.; Rajca, A.; Johnson, J. A. Redox-Responsive Branched-Bottlebrush Polymers for in Vivo MRI and Fluorescence Imaging. *Nat. Commun.* **2014**, *5* (1), 1–9.

(18) Nguyen, H. V. T.; Chen, Q.; Paletta, J. T.; Harvey, P.; Jiang, Y.; Zhang, H.; Boska, M. D.; Ottaviani, M. F.; Jasanoff, A.; Rajca, A.; Johnson, J. A. Nitroxide-Based Macromolecular Contrast Agents with Unprecedented Transverse Relaxivity and Stability for Magnetic Resonance Imaging of Tumors. *ACS Cent. Sci.* **2017**, *3* (7), 800–811.

(19) Moral, M.; Domínguez, R.; Fernández-Liencres, M. P.; Garzón-Ruiz, A.; García-Martínez, J. C.; Navarro, A. Photophysical Features and Semiconducting Properties of Propeller-Shaped Oligo(Styryl)Benzenes. *J. Chem. Phys.* **2019**, *150* (6).

(20) Kunz, T. K.; Wolf, M. O. Electrodeposition and Properties of TEMPO Functionalized Polythiophene Thin Films. *Polym. Chem.* **2011**, *2* (3), 640–644.

(21) Breuer, E.; Aurich, H. U.; Nielsen, A.; Patai, S.; Rappoport, Z. *Nitrones, Nitronates and Nitroxides (1989)*; Breuer, E., Aurich, H. G., Nielsen, A., Eds.; John Wiley & Sons, Inc.: Chichester, UK, 1989.

(22) Badetti, E.; Lloveras, V.; Muñoz-Gómez, J. L.; Sebastián, R. M.; Caminade, A. M.; Majoral, J. P.; Veciana, J.; Vidal-Gancedo, J. Radical Dendrimers: A Family of Five Generations of Phosphorus Dendrimers Functionalized with TEMPO Radicals. *Macromolecules* **2014**, *47* (22), 7717–7724.

(23) Chernick, E. T.; Casillas, R.; Zirzlmeier, J.; Gardner, D. M.; Gruber, M.; Kropp, H.; Meyer, K.; Wasielewski, M. R.; Guldi, D. M.; Tykwinski, R. R. Pentacene Appended to a TEMPO Stable Free Radical: The Effect of Magnetic Exchange Coupling on Photoexcited Pentacene. *J. Am. Chem. Soc.* **2015**, *137* (2), 857–863.

(24) Guzen, K. P.; Guarezemini, A. S.; Órfão, A. T. G.; Cella, R.; Pereira, C. M. P.; Stefani, H. A. Eco-Friendly Synthesis of Imines by Ultrasound Irradiation. *Tetrahedron Lett.* **2007**, *48* (10), 1845–1848.

(25) Lakowicz, J. R. *Principles of Fluorescence Spectroscopy*, 3rd ed.; Springer: New York, 2006.

(26) Badetti, E.; Lloveras, V.; Wurst, K.; Sebastián, R. M.; Caminade, A. M.; Majoral, J. P.; Veciana, J.; Vidal-Gancedo, J. Synthesis and Structural Characterization of a Dendrimer Model Compound Based on a Cyclotriphosphazene Core with TEMPO Radicals as Substituents. *Org. Lett.* **2013**, *15* (14), 3490–3493.

(27) Garcia-Martinez, J. C.; Diez-Barra, E.; Rodriguez-Lopez, J. Conjugated Dendrimers with Oly (Phenylenevinylene) and Poly (Phenyleneethynylene) Scaffolds. *Curr. Org. Synth.* **2008**, *5* (3), 267–290.

(28) Domínguez, R.; Moral, M.; Fernández-Liencres, M. P.; Peña-Ruiz, T.; Tolosa, J.; Canales-Vázquez, J.; García-Martínez, J. C.; Navarro, A.; Garzón-Ruiz, A. Understanding the Driving Mechanisms of Enhanced Luminescence Emission of Oligo(Styryl)Benzenes and Tri(Styryl)-s-Triazine. *Chem. - A Eur. J.* **2020**, *26* (15), 3373–3384.

(29) Ortiz-Bustos, J.; Hierro, I. del; Sánchez-Ruiz, A.; García-Martínez, J. C.; Pérez, Y. Tuning of Type-I and Type-II Mechanisms for Visible Light Degradation in Tris(Styryl)Benzene-Sensitized TiO2 Nanoparticles. *Dye. Pigment.* **2021**, *184*, 108802.

(30) Sánchez-Ruiz, A.; Sousa-Hervés, A.; Tolosa Barrilero, J.; Navarro, A.; Garcia-Martinez, J. C. Aggregation-Induced Emission Properties in Fully π-Conjugated Polymers, Dendrimers, and Oligomers. *Polymers (Basel).* **2021**, *13* (2), 213.

(31) Domínguez, R.; Tolosa, J.; Moral, M.; Bravo, I.; Canales-Vázquez, J.; Rodríguez-López, J.; Garzón-Ruiz, A.; García-Martínez, J. C. PH-Controlled Self-Assembly of X-Shaped Conjugated Molecules: The Case of 1,2,4,5-Tetrastyrylbenzene. *J. Phys. Chem. C* **2018**, *122* (34), 19937–19945.

(32) Lee, H.; Shahrivarkevishahi, A.; Lumata, J. L.; Luzuriaga, M. A.; Hagge, L. M.; Benjamin, C. E.; Brohlin, O. R.; Parish, C. R.; Firouzi, H. R.; Nielsen, S. O.; Lumata, L. L.; Gassensmith, J. J. Supramolecular and Biomacromolecular Enhancement of Metal-Free Magnetic Resonance Imaging Contrast Agents. *Chem. Sci.* **2020**, *11* (8), 2045–2050.

(33) de Lera-Garrido, F.; Sánchez-Ruiz, A.; Rodríguez-López, J.; Tolosa, J.; García-Martínez, J. C. Enhancement of Emission by Surfactant-Induced Aggregation in Poly(Phenylenevinylene)-Based Lipochromophores. *Dye. Pigment.* **2020**, *179* (December 2019).

(34) Liu, W.; Guo, R. The Interaction between Morin and CTAB Aggregates. *J. Colloid Interface Sci.* **2005**, *290* (2), 564–573.

Chapter 6 *In vivo* MRI studies of G3-Tyr(PROXYL)-COONa radical dendrimer

6.1 Introduction

In this Thesis we have developed various radical dendrimers with potential application as MRI contrast agents giving some of them very good results *in vitro* (either MRI, stability or cytotoxicity), demonstrating they are excellent candidates to be used as MRI contrast agents suited for biomedical applications. However, it is necessary to determine if they can work properly as contrast agents *in vivo* and can maintain the properties observed *in vitro* leading to a good diagnostic of tumors, for example. Therefore, it is necessary to carry out biodistribution studies in both healthy and tumor-bearing mice to consider radical dendrimers as a plausible alternative to Gd-based MRI contrast agents.

We have focused on the family of radical dendrimers based on PPH dendrimer with tyrosine as a liker Gn-Tyr(PROXYL)-COOLi that showed excellent water solubility, high relaxivity, and no cytotoxicity (Chapter 2). Among them, the G3 generation has been the compound of choice to carry out these studies since it showed the highest relaxivity (ca. 13 $mM^{-1}s^{-1}$), the highest stability against reduction and large molecular size. Therefore, in this Chapter, we have explored the *in vivo* MRI potential characteristics of the highest generation of such family of radical dendrimers (G3-Tyr(PROXYL)-COOLi) in healthy and GL261 glioblastoma-bearing mice, along with its *in vivo* toxicity and stability.

To the best of our knowledge, there are only two examples in the literature about *in vivo* studies using radical dendrimers and very few reports using other kind of macromolecular polynitroxides. For example, Winalski and co-workers described that despite the low solubility in water of the third-generation polypropylenimine (PPI) dendrimers conjugated with nitroxides, its intraarticular administration to rabbit stifle joints produced significant enhancement of articular cartilage in T_1-weighted images.[1] On the other hand, biodistribution studies were performed with PPI dendrimers conjugated with spirocyclohexyl nitroxides and PEG chains, providing selectively enhanced magnetic resonance imaging in mice for over 1 h.[2] Only more recently, other kind of macromolecular polynitroxides not based on dendrimers but on polymers or polymeric nanoparticles have shown interesting properties as MRI CA. For example, nitroxide-

functionalized brush-arm star polymer organic radical contrast agents (BASP-ORCAs) have shown very high r_2 relaxivity and accumulation in murine subcutaneous tumors (A459 tumor-bearing NCR-NU mice) for long time following systemic administration.[3] Linear and cross-linked poly(carboxylate ester) PEG-modified PROXYL systems were used to provide MR imaging contrast to breast cancer tumors.[4] In addition, amphiphilic poly(ethylene glycol)-b-polycarbonate-based diblock copolymers containing pendant persistent PROXYL radicals were locally administered in the hindlimb muscle of a female C57BL/6J mouse.[5] Finally, when adult female BALB/c nude mice bearing subcutaneous tumors of HeLa cells in their back were intravenously injected with polyacetylenes containing TEMPO and PEG the MRI signal intensity was significantly increased in the tumor parenchyma.[6]

While dendrimer-based magnetic resonance imaging agents decorated with Gd have been reported for brain cancer,[7] nothing it is described with metal-free organic water-soluble radical dendrimers in this kind of cancer.

To carry out such studies we have synthesized the corresponding sodium salt derivative instead of the described lithium salt derivative in Chapter 2, in order to improve biocompatibility and safety.

6.2 Synthesis of G3-Tyr(PROXYL)-COONa

The synthesis of G3-Tyr(PROXYL)-COONa (**39**) dendrimer was made following Scheme 2-10 (Chapter 2). The corresponding methyl ester derivative G3-Tyr(PROXYL)-COOMe was hydrolyzed with NaOH in THF:H_2O (1:1), resulting in the water soluble G3-Tyr(PROXYL)-COONa (**39**) dendrimer (Scheme 6-1). Dialysis was used to purify it and the full functionalization of G3 dendrimer with radicals was confirmed by EPR.

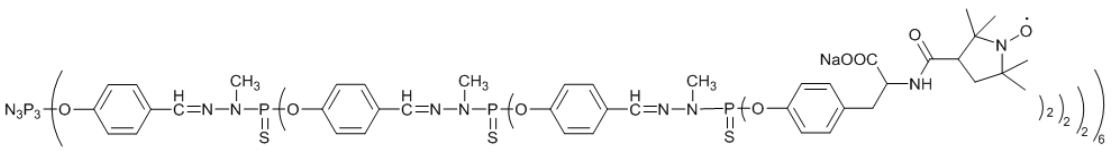

Scheme 6-1. Structure of G3-Tyr(PROXYL)-COONa (**39**) radical dendrimer.

6.3 Endotoxin analysis of G3-Tyr(PROXYL)-COONa radical dendrimer.

Before *in vivo* studies, endotoxin analysis of G3-Tyr(PROXYL)-COONa (**39**) radical dendrimer was carried out to discard the presence of such a toxin in the G3 sample to be administered to mice. We made the analysis at two different concentrations: 0.4 mg/mL and 4 mg/mL. In the sample of lower concentration, the value obtained (0.02 EU/mL) was outside the detection range, and in the higher concentrated sample it was detected a very low endotoxin level: 0.034 ± 0.003 EU/mL. These endotoxin levels are acceptable, since the limit for administration in mice would be 1 EU/mL (5 EU/kg for the usual routes of administration).

6.4 *In vivo* biodistribution

The preliminary biodistribution studies (MRI-based) were performed with n=3 wild type (wt) female mice. With this experiment, we wanted to assess T_1 changes in different organs to check for the biodistribution of G3 after intravenous administration. The dose administered was first planned to be 0.00625 mmol/Kg in dendrimer (0.3 mmol/Kg per radical unit). The G3-Tyr(PROXYL)-COONa (**39**) administration produced slight enhancement in different organs of wt mice measured with whole body T_1w MRI (Figure 6-1), confirmed by decrease of T_1 values calculated in T_1 maps. Enhancement was mostly observed in kidney cortex and pelvis, suggesting the relevance of renal excretion for these compounds.

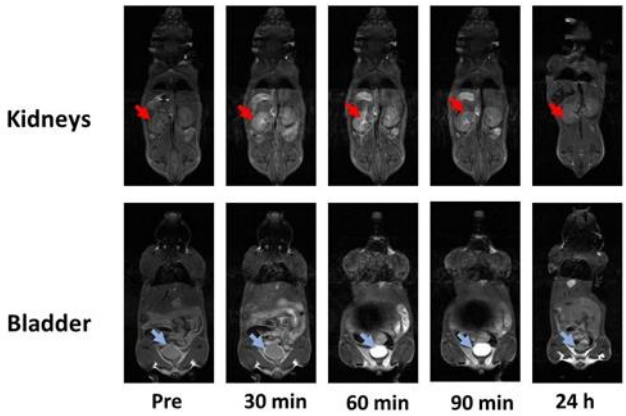

Figure 6-1. *T*1w MRI at different times after G3-Tyr(PROXYL)-COONa (**39**) radical dendrimer administration (0.00625mmol/kg). The main enhancement was seen in kidney cortex/pelvis and bladder. Upper and lower rows belong to the same animal and same time point.

An additional mouse administered with the same dose was euthanized to check some chosen organs (kidneys, liver, urine) by electron paramagnetic resonance (EPR) (Figure 6-2). A similar mass of kidney and liver tissues was analyzed by EPR, using a flat tissue cell. For urine analysis, we had to dilute the collected urine to the half with Mili-Q water to get the optimum volume to be measured in a flat cell (a special EPR cell for aqueous solutions).

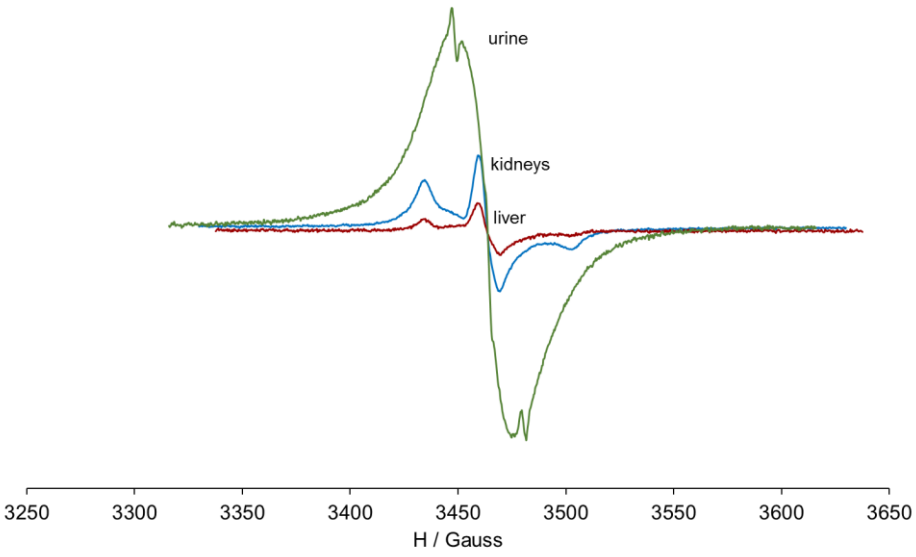

Figure 6-2. EPR spectra of kidneys, liver and urine from healthy mice after 0.00625 mmol/Kg intravenous administration of G3-Tyr(PROXYL)-COONa (**39**) radical dendrimer for biodistribution assays. The urine spectrum was made from the urine collected diluted to the half.

In Figure 6-2, we can observe three important features: i) The amount of G3 radical

dendrimer is much higher in urine than in kidneys and liver, ii) kidneys showed much stronger radical signal intensity than liver, in agreement with the whole body T_1w MRI, suggesting excretion of the radical dendrimer through the kidneys, and iii) the EPR spectrum shape of the urine sample was almost identical to the G3 spectrum before injection (see Figure 2-3 from Chapter 2). This means that the radical character of PROXYL radicals in G3-Tyr(PROXYL)-COONa (**39**) radical dendrimer was not quenched by circulating in the bloodstream, passing from the blood to kidneys and bladder. This is a very important result that demonstrates the high stability of the radicals when anchored to the dendrimer, in contrast to the fast reduction *in vivo* that suffer isolated nitroxides, especially in the bloodstream and tissues, losing their contrast ability shortly after injection.

On the other hand, the EPR spectra shape of kidneys and liver is totally different from that of urine, since the radical dendrimer is not found in liquid conditions (isotropic conditions) but within a dense tissue of an organ, thus, under anisotropic conditions, making the spectral shape being in the slow-motion regime, close to the rigid limit. In these two cases, we cannot discard the inactivation of some radicals of the dendrimer, but, in any case, the observation of radical dendrimer EPR signal more than 1.5 hours after injection also confirms its stability *in vivo*.

The G3 radical dendrimer was also administered to n=2 wt mice which were followed during one month (not shown) with no consistent signs of harm.

6.5 *In vivo* studies with GL261 glioblastoma-bearing mice.

6.5.1 Preliminary *in vivo* MRI studies.

The initial G3 dose administered to GL261 glioblastoma (GB)-bearing mice was the same than for biodistribution studies, that is, 0.00625 mmol/Kg in dendrimer (0.3 mmol/kg in radical). Whole set of MRI studies, including DCE-MRI were performed as described in Appendix B (Materials and Methods). However, the overall results achieved were poor, considering differences in relaxivity. G3-Tyr(PROXYL)-COONa (**39**) administration at this dose only produced hardly noticeable tumor enhancement, not enough to be considered as a suitable contrast agent candidate. The slight enhancement produced only in a peripheral part of the tumor suggested that increasing the dose injected

could help to achieve suitable enhancement. One mouse was euthanized and EPR was performed on selected organs (kidneys, liver, brain tumor, healthy brain and muscle) to check the amount of G3 radical dendrimer and confirm whether it entered the brain tumor or not (Figure 6-3). A similar mass of the different organs (about 47 mg each) was weighed. From such spectra, we can remark two important things: i) G3 radical dendrimer was found mainly in kidneys, then, in liver and in lower amount in the brain tumor, ii) a certain amount of G3 radical dendrimer was detected into the brain tumor, while healthy surrounding brain barely show G3 signal, suggesting that G3 radical dendrimer can selectively accumulate in tumors with few spreading to surrounding brain. This is a relevant and desirable characteristic in a contrast agent to be used for brain tumors. Since such G3 amount was not enough to produce suitable tumor enhancement in T_1 weighted MRI, an increase in the dose of G3-Tyr(PROXYL)-COONa (**39**) concentration administered to GL261 tumor-bearing mice was necessary to improve the tumor enhancement.

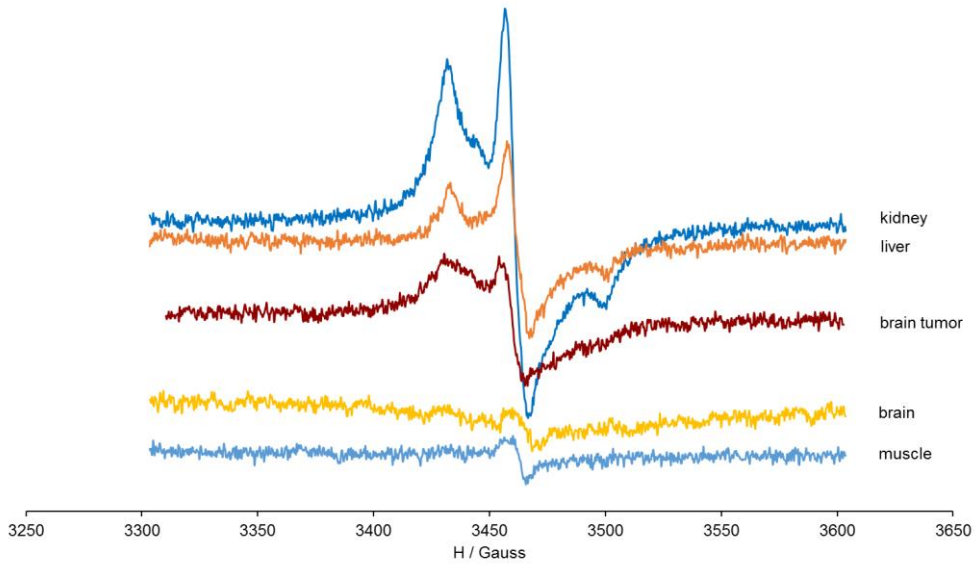

Figure 6-3. EPR spectra of kidneys, liver, brain tumor, contralateral healthy brain and muscle from GL261 tumor-bearing mice after 0.00625 mmol/Kg administration of G3-Tyr(PROXYL)-COONa (**39**) radical dendrimer.

In the search for a suitable concentration to perform the *in vivo* MRI contrast enhancement studies with G3-Tyr(PROXYL)-COONa (**39**) radical dendrimer, dose adjustment was done having in mind the *in vitro* MRI results (Figure 2-6, Chapter 2). Those results showed that relaxivity r_1 of G3-Tyr(PROXYL)-COONa (**39**) compound

(ca. 13 $mM^{-1}s^{-1}$) was 4 times higher than for a Gd complex (for example Gd-DTPA, 3.2 $mM^{-1}s^{-1}$). Taking into account these data and the standard dose of Gd complexes of 0.1 mmol/kg, we decided to prepare 4 times less concentrated dose for G3 compound, i.e. 0.025 mmol/kg. Thus, we increased the initial G3 radical dendrimer concentration from 0.00625 mmol/Kg (0.3 mmol/kg in radical) to 0.025 mmol/Kg (1.2 mmol/Kg in radical). This new G3 concentration resulted to be also completely soluble in water, demonstrating the high degree of water solubility of that radical dendrimer.

6.5.2 Tolerability with 0.025 mmol/Kg dose.

Previous to MRI studies, a tolerability study with 3 healthy wt C57/BL6 females were administered with 0.025 mmol/Kg G3-Tyr(PROXYL)-COONa (**39**) radical dendrimer. Mice were housed at the animal facility and followed-up for two months. The first 10 days animals were weighted every day and their weight evolution was the expected according to Charles River growth chart for healthy C57/BL6 females of this age. Figure 6-4 shows the variation of weight along time. Administered mice did not show toxicity symptoms and did not experiment body weight loss during the whole follow-up. Their overall state such as fur aspect, hydration and behavior/activity was satisfactory and the final weight was within normal values according to the standard growth chart. These important results demonstrate the non-toxicity of G3-Tyr(PROXYL)-COONa (**39**) radical dendrimer *in vivo* after systemic intravenous tail-vein injection at this dose.

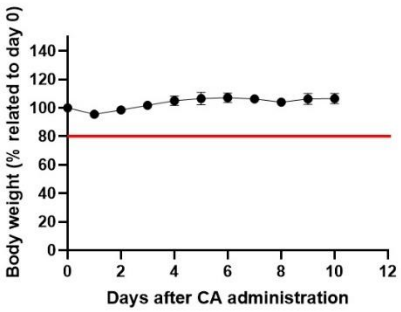

Figure 6-4. Percentage of body weight variation of mice injected with G3-Tyr(PROXYL)-COONa (**39**) radical dendrimer at dose 0.025 mmol/Kg in dendrimer. The red line indicates the 20% weight reduction point.

6.5.3 *In vivo* MRI studies with 0.025 mmol/Kg of G3.

A dose of 0.025 mmol/kg in dendrimer was intravenously injected to n=3 GL261 glioblastoma-bearing mice and experiments conducted as for the lower dose previously described. This dose produced noticeable relative contrast enhancement (RCE) in tumor-bearing mice (Figure 6-5 and Figure 6-6).

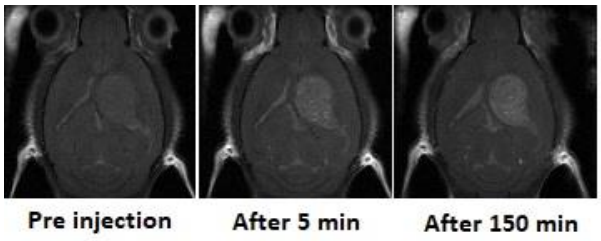

Figure 6-5. Axial *T*1w MRI for follow-up of tumor contrast enhancement before and after 5 min (ca. maximum enhancement) and 150 min (final of *T*1w MRI follow-up) of G3-Tyr(PROXYL)-COONa (**39**) radical dendrimer administration (0.025 mmol/Kg) to GL261 GB-bearing mice.

Changes observed in T_1 values were mostly seen in tumors rather than in contralateral brain. T_1 values were calculated before and after G3 administration with T_1 map sequences. T_1 decrease in the tumor was 19.2 % while it was not detected any decrease in the corresponding contralateral part.

The relative contrast enhancement and the kinetics of uptake and washout of G3-Tyr(PROXYL)-COONa (**39**) radical dendrimer at 0.025 mmol/Kg were compared with Gd-DTPA administration at the standard dose 0.1 mmol/kg (as well as at a lower dose 0.04 mmol/kg). Only the first 60 minutes in the first DCE-MRI experiment of G3 were used for comparison with Gd. Remarkably, the RCE of G3-Tyr(PROXYL)-COONa (**39**) radical dendrimer in the tumor at 0.025 mmol/Kg was similar, although slightly lower, than the RCE obtained with Gd-DTPA at the standard dose 0.1 mmol/Kg and proved higher than RCE obtained with Gd at 0.04 mmol/Kg (Figure 6-6). On the other hand, the kinetics of washout was completely different between both contrast agents. The contrast enhancement with Gd-DTPA starts to decrease sharply after the first 5-6 minutes, suggesting a fast washout, while G3-Tyr(PROXYL)-COONa (**39**) enhancement proved mostly sustained along the time measured (Figure 6-6). In fact, 3 h after administration, relevant T_1 decrease could still be measured in the tumor area and in different organs, showing a persistence of G3 enhancement well beyond the washout time of Gd.

This is also a very important point to highlight, that is, an improvement in the

imaging times that provides G3 compared to Gd complexes, which shows shorter imaging times.

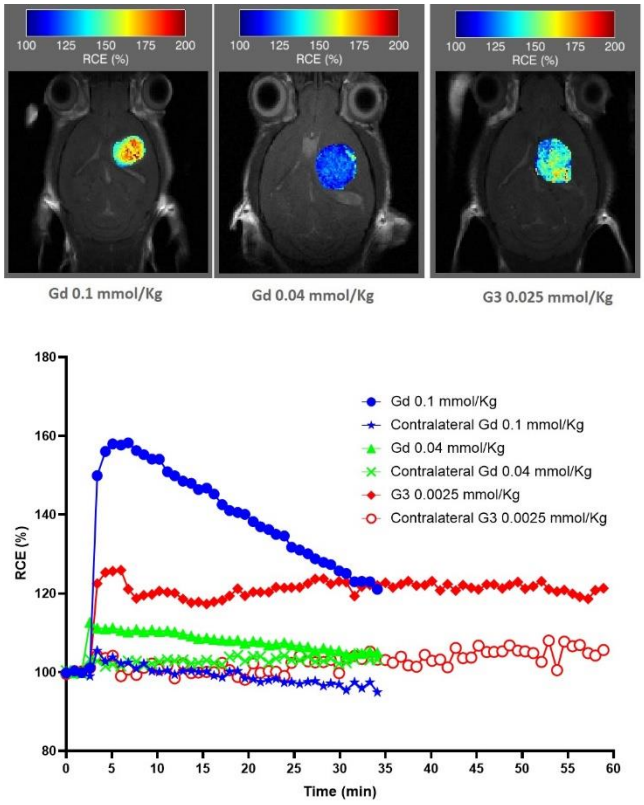

Figure 6-6. Top: Colour-code scale for RCE (Gd 0.1 and 0.04 mmol/Kg, 30 minutes and G3 0.025 mmol/Kg, 60 minutes). Bottom: region of interest (ROI) kinetics for these agents, showing the slower washout of G3. Maximum RCE calculated was 158% for Gd 0.1 mmol/Kg, 113% for Gd 0.04mmol/Kg and 126% for G3 0.025 mmol/Kg. Contralateral enhancement was reproducible in all cases (102 ±3%).

6.5.4 Confirmation of biodistribution with the 0.025 mmol/Kg dose

The biodistribution for 0.00625 mmol/Kg was expected to be fully comparable with the higher dose finally chosen for MRI studies, 0.025 mmol/kg. For confirmation purposes, one of the GL261-GB bearing mice was explored with whole body MRI 3h after G3 administration, once DCE-MRI studies were finished. Although the timing did not completely match, the main contrast enhancement and T_1 value decrease were seen in kidney cortex and pelvis (41-59% in comparison with basal measurements in wt mice) and bladder (95% decrease). These values were in the range of those obtained for Gd-DTPA after 0.5 h, reinforcing the difference between the pharmacokinetics of both contrast agents.

In addition, a GL261-GB bearing mice with 0.025 mmol/Kg dose was euthanized

after 3 hours and EPR was performed on selected organs (bladder, kidneys, liver, heart, brain tumor, healthy brain and muscle) to check the amount of G3 radical dendrimer in them. Similar organ tissue mass was analyzed by EPR (around 52 mg each) and the corresponding spectra are plotted in Figure 6-7.

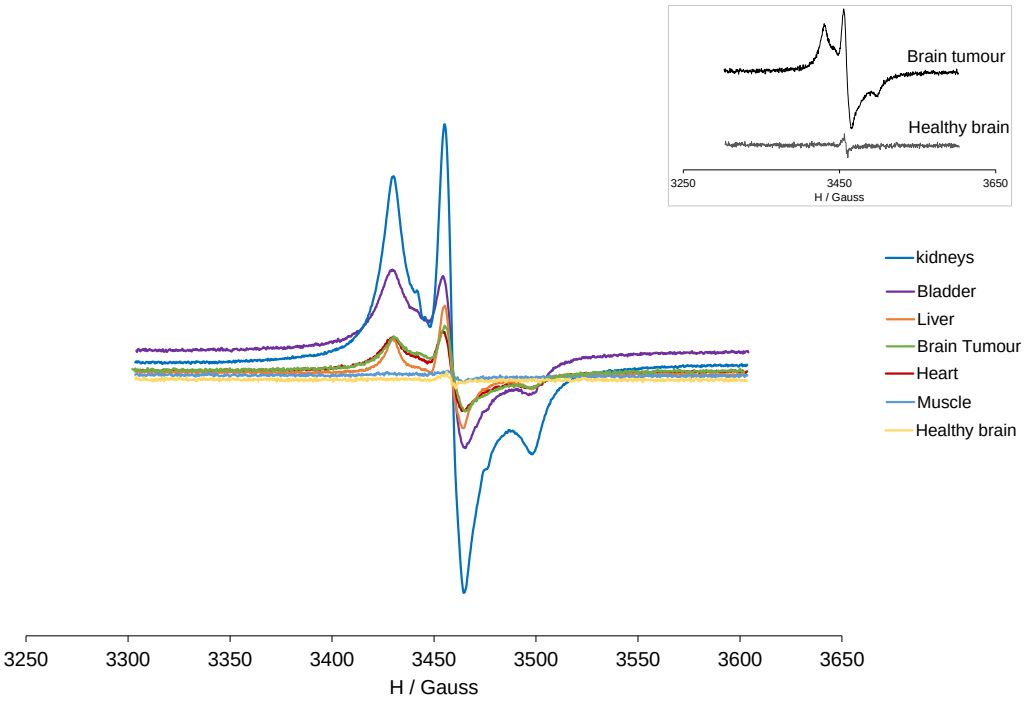

Figure 6-7. EPR spectra of kidneys, bladder, liver, heart, muscle, brain tumor and contralateral healthy brain from GL261 tumor-bearing mice after 0.025 mmol/Kg administration of G3-Tyr(PROXYL)-COONa (**39**) radical dendrimer.

The largest EPR signal intensity (largest amount of G3-Tyr(PROXYL)-COONa (**39**) radical dendrimer) was found in kidneys followed by bladder, then in liver, brain tumor and heart, and finally almost no EPR signal was detected in the healthy surrounding brain and muscle, similarly to what was obtained with the lower dose. In fact, it is worth mentioning that it was observed approximately four times more EPR signal intensity in organs like liver or kidneys with the higher dose compared with that with the lower dose. Thus, this increase in the EPR signal followed the same 4-fold increase ratio of the administered concentrations, i.e. from 0.00625 to 0.025 mmol/kg (see Figure 6-8 as an example), and demonstrates that the biodistribution is similar in both administered doses.

It is also important to remark that the selective accumulation behavior of G3-Tyr(PROXYL)-COONa (**39**) in tumor brain is reproduced at the higher dose (see inset of Figure 6-7). In addition, the observation of intense EPR signal after 3 h of intravenous administration supports again the stability of PROXYL radicals *in vivo*, farther beyond

that of isolated nitroxides (minutes). Related to this, the EPR signal observed in the heart means long circulation half-life of the radical dendrimer.

All these features make G3-Tyr(PROXYL)-COONa (**39**) radical dendrimers capable of imaging tumors over clinically meaningful time scales following systemic administration, at longer time periods than Gd complexes, without concerns over long-term tissue accumulation of metals.

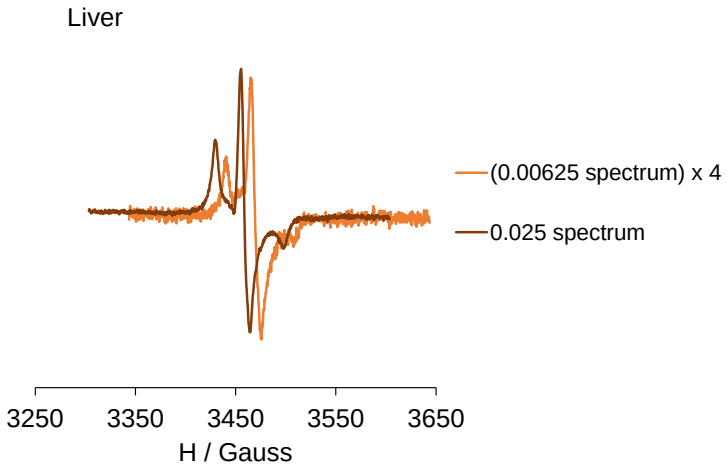

Figure 6-8. EPR spectra of liver at 0.00625 mmol/kg dose of G3-Tyr(PROXYL)-COONa (**39**) radical dendrimer enlarged 4 times compared with the one at 0.0025 mmol/kg dose.

6.6 Conclusions

- The contrast ability *in vivo* of G3-Tyr(PROXYL)-COONa (**39**) (G3) radical dendrimer specially designed to act as a T_1 contrast agent for MRI has been described in healthy and GL261 glioblastoma-bearing mice.
- No signs of toxicity or weight loss were detected in mice after systemic intravenous tail-vein injection of the radical dendrimer.
- Biodistribution studies show enhancement mostly in kidney cortex and pelvis suggesting the relevance of renal excretion for this compound, confirmed also by EPR measurements.
- G3 radical dendrimer at 0.025 mmol/Kg dose provides similar contrast enhancement on murine GL261 glioblastoma tumor than commercial Gd-based contrast agents at the standard dose of 0.1 mmol/Kg.
- The observed selective accumulation of G3 radical dendrimer in the brain tumor is a relevant and desirable characteristic in a contrast agent to be used for brain

tumors.

- Compared to the standard Gd-DTPA complex, G3-Tyr(PROXYL)-COONa (**39**) allows tumor imaging over longer time (≥3 h) and with slower clearance.
- A high stability in biological media of the radicals anchored on the dendrimer surface has been demonstrated *in vivo*, being much higher than that of isolated nitroxides that are rapidly reduced (half-lives on the order of minutes).

The high stability and contrast enhancement obtained with G3-Tyr(PROXYL)-COONa (**39**) radical dendrimer species demonstrates that the two major limitations of nitroxyl radicals have been overcome, not only *in vitro* but also *in vivo*. These important features together with the selective accumulation in the brain tumor and longer imaging times than Gd-based CA, makes G3-Tyr(PROXYL)-COONa (**39**) radical dendrimer a viable alternative to metal-based MRI contrast agents, particularly on MRI analysis of glioblastoma tumors.

6.7 Reference

(1) Winalski, C. S.; Shortkroff, S.; Mulkern, R. V.; Schneider, E.; Rosen, G. M. Magnetic Resonance Relaxivity of Dendrimer-Linked Nitroxides. *Magn. Reson. Med.* **2002**, *48* (6), 965–972.

(2) Rajca, A.; Wang, Y.; Boska, M.; Paletta, J. T.; Olankitwanit, A.; Swanson, M. A.; Mitchell, D. G.; Eaton, S. S.; Eaton, G. R.; Rajca, S. Organic Radical Contrast Agents for Magnetic Resonance Imaging. *J. Am. Chem. Soc.* **2012**, *134* (38), 15724–15727.

(3) Nguyen, H. V. T.; Chen, Q.; Paletta, J. T.; Harvey, P.; Jiang, Y.; Zhang, H.; Boska, M. D.; Ottaviani, M. F.; Jasanoff, A.; Rajca, A.; Johnson, J. A. Nitroxide-Based Macromolecular Contrast Agents with Unprecedented Transverse Relaxivity and Stability for Magnetic Resonance Imaging of Tumors. *ACS Cent. Sci.* **2017**, *3* (7), 800–811.

(4) Guo, S.; Wang, X.; Dai, Y.; Dai, X.; Li, Z.; Luo, Q.; Zheng, X.; Gu, Z.; Zhang, H.; Gong, Q.; Luo, K. Enhancing the Efficacy of Metal-Free MRI Contrast Agents via Conjugating Nitroxides onto PEGylated Cross-Linked Poly(Carboxylate Ester). *Adv. Sci.* **2020**, *7* (14).

(5) Chan, J. M. W.; Wojtecki, R. J.; Sardon, H.; Lee, A. L. Z.; Smith, C. E.; Shkumatov, A.; Gao, S.; Kong, H.; Yang, Y. Y.; Hedrick, J. L. Self-Assembled, Biodegradable Magnetic Resonance Imaging Agents: Organic Radical-Functionalized Diblock Copolymers. *ACS Macro Lett.* **2017**, *6* (2), 176–180.

(6) Huang, L.; Yan, C.; Cui, D.; Yan, Y.; Liu, X.; Lu, X.; Tan, X.; Lu, X.; Xu, J.; Xu, Y.; Liu, R. Organic Radical Contrast Agents Based on Polyacetylenes Containing 2,2,6,6-Tetramethylpiperidine 1-Oxyl (TEMPO): Targeted Magnetic Resonance (MR)/Optical Bimodal Imaging of Folate Receptor Expressing HeLa Tumors in Vitro and in Vivoa. *Macromol. Biosci.* **2015**, *15* (6), 788–798.

(7) Ding, L.; Lyu, Z.; Dhumal, D.; Kao, C. L.; Bernard, M.; Peng, L. Dendrimer-Based Magnetic Resonance Imaging Agents for Brain Cancer. *Sci. China Mater.* **2018**.

Chapter 7 General Conclusions

With the aim of preparing water-soluble metal-free MRI contrast agents based on organic radical dendrimers, various methods have been used in this Thesis:

- Tyrosine and lysine amino acids, have been chosen as linkers between the branches and radicals of PPH dendrimers to allow radical anchoring and confer solubility in water at the same time.

- Four generations of PPH dendrimers with tyrosine as linker, fully functionalized with up to 48 PROXYL radicals (Gn-Tyr(PROXYL)-COOLi, n=0-3 radical dendrimers) have been characterized by EPR, DLS and TEM and their cytotoxicity and MRI relaxivity have been studied. They are fully soluble in water, do not show cytotoxicity, and their relaxivity per molecule is high, increasing from 1.39 $mM^{-1}s^{-1}$ in G0 to 12.96 $mM^{-1}s^{-1}$ in G3. Remarkably, the relaxivity of G3-Tyr(PROXYL)-COOLi is four times higher than the most widely used Gd-DPTA in clinics (3.2 $mM^{-1}s^{-1}$).

- Lysine linker has been properly anchored to four generations of PPH dendrimers (Gn-Lys(BOC)-COOMe, n=0-3). However, only water-soluble G0-Lys(PROXYL)-COOLi radical dendrimer has been achieved since generations higher than G0 show lysine release through P-N bond cleavage under acid conditions, preventing the obtaining of radical dendrimers with this linker in them. We have been able to determine that G1-Lys(BOC)-COOLi presents P-N bond cleavage at pH 7.7 in aqueous solution. Therefore, generations higher than G0 of these new lysine-functionalized PPH dendrimers cannot be used to prepare water-soluble contrast agents, but, interestingly, they might be used to prepare pH-controlled degradable dendrimers or dendrimers with pH-controlled release properties, opening a new field of research.

- We have carried out stability studies under acid conditions with lysine and tyrosine functionalized PPH dendrimers and we have demonstrated that P-O bonds are more stable and more resistant to hydrolysis than P-N bonds, and, on the other hand, that P-N bonds with P from the core are more stable than P-N bonds with P from the branches. Preliminar theoretical calculations have been performed comparing the different P-N bond stability

between G0 and G1-Lys dendrimers, suggesting that the activation of the phosphine group of model G1 is much more feasible than that of model G0.

- Two generations of water-soluble oligoethylene glycol (OEG)-based dendrimers fully functionalized with 5 and 20 PROXYL organic radicals (Gn-OEG-PROXYL, n=0,1) have been synthesized and characterized. The resulting radical dendrimers are soluble in water, non-cytotoxic and present a good relaxivity. G1-OEG-PROXYL radical dendrimer presents a r_1 relaxivity value (3.4 $mM^{-1}s^{-1}$) similar than the most widely used Gd(III) complexes in clinics (e.g. Gd-DTPA, 3.2 $mM^{-1}s^{-1}$).

- We have prepared three generations of radical dendritic systems based on amphiphilic dendritic-linear-dendritic polymers. These species are based on (bis-MPA) dendrons at the end of a poly(ethylene glycol) chain and have been fully functionalized by click chemistry with 4, 8 and 16 TEMPO radical units, respectively (G1-, G2- and G3-MPA-PEG20k-TEMPO), showing limited solubility in water. We have been able to prepare homogeneous nanoparticles of G2 species (G2 NPs) as a stable colloid in water for at least one month. While these nanoparticles show spherical morphology by TEM, G2 species directly dissolved in water are organized forming nanofibers. G2 NPs present slightly higher relaxivity than G2, probably because of the higher rigidity of nanoparticles in front of the more flexible nanofibers structures. G2 species have been found to be non-cytotoxic.

- Fluorescent-magnetic radical dendrimers have been prepared as potential bimodal imaging agents. Six radical dendrimers based on fluorescent oligo(styryl)benzenes, with different linking bonds between the radicals and the dendrimers (amido, imino and amino linkers) have been synthesized and characterized. They present simultaneously fluorescence and relaxivity in organic solvents. CTAB micelles have been prepared to obtain aqueous dispersions of such radical dendrimers. Such micellar systems, with the radical dendrimers encapsulated, maintain both magnetic and fluorescent properties.

- The contrast ability *in vivo* of G3-Tyr(PROXYL)-COONa (G3) radical dendrimer has been studied in healthy and GL261 glioblastoma-bearing mice. Biodistribution studies show enhancement mostly in kidney cortex and pelvis suggesting the relevance of renal excretion for this compound, confirmed also by EPR measurements. G3 radical

dendrimer at 0.025 mmol/Kg dose provides similar contrast enhancement on murine GL261 glioblastoma tumor than commercial Gd-based contrast agents at the standard dose of 0.1 mmol/Kg. No signs of toxicity or weight loss were detected in mice after systemic intravenous tail-vein injection of the radical dendrimer and this species shows longer circulation time than Gd-based CA.

Chapter 8 Experimental part

8.1 Radical dendrimers based on PPH dendrimers

8.1.1 Synthesis of PPH dendrimers

G0' (1)

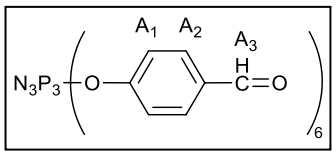

1.5 g of hexachlorocyclotriphosphazene (G0) (4.3 mmol, 1 eq), 4.22 g of 4-hydroxybenzaldehyde (34.5 mmol, 8 eq) and 22.5 g of Cs_2CO_3 (69 mmol, 16 eq) were added into a dried flask, followed by the addition of 60 mL of anhydrous THF. After the reaction proceeded for 15 minutes under argon atmosphere in an ice bath, the ice bath was removed and the solution was stirred at room temperature overnight. Subsequently, the reaction mixture was filtrated to eliminate the solid. The solution was concentrated under vacuum and then dissolved with minimum THF. The solution was precipitated with n-pentane three times. The obtained product, G0' was dried overnight under vacuum, as a white powder (3.157 g, 85%).

Characterization:

- ^{31}P {^{1}H} NMR (250 MHz, $CDCl_3$): δ 7.2 (s, P_0) ppm.
- ^{1}H NMR (250 MHz, $CDCl_3$): δ 7.1 (d, 12H, $JH_{A1}H_{A2}$=7.5 Hz, H_{A1}), 7.7 (d, 12H, $JH_{A1}H_{A2}$=7.5 Hz, H_{A2}), 9.9 (s, 6H, H_{A3}) ppm.
- ^{13}C NMR (360 MHz, $CDCl_3$): δ 121.2, 131.4, 133.7, 154.5, 190.5 ppm.
- IR-ATR (cm^{-1}): 1700 ν (CH=O), 1598 ν (CCAr) and δ (CCH), 1274 ν (PN), 1205 δ (PNN), 1100 δ (NCH), 943 ν (P-O).

Dichlorophosphonomethylhydrazide (9)

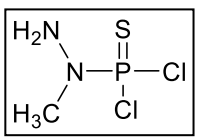

2.40 mL of thiophosphorylchloride (23.7 mmol, 1 eq) was added into a dried flask and dissolved in 40 mL of anhydrous chloroform. Then, the flask was put in an acetone bath and cooled down to -60 ºC with a cooler. 2.18 mL of methylhydrazine (47.30 mmol, 2 eq) was dissolved in 60 mL of chloroform and added into the flask drop by drop with a dropping funnel. After the mixture was stirred under argon atmosphere at -60 ºC for 30 minutes, the cooler was removed and the reaction mixture was stirred overnight at room temperature. The mixture

solution was filtrated with a cannula to remove the salt and the filtrate was stored as the product (concentration, 0.236 mM).

Characterization:

- ^{31}P {^{1}H} NMR (250 MHz, $CDCl_3$): δ 68.5 (s, P) ppm.
- ^{1}H NMR (250 MHz, $CDCl_3$) δ 1.24 (t, 2H), 3.17 (s, 3H), 3.24 (s, 3H), 3.72 (q, 2H) ppm.

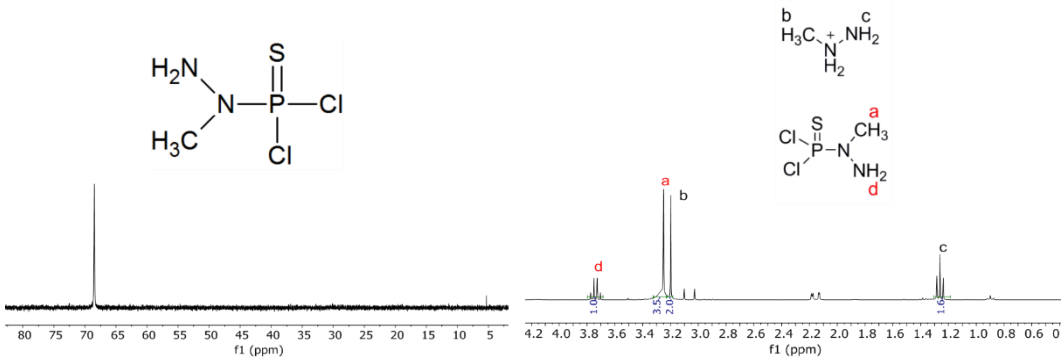

G1 (2)

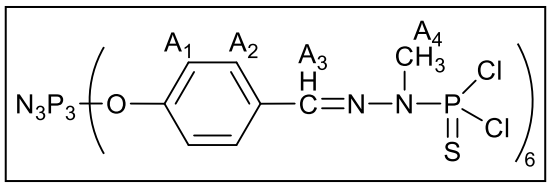

The dendrimer with chlorine as a terminal group was synthesized as follows. 0.4 g of dendrimer G0' (**1**) (0.5 mmol, 1 eq) was added into the flask, followed by three vacuum/argon cycles. 12 mL of THF was added to dissolve the reactant. The flask was put into an ice bath. Then 30 mL of dichlorophosphonomethylhydrazide (**9**) (7 mmol, 14 eq) was added into the flask drop by drop via syringe. The mixture was stirred for 30 minutes under argon atmosphere and in the ice bath. After that, the ice bath was withdrawn and the reaction proceeded overnight at room temperature. After the full conversion was confirmed by ^{31}P NMR, the reaction was stopped and the reaction solution was concentrated. Subsequently, the crude was dissolved in a minimum amount of THF precipitated three times with n-pentane. The product was obtained as a pale yellow powder after being dried under vacuum overnight (0.8681 g, 95%).

Characterization:

- ^{31}P {^{1}H} NMR (250 MHz, $CDCl_3$) δ: 8.4 (s, P_0), 62.7(s, P_1) ppm.
- ^{1}H NMR (250 MHz, $CDCl_3$) δ: 3.48 (d, 18H, $JH_{A4}P_1$= 15 Hz, H_{A4}), 7.05 (d, 12H, $JH_{A1}H_{A2}$, H_{A1}), 7.60 (d, 12H, $JH_{A2}H_{A1}$= 7.5 Hz, H_{A2}), 7.63 (s, 8H, H_{A3}) ppm.

- ^{13}C NMR (360 MHz, $CDCl_3$) δ 151.8, 140.8, 140.6, 131.4, 128.7, 121.5, 32.2, 32.0 ppm.
- IR-ATR (cm^{-1}): 1606, 1504, 1465, 1406, 1369, 1154, 939, 832, 781, 743, 684.

G1 prima (3)

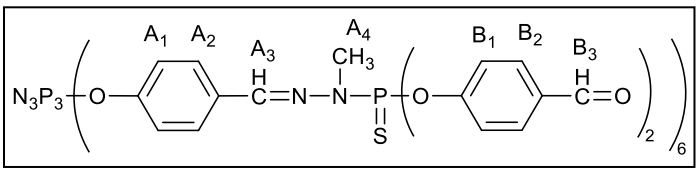

0.60 g of G1(**2**) (0.3mmol, 1 eq), 0.64 g of 4-hyroxybenzaldehyde (5.3 mmol, 16 eq), and 3.4 g of Cs_2CO_3 (10.5 mmol, 32 eq) were added into a flask, followed by three argon/vacuum cycles. Then, 10 mL of the anhydrous THF was added into the flask and the flask was put in an ice bath. After being stirred for 30 minutes under argon atmosphere, the ice bath was withdrawn and the reaction underwent overnight at room temperature. The reaction mixture was filtrated and the solution was concentrated. A minimum amount of THF was added to dissolve. The product was obtained as a pale yellow powder after being precipitated with n-pentane three times and dried under vacuum (0.765 g, 81%).

Characterization:

- ^{31}P {^1H} NMR (250 MHz, $CDCl_3$): δ 8.2 (s, P_0), 60.7(s, P_1) ppm.
- ^1H NMR (250 MHz, $CDCl_3$): δ 3.3 (d, 18H, $JH_{A4}P_1$=10 Hz, H_{A4}), 7.0 (d, 12H, $JH_{A1}H_{A2}$=7.5 Hz, H_{A1}), 7.3 (d, 24H, $JH_{B1}H_{B2}$=7.5 Hz, H_{B1}), 7.6 (d, 12H, $JH_{A2}H_{A1}$=7.5 Hz, H_{A2}), 7.6 (s, 6H, H_{A3}), 7.8 (d, 24H, $JH_{B2}H_{B1}$=7.5 Hz, H_{B2}), 9.9 (s, 12H, H_{B3}) ppm.
- ^{13}C {^1H} NMR (360 MHz, $CDCl_3$): δ 33.03, 121.46, 122.01, 128.33, 131.52, 133.78, 139.53, 151.55, 155.14, 190.73 ppm.
- IR-ATR (cm^{-1}): 1700 ν(CH=O), 1595, 1496, 1422, 1361, 1294, 1193, 1146, 909, 823, 776, 722.

G2 (4)

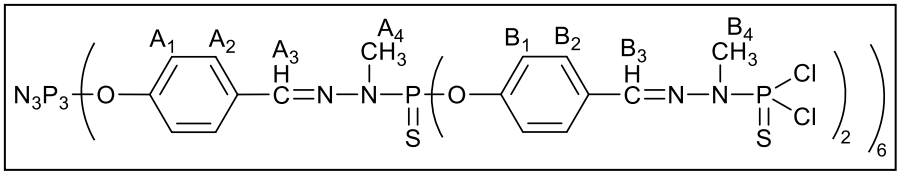

0.5 g of G1 prima (**3**) (0.18 mmol, 1 eq) was added into a flask, followed by three argon/vacuum cycles. Then 15 mL of anhydrous chloroform was added to dissolve. 15 mL of dichlorophosphonomethylhydrazide (**9**) (3.5 mmol, 20 eq) was added into the flask via a syringe. The reaction was stirred under an argon atmosphere and in an ice bath for

one hour. After being confirmed by ^{31}P NMR that the conversion had finished, the reaction solution was concentrated and dissolved in minimum $CHCl_3$. The dendrimer G2 was obtained as a white powder after being precipitated with n-pentane/ether (v/v, 1/2) three times and dried under vacuum (0.788 g, 94%).

Characterization:

- ^{31}P {^1H} NMR (250 MHz, $CDCl_3$): δ 8.4 (s, P_0), 62.1(s, P_1), 62.9 (s, P_2) ppm.
- ^1H NMR (250 MHz, $CDCl_3$): δ 3.3 (d, 18H, $JH_{A4}P_1$=10 Hz, H_{A4}), 3.4 (d, 36H, $JH_{B4}P_2$=13.8 Hz, H_{B4}), 7.0 (d, 12H, $JH_{A1}H_{B1}$=8.45 Hz, H_{A1}), 7.2 (d, 24H, $JH_{B1}H_{B2}$=7.32 Hz, H_{B1}), 7.6-7.7 (m, 54H, H_{A2}, H_{A3}, H_{B2}, H_{B3}) ppm.
- ^{13}C {^1H} NMR (360 MHz, $CDCl_3$): δ 31.86, 33.15, 121.38, 121.87, 128.32, 128.74, 131.6, 132.01, 139.00, 140.43, 151.22, 151.78 ppm.
- IR-ATR (cm^{-1}): 1600, 1502.27, 1365, 1217, 908, 833, 779.

G2 prima (5)

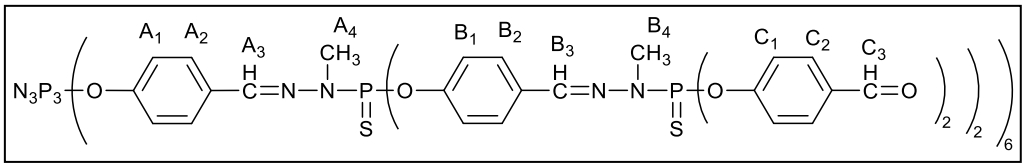

300 mg of G2 (**4**) (0.0627 mmol, 1 eq), 244.9 mg of 4-hyroxybenzaldehyde (2.005 mmol, 32 eq), and 1.306g of Cs_2CO_3 (4.011 mmol, 64 eq) were added into a flask, followed by three argon/vacuum cycles. Then, 15 mL of anhydrous THF was added into the flask via a syringe. The reaction was stirred under argon atmosphere in an ice bath for 30 min. After that, the ice bath was removed. The reaction underwent overnight. Finally, the reaction mixture was filtrated, the filtrate was concentrated and dissolved in a minimum of THF. The solution was precipitated with n-pentane three times. The product was obtained after being dried under vacuum overnight (310.3 mg, 73%).

Characterization:

- ^{31}P {^1H} NMR (250 MHz, $CDCl_3$): δ 8.4 (s, P_0), 60.4 (s, P_2), 62.4 (s, P_1) ppm.
- ^1H NMR (250 MHz, $CDCl_3$): δ 3.2 (d, 18H, $JH_{A4}P_1$=10Hz, H_{A4}) 3.3 (d, 36H, ,$JH_{B4}P_2$=10Hz, H_{B4}), 6.9 (d, 12H, $JH_{A1}H_{A2}$=7.5 Hz, H_{A1}), 7.2 (d, 24H, $JH_{B1}H_{B2}$=7.5 Hz, H_{B1}), 7.33 (d, 48H, $JH_{C1}H_{C2}$=7.5 Hz, H_{C1}), 7.55-7.83 (m, 108H, H_{A2}, H_{A3}, H_{B2}, H_{B3}, H_{C2}), 9.9 (s, 24H, H_{C3}) ppm.
- ^{13}C {^1H} NMR (360 MHz, $CDCl_3$): δ 33.04, 122.00, 128.42, 131.54, 133.69, 139.66, 151.51, 155.08, 190.82 ppm.
- IR-ATR (cm^{-1}): 1698, 1592, 1499, 1367, 1208, 1151, 908, 835, 783, 729.

G3 (6)

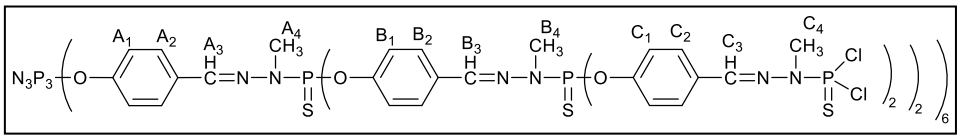

170 mg of G2 prima (**5**) (24.8 µmol, 1 eq) was added into a flask, followed by three argon/vacuum cycles. 4 mL of $CHCl_3$ was added into the flask. The flask was put in an ice bath to cool down. Next, 3.16 mL of dichlorophosphonomethylhydrazide (**9**) (0.745 mmol, 30 eq) was added to the flask via a syringe. After 2 hours, the reaction was checked by ^{31}P NMR in order to confirm that the reaction had finished. Thereafter, the reaction mixture was filtrated and the filtrate was concentrated and precipitated with n-pentane/ether (v/v, 1/2) three times. The product was obtained after being dried under vacuum overnight (240.4 mg, 91%).

Characterization:

- ^{31}P $\{^1H\}$ NMR (100 MHz, $CDCl_3$): δ 8.6 (s, P_0), 62.1 (s, P_2), 62.5 (s, P_1), 63.0 (s, P_3) ppm.
- ^1H NMR (250 MHz, $CDCl_3$): δ 3.2 (m, 126H, H_{A4}, H_{B4}, H_{C4}), 6.9 (m, 12H, H_{A1}), 7.1-7.2 (m, 72H, H_{B1}, H_{C1}), 7.5-7.7 (m, 126H, H_{A2}, H_{B2}, H_{C2}, H_{A3}, H_{B3}, H_{C3}) ppm.
- ^{13}C $\{^1H\}$ NMR (360 MHz, $CDCl_3$): δ 31.96, 33.05, 121.90, 128.37, 128.86, 131.82, 132.20, 139.05, 140.80, 151.17, 151.70 ppm.
- IR-ATR (cm^{-1}): 1600, 1500, 1462, 1365, 1188, 1155, 1012, 907, 834, 781, 727.

G3 prima (7)

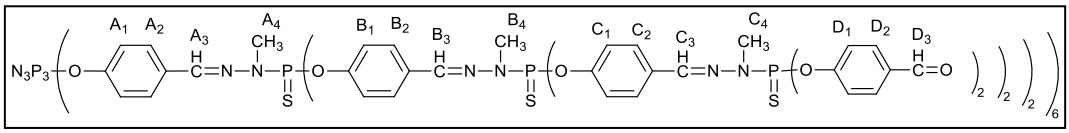

600 mg of G3 (**6**) (56 µmol, 1 eq), 438 mg of 4-hyroxybenzaldehyde (3.59 mmol, 64 eq) and 2.337 g of Cs_2CO_3 (7.17 mmol, 128 eq) were added into a flask, followed by three argon vacuum cycles. Then the flask was put in an ice bath. 15 mL of THF was added via a syringe. After the reaction mixture was stirred overnight, ^{31}P NMR was used to monitor the reaction. Then, the reaction mixture was filtrated, and the filtrate was precipitated with n-pentane three times. The product was obtained after being dried under vacuum (0.763 g, 92 %).

Characterization:

- ^{31}P {^{1}H} NMR (250 MHz, $CDCl_3$): δ 8.4 (s, P_0), 60.4 (s, P_3), 62.4 (s, P_2), 62.7 (s, P_1) ppm.
- ^{1}H NMR (250 MHz, $CDCl_3$): δ 3.3 (m, 126H, H_{A4}, H_{B4}, H_{C4}), 6.9 (m, 12H, H_{A1}), 7.2 (m, 72H, H_{B1}, H_{C1}), 7.3 (m, 96H, H_{D1}), 7.5-7.8 (m, 180H, H_{A2}, H_{A3}, H_{B2}, H_{B3}, H_{C2}, H_{C3}, H_{D2}), 9.9 (s, 48H, H_{D3}) ppm.
- ^{13}C {^{1}H} NMR (360 MHz, $CDCl_3$): δ 33.08, 122.02, 128.41, 131.53, 133.65, 139.64, 151.48, 155.19, 190.90.
- IR-ATR (cm^{-1}): 1698, 1598, 1499, 1368, 1206, 1153, 911, 833, 782, 727.

G4 (8)

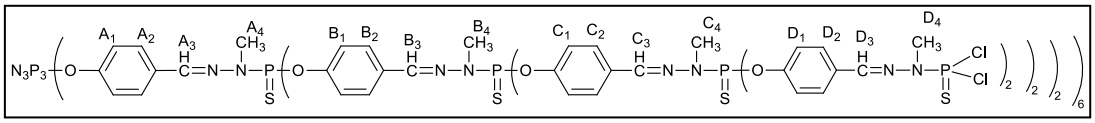

200 mg of G3 prima (**7**) (13.5 µmol, 1 eq) was added into a flask, and then 6 mL of $CHCl_3$ was added to dissolve. Next, 3.66 mL of dichlorophosphonomethylhydrazide (**9**) (1.0797 mmol, 80 eq) was added to the flask. The flask was put in an ice bath. After the reaction mixture was stirred for one hour, ^{31}P NMR was used to confirm the completion of the reaction. Then, the reaction was stopped and the reaction mixture was filtrated and the filtrate was concentrated and precipitated with n-pentane/ether (v/v,1/2) three times (0.259 g, 85%).

Characterization:

- ^{31}P {^{1}H} NMR (250 MHz, $CDCl_3$): δ 8.4 (s, P_0), 62.09 (s, P_3), 62.56 (m, P_2, P_1), 63.09 (s, P_4) ppm.
- ^{1}H NMR (250 MHz, $CDCl_3$): δ 3.3 (m, 270H, H_{A4}, H_{B4}, H_{C4}, H_{D4}), 6.9 (m, 12H, H_{A1}), 7.1-7.2 (m, 168H, H_{B1}, H_{C1}, H_{D1}), 7.5-7.7 (m, 270H, H_{A2}, H_{B2}, H_{C2}, H_{D2}, H_{A3}, H_{B3}, H_{C3}, H_{D3}) ppm.
- ^{13}C {^{1}H} NMR (360 MHz, $CDCl_3$): δ 31.97, 33.20, 121.90, 128.38, 128.76, 131.49, 132.14, 139.08, 140.78, 151.28, 151.84 ppm.
- IR-ATR (cm^{-1}): 1600, 1502, 1463, 1407, 1365, 1300, 1239, 1189, 1155, 1135, 1014, 907, 834, 781, 727, 689.

NMR and IR of PPH dendrimers

^{31}P NMR of Gn and Gn' PPH dendrimers

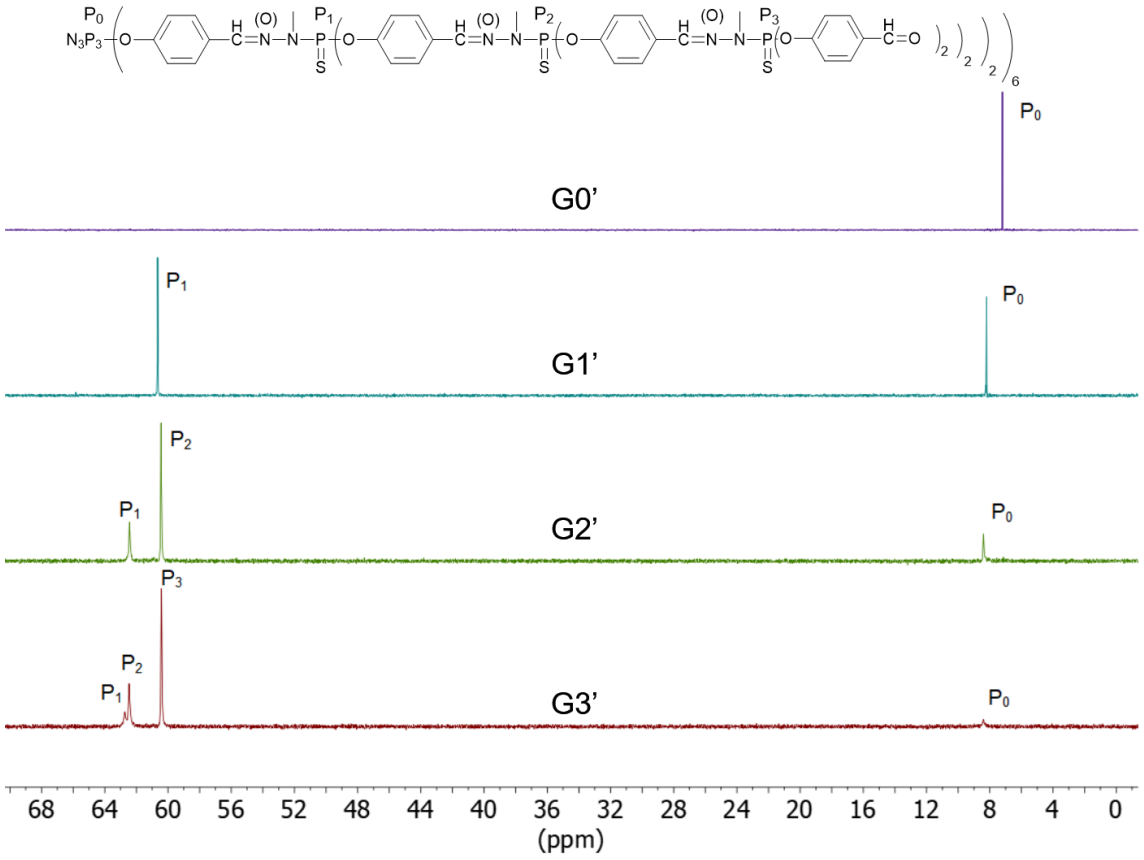

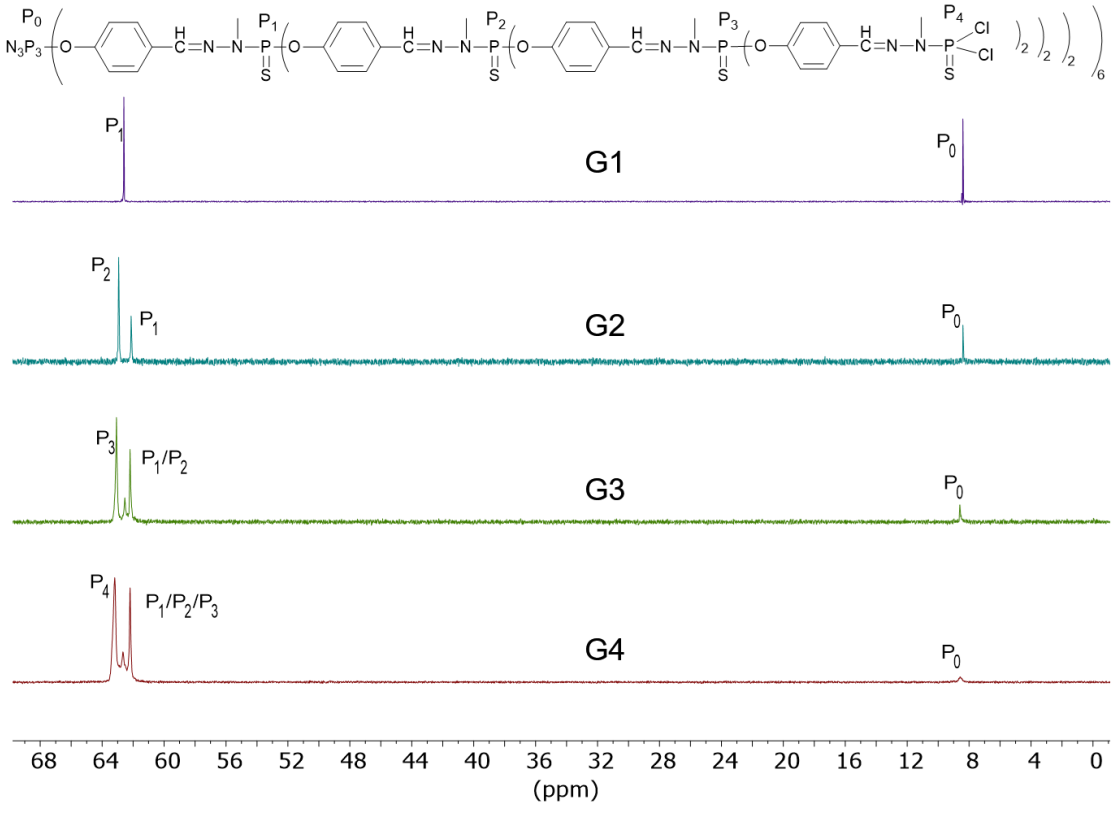

^{1}H NMR of Gn' and Gn PPH dendrimers

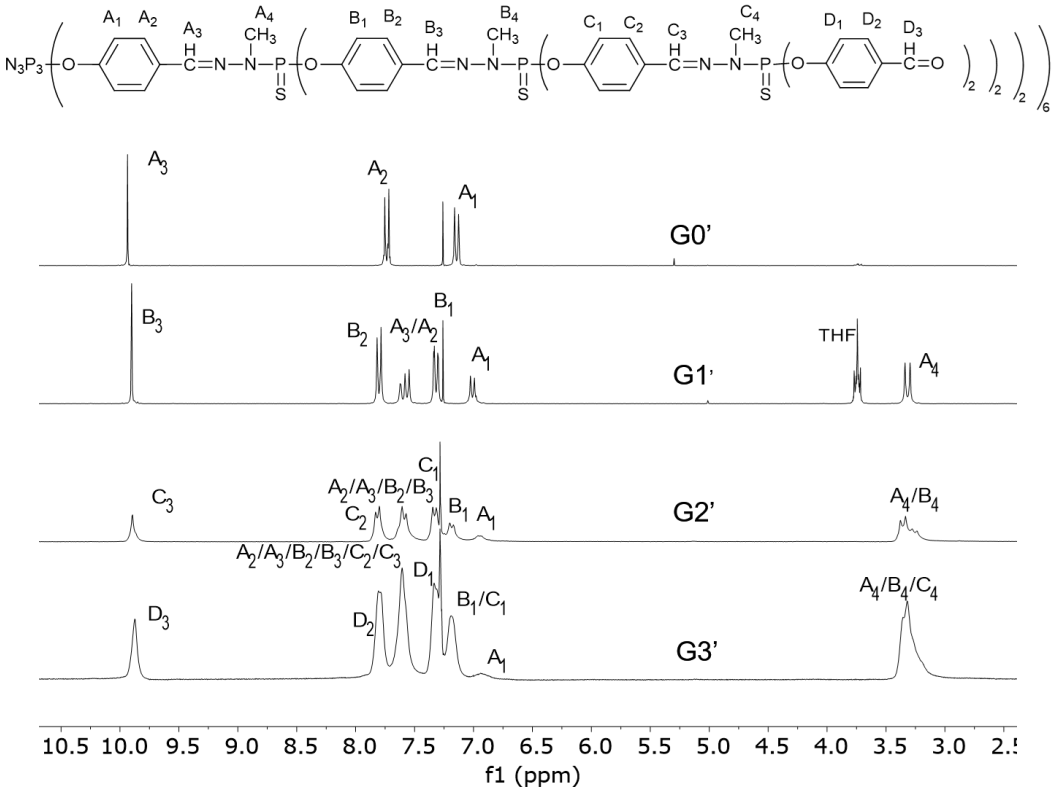

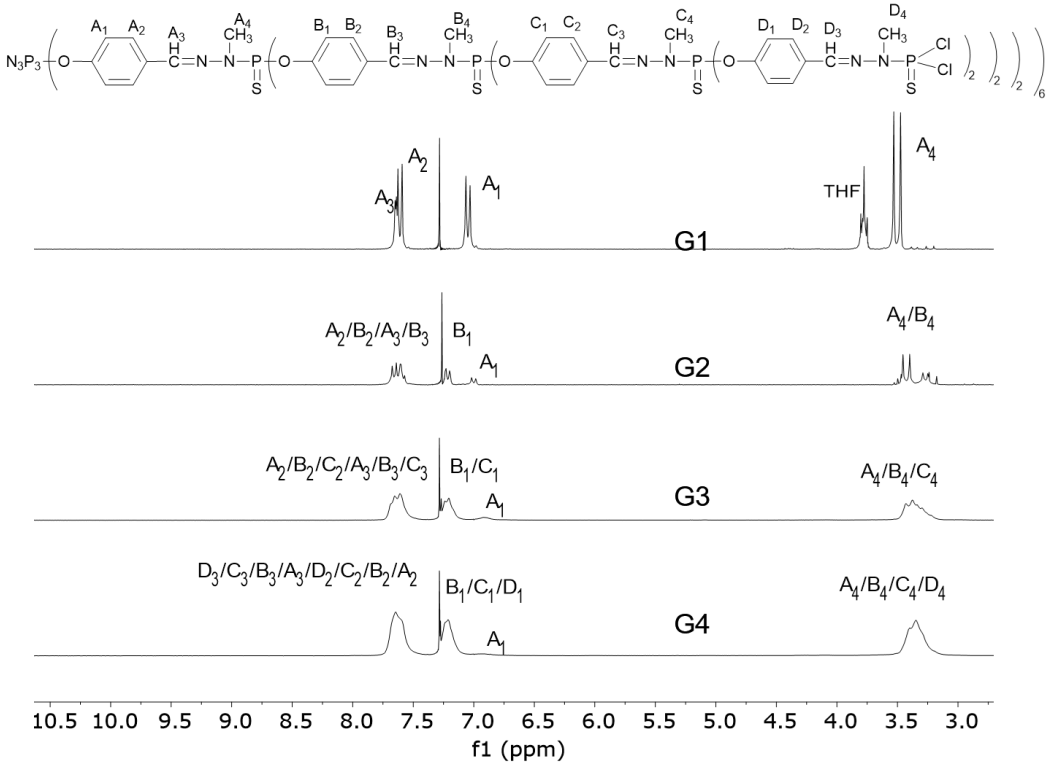

^{13}C NMR of Gn' and Gn PPH dendrimers

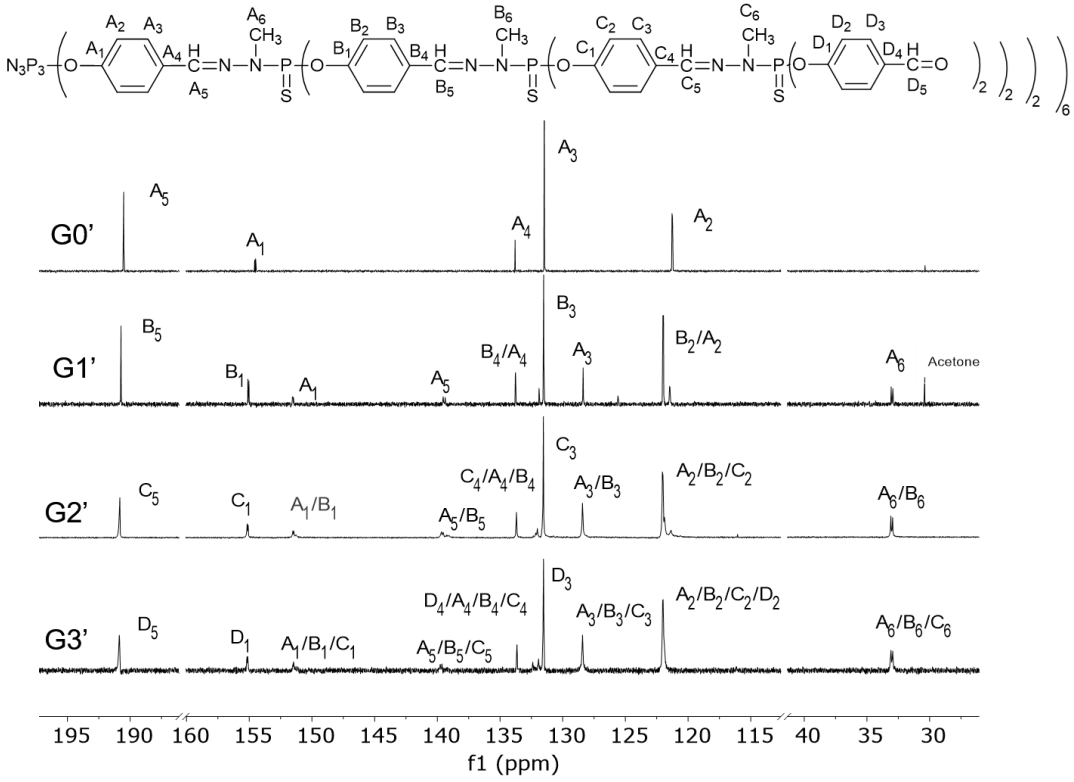

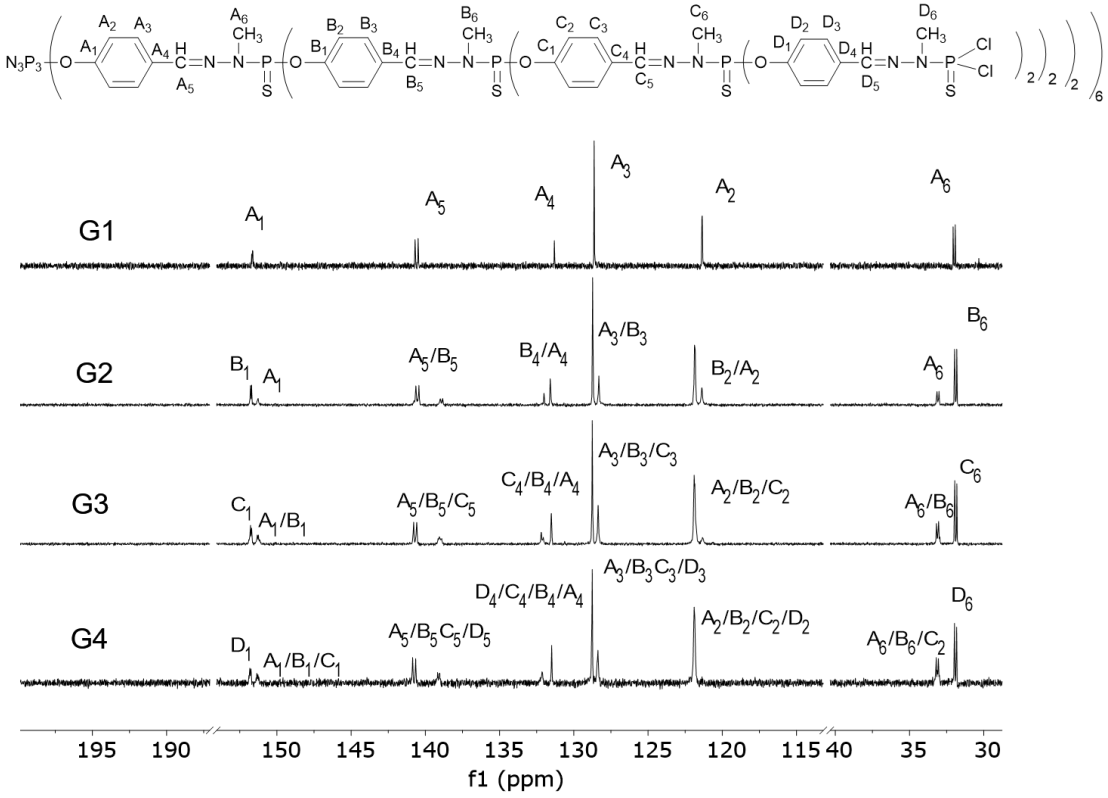

IR of Gn' and Gn PPH dendrimers

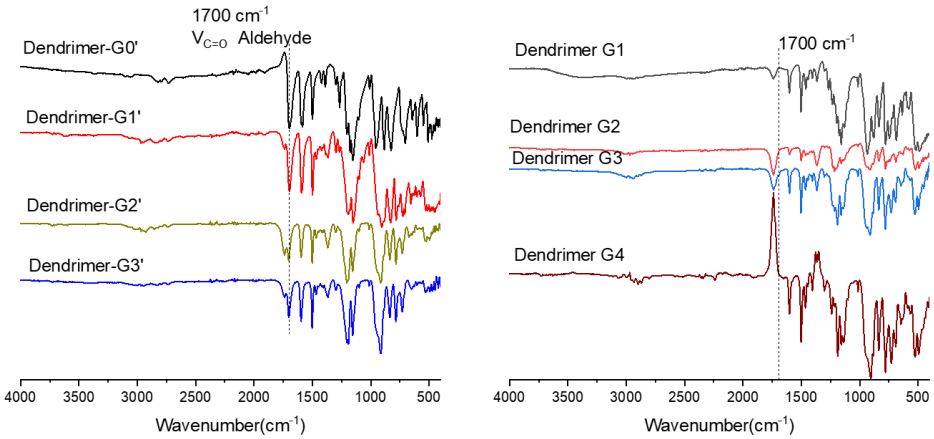

8.1.2 Attempted Synthesis of PROXYL-Lys(Gn)-COOLi radical dendrimers

PROXYL-Lys(BOC)-COOMe (10)

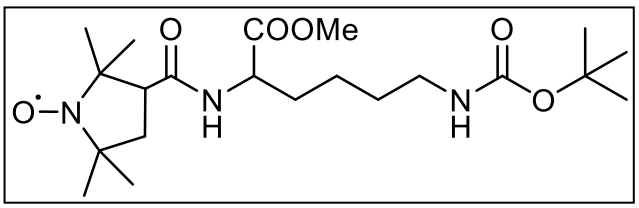

In 25 mL of round bottom flask 150 mg of 3-carboxy-PROXYL (0.81 mmol, 1.2 eq) and 306.35 mg of HATU (0.81 mmol, 1.2 eq) were added, and the reagents were dissolved in 12 mL of DCM. 467µL of DIEA (2.68 mmol, 4 eq) was added. After being stirred for 10 min, 198.6 mg of H-Lys(BOC)OMe•HCl (0.67 mmol, 1 eq) was added. The reaction proceeded at room temperature overnight. After that, the reaction mixture was extracted with the equivalent of water five times. The organic phase was dried by $MgSO_4$. The product was obtained after being purified by column chromatography on silica gel (DCM/MeOH 98/2, Rf= 0.33). (260 mg, 90.9%)

Characterization:

- IR-ATR (cm^{-1}): 3323 (NH carbamate), 2972, 2928 (NH amide), 2865, 1742, 1662, 1525 (N-C=O amide), 1458, 1365, 1252, 1169, 1018, 840, 773.
- EPR (DCM): g = 2.0054; a_N = 14.6 G; ΔH_{pp} = 1.2 G.

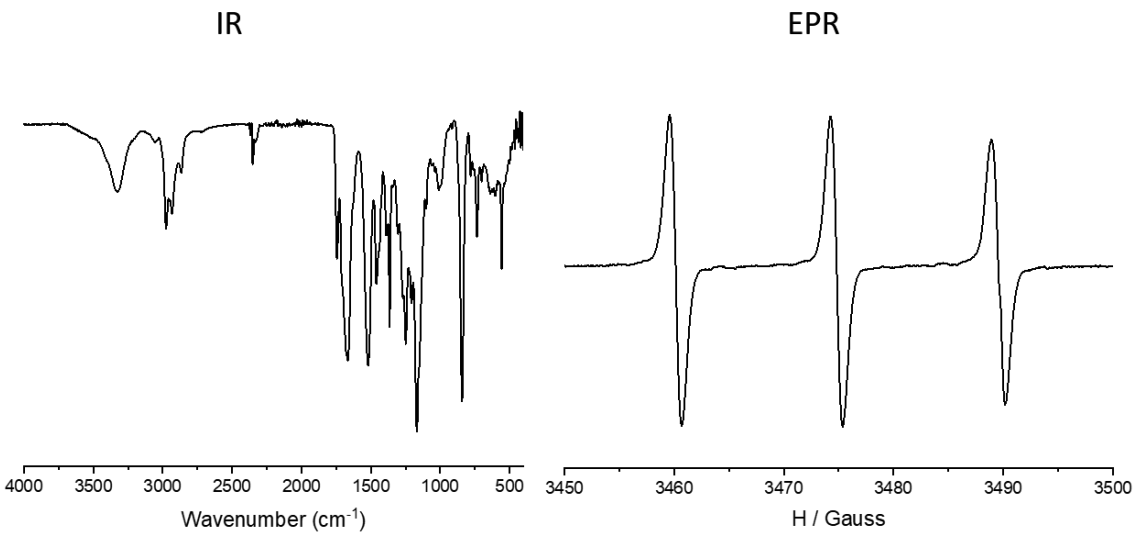

PROXYL-Lys-COOMe (11)

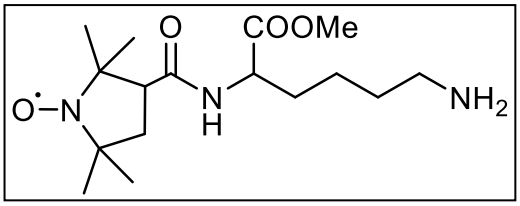

261 mg of PROXYL-Lys(BOC)-COOMe (**10**) (609 µmol, 1 eq) was dissolved in 4 mL of anhydrous DCM in a round bottom flask. Then the flask was put in an ice bath to cool down. 1.6 mL of TFA (13.398 mmol, 22 eq) was added into the flask. After the reaction was stirred in the ice bath for 30 min, the ice bath was removed. Next, the reaction proceeded at room temperature overnight. After that, the solvent was removed by evaporation, the residue was washed with DCM and MeOH three times respectively. Finally, the product was obtained after being dried under vacuum. (267 mg, 98%)

Characterization:

- IR-ATR (cm^{-1}): (2963, 2925, 2854, 1785, 1748, 1656, 1533, 1458, 1443, 1379, 1321, 1155, 1012, 843, 796, 724, 706).
- EPR (DCM): g = 2.0053; a_N = 14.6 G; ΔH_{pp} = 1.2 G.

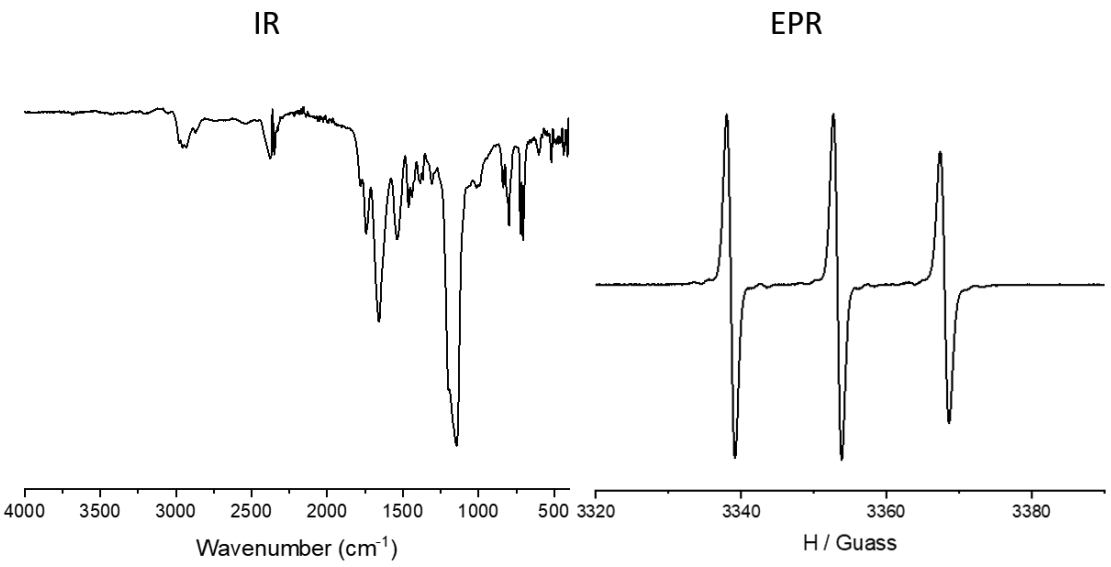

Attempted synthesis of PROXYL-Lys(G0)-COOMe (12)

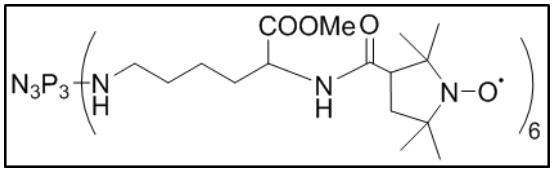

11 mg of G0 (33.83 µmol, 1 eq) and 263.8 mg of Cs_2CO_3 (811.94 µmol, 24 eq) were added into a flask. Then the flask was put into an ice bath. 100 mg of PROXYL-Lys-COOMe (**11**) (304.48 µmol, 9 eq) was dissolved in anhydrous THF and transferred into the flask. After 10 minutes in the ice bath, the reaction mixture was stirred in for 16 hours at room temperature. After that, the reaction was stopped. The solid was removed by filtration and the solution was concentrated. The crude was dissolved in DCM, and purified by column chromatography on silica gel (DCM/MeOH, v/v, 95/5). (20 mg, 28 %). See the explanation of Chapter 2 about its non-fully substitution.

Characterization:

- IR-ATR (cm^{-1}): 3326, 3072, 3043, 2981, 2930, 2862, 1740, 1643, 1535, 1465, 1361, 1301, 1256, 1203, 1170, 1148, 1098, 1012, 731.
- EPR (DCM): g = 2.0054; intramolecular spin-exchange interaction among radicals, alternating line width effect (a_N of the main three lines: 14.6 G).

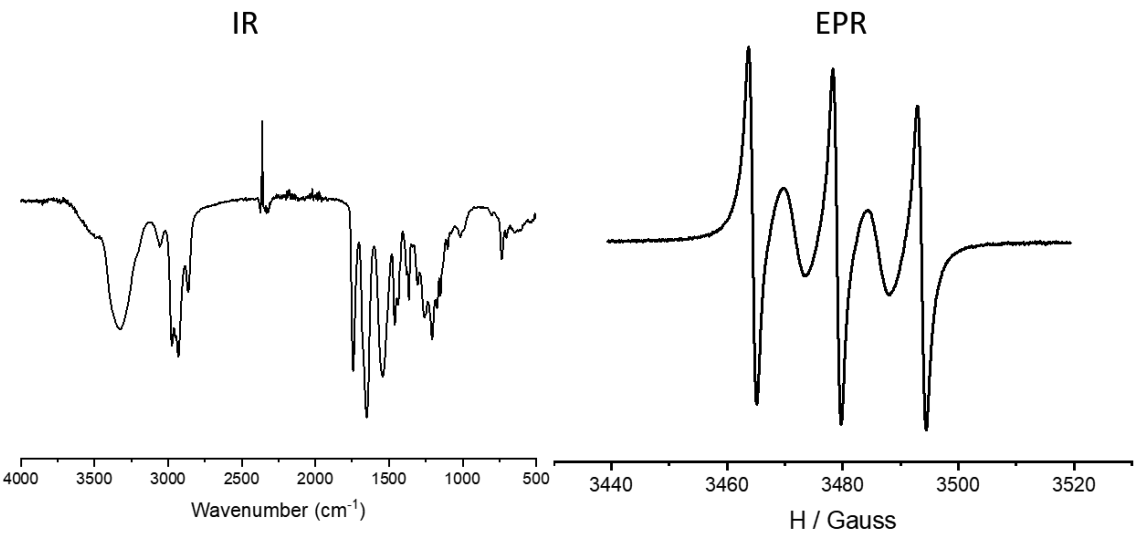

Attempted synthesis of PROXYL-Lys(G0)-COOLi (13)

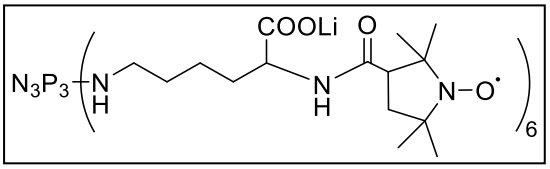

226 mg of PROXYL-Lys(G0)-COOMe (**12**) (107.62 µmol, 1 eq) was added into a flask, followed by addition of 352.31 mg of LiOH•H_2O (8.40 mmol, 78 eq). Then 4 mL of anhydrous THF and 2 mL of H_2O were added into the flask. After 16 h, the reaction was stopped, and THF was removed by concentration. The product was purified by ultrafiltration to remove excess of LiOH•H_2O. (30 mg, 13.6%). It was characterized by quantitative EPR and MRI showing that it was non-fully functionalized (see Chapter 2).

Attempted synthesis of PROXYL-Lys(G1)-COOLi (14)

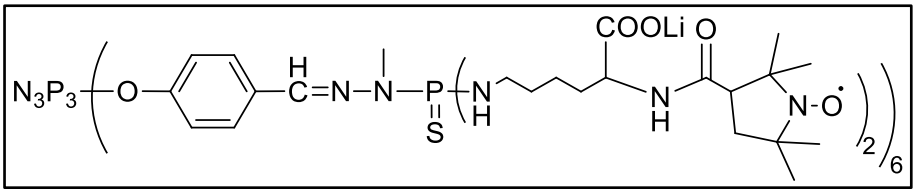

59.69 mg of G1 (**2**) (32.65 µmol, 1 eq) and 260 mg of PROXYL-Lys-COOMe (**11**) (587.66 µmol, 18 eq) were added into a flask. 4 mL of THF was added into the flask to dissolve G1 and PROXYL-Lys-COOMe (**11**). Then the flask was put into an ice bath. 180 µL of TEA (1305.92 µmol, 40 eq) was added into the flask. After 1 hour in the ice bath, the reaction mixture was stirred for overnight at room temperature. The solid was removed by filtration. The solution was concentrated.

174 mg of PROXYL-Lys(G1)-COOMe (32.64 µmol, 1 eq) was added into a flask,

followed by addition of 189.05 mg of LiOH•H_2O (4.50 mmol, 138 eq). Then 4 mL of THF_{anh} and 2 mL of H_2O were added into the flask. After 39 h, the reaction was stopped, and THF was removed by concentration. The product was obtained after ultrafiltration and lyophilization (69.8 mg, 41%). It was characterized by quantitative EPR and MRI showing that it was not fully functionalized (see Chapter 2).

Attempted synthesis PROXYL-Lys(G2)-COOLi (15)

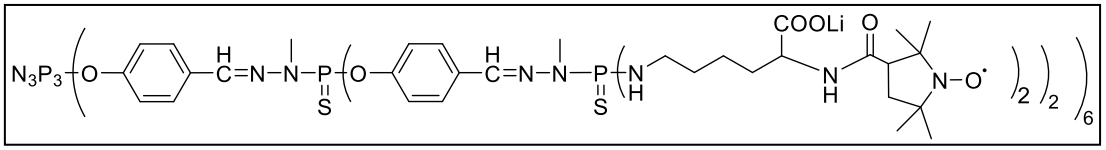

70.9 mg of G2 (14.69 µmol, 1 eq) and 260 mg of PROXYL-Lys-COOMe (587.66 µmol, 48 eq) were added into a flask. 4 mL of THF was added into the flask to dissolve G2 (**4**) and PROXYL-Lys-COOMe (**11**). Then the flask was put into an ice bath. 122 µL of TEA (881 µmol, 60 eq) was added into the flask. After 30 min, the ice bath was removed. The reaction mixture was stirred for overnight at room temperature. The produced suspended solid was removed by filtration. The solution was concentrated.

173 mg of PROXYL-Lys(G2)-COOMe (14.69 µmol, 1eq) was added into a flask, followed by addition of 193.2 mg of LiOH•H_2O (4.58 mmol, 312 eq). Then 4 mL of THF_{anh} and 2 mL of H_2O were added into the flask. After 39 h, the reaction was stopped, and THF was removed by concentration. The product was obtained after ultrafiltration and lyophilization (80.9 mg, 47.3%). It was characterized by quantitative EPR and MRI showing that it was non-fully functionalized (see Chapter 2).

Attempted synthesis of PROXYL-Lys(G3)-COOLi (16)

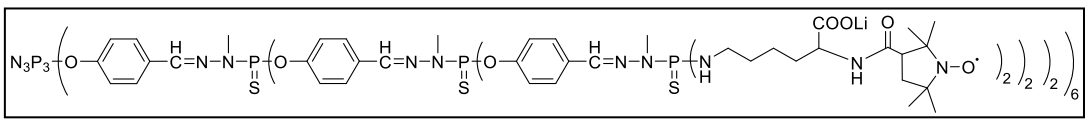

92.5 mg of G3 (8.59 µmol, 1 eq) and 228 mg of PROXYL-Lys-COOMe (**11**) (587.66 µmol, 18 eq) were added into a flask. 10 mL of THF was added into the flask to dissolve G3 (**6**) and PROXYL-Lys-COOMe (**11**). Then the flask was put into an ice bath. 100 µL of TEA (1305.92 µmol, 40 eq) was added into the flask. After being stirred for 30 min in the ice bath, the reaction mixture was stirred overnight at room temperature. The suspended solid was removed by filtration. The solution was concentrated.

212 mg of PROXYL-Lys(G3)-COOMe (8.58 µmol, 1 eq) was added into a flask,

followed by addition of 224 mg of $LiOH•H_2O$ (5.35 mmol, 624 eq). Then 4 mL of THF_{anh} and 2 mL of H_2O were added into the flask. After 39 h, the reaction was stopped, and THF was removed by concentration. The product was obtained after ultrafiltration and lyophilization (83.3 mg, 40%). It was characterized by quantitative EPR and MRI showing that it was non-fully functionalized (see Chapter 2).

8.1.3 Synthesis of Gn-Lys(PROXYL)-COOLi radical dendrimers

G0-Lys(BOC)-COOMe (17)

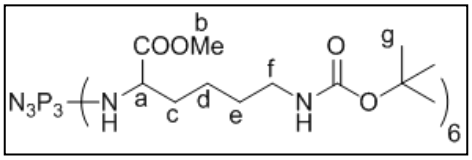

50 mg of PPH dendrimer G0 (0.144 mmol, 1 eq) and 341.47 mg of H-Lys(BOC)-OMe•HCl (1.15 mmol, 8 eq) were added into a flask and dissolved in toluene (12 mL). Afterwards, 641 µL of TEA (4.6 mmol, 32 eq) was added with syringe. The reaction solution was stirred for 9 days at 105 °C. ^{31}P NMR was used to follow the reaction. After 9 days, the white solid was removed by filtration, and the filtrate was concentrated by rotary evaporator, and precipitated with n-pentane three times. The product was provided in the n-pentane phase and was dried under vacuum. (TLC, DCM/MeOH 15/1 Rf=0.27) (110.4 mg, 45.4%)

Characterization:

- ^{31}P $\{^1H\}$ NMR (250 MHz, $CDCl_3$): δ 15 (s, P_0) ppm.
- ^1H NMR (250 MHz, $CDCl_3$): δ 3.7 (s, 3H, H_b), 3.4 (t, 1H, H_a), 3.0 (m, 2H, H_f), 1.4-1.8 (m, 15H, H_c, H_d, H_e, H_g) ppm.
- ^{13}C $\{^1H\}$ NMR (360 MHz, $CDCl_3$): δ (22.8, 28.4, 29.8, 34.4, 40.3, 52.0, 54.2, 156.0, 176.4) ppm.
- MS (MALDI-TOF, positive, matrix): 1690 m/z.

  Calculated: $C_{72}H_{138}N_{15}O_{24}P_3$, 1690.90.

^{31}P NMR (a), ^{1}H NMR (b), ^{13}C NMR (c), and MALDI-TOF (d) of G0-Lys(BOC)-COOMe (17)

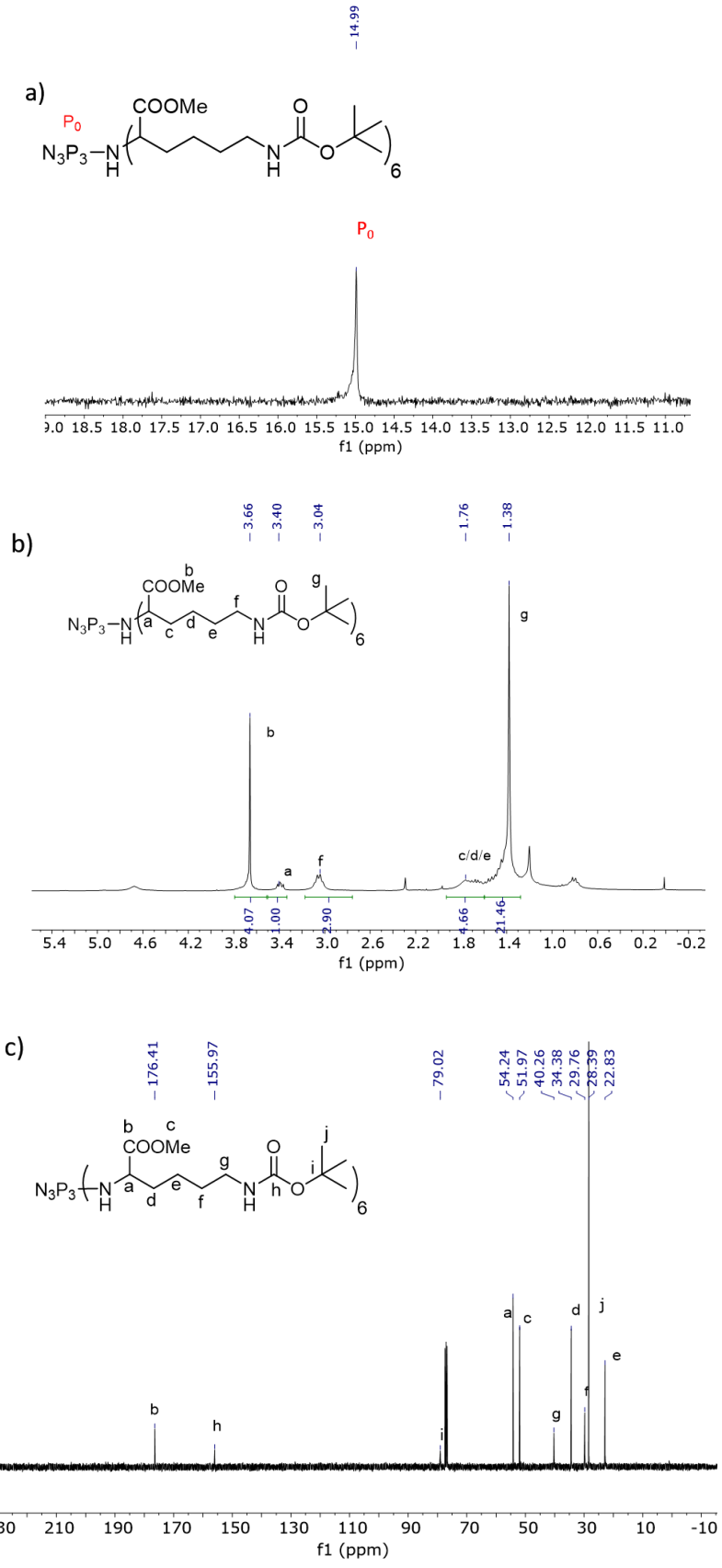

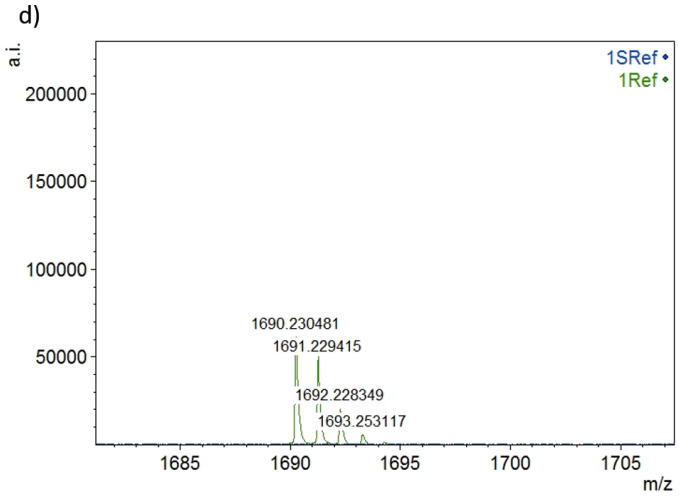

G1-Lys(BOC)-COOMe (18)

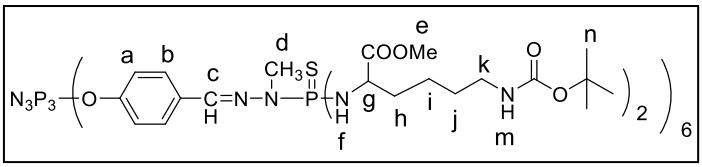

50 mg of G1 (**2**) dendrimer (0.027 mmol, 1 eq) and 129.92 mg of H-Lys(BOC)-OMe•HCl (0.44 mmol, 16 eq) were added into the flask. Subsequently, toluene (10 mL) was added to dissolve these two reactants. Then, 114.4 µL of TEA (0.82 mmol, 30 eq) was added into the flask. The reaction mixture was stirred overnight. After the being checked by ^{31}P NMR to confirm the substitution finished, the reaction was stopped. The produced white solid was isolated by filtration. The filtrate was concentrated and dissolved in CH_2Cl_2 and washed with 0.05 M HCl five times. The organic phase was dried with $MgSO_4$. The product was provided after filtration and concentration (101.5 mg, 82.3%) (TLC, DCM/MeOH 40/1, Rf=0.46).

Characterization:

- ^{31}P {^1H} NMR (250 MHz, $CDCl_3$): δ 8.4 (s, P_0), 67.8 (s, P_1) ppm.
- ^1H NMR (250 MHz, $CDCl_3$): δ 7.48-7.53 (m, 18H, H_b, H_c), 4.68 (m, 12H, H_m), 4.03 (m, 12H, H_g), 3.57-3.63 (d, 36H, H_e), 3.13-3.18 (d, 18H, H_d), 3.04-3.06 (m, 24H, H_k), 1.42-1.69 (m, 180H, H_h, H_i, H_i, H_n) ppm.
- ^{13}C {^1H} NMR (360 MHz, $CDCl_3$): δ (22.4, 28.4, 29.6, 31.5, 40.3, 52.2, 54.3, 79.0, 121.1, 127.8, 132.5, 136.9, 150.8, 156.0, 174.3) ppm.
- MS (MALDI-TOF, positive, matrix): 4538 m/z.

  Calculated: $C_{192}H_{324}N_{39}O_{54}P_9S_6$, 4514.05.

^{31}P NMR (a), ^{1}H NMR (b), ^{13}C NMR (c), and MALDI-TOF (d) of G1-Lys(BOC)-COOMe

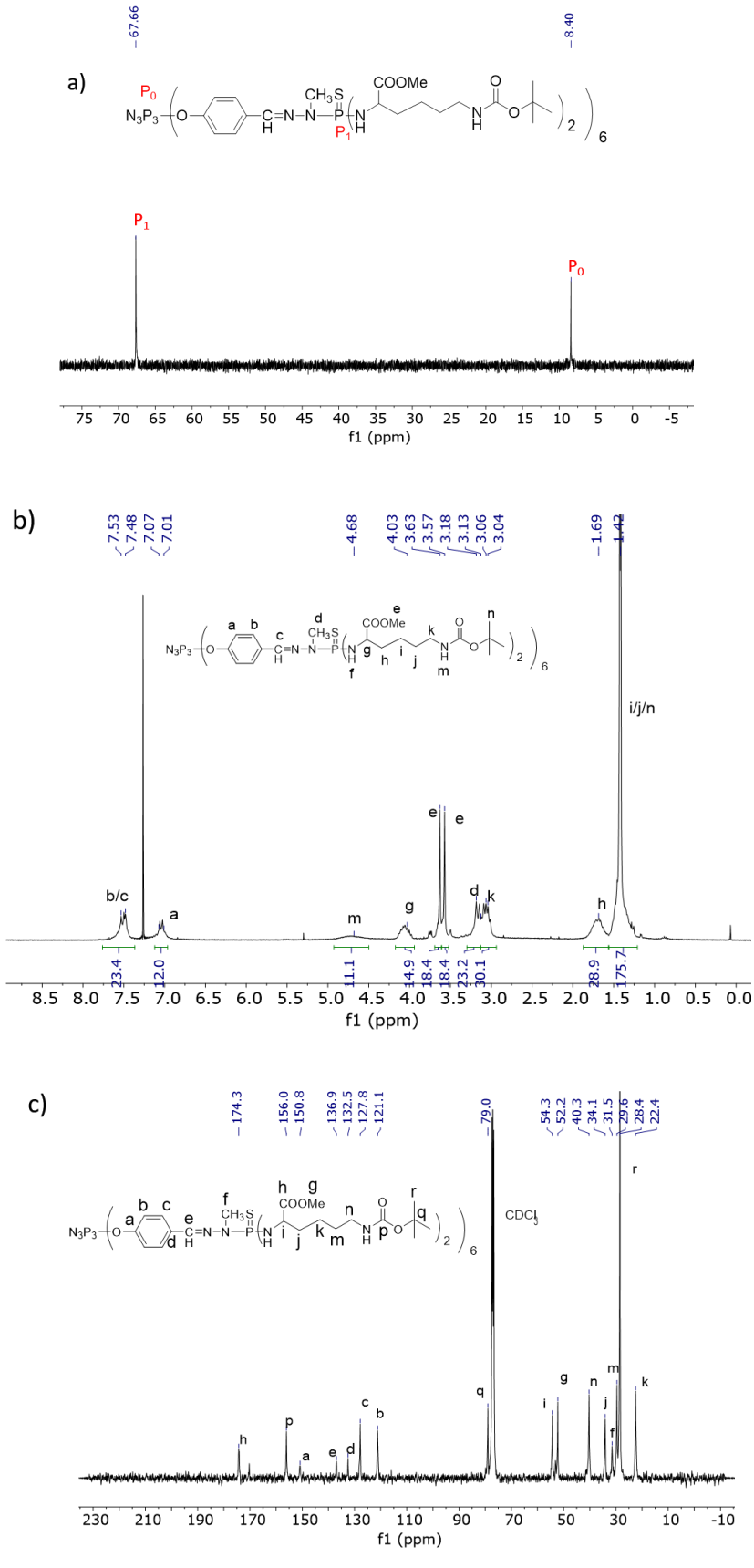

d)

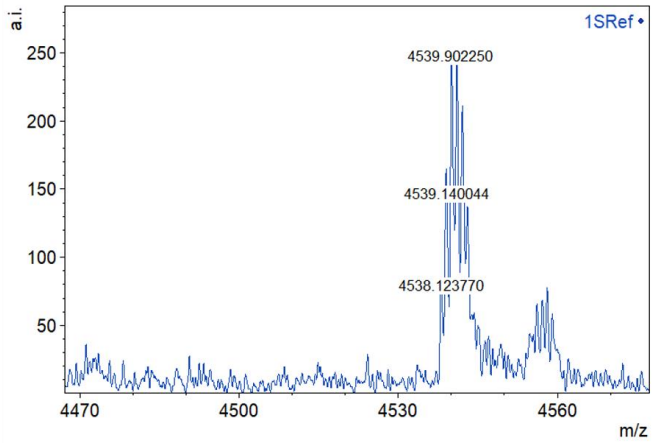

G2-Lys(BOC)-COOMe (19)

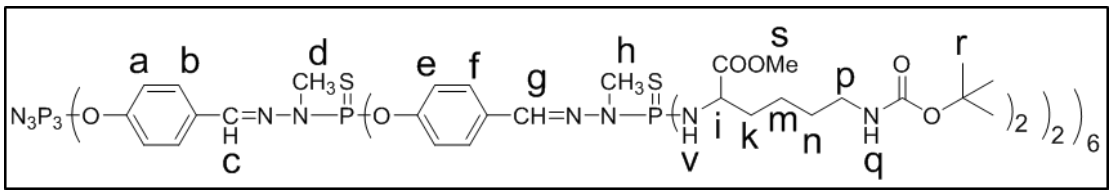

30 mg of G2 (**4**) dendrimer (0.0063 mmol, 1 eq) and 52.09 mg of H-Lys(BOC)-OMe•HCl (0.18 mmol, 28 eq) were added into a dried flask. 10 mL of toluene was added to dissolve these two reactants. Then, 52 µL of TEA (0.38 mmol, 60 eq) was added into the flask. The reaction mixture was stirred in an ice bath for 40 min. After that, the ice bath was removed. The reaction proceeded overnight at room temperature. Next, the white solid was isolated by filtration. Finally, the product was purified by column chromatography on silica gel (DCM/EtOH, 35/1). After being dried under vacuum, product was obtained (41.9 mg, 69%).

Characterization:

- ^{31}P {^{1}H} NMR (250 MHz, $CDCl_3$): δ 8.4 (s, P_0), 62.8 (s, P_1), 66.7 (s, P_2) ppm.
- ^{1}H NMR (250 MHz, $CDCl_3$): δ 7.42-7.56 (m, 54H, H_c, H_g, H_b, H_f), 4.68 (m, 24H, H_q), 3.70-3.73 (m, 24H, H_i), 3.56-3.60 (d, 72H, H_s), 2.88-3.29 (m, 102H, H_d, H_h, H_p), 1.66 (k, 48H, H_k), 1.40-1.42 (m, 312H, H_m, H_n, H_r) ppm.
- ^{13}C {^{1}H} NMR (360 MHz, $CDCl_3$): δ (22.4, 28.4, 29.6, 31.4, 40.3, 52.2, 54.3, 79.0, 121.7, 126.8, 127.8, 128.5, 132.1, 136.7, 150.2, 156.2, 174.4) ppm.

^{31}P NMR (a), ^{1}H NMR (b), and ^{13}C NMR (c) of G2-Lys(BOC)-COOMe (19)

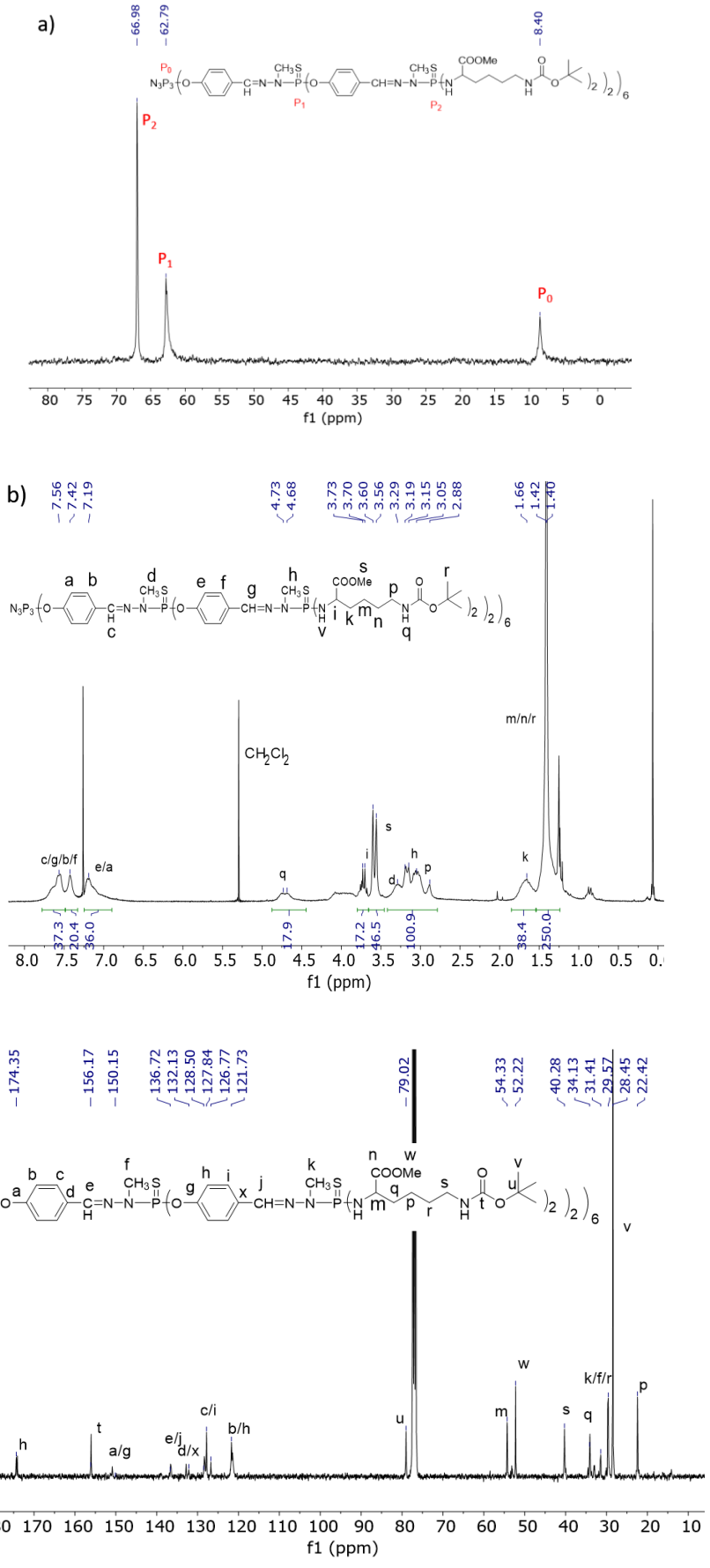

G3-Lys(BOC)-COOMe (20)

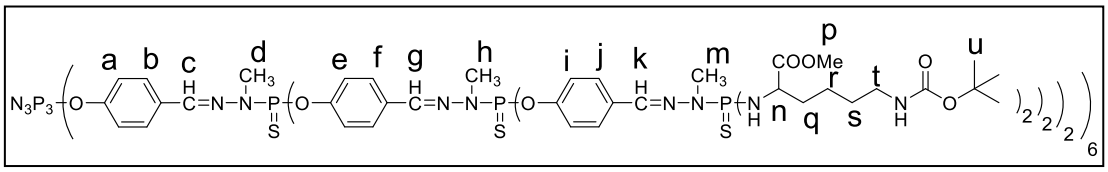

50 mg of G3 (**6**) dendrimer (0.0047 mmol, 1 eq) and 77.6 mg of H-Lys(BOC)-OMe•HCl (0.26 mmol, 1 eq) were added into the flask. Subsequently, THF (10 mL) was added to dissolve these two reactants. 78.1 µL of TEA (0.56 mmol, 120 eq) was added into the flask. The solution was stirred in an ice bath for 1 hour, then at room temperature for 2 days. After the completion was confirmed by ^{31}P NMR, the solution was concentrated and the residues was dissolved in $CHCl_3$ and washed with 0.05 M HCl 6 times. The organic phase was dried with $MgSO_4$. The product was provided after filtration and being dried under vacuum. TLC (DCM/EtOH, 30/1, Rf=0.44) (32.5 mg, 32.4%)

Characterization:

- ^{31}P {^{1}H} NMR (250 MHz, $CDCl_3$): δ 8.6 (s, P_0), 61.8 (s, P_1), 62.8 (s, P_2) 67.0 (s, P_3) ppm.
- ^{1}H NMR (250 MHz, $CDCl_3$): δ 7.58-7.78 (m, 126H, H_c, H_g, H_k, H_b, H_f, H_g), 7.18 (m, 84H, H_a, H_e, H_i,), 4.01 (m, 48H, H_n), 3.55-3.59 (d, 144H, H_p), 3.17-3.59 (m, 222H, H_d, H_h, H_m, H_t), 1.40-1.69 (m, 720H, H_m, H_n, H_r) ppm.

^{31}P NMR (a), and ^{1}H NMR (b) of G3-Lys(BOC)-COOMe (20)

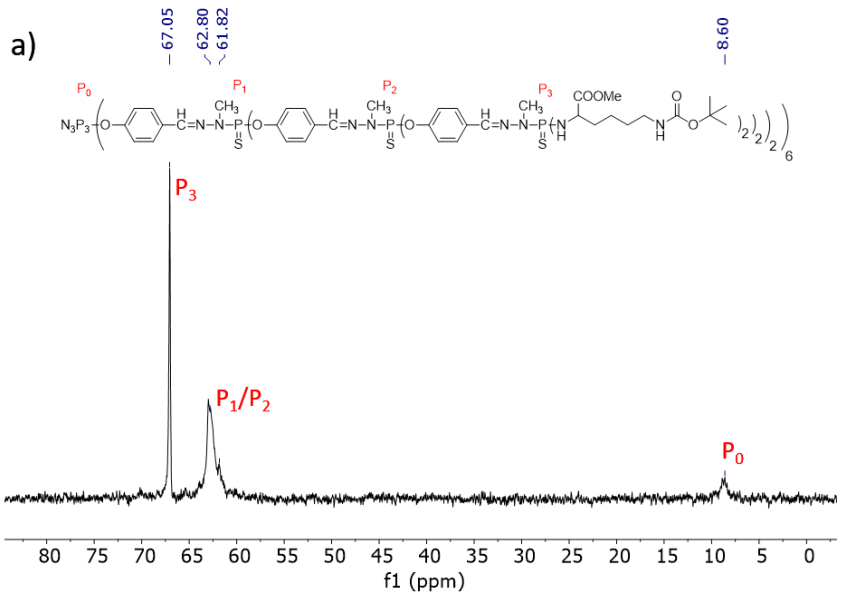

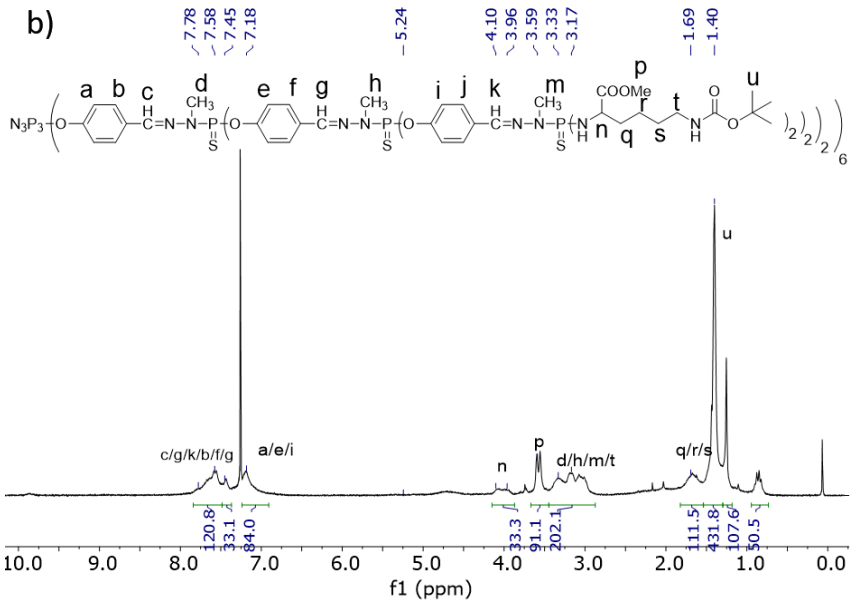

G0-Lys-COOMe (21)

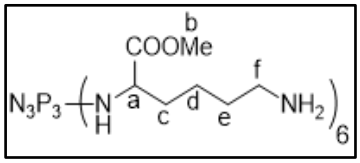

110 mg of G0-Lys(BOC)-COOMe (**17**) (65 µmol, 1 eq) was added into a 25 mL of dried flask. Then, 10 mL of anhydrous DCM was added into the flask to dissolve. The flask was put in an ice bath. Next, 0.6 mL of TFA (7.82 mmol, 120 eq) was added into the solution. After the reaction solution was stirred in an ice bath for 2 hours. The ice bath was removed, and the reaction proceeded in room temperature overnight. The product was purified by washing with DCM and MeOH three times respectively. Finally, the product was dried under vacuum (115 mg, 99%).

Characterization:

- ^{31}P {^{1}H } NMR (250 MHz, MeOD): δ 16.7 (s, P_0) ppm.
- ^{1}H NMR (250 MHz, $CDCl_3$): δ 3.96 (t, 1H, H_a), 3.84 (s, 3H, H_b), 2.96 (t, 2H, H_f), 1.54-1.92 (m, 6H, H_p, H_e, H_d) ppm
- MS (MALDI-TOF, positive, matrix): 1089.73 m/z. Calculated: $C_{42}H_{90}N_{15}O_{12}P_3$, 1090.87.

^{31}P NMR (a), ^{1}H NMR (b), and MALDI-TOF (c) of G0-Lys-COOMe (21)

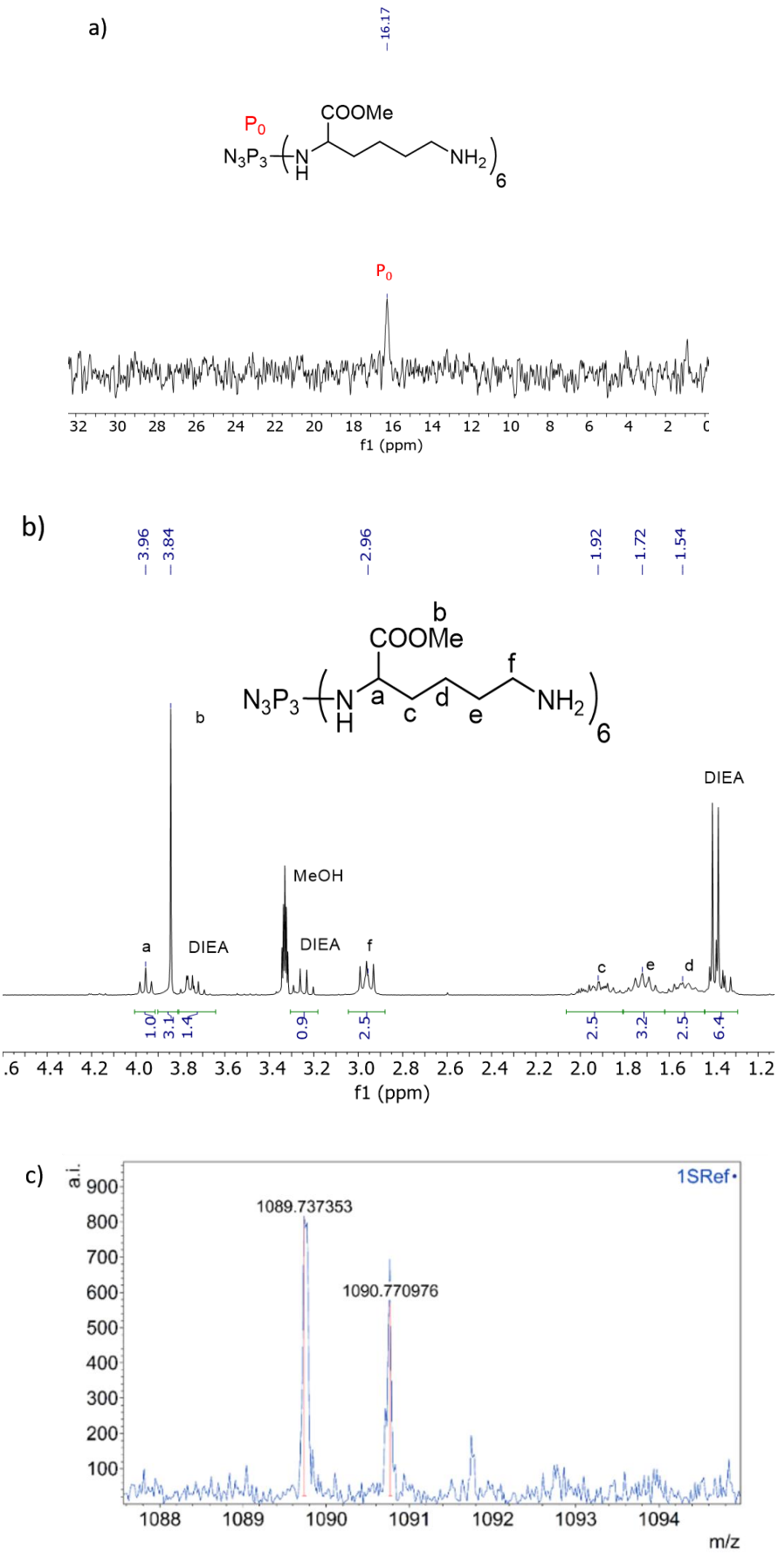

G0-Lys(PROXYL)-COOMe (22)

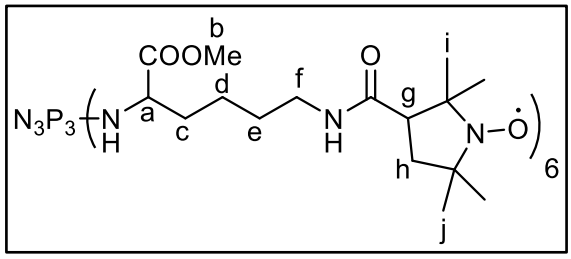

177.57 mg of HATU (7.2 eq, 0.47 mmol) and 87.0 mg of 3-carboxy-PROXYL (0.47 mmol, 7.2 eq) were added into a flask containing 115 mg of G0-Lys-COOMe (**21**) (0.06 mmol, 1 eq). Next, 10 mL of anhydrous dichloromethane was added into the flask to dissolve. After the reaction mixture was stirred for 20 min, 790 µL of DIEA (1.82 mmol, 70 eq) was added into the flask. Then the reaction was stirred at room temperature overnight. The reaction mixture was washed with water three times and the organic phase was dried with $MgSO_4$ overnight. Finally, the product was purified by column chromatography on silica gel (DCM/MeOH, 10/1) (57.7 mg, 42%).

Charaterization:

- ^{1}H NMR (phenylhydrazine) (250 MHz, DMSO-d_6): δ 1.02-1.24 (m, 12H, H_i, H_j), 1.37 (m, 2H, H_h), 1.52 (m, 2H, H_d), 1.67 (m, 2H, H_e), 2.0 (m, 2H, H_c), 2.94 (g, 1H, H_g), 3.13 (f, 2H, H_d), 3.61 (m, 3H, H_b), 4.20 (m, 1H, H_a) ppm.
- MS (MALDI-TOF, positive, matrix): 2100.56 m/z. Calculated: $C_{96}H_{174}N_{21}O_{24}P_3^{6\bullet}$, 2099.46.
- EPR (DCM): g = 2.0051; intramolecular spin-exchange interaction among radicals, alternating line width effect (a_N of the main three lines: 14.6 G). By quantitative EPR study it showed the same area (double integral) than G0-Tyr(PROXYL)-COOMe and around six times more than PROXYL free radical.

^{1}H NMR (a), EPR (b), and MALDI-TOF (c) of G0-Lys(PROXYL)-COOMe (22)

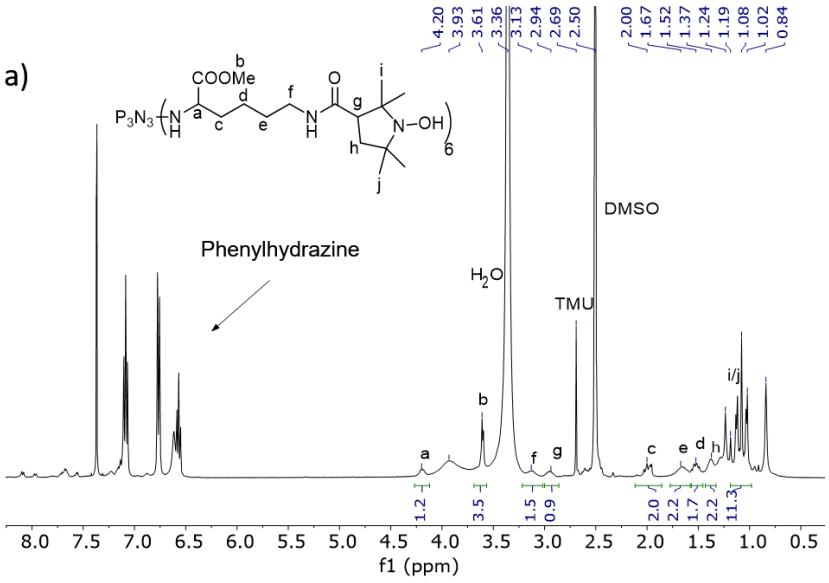

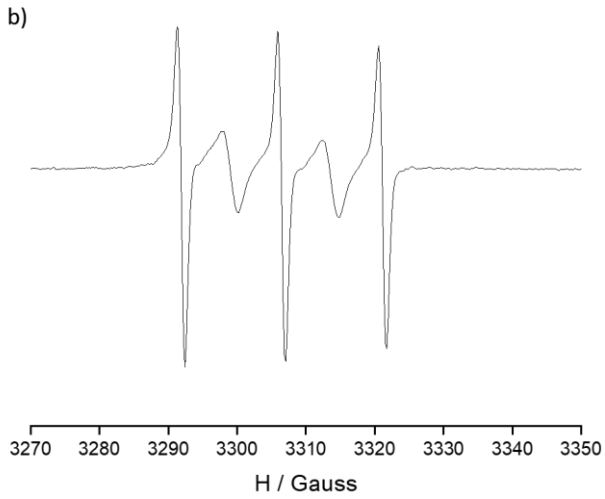

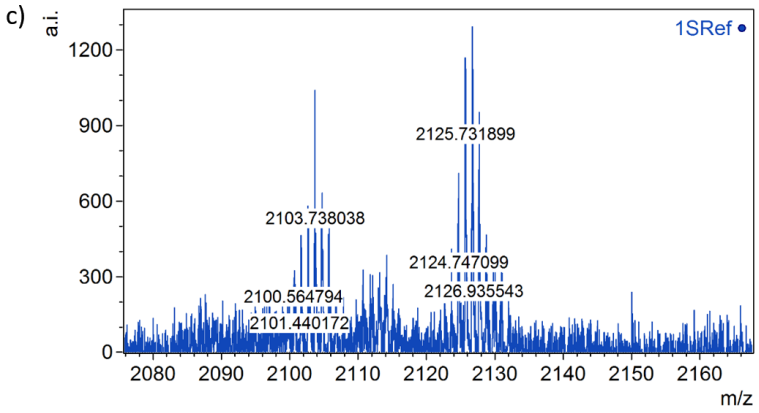

G0-Lys(PROXYL)-COOLi (23)

10.4 mg of G0-Lys(PROXYL)-COOMe (**22**) (4.95 µmol, 1 eq) was added into a flask, followed by addition of 16.21 mg of LiOH•H_2O (8.40 mmol, 78 eq). Then 4 mL of anhydrous THF and 2 mL of H_2O were added into the flask. After 16 h, the reaction was stopped, and THF was removed by concentration. The product was purified by ultrafiltration to remove excess of LiOH•H_2O (1 mg). Quantitative EPR showed it has the same area (double integral) than precursor G0-Tyr(PROXYL)-COOLi (**22**) and around six times higher than PROXYL free radical.

G1-Lys-COOMe (24)

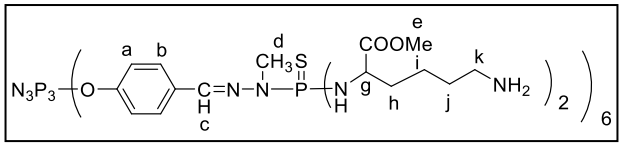

As for the synthesis of G1-Lys-COOMe (**24**), initially we used the same method as G0-Lys-COOMe

(**21**). But we found that the acids could destroy the dendrimer, which was verified by ^{31}P NMR. Finally, we found that $SnCl_4$ could successfully deprotect the BOC group. This specific step was described as following.

20 mg of G1-Lys(BOC)-COOMe (**18**) (0.0044 mmol, 1 eq) was dissolved in 600 µL of CD_2Cl_2. Then the solution was added into the $SnCl_4$ (24 µL, 0.213 mmol) solution in anhydrous CH_2Cl_2 under argon atmosphere in order to prevent the $SnCl_4$ from being contacted with water in the air. Once the dendrimer solution was added into the $SnCl_4$ solution, white solid was observed. After 30 min, the liquid part was taken out and the solid part was dried under vacuum as product (9.2 mg, 62.7%).

Characterization:

- ^{31}P {^1H } NMR (250 MHz, MeOD): δ 8.4 (P_0), 66.81 (P_1) ppm.
- ^1H NMR (250 MHz, MeOD): δ 7.33-7.67 (m, 18H, H_b, H_c), 7.06 (m, 12H, H_a), 4.09 (t, 12H, H_g), 3.86 (s, 36H, H_e), 3.75 (m, 18H, H_d), 2.98 (t, 24H, H_k), 1.57-1.96 (m, 72H, H_h, H_i, H_j) ppm.

^{31}P NMR (a), and ^1H NMR (b) of G1-Lys-COOMe (24)

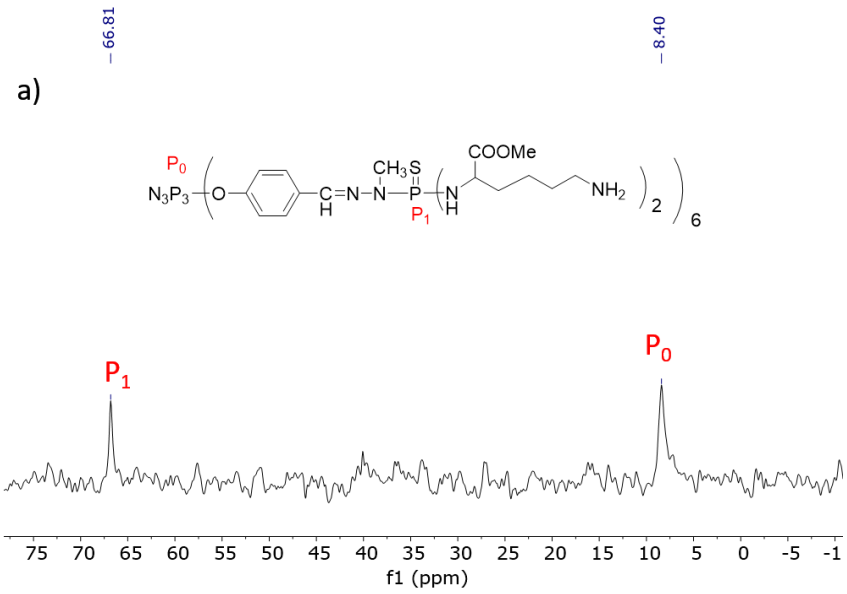

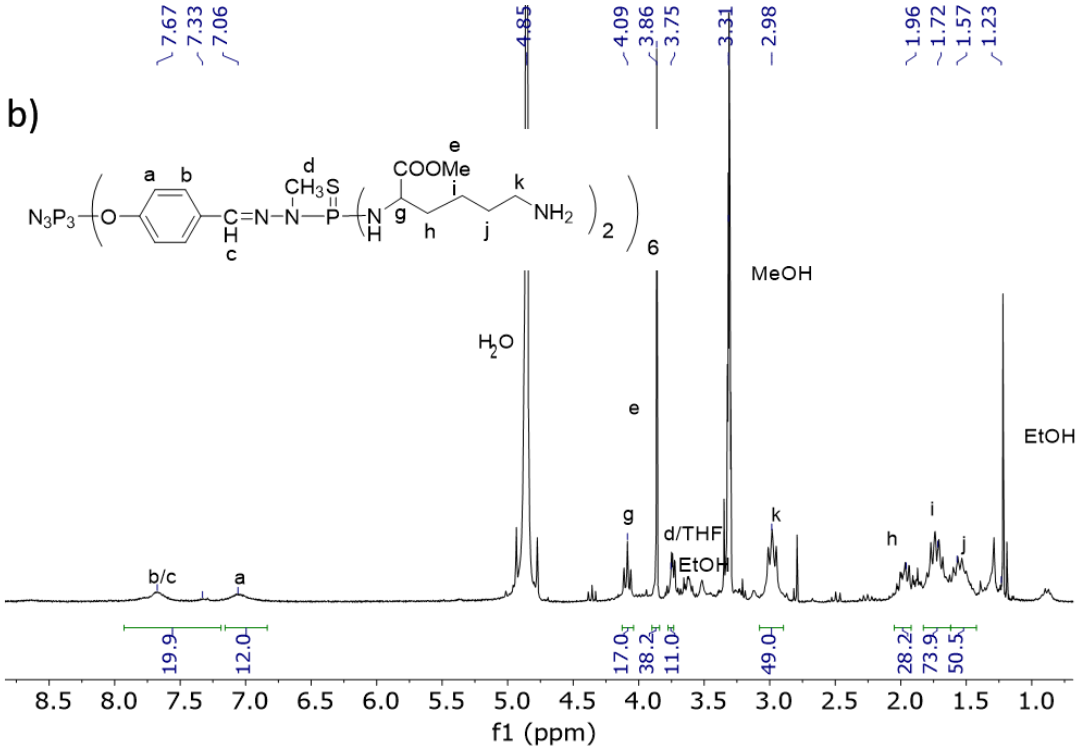

G1-Lys(PROXYL)-COOMe (25)

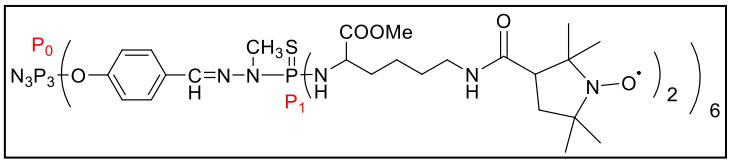

40 mg of G1-Lys-COOMe (**24**) (0.01 mmol, 1 eq) was dissolved in 5 mL of DMSO solution. 70 µL of DIEA (40 mmol, 33 eq), 88.22 mg of HATU (0.23 mmol, 19.2 eq) and 43.21 mg of 3-carboxy-PROXYL (19.2 eq, 0.23 mmol) was added into the solution of G1-Lys-COOMe. Then the solution was stirred at room temperature overnight. The product was purified by extracting with saturated $NaHCO_3$ four times in DCM. The organic phase was dried with $MgSO_4$ followed by dried under vacuum. The crude was dissolved in DCM, and purified by GPC column (CH_2Cl_2, Bio-Beads ^{TM} S-X1). The product G1-Lys(PROXYL)-COOMe was characterized by ^{31}P NMR and EPR (39.9 mg, 62%).

Characterization

- ^{31}P {^{1}H } NMR (250 MHz, DMSO-d_6): δ 8.4 (s, P_0), 67.0 (s, P_1) ppm.
- EPR (DCM): g = 2.0051; intramolecular spin-exchange interaction among radicals, alternating line width effect. Quantitative EPR showed the same area (double integral) than G1-Tyr(PROXYL)-COOMe and approximately 12 times more than PROXYL free radical.

^{31}P (a) NMR and EPR (b) of G1-Lys(PROXYL)-COOMe (25)

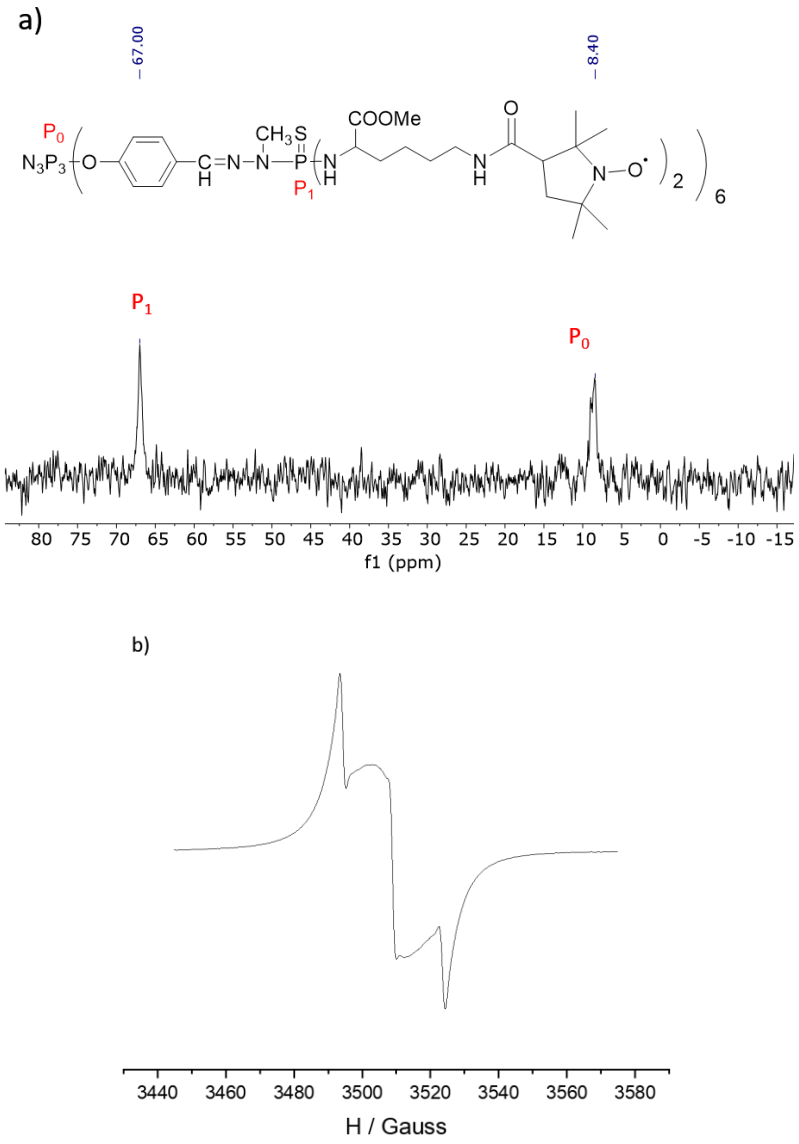

G1-Lys(BOC)-COOLi (26)

See materials and methods part (Appendix B).

G1-Lys(PROXYL)-COOLi (27)

See materials and methods part (Appendix B).

8.2 Radical dendrimers based on oligoethylene glycol (OEG) dendrimers

Synthesis of G0-OEG-PROXYL radical dendrimers (28)

3-carboxy-proxyl (25.312 mg; 1.3 eq. per group) and HATU (52.19 mg; 1.3 eq. per group) were dissolved in anhydrous DCM (2 mL) in a 25 mL round flask. Then, triethylamine (71 μL; 25 eq.) was added with a syringe and it was let to stir at room temperature for 15 minutes. In another 25 mL round flask under an argon atmosphere, G0-OEG-NH_2(•8 HCl) dendrimer (50.0 mg, 1 eq.) was dissolved in anhydrous DCM (2 mL). Then, triethylamine (80 μL; 28 eq.) was added with a syringe and was let to stir for 15 minutes. Subsequently, the mixture of the first flask containing 3-carboxy-proxyl was transferred to the second one containing the G0-OEG-NH_2 dendrimer. The reaction mixture was let to stir at room temperature overnight. The reaction was monitored by TLC using ninhydrin. The product was purified by ultrafiltration in a mixture of water/acetone (10%/90%), (61% yield).

Characterization:

- ^{1}H NMR (250 MHz, DMSO-d_6): δ 1.13-1.27 (m, 14H, H_A, H_B, H_C,), 1.8 (m, 4H, H_a, H_b,), 1.9 (m, 16H, H_b), 3.25-3.65 (m, 18H, H_{c-m}).
- MALDI-TOF MS (dithranol, linear mode m/z): 2247.31 $[M+H]^+$. Calculated mass for $C_{109}H_{203}N_{18}O_{30}$: 2245.92.
- IR (ATR, cm^{-1}): 3303 (-N-H-)st; 1650 (C=O)st; 1364 (N-O.)st; 1290 (-C-H-) bend; 1100 (-C-O-C-)st.
- EPR (DCM): g = 2.0055; intramolecular spin-exchange interaction among radicals, alternating line width effect (see text Chapter 3).

Synthesis of G1-OEG-PROXYL radical dendrimers (29)

3-carboxy-PROXYL (13.00 mg, 1.5 eq. per group) and HATU (26.1 mg, 1.5 eq. per group) were dissolved in 3 mL of anhydrous DCM in a round flask, then triethylamine (50 μL; 154 eq.) was added and it was let to stir at room temperature for 30 min. G2-OEG-NH_2(•38 HCl) dendrimer (17 mg; 1 eq.) was dissolved in 3 mL of DCM in another round flask. The solution containing 3-carboxy-PROXYL was transferred into the flask containing G2-OEG-NH_2 dendrimer and the reaction mixture was let to stir at room temperature overnight. The reaction was monitored by TLC using ninhydrin. The product was purified by ultrafiltration in water, and obtained with a 54% yield.

Characterization:

- IR (ATR, cm^{-1}): 3303 (-N-H-)st; 1650 (C=O)st; 1364 (N-O.)st; 1290 (-C-H-) bend; 1100 (-C-O-C-)st.
- EPR(DCM): g = 2.0055; intramolecular spin-exchange interaction among radicals, alternating line width effect (see text Chapter 3).

8.3 Nanoparticles based on the bis-MPA radical dendrimers

G1-MPA-PEG20k-TEMPO (30)

50 mg of G1-MPA-PEG20k-alkyne (2.4 µmol, 1 eq) and 2.3 mg of N_3-TEMPO (11.7 mmol, 4.8 eq) were added into a flask. Next, 3 mL of anhydrous THF was added into the flask, and the solution was bubbled with argon for 5 min. Then, 2 mL of MeCN and 0.8 mg of CuI were added and the solution was bubbled for another 2 min. Subsequently, 40 µL of DIEA was added to the solution. The reaction mixture was stirred at room temperature for 21 h. After that, the solution was concentrated under a vacuum. The compounds were dissolved in 3 mL of water and transferred to a dialysis bag (MWCO, 0.1-0.5 kDa). The product was purified in 500 mL of Mili-Q water by dialysis. The water was changed after 2 h, 6 h, 23 h. The product was obtained after lyophilization as a white powder (48 mg, 91%).

Characterization:

- ^{1}H NMR (phenylhydrazine) (250 MHz, DMSO-d_6): δ 1.1 (d, 48H, H_a), 1.3 (s, 6H, H_h), 1.9 (m, 16H, H_b), 2.7-2.8 (m, 16H, H_e, H_f), 3.5 (s, PEG), 4.1 (s, 12H, H_g), 4.8 (m, 4H, H_c), 8.0 (s, 4H, H_d) ppm.
- EPR (DCM): g = 2.0061; intramolecular spin-exchange interaction among radicals, alternating line width effect (see text Chapter 4).

G2-MPA-PEG20k-TEMPO (31)

40 mg of G2-MPA-PEG20k-alkyne (1.9 µmol, 1 eq) and 3.6 mg of N_3-TEMPO (11.7 µmol, 9.6 eq) were added into a flask. Next, 3 mL of anhydrous THF and 1.5 mL of anhydrous MeCN were added into the flask, and the solution was bubbled with argon for 5 min. Then, 0.6 mg of CuI was added and the solution was bubbled for another 2 min. Subsequently, 62 µL of DIEA was added to the solution. The reaction mixture was stirred at r.t overnight. After that, the solution was concentrated under a vacuum. The compounds were dissolved in 3.3 mL of mixture solvent of EtOH and H_2O (1/10, v/v) and transferred

to a dialysis bag (MWCO, 0.1-0.5 kDa). The product was purified in 500 mL of Mili-Q water by dialysis. The water was changed after 2 h, 6 h, 23 h. The product was obtained after lyophilization as a white powder (41.9 mg, 97%).

Characterization:

- ^{1}H NMR (phenylhydrazine) (250 MHz, $CDCl_3$): δ 0.8-1.4 (m, 114H, H_a, H_h, H_j), 2.2 (m, 32H, H_b), 2.8-3.0 (m, 32H, H_e, H_f), 3.6 (s, PEG), 4.2-4.3 (d, 24H, H_g, H_i), 4.8 (m, 8H, H_c) ppm.
- EPR (DCM): g = 2.0055, intramolecular spin-exchange interaction among radicals, alternating line width effect (see text Chapter 4).

G3-MPA-PEG20k-TEMPO (32)

30 mg of G3-MPA-PEG20k-alkyne (1.3 μmol, 1 eq) and 4.92 mg of N_3-TEMPO (19.2 μmol, 19.2 eq) were added into a flask. Next, 3 mL of anhydrous THF and 1.5 mL of anhydrous MeCN were added into the flask, and the solution was bubbled with argon for 5 min. Then, 1.9 mg of CuI was added and the solution was bubbled for another 2 min. Subsequently, 90 μL of DIEA was added to the solution. The reaction mixture was stirred at room temperature for 20 h. After that, the solution was concentrated under a vacuum. The compounds were dissolved in 3.3 mL of mixture solvent of MeOH and H_2O (1/10, v/v) and transferred to a dialysis bag (MWCO, 0.1-0.5 kDa). The product was purified in 500 mL of Mili-Q water by dialysis. The water was changed after 2 h, 6 h, 23 h. The product was obtained after lyophilization as a white powder (33.1 mg, 98%).

Characterization:

- ^{1}H NMR (phenylhydrazine) (250 MHz, $CDCl_3$): δ 1.2-1.3 (m, 234H, H_a, H_h, H_j, H_l), 2.1 (m, 64H, H_b), 2.8-3.0 (m, 64H, H_e, H_f), 3.6 (s, PEG), 4.2 (m, 56H, H_g, H_i, H_k), 5.2 (m, 16H, H_c) ppm.
- EPR (DCM): g = 2.0060, intramolecular spin-exchange interaction among radicals, alternating line width effect (see text Chapter 4).

Preparation of nanoparticles with G2-MPA-PEG20k-TEMPO

4.6 mg of G2-MPA-PEG20k-TEMPO (**31**) was firstly dissolved in 1 mL of acetone (HPLC grade). Next, the solution was injected into 5 mL of water with an injection speed of 1 mL/h with an injection pump, meanwhile, the aqueous solution was being stirred at 200 rpm. After the injection finished, the solution was stirred in the fume hood overnight. Then the nanoparticles colloid was dialyzed in water. The water was changed after 2 h, 15 h, 19 h and 20 h. Finally, the nanoparticles dispersion was stored at 4 °C.

8.4 Bimodal fluorescent magnetic radical dendrimers

tri-amido-TEMPO (33)

20.0 mg of tri-acid dendrimer (0.13 mmol, 1 eq) was added into a round-bottom flask and dissolved in 6 mL of THF_{anh}, then 49.74 mg of HATU (0.13 mmol, 3.3 eq) was added under argon atmosphere. 22.4 mg of 4-amino-TEMPO (0.13 mmol, 3.3 eq) was dissolved in a vial with 1 mL of THF_{anh} and transferred into the flask containing the tri-acid and HATU. After the solution was stirred for 10 min, 22.7 μL of DIEA (0.13 mmol, 3.3 eq) was added into the flask with a syringe and the mixture was stirred overnight. Then, THF was removed under vacuum, and the solid was dissolved in DCM. The organic phase in DCM was extracted five times with MiliQ water and dried with $MgSO_4$. After that, the product tri-amido-TEMPO (**33**) was obtained after purification by column chromatography on silica gel (DCM/EtOH, 40/1, v/v, Rf=0.33), and being dried under vacuum, (33.5 mg, 87.67 %).

Characterization:

- ^{1}H NMR (phenylhydrazine) (250 MHz, DMSO-d_6): δ 1.1 (d, 36H, H_a), 1.5-1.7 (m, 12H, H_b), 4.2 (s, 3H, H_c), 7.5-7.9 (m, 21H, H_d, H_e, H_f, H_g, H_h) ppm.
- IR (cm^{-1}): 3299 ν(NH), 2972 ν(CH), 2928 ν(CH), 2852 ν(CH), 1630 ν(CO), 1537, 1500, 1458, 1364, 1323, 1263, 1242, 1179, 964, 859, 847.
- MS (MALDI-TOF, positive mode): 977.2 m/z.
  Calculated: $C_{60}H_{75}N_6O_6^{3\bullet}$, 976.30.
- EPR (THF): g = 2.0059; a_N = 15.5 G; ΔH_{pp} = 1.61 G.

tetra-amido-TEMPO (34)

The synthesis of the tetra-amido-TEMPO (**34**) was similar to the synthesis of tri-amido-TEMPO (**33**). 20 mg of tetra-acid (0.03 mmol, 1 eq) and 50.49 mg HATU (0.13 mmol, 4.4 eq) were added into a round-bottom flask, and 8 mL of THF_{anh} were added into the flask. 22.74 mg of 4-amino-TEMPO (0.13 mmol, 4.4 eq) was weighed and dissolved in a vial with 2 mL of THF_{anh} and transferred into the flask. After the solution was stirred for 10 min, 23 μL of DIEA (0.13 mmol, 4.4 eq) was added. The reaction mixture was stirred overnight. 1.5 mL of DMSO was added to the flask. After being stirred for another 4 hours, THF was removed under vacuum and the residue part was dissolved in DCM.

The solution in DCM was extracted with water five times. The organic phase was dried with $MgSO_4$ and purified by column chromatography on silica gel (DCM/MeOH, 20/1, v/v, Rf=0.44) to obtain the product (21.1 mg, 53%).

Characterization:

- ^{1}H NMR (phenylhydrazine) (250 MHz, DMSO-d_6): δ 1.1 (d, 48H, H_a), 1.5-1.7 (m, 16H, H_b), 4.2 (s, 4H, H_c), 7.5-8.2 (m, 26H, H_d, H_e, H_f, H_g, H_h) ppm.
- IR (cm^{-1}): 3297 ν(NH), 2970 ν(CH), 2925 ν(CH), 2854 ν(CH), 1632 ν(CO), 1600, 1531, 1498, 1458, 1362, 1320, 1267, 1240, 1176, 957, 864, 759.
- MS (MALDI-TOF, positive mode): 1277.2 m/z.
  Calculated: $C_{78}H_{98}N_8O_8^{4\bullet}$, 1275.69.
- EPR (THF): g = 2.0064; a_N = 15.5 G; ΔH_{pp} = 1.64 G.

tri-imino-TEMPO (35)

20.0 mg of tri-aldehyde (0.04 mmol, 1 eq) was added into the flask and then 2 mL of THF was added to dissolve it. 24.76 mg of 4-amino-TEMPO (0.14 mmol, 3.3 eq) was weighed and put into a vial, and THF_{anh} (1 mL) was used to dissolve the radical. The solution of amino-TEMPO was transferred into the flask containing the tri-aldehyde. Al_2O_3 (32 mg) was added into the flask to accelerate the reaction and we sonicated the reaction mixture for 6 h. After filtration to remove Al_2O_3, the reaction solution was precipitated with *n*-pentane twice. The product was obtained as solid and dried under vacuum (25 mg, 62.5%).

Characterization:

- ^{1}H NMR (phenylhydrazine) (250 MHz, DMSO-d_6): δ 1.1 (d, 36H, H_a), 1.6 (m, 12H, H_b), 3.7 (s, 3H, H_c), 7.4-7.8 (m, 21H, H_e, H_f, H_g, H_h, H_i), 8.5 (d, 3H, H_d) ppm.
- IR (cm^{-1}): 3027 , 2973 ν(CH), 2928 ν(CH), 2863 ν(CH), 1637 ν(C=N), 1600, 1509, 1560, 1414, 1360, 1346, 1306, 1240, 1216, 1173, 1046, 960, 849, 806, 566.
- MS (MALDI-TOF, positive mode): 929.2 m/z.
  Calculated: $C_{60}H_{75}N_6O_3^{3\bullet}$, 928.30.
- EPR (THF): g = 2.0060; a_N = 15.4 G; ΔH_{pp} = 1.59 G.

tetra-imino-TEMPO (36).

The synthesis of the tetra-imino-TEMPO (**36**) was similar to the synthesis of tri-amido-TEMPO (**35**). 20 mg of tetra-aldehyde (0.03 mmol, 1 eq) was added into a flask and

dissolved in THF_{anh} (8 mL). 22.9 mg of 4-amino-TEMPO (0.13 mmol, 4 eq) was weighed and dissolved with THF (2 mL) in a vial. The solution was transferred into the flask with a syringe. Al_2O_3 (30 mg) was added to the solution and the reaction mixture was stirred for 8h under sonication. After filtration to remove Al_2O_3 and precipitation with n-pentane three times, the product was obtained and dried under vacuum (34.4 mg, 85%).

Characterization:

- ^{1}H NMR (phenylhydrazine) (250 MHz, DMSO-d_6): δ 1.1 (d, 48H, H_a), 1.6 (m, 16H, H_b), 3.6 (s, 4H, H_c), 7.5-8.1 (m, 26H, H_e, H_f, H_g, H_h, H_i), 8.5 (s, 4H, H_d) ppm.
- IR (cm^{-1}): 3030, 2971 ν(CH), 2930 ν(CH), 2855 ν(CH), 1637 ν(C=N), 1601, 1560, 1508, 1464, 1414, 1360, 1343, 1302, 1240, 1221, 1172, 1105, 1048, 957, 901, 856, 809, 532.
- MS (MALDI-TOF, positive mode): 1212.2 m/z.

  Calculated: $C_{78}H_{98}N_8O_4^{4\bullet}$, 1211.69.
- EPR (THF): g = 2.0053; a_N = 15.4 G; ΔH_{pp} = 1.56 G.

tri-amino-TEMPO (37).

31.7 mg of tri-imino-TEMPO (**35**) (0.03 mmol, 1 eq) was added into a flask, 4 mL of $CHCl_3$ and 2 mL of CH_3OH were added to dissolve the reagent. The flask was put into an ice bath. $NaBH_4$ (0.1 mmol, 3.66 mg) was added to the flask. Then, the reaction mixture was stirred in an ice bath overnight. After that, the reaction solution was concentrated, and DCM was added into the flask to dissolve the product and extracted with water three times. The product was obtained after the organic phase was dried (31.0 mg, 97.17%).

Characterization:

- ^{1}H NMR (phenylhydrazine) (250 MHz, DMSO-d_6): δ 1.0 (d, 36H, H_a), 1.2-1.8 (m, 12H, H_b), 2.8 (s, 3H, H_c), 3.7 (s, 6H, H_d), 7.2-7.7 (m, 20H, H_e, H_f, H_g, H_h, H_i) ppm.
- IR (cm^{-1}): 3300 ν(NH), 3024 ν(CH), 2969 ν(CH), 2926 ν(CH), 2855 ν(CH), 1585, 1510, 1456, 1360, 1310, 1241, 1217, 1175, 1104, 1017, 959, 892, 842, 795, 737, 704, 681, 640, 558, 540, 509.
- MS (MALDI-TOF, positive mode): 936.1 m/z.

  Calculated: $C_{60}H_{81}N_6O_3^{3\bullet}$, 934.35.
- EPR (THF): g = 2.0057; a_N = 15.4 G; ΔH_{pp} = 1.62 G.

tetra-amino-TEMPO (38).

30.9 mg of tetra-imino-TEMPO (**36**) (0.02 mmol, 1 eq) was added into a flask, 4 mL of $CHCl_3$ and 2 mL of CH_3OH were added to dissolve the reagent. The flask was put into an ice bath. $NaBH_4$ (2.8 mg, 0.07 mmol) was added to the flask. Then the reaction mixture was stirred in an ice bath overnight. After that, the reaction solution was concentrated, and DCM was added into the flask to dissolve the product and the organic solution extracted with water three times. The product was obtained after the organic phase was dried (28.7 mg, 95%).

Characterization:

- ^{1}H NMR (phenylhydrazine) (250 MHz, DMSO-d_6): δ 1.0 (d, 48H, H_a), 1.2-1.8 (m, 16H, H_b), 2.8 (s, 4H, H_c), 3.7 (s, 8H, H_d), 7.4-7.7 (m, 26H, H_e, H_f, H_g, H_h, H_i) ppm.
- IR (cm^{-1}): 3300 ν(NH), 3017, 2970 ν(CH), 2927 ν(CH), 2849 ν(CH), 1509, 1455, 1360, 1241, 1174, 1099, 956, 853, 798, 728, 611.
- MS (MALDI-TOF, positive mode): 1220.3 m/z.
  Calculated: $C_{78}H_{106}N_8O_4^{4\bullet}$, 1219.76.
- EPR (THF): g = 2.0057; a_N = 15.4 G; ΔH_{pp} = 1.40 G.

8.5 Synthesis of G3-Tyr(PROXYL)-COONa

Under dark conditions, 110 mg of G3-Tyr(PROXYL)-COOMe (4.17 µmol, 1 eq) was added into a round-bottomed flask equipped with a stir bar and dissolved in 2 mL of THF. 129 mg of NaOH (3.0 mmol, 720 eq) were dissolved in 2 mL of Mili-Q water and transferred to the THF solution of G3-Try(PROXYL)-COOMe. The reaction mixture was let to stir at room temperature overnight. Afterwards, THF was removed under vacuum and the aqueous solution was purified by dialysis (MWCO, 0.1-0.5 kDa) to remove the excess of NaOH. The external water was changed after 2, 4, 21 and 46 h. Then, the aqueous solution of the dialysis bag was collected and the water eliminated by freeze-drying to afford the final product G3-Try(PROXYL)-COONa (**39**) as a pale yellow solid in a (74.5 mg, 67%). It was checked by quantitative EPR that it has the same area (double integral) than G3-Tyr(PROXYL)-COOLi.

Appendix A List of Publications

Related to this Thesis:

1. Pinto, L. F.; Lloveras, V.; Zhang, S.; Liko, F.; Veciana, J.; Muñoz-Gómez, J. L.; Vidal-Gancedo, J. Fully Water-Soluble Polyphosphorhydrazone-Based Radical Dendrimers Functionalized with Tyr-PROXYL Radicals as Metal-Free MRI T1 Contrast Agents. *ACS Appl. Bio Mater.* **2020**, *3* (1), 369–376.

2. Zhang, S.; Lloveras, V.; Pulido, D.; Liko, F.; Pinto, L. F.; Albericio, F.; Royo, M.; Vidal-Gancedo, J. Radical Dendrimers Based on Biocompatible Oligoethylene Glycol Dendrimers as Contrast Agents for MRI. *Pharmaceutics* **2020**, *12* (8), 1–15.

3. Zhang, S.; Lloveras, V.; Lope, S.; Calero, P.; Wu, S.; Candiota, A. P.; Vidal-Gancedo, J. Metal-free Radical Dendrimers as MRI Contrast Agents for Glioblastoma Diagnosis: Ex vivo and In vivo Approaches. *In preparation*.

4. Zhang, S.; Lloveras, V.; Shirdel, E.; Wu, Y.; Ujaque, G.; Vidal-Gancedo, J. pH-controlled Release of Amino Acid Functionalized Phosphorus Dendrimers. *In preparation.*

Not directly related to this Thesis:

1. Badetti, E.; Lloveras, V.; Amadio, E.; Di Lorenzo, R.; Olivares-Marín, M.; Tesio, A. Y.; Zhang, S.; Pan, F.; Rissanen, K.; Veciana, J.; Tonti, D.; Vidal-Gancedo, J.; Zonta, C.; Licini, G. Organic Polyradicals as Redox Mediators: Effect of Intramolecular Radical Interactions on Their Efficiency. *ACS Appl. Mater. Interfaces* **2020**, *12* (41), 45968–45975.

Appendix B Materials and Methods

Reagents and solvents.

Commercial reagents have been directly used. Commercial solvents have been used directly, except for the following:

- THF has been distilled over metallic sodium and benzophenone under N_2(g).
- Toluene has been distilled over metallic sodium and benzophenone under N_2(g).
- CH_2Cl_2 has been distilled over CaH_2 and under N_2(g).
- $CHCl_3$ has been distilled over CaH_2 and under N_2(g).

The synthesis and handling of radical derivatives in solution has been performed under dark conditions in the dark room facility of ICMAB.

Instrumentation and methods.

Nuclear magnetic resonance (NMR) spectroscopy

The NMR spectra have been performed in SeRMN service of UAB using the next spectrometers: Bruker Avance DRX-250, Bruker DXP-360 MHz, Bruker Advance III-400 MHz. The chemical shifts of $^{31}P\{1H\}$ spectra are expressed in ppm using as an internal reference H_3PO_4 85% in water for ^{31}P NMR (0 ppm). The chemical shifts of ^{1}H spectra are expressed in ppm using as an internal reference tetramethylsilane (TMS) (0 ppm). The chemical shifts of ^{13}C spectra are expressed in ppm using as an internal reference the carbon traces of the solvent.

Ultraviolet-visible (UV-Vis) spectroscopy

The UV-Vis spectra have been recorded in a double beam JASCO V-770 spectrophotometer, the cuvettes used are made of quartz of 3 ml of volume and 1 cm of optical path length. The wavelenght range used was from 200 to 800 nm.

Infrared (FT-IR) spectroscopy

FT-IR spectra have been recorded in a FT/IR-4700 from JASCO (Tokyo, Japan) with an ATR (attenuated total reflectance) accessory, in the 400–4000 cm^{-1} range with 4 cm^{-1} resolution.

Mass spectrometry

The mass spectra has been recorded in a MALDI-TOF BIFLEX spectrometer (Bruker-Franzen Analytik) equipped with a pulsed nitrogen laser (337 nm), using 19 kV acceleration voltage, at UAB.

Electron paramagnetic resonance (EPR) spectroscopy

EPR spectra have been obtained with an X-Band (9.4 GHz) Bruker ELEXSYS E-500 spectrometer equipped with a ST8911 microwave cavity, a Bruker variable temperature unit, a field frequency lock system Bruker ER 033 M and with a NMR Gaussmeter Bruker ER 035 M. The modulation amplitude was kept well below the line width, and the microwave power was well below saturation. All liquid samples were previously degassed with Ar. EPR spectra of organic solutions have been performed with standard 4 mm-diameter quartz EPR tubes, for aqueous solution we have used a flat quartz EPR cell and the EPR spectra of the animal organs have been carried out with a special quartz flat tissue cell.

Size exclusion chromatography (SEC)

SEC analyses have been carried out using an Agilent 1260 infinity II liquid chromatography system apparatus equipped with a diode array detector under the following conditions: a PSS Suprema pre-column (10 µm, 8 × 50 mm) and a PSS Suprema analytical column (10 µm, 100 Å, 8 × 300 mm) with a diode array detector were used for aqueous solution as eluent, a PSS Suprema pre-column (10 µm, 8 x 50 mm) and a PSS Suprema analytical column (10 µm, 100 Å, 8 × 300 mm) were used for organic solvent ($CHCl_3$). Radical dendrimers were dissolved in the eluent to reach a final concentration of 1 mg/mL and filtered through 0.2 µm nylon filter before injection, using a flow rate of 0.5 mL/min. For aqueous solution, LiCl in water (0.25 mM) was used as eluent.

Dynamic light scattering (DLS)

DLS measurements have been carried out on a Nano-S Zetasizer (Malvern Instrument Ltd., Malvern, UK) with back scattering detector (173º, 633 nm laser wavelength) to measure hydrodynamic size (diameter) in batch mode at 25 ℃. Samples were prepared at a concentration of 1 mg/mL in 30 mM phosphate buffer pH 7.4 or in Mili-Q water. The samples were filtered through 0.2 μm or 0.45 μm PTFE filter before analysis. A minimum of 3 measurements per sample were made.

Z-Potential

Z-Potential experiments were carried out on the same Zetasizer Nano ZS dynamic light scattering (DLS) instrument (Malvern Panalytical, Malvern, UK). Dendrimers samples were prepared at a concentration of 1 mg/mL in water. A minimum of 3 measurements per sample were made.

Transmission electron microscopy (TEM)

TEM images were performed in a JEOL 1210 microscope operating at 120 kV and equipped with a Gathan sample holder.

Fluorescence spectroscopy

Fluorimetry studies have been performed in a Varian Cary Eclipse fluorimeter from the Laboratori de Luminescència i Espectroscòpia de Biomolècules (LLEB), at the UAB, in an auto-service regime, excitation slit 5 nm, emission 5 nm.

Magnetic resonance imaging (MRI)

Magnetic resonance imaging experiments have been carried out in a BioSpec 70/30 Bruker system using a 7.0 T horizontal-bore superconducting magnet equipped with actively shielded gradients (B-GA12 gradient coil inserted into a B-GA20S gradient system), from the SeRMN service of UAB.

Relaxometric measurements

Longitudinal (r_1) and transverse (r_2) relaxivities were determined per concentration

of molecule or radical units. A range of concentrations of the compound were prepared. Relaxivity measurements were obtained at room temperature. The software used for the calculations of T_1 and T_2 relaxations was Paravision 6.0 (Bruker Software). *r_1 relaxivity*. Series of axial T_1-weighted (T1W) images were acquired for each concentration of compound to obtain T_1 maps based on a magnetization saturation experiment and the following parameters: repetition time (TR) = 70−6000 ms, echo time (TE) = 9.2 ms, field of view (FOV) = 2.5 × 2.5 cm, averages (Av) = 1, acquisition matrix (Mtx) = 128 × 128. The T_1 values were calculated from the mean signal in the region of interest (ROI) for each repetition time, adjusted to the equation: S = So [1 − (−TR/T1)]. *r_2 relaxivity*. T_2 maps were calculated from multi spin echo images with a TR of 2 s. A total of 25 echo images were acquired with a TE of 8.02 ms, which was also the interval time between echo image acquisitions. T_2-map parameters were as follows: 1 axial slice of 2 mm thickness; TR = 3200 ms; TE = 8.02 ms (25 echo times with interval of 8.02 ms in between), 1 average. Field of view (FOV): 35 × 35 mm; Mtx: 256 × 256. The T_2 values were calculated from mean signal in the ROI for each echo image, adjusted according to the equation: S = So (−TE/T2)].

Chromatographic techniques

• Thin layer chromatography (TLC): The TLC was performed over chromatoplates of silica gel with aluminum support (60F, 0.2 mm, Merk).

• Column chromatography: The purification by column chromatography has been carried out with silica gel (Chromatogel 60 ÅCC, 230-400 mesh).

• Size exclusion chromatography: The purification by size exclusion was performed using CH_2Cl_2 HPLC grade as eluent and Bio-BeadsTMS-X1 as stationary phase.

Ultrafiltration

Ultrafiltration of radical dendrimers was performed on solvent-resistant stirred cells from EMD Millipore (Billerica, MA, USA) with regenerated cellulose membranes (1, 3 and 5 kDa). Ultrapure water (Milli-Q, EMD Millipore) or mixtures of ultrapure water and HPLC grade acetone were used for ultrafiltration.

Dialysis

Dialysis of radical dendrimers was performed with a dialysis kit (MWCO 100-500 Da, Thermo Fisher Scientific Inc.). The solution of crude radical dendrimers was added to the dialysis kit and dialyzed against ultrapure water. The water was changed at different interval times.

Reduction of organic radicals for NMR characterization

The NMR characterization of organic radicals and in particular of radical dendrimers is usually difficult and incomplete because the paramagnetic character of the radical influences in broadening the signals corresponding to the nuclei close to the areas of the molecule in which the spin density of the unpaired electron is appreciable. To avoid this, ascorbic acid is usually used to cancel the radical character (like we have done in G0-OEG-PROXYL compound) and thus be able to have an NMR spectrum that allows us to characterize the entire molecule by NMR. Since ascorbic acid is generally used in aqueous media, an exhaustive literature search has been carried out to be able to do it in organic solvents. We chose mainly two ways of reduction of the nitroxide radicals, phenylhydrazine and hydrazobenzene, both of them have been adopted to reduce the nitroxide to hydroxylamine for the characterization by ^{1}H NMR. Considering there are more protons in hydrazobenzene, we decided to use phenylhydrazine in our cases, to minimize the interference produced by the protons from the reducing agents.

The specific procedure for radical dendrimers has been the following: 3-5 mg of radical dendrimers (amido-TEMPO, imino-TEMPO, amino-TEMPO derivatives, Gn-MPA-PEG20k-TEMPO and G0-Lys(PROXYL)-COOMe radical dendrimers) were dissolved in approximately 500 μL of $CDCl_3$ or DMSO-d_6. Then, 2-4 μL of phenylhydrazine was added into the solution of radical dendrimers. After 30 min at room temperature, the solution was transferred to a NMR tube to perform the NMR measurements. In general, DMSO-d_6 is better to be used for these kinds of experiments since the polarity of hydroxylamine products is high.

G0-OEG-PROXYL radical dendrimer (25.86 mg; 1 eq.) was dissolved in H_2O (2mL) in a 10 mL round flask. Subsequently, ascorbic acid excess (103.6 mg; 10 eq. per group) was added and it was stirred for around 6 h. The product was purified by ultrafiltration in water/acetone mixture (10%/90%) giving quantitative yield.

^{1}H NMR and ^{31}P NMR for checking the stability of Gn-Lys(BOC)-COOMe (n=0, 1, 3) and G1-Tyr(BOC)-COOMe

10-20 mg of dendrimers were dissolved in 600 mL of CD_2Cl_2 and characterized by ^{1}H NMR and ^{31}P NMR. Next, different equivalents (1 eq, 5 eq, 20 eq) of TFA were added to the solution, and the solution was characterized by ^{1}H NMR and ^{31}P NMR at defined time interval.

ESI-MS of G0-Lys(BOC)-COOMe (17) and G1-Lys(BOC)-COOMe (18)

The ESI-MS spectra of G0-Lys(PROXYL)-COOMe and G1-Lys(PROXYL)-COOMe were performed under different conditions, with acid (TFA) and without acid. Given the requirement of the equipment, we had to dilute the solution before injection and use a maximum amount of 0.1% TFA and acetonitrile as solvent.

Specifically, 0.924 mg of G0-Lys(BOC)-COOMe (**17**) was dissolved in 200 μL of acetonitrile. Next, 100 μL of the dendrimer solution was taken and diluted with 3.9 mL of acetonitrile to prepare a solution without acid as a reference. 100 μL of radical dendrimer solution was mixed with 4 μL of TFA (36 eq per branch). After 10 min, the radical dendrimer solution containing TFA was diluted with 3.9 mL of acetonitrile to obtain a solution of 4 mL. Last, these two solutions were sent to SAQ service from UAB for ESI-MS measurements.

1.01 mg of G1-Lys(BOC)-COOMe (**18**) was dissolved in 200 μL of acetonitrile. Next, 100 μL of the dendrimer solution was taken out and diluted with 4.9 mL of acetonitrile to prepare a solution without acid as a reference. 100 μL of dendrimer solution was mixed with 5 μL of TFA (50 eq per branch). After 10 min, the dendrimer solution containing TFA was diluted with 4.9 mL of acetonitrile to obtain a solution of 5 mL. Last, these two solutions were sent to SAQ service from UAB for ESI-MS measurements.

UV-Vis of G1-Lys(BOC)-COOMe (18)

0.5 mg of G1-Lys(BOC)-COOMe (**18**) was dissolved in 3 mL of $CHCl_3$, and characterized by UV-Vis. Next, 2 μL of TFA (20 eq per branch) was added to the dendrimer solution. Then, the solution was characterized by UV-Vis at different times. The stability of G1 (**2**) dendrimer was also checked in this way, using 0.2 mg of G1 (**2**) dendrimer, mixed with 2 μL of TFA.

Neutralization of the basic solution of G1-Lys(BOC)-COOLi (26)

14.7 mg of G1-Lys(BOC)-COOMe (**18**) were dissolved in 2 mL of THF. Next, 1 mL of Mili-Q water which contains 17 mg of $LiOH•H_2O$ was mixed with the dendrimer solution. Then the solution was stirred overnight. After that, the THF was evaporated under vacuum. The aqueous basic solution was characterized by ^{31}P NMR. After confirmation of the integrity of the structure by ^{31}P NMR. The solution was neutralized by adding 0.5 M citrate acid and citric buffer (pH 5), to adjust the pH gradually. Then, the solution was characterized by ^{31}P NMR.

Neutralization of the basic solution of G1-Lys(PROXYL)-COOLi (27)

3 mg of G1-Lys(PROXYL)-COOMe (**25**) were dissolved in 500 μL of Mili-Q water with 8.445 mg of $LiOH•H_2O$, followed by 100 μL of THF. Then the solution was characterized by EPR. 210 μL of the radical dendrimers solution was taken and the pH of the solution was adjusted with 2 M citrate acid (20 μL) and pH 5 citric buffer (10 μL) to pH 6. And the solution was characterized by EPR.

Endotoxin analysis

Endotoxin analysis of G3-Tyr(PROXYL)-COONa (**39**) were carried out at the Vall d'Hebron Research Institute (VHIR) by the manager of Área Tecnológica de Validación Funcional y Ensayos Preclínicos del CIBBIM-Nanomedicina of NANBIOSIS U20 of the CIBER-BBN.

***In vitro* cytotoxicity assays**

In vitro cell viability assays of Gn-Tyr-PROXYL radical dendrimers (n=0-3) were conducted with the fetus normal lung tissue cell line (MRC-5). The cells were incubated with Gn-Tyr-PROXYL dendrimers (n=0-3) at different concentrations ranging from 0.016 to 2mM per radical unit, for 24 and 48 h. Cell viability was determined by MTT assay, in the Cell cultures, Antibody production and Cytometry Services of UAB.

In vitro cytotoxicity assays of G0- and G1-OEG-PROXYL and G2-MPA-PEG20k-

TEMPO compounds were conducted with a Vero cell line (ATCC® CCL-81™) in ICN2-ICMAB Biolab facility. Vero cell line was initiated from the kidney of a normal adult African green monkey. G0- and G1-OEG-PROXYL and G2-MPA-PEG20k-TEMPO samples were filtered and serially diluted in DMEM+10%PBS media. Then, the cells were mixed in each solution (1×10^4 cells/well) to avoid pipetting errors. The dilutions, control and blank were seeded. The XTT kit (CyQUANT™ XTT Cell Viability Assay) was added at 24 h and 48 h. The reading was performed 4h after the tetrazolium was added. From each concentration quadruplicates were prepared and measured.

Animal Experimental Design

Tolerability and biodistribution studies were performed in healthy mice following the UAB animal work protocol. For biodistribution studies, a 0.00625 mmol/Kg dosage was used, with the objective of assessing through MRI studies the main organs related to G3-Tyr(PROXYL)-COONa (**39**) radical dendrimer metabolization, which is not expected to vary for different doses. However, tolerability studies were performed with the 0.025 mmol/Kg dosage foreseen in the DCE-MRI studies with the objective to ensure that no harmful effect was seen in the case of healthy C57BL/6 female mice.

Image analysis

Mice were positioned in a dedicated bed, which allowed suitable anaesthesia delivery (isoflurane, 1.5%-2.0% in O_2 at 1 L/min), with an integrated circuit of heating water for maintaining proper body temperature. Respiratory frequency was monitored with the help of a pressure probe and kept between 60 - 80 breaths/min. The 7T Bruker BioSpec 70/30 USR spectrometer (Bruker BioSpin GmbH, Ettlingen, Germany) equipped with a mini-imaging gradient set (400 mT/m) was used for acquisitions. A 72-mm inner-diameter linear volume coil was used as transmitter, and a dedicated mouse brain quadrature surface coil was used as receiver for MRI studies.

***In vivo* MRI studies**

In vivo MRI studies were conducted at the joint nuclear magnetic resonance facility of the Universitat Autònoma de Barcelona and Centro de Investigación Biomédica en Red-Bioingeniería, Biomateriales y Nanomedicina (CIBER-BBN), Unit 25 of

NANBIOSIS (www.nanbiosis.es) following the UAB animals work protocol. Mice anesthesia was performed with isoflurane (B.Braun, Melsungen, Germany) at 0.5-1.5% in O_2, and respiratory frequency was maintained between 40–60 breaths/min. Body temperature was maintained with a recirculating water system incorporated in the animal bed, and measured with a rectal probe. Respiration rate and temperature were constantly monitored (SA Instruments, Inc., New York, USA). Before immobilization in the animal holder, each mouse was cannulated in the tail vein using a home-built multi-delivery polyethylene tubing system. In this case, a 30G 2-way catheter was connected through polyethylene tubing, to 2 independent 1 mL syringes (Becton-Dickinson S.A., Madrid, Spain) loaded with heparinized-saline (40 U/ml) (0.9% NaCl, B.Braun and heparin, Mayne Pharma España, Madrid, Spain).

The MRI studies to assess contrast enhancement was performed with GL261 glioma GB-bearing mice following the UAB animals work protocol. Contrast agents administration (both G3-Tyr(PROXYL)-COONa radical dendrimer and Gd-based commercial CA) was done intravenously under anesthesia. The MRI exploration was performed, and animals left to recover in a warm environment. Mice were euthanized after the whole procedure was finished.

T_1 maps were performed with RARE-VTR sequence with FOV 17.6×19.28 mm; MTX, 128×128 matrix (138×150 μm/pixel); with Teff 7.5 ms and TR list: 100, 400, 700, 1000, 1300, 1700, 2000, 2600, 3500 and 5000 ms. NR=1, TAT 19 m 31s.

Dynamic Contrast Enhanced (DCE)-T_1 MRI studies.

Three glioma-bearing mice were injected with gadopentetate dimeglumine and another three were injected with G3-Tyr(PROXYL)-COONa (**39**). A DCE T1 study was then performed using three coronal sections. For this, a MSME sequence was used with: FOV 17.6×17.6 mm, MTX, 128×128 matrix (138×138 μm/pixel); TR/TE, 200/8.5 ms; ST, 1 mm; NA, 2; NR, 70; TAT, 59 min 44 s. The contrast bolus was administered after the third repetition of the complete T_1-weighted sequence (about 2.5 min after the start of the image acquisition protocol). DCE-MRI data were analyzed with DCE-@urLAB (http://oa.upm.es/28901/).

Appendix C Electron Paramagnetic Resonance (EPR)

To describe a paramagnetic isolated system under a magnetic field B_0, in EPR is used the formalism of Spin Hamiltonian. If we consider the paramagnetic system with an unpaired electron and some nuclei with nuclear spin quantum number I≠0, the spin Hamiltonian can be written as follows:

$$H = \mu_B \overline{BgS} - \mu_N \overline{Bg_N I} + \overline{IAS} + \overline{SDS} \quad (1)$$

In this expression first appears the electronic Zeeman interaction between the unpaired electron and the magnetic field, second the nuclear interaction between the nuclei with I≠0 and the magnetic field, then the hyperfine interaction between the electron spin and the nuclei with I≠0 and, finally, the dipolar interaction or zero field splitting between two or more unpaired electrons.

EPR spectra in solution.

EPR spectra of radicals in solution, especially those of organic radicals, are the easiest to interpret. In the case of a radical with an unpaired electron and in isotropic conditions, the expression of the spin Hamiltonian is reduced to:

$$H = \mu_B B g \bar{S} \quad (2)$$

and, since the energy E is proportional to the magnetic moment, the quantization of spin angular momentum ($m_s = \pm\frac{1}{2}$) determines the quantization of the electron energy levels in a magnetic field, obtaining in this case two levels:

$$E_\propto = +\frac{1}{2} g\mu_B$$

$$E_\beta = -\frac{1}{2} g\mu_B \quad (3)$$

The resonance equation corresponding to the transition between the α and β states (Figure C1) is:

$$\Delta E = E_\propto - E_\beta = g\mu_B = hv \quad (4)$$

Therefore, the EPR spectrum will consist of a single line centered at the resonance field corresponding to the g factor and with a linewidth (ΔH_{pp}) characteristics of the radical. The EPR spectra are always represented as a first derivative of the absorption signal for technical and historical reasons.

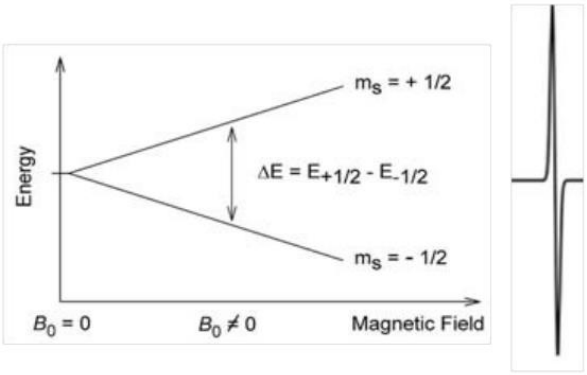

Figure C1. Representation of the energy separation of an electron spin under a magnetic field B_0 and the corresponding EPR spectrum

If in the paramagnetic system, for example an organic radical, there are nuclei with I≠0, we also must take into account the hyperfine interaction. A radical having a nucleus with $I = +\frac{1}{2}$, as a hydrogen atom, manifests a hyperfine splitting, *a*, which is proportional to the electron spin density on that atom. It presents an energy diagram and spectrum as that depicted in Figure C2a, which shows two lines with the same intensity 1:1. A nucleus with I=1, as a nitrogen atom, presents an energy diagram and spectrum as that depicted in Figure C2b which shows three lines with the same intensity 1:1:1. In general, the rules for calculating the number of signals and their relative intensities are similar to those used in NMR. This spectrum is the characteristic of nitroxyl radicals since the unpaired electron interacts mainly with one nitrogen atom.

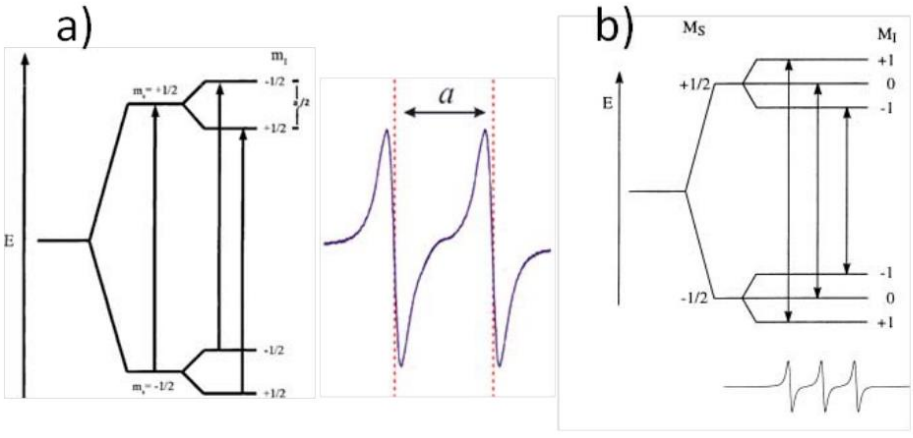

Figure C2. Energy states of a system with one unpaired electron and one nucleus with **a)** $I = \frac{1}{2}$, **b)** $I = 1$ and its corresponding EPR spectrum.

A radical system can have atoms of the same type with different hyperfine splitting

due to its different position in the molecule and groups of atoms that show the same hyperfine constant because they are equivalent. The number of lines (2I+1) in the spectrum and their intensity can be predicted with the Pascal triangle (Figure) (e.g., one unpaired electron that interacts with three equivalent nuclei of spin $I = \frac{1}{2}$ generates an EPR spectrum with four lines with relatives intensities 1:3:3:1).

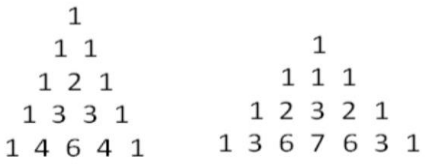

Figure C3. Pascal triangle for nucleus $I = \frac{1}{2}$ (left) and for I=1 (right).

In general, there are some rules to interpret the EPR spectra in solution when the conditions are isotropic and the splitting is of first order:

1. The spectrum must be symmetrical with respect to a central point.
2. The absence of a central line indicates an odd number of equivalent nuclei.
3. The separation between the two outer lines, always give the value of the smallest hyperfine splitting.
4. When in the molecule only appears nuclei with spin $I = \frac{1}{2}$, the sum $\sum_j n_j|a_j|$ is equal to the total extension of the spectrum; where n_j is the number of nuclei with hyperfine splitting a_j.
5. The maximum possible number of lines is given by the expression $\prod_j(2n_j + I_j + 1)$ where n_j is the number of equivalent nuclei with spin I_j.
6. The best proof of the correct interpretation is the simulation of the spectrum.

Under the conditions described above, the three fundamental parameters that define an EPR spectrum in isotropic conditions are the *g* factor, the line width and the coupling constant.

- The g factor (g) is a no dimensional parameter that is related to the magnetic field (B_0), and the frequency and it can be considered similar to the chemical shift in NMR.

- The coupling constant of the electron with the specific nuclei with nuclear spin different to zero ($I \neq 0$) is represented as a (in Gauss).

- The line width of the lines of the spectrum (ΔH_{pp}) (in Gauss).

In the nitroxyl radicals like TEMPO or PROXYL, the spin density is mainly located on the N-O• bond, for this reason, the unpaired electron couples with the nitrogen atom with a remarkable hyperfine coupling constant. ^{14}N has a nuclear spin I=1, so the transitions are between mI=-1,0,+1 (Figure C2b). Consequently, 3 lines of relative intensity 1:1:1 appeared in the EPR spectrum obtained at room temperature, i.e. in isotropic conditions.

Zero field splitting. Fine-structure.

These contributions may appear in systems with $I > \frac{1}{2}$ and express the energy splitting between different levels that take place in the absence of applied magnetic field. The simplest case corresponds to a biradical.

When a system contains two unpaired electrons that interact between them, appear two states of different energy, a symmetric one (triple state, S=1) and an antisymmetric one (singlet state, S=0). These two states present relative energies that depends on the sign and magnitude of the exchange integral *J*. The triplet state has three different configurations that present different energies even in absence of an external magnetic field due to the magnetic field generated by each electron over the other (zero field splitting).

We can say that, in the simplest case of system with S=1, the zero field splitting component of the spin Hamiltonian is:

$$H = \overline{SDS} \tag{5}$$

Where $\overline{D}$ is a symmetrical tensor of zero trace. The resolution of the corresponding secular determinant shows that the solution can be written in function of two parameters, *D* and *E* and they define completely the system. It is important to highlight the dependence of *D* parameter with the average distance between the two electrons that are interacting, while *E* parameter only depends on the wave function symmetry. Normally, EPR transitions are limited to the transitions with $\Delta m_s = \pm 1$. However, for triplet states at low fields a forbidden transition with $\Delta m_s = \pm 2$ can also been observed. This transition is observed at a magnetic field half of that predicted by the *g* value, is normally referred as half-field transition, and is often related to systems with two or more electrons.

Exchange interaction

Another consequence of having two or more unpaired electrons in a radical molecule is the exchange interaction. The exchange interaction is a direct consequence of the Pauli principe. For a two-electron system, it is described by the following term with adds to the spin Hamiltonian.

$$H = J \cdot S_1 \cdot S_2 \quad (6)$$

Were S_1 and S_2 are the electron spin angular momentum operators for the two electrons and J is the exchange coupling constant as previously commented. A positive value of J corresponds to the singlet been lower in energy than the triplet, which result from an antiferromagnetic interaction between the two electrons. A negative value of J (the singlet is higher in energy than the triplet) is typical of a ferromagnetic interaction. A strong exchange requires the two unpaired electrons be very close to each other. When it happens, if the hyperfine constant a is significantly smaller than the exchange constant J, such systems show EPR spectra split by the hyperfine interaction with nuclei from both radical units, however the distance between the hyperfine lines is $a/2$ rather than a. For instance, two nitroxyl radicals with strong exchange coupling show five-line spectra with 1:2:3:2:1 intensity ratio and the separation between them is half of that observed for similar monoradicals.

Dipole-dipole interaction

The dipole-dipole interaction in systems with well-separated electrons (e.g. diradicals) averages out zero for rapidly molecular tumbling and the EPR spectra is dominated by the exchange interaction. In frozen conditions, the spectra is controlled not only by the exchange interaction but also by anisotropic hyperfine interaction and anisotropic dipole-dipole interaction become more and more complex. Fortunately, EPR spectra in frozen solutions of di- or poly-organic radicals are much simpler if the distance between the radicals is short (about 1-3 nm). In these conditions, the exchange interaction becomes negligible and the EPR spectra are thus dominated by the dipolar interaction. The effect of dipole-dipole interaction at short radical distances is only a line broadening that depends on the distance between radicals. This effect could be estimated by the empirical ratio of peak heights d_1/d in nitroxides (Figure C4). This parameter is shown to be sensitive to the distance between adjacent nitroxides and hence a convenient measure

of the strength of the dipole-dipole interactions (e. g., the higher the ratio, the shorter the distance between the radical centers and hence the higher the radical interactions).

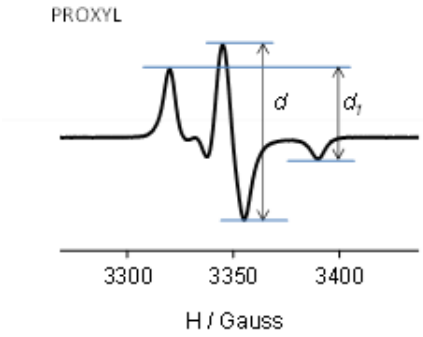

Figure C4. Representation of the d and d_1 used to calculate d_1/d parameter in the typical spectrum of a nitroxide radical in frozen solution conditions.

References

1. Weil John A., Bolton James R. and Wertz, Electron Paramagnetic Resonance, **1994**, Jonh Wiley & Sons, New York.

2. Atherton, N.M., Principles of Electron Resonance, **1993**, Ellis Horwood Limited, London.

3. Chechik, V.; Carter, E.; Murphy, D., Electron Paramagnetic Resonance, **2016**, Oxford University Press, USA.